

PhD 11893

A STUDY OF PLASTICITY THEORIES AND  
THEIR APPLICABILITY TO SOILS

by

Guy Timmouth Houlsby

A dissertation submitted for the  
degree of Doctor of Philosophy  
at the University of Cambridge



St. John's College

January 1981

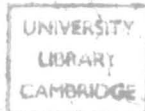
## SUMMARY

A review of the types of rate independent theories for soils is given, together with a more detailed survey of plasticity theories. The contributions of particulate mechanics are briefly summarised. The remainder of the dissertation is divided into two parts, dealing respectively with a theoretical and experimental study of the applicability of plasticity theory to soils. Some additional information is given in Appendices.

Part I begins with some theoretical preliminaries. Kinematic variables and their conjugate forces, internal variables and the theoretical restrictions on plasticity theory are introduced. The need for a less restrictive approach is explained, and this is met by a thermomechanical formulation of plasticity theory. Some implications of the theory and some specific examples are given, including models involving non-associated flow and the principle of effective stress.

A detailed discussion of the derivation of the Modified Cam-Clay model from the thermomechanical method is given, including comparisons with earlier energy theories for clays. The model is extended to general stress states and to large strain theory. Some modifications of the model are then considered, including changes to the yield locus and a study of a shear modulus dependent on pressure or preconsolidation pressure. Experimental data on the variation of the shear modulus are discussed. Part I concludes with two aspects of soil behaviour not yet included in the thermomechanical approach: the generalisation of yield loci in the octahedral plane and the development of anisotropy.

The material for experimental study is described, and the types of test for the applicability of plasticity theory discussed. An investigation of the effect of stress and of stress history on a dense sand in triaxial compression, using a programme of stress cycle tests,



is outlined. A computer controlled triaxial machine necessary for the tests is described, with details of the datalogging and control system and the sample preparation procedure. The method of analysis for the tests is given, including a method of fitting elastic and plastic properties to the data. The results of the tests are presented. The elastic properties are anisotropic and depend on stress and stress history. The plastic properties are strongly history dependent, and significant secondary plastic strains on unloading were observed.

Finally some conclusions from both the theoretical and experimental work are drawn together and some topics for future work suggested. The application of the thermomechanical approach in describing soils is emphasised.

## CONTENTS

Summary	1
Contents	3
Preface	6
1. Introduction and Review	7
1.1 Theoretical Models for Soils	7
1.2 Notation and Terminology	10
1.3 Rate Independent Theories for Soils	12
1.4 Plasticity Theories for Soils	16
1.5 The Contribution of Particulate Mechanics	22
Part I Theoretical Study	
2. Theoretical Background to Plasticity Theory for Soils	26
2.1 Kinematic Variables and Conjugate Forces	26
2.2 The Use of Internal Variables in Plasticity	29
2.3 Theoretical Restrictions Imposed on Plasticity Theory	31
2.4 The Need for a Less Restrictive Approach	34
3. A Thermomechanical Formulation of Plasticity Theory	36
3.1 Introduction to Thermomechanical Methods	36
3.2 Ziegler's Thermomechanical Formulation	38
3.3 Some Implications of Ziegler's Formulation for Conventional Plasticity Theory	44
3.4 Derivation of Specific Elastic-Plastic Models from Thermomechanics	50
3.5 Effective Stress Models for Soils	53
4. Derivation of the Modified Cam-Clay Model from Thermomechanics	58
4.1 The Cam-Clay Models	58

4.2	Derivation of the Modified Cam-Clay Model from Thermomechanics	59
4.3	Comparisons with Alternative Energy Theories for Clays	68
4.4	Extension of the Modified Cam-Clay Model to General Stress States	75
4.5	Extension to Large Strain Theory	77
5.	Variations on Modified Cam-Clay and Comparisons with Experimental Data	84
5.1	Numerical Calculations Using Modified Cam-Clay Models	84
5.2	A Change in the Dissipation Function	87
5.3	A Pressure Dependent Shear Modulus	93
5.4	Elastic-Plastic Coupling	95
5.5	Experimental Data on the Variation of the Shear Modulus of a Clay	100
6.	Further Aspects of the Behaviour of Clays	110
6.1	Generalisation of Yield Loci in the Octahedral Plane	110
6.2	Anisotropy and the Effects of Stress History	120
	Part II Experimental Study	
7.	The Experimental Programme	127
7.1	The Choice of Material for Experimental Study	127
7.2	Experimental Testing of Plasticity Theory	131
7.3	Stress Probe and Stress Cycle Tests	135
7.4	The Effect of Stress and of Stress History	139
8.	A Triaxial Apparatus for Stress Cycle Tests	145
8.1	A Computer Controlled Triaxial Machine	145
8.2	The Transducers and Their Calibration	140
8.3	Automatic Data Logging and Motor Control by the PDP-8E Computer	156
8.4	The Triaxial Testing Control Program	158
8.5	Sample Preparation	163

9.	Stress Cycle Tests on Dense Sand	169
9.1	Analysis of Stress Cycle Tests	169
9.2	Optimisation of Elastic and Plastic Properties	174
9.3	Constraints on the Minimisation Procedure	179
9.4	Representation of Stress Cycle Results	182
9.5	Variation and Interpretation of Elastic Properties	188
9.6	Variation of Plastic Properties	199
10.	Conclusions	210
10.1	The Use of Thermomechanics in Soil Modelling	210
10.2	The Modified Cam-Clay Models	211
10.3	Results of Stress Cycle Tests on Dense Sand	212
10.4	The Applicability of Plasticity Theory to Soils	215
	Notation	217
	References	220
	Appendix A The Work Input to a Granular Material	226
	Appendix B Homogeneity of Response	231
	Appendix C Stress and Strain Calculations for Triaxial Tests	237

## PREFACE

The work described in this dissertation was carried out as part of the continuing research into the stress-strain behaviour of soils by the Soil Mechanics Group at Cambridge. During this work I was supported by the Science Research Council. I am grateful also to St. John's College, both for a Studentship and for generous grants towards my attendance at conferences.

Many members of the Engineering Department have been of assistance to me during my work, and only a few may be mentioned here. I am extremely grateful to Professor C.P. Wroth (now at the Department of Engineering Science, Oxford University) for his invaluable guidance throughout this research. The staff of the soil mechanics laboratory (in particular Mr R.E. Ward, Mr W. Gwizdala and Mr A. Balodis) were of great help with experimental work, and I am also grateful to the C.U.E.D. computing staff for their help. I wish also to thank Mrs P. Lister for her careful typing of this dissertation.

The tests on Kaolin described in Section 5.4 were carried out by Mr C.S. Davidson as an Engineering Tripos, Part II, Research Project in co-operation with myself and under the supervision of Dr M.F. Randolph. I am very grateful to Charles Davidson for his careful work on this project.

Finally I am always grateful to my parents for their continuing support and encouragement for my research.

This dissertation is the result of my own original work and includes nothing which is the outcome of work done in collaboration. In particular the use of thermo-mechanical methods in the derivation of plasticity theory, and the use of stress cycle tests for investigating the behaviour of soils are new developments.

G.T. Houlsby

## CHAPTER 1

## INTRODUCTION AND REVIEW

The subject of theoretical models for soils is first introduced, and the range of this dissertation outlined. After a brief explanation of the terminology which will be used, a review of the types of rate independent theories for soils is given, followed by a more detailed survey of plasticity theories. The possible contributions of particulate mechanics are summarised.

### 1.1 Theoretical Models for Soils

The study of theoretical models for soils is now over two hundred years old, dating from the analysis of the failure of a soil mass by Coulomb in 1773 (see Heyman (1972)). The mechanical behaviour of soils is still, however, far from being properly understood, even for the simplest of laboratory prepared materials. The application of plasticity theory to soils, a subject which has been studied extensively during the last quarter of a century, is still therefore a topic which must be examined critically.

The subject of theoretical soil mechanics may be approximately divided into two fields, the characterisation of the soil (the study of constitutive relations) and the solution of boundary value problems; this dissertation is entirely concerned with the former. Within the subject of constitutive relations it is first necessary to distinguish carefully between three regions of study. The first is the study of the behaviour and properties of the real material: for instance the experimental measurement of the variation of the shear modulus of a sand. The second field is the study of the applicability of a particular theory to a soil: in the above example the question would arise as to whether an elastic shear modulus reasonably represented the behaviour of the soil within the range of interest. The third subject is the study of the theory itself: it may be the case for instance that any properly

expressed theory using a variable shear modulus must comply with certain fundamental theoretical conditions. The three topics have been introduced in reverse order from the logical procedure in practice; a theory must be properly formulated first, its applicability to soils assessed and finally the properties for individual soils determined. The topics studied in this dissertation relate to the proper formulation of plasticity theories, and the assessment of the suitability of these theories for soils.

The study of the theory itself is necessary because unfortunately many models for soils are either incomplete or inconsistent with the principles of continuum mechanics. Various theoretical criteria must be satisfied before any study of the usefulness of a theory in its application to soils.

The usefulness of a model is emphasised since in choosing a theoretical idealisation of a soil one is not always primarily concerned with accuracy: the best model for solving an engineering problem is not necessarily that which most closely fits the stress-strain curve for the chosen laboratory or field tests. Soil is a very complex material, and any model which achieves a high degree of accuracy is likely also to be complex. A simpler model may have advantages which may outweigh any loss in precision; for instance the use of linear elasticity allows the application of many standard solutions for stresses and displacements. Complex models also have the disadvantage that they may involve many parameters and functions which are difficult to determine, and may be of unknown significance if the conditions in the real problem depart in any way from those from which the model was derived.

Finally, and perhaps most importantly, the complex models are unlikely to give an engineer a true understanding of soil behaviour. A theory is seen as more than a mere encoding of test data in a concise form, but it should embody some explanation of the mechanisms underlying

the behaviour. To draw an analogy from astronomy, the approach used in many of today's theories in soil mechanics seems remarkably similar to that of Ptolemy in his system of epicycles which, whilst fitting (at least approximately) the motion of most of the planets, did nothing to explain that motion. Ptolemy's approach was totally superseded once a theory which provided an explanation was found; the purely phenomenological approach is therefore rejected in the following, where theories based on relatively simple hypotheses are studied. Although a certain degree of complexity must be admitted to provide tolerable accuracy, an emphasis is placed on relatively simple theories; it is felt that only by adopting this approach can some progress be made towards an understanding of soil behaviour.

The work presented in this dissertation is arranged as follows. This Chapter continues with an outline of the terminology which will be used, followed by reviews of three different topics. The different possible structures for rate independent theories are first reviewed, then a more detailed, but selective, review made of plasticity theories for soils. A short survey of the contribution of particulate mechanics to the understanding of soil behaviour is given; these ideas provide some background for the continuum mechanics theories which will be examined later.

The remainder of the dissertation is divided into two halves; Part I deals mainly with the study of theories for soils (principally for clays) although it draws slightly on experimental data. In Chapter 2 certain preliminary problems in continuum mechanics are discussed, leading to a study of the restrictions which are usually imposed on plasticity theory and their over-restrictive nature for soils. An alternative approach to plasticity theory is given in Chapter 3, successfully imposing the restrictions of thermodynamics without introducing the unrealistic requirement of normality of plastic strain increments to the yield locus. The new approach is developed in Chapters 4 and 5 where the Modified Cam-Clay model is derived in terms of the thermomechanical method, and it is

shown how the method allows proper treatment of some alterations to the simple model. Part I is completed by a Chapter in which some aspects of soil behaviour not yet accommodated in the thermomechanical method are discussed.

Part II is an experimental study, essentially separate from Part I; it begins with a discussion of the ways in which the applicability of plasticity theory to soils may be tested experimentally, leading to a programme of "stress cycle" tests which are used to study the effects of stress and of stress history on the behaviour of a sand. A computer controlled triaxial apparatus, necessary for these tests, is described. The results of the tests are presented and interpreted in terms of elasticity and plasticity theory.

In Chapter 10 some conclusions from Parts I and II are drawn together. Some additional material is presented in Appendices. Appendix A is a copy of a publication on which Section 2.1 is based, and Appendix B is a brief discussion of an extension of the ideas presented in Chapter 3 to the analysis of non-homogeneous behaviour. Details of calculations for the triaxial test are given in Appendix C.

## 1.2 Notation and Terminology

Before proceeding further it is useful to define various terms which will be used. Cartesian tensors are used through this work, and the summation convention implied by a repeated index. The following notation is used for the invariants of a Cartesian tensor  $t_{ij}$  :

$$t_{(1)} = t_{ii} \quad (1.2.1)$$

$$t_{(2)} = \frac{1}{2} (t_{ij}t_{ji} - t_{ii}t_{jj}) \quad (1.2.2)$$

$$t_{(3)} = \frac{1}{6} (2t_{ij}t_{jk}t_{ki} - 3t_{ij}t_{ji}t_{kk} + t_{ii}t_{jj}t_{kk}) \quad (1.2.3)$$

The deviator of a tensor is indicated by a dash notation and is given by:

$$t'_{ij} = t_{ij} - \frac{1}{3} t_{(1)} \delta_{ij} \quad (1.2.4)$$

where  $\delta_{ij}$  is the Kronecker delta. It is convenient to note the following differentials:

$$\frac{\partial t_{(1)}}{\partial t_{ij}} = \delta_{ij} \quad (1.2.5)$$

$$\frac{\partial t'_{(2)}}{\partial t_{ij}} = t'_{ij} \quad (1.2.6)$$

A dot notation is used to indicate differentiation with respect to time, and a superposed dot on an invariant is used to indicate the appropriate invariant of the rate of change of the tensor (as opposed to the rate of change of the invariant of the tensor). Partial differentiation with respect to spatial coordinate  $x_i$  is indicated by a comma notation, thus:

$$\frac{\partial y}{\partial x_i} = y_{,i} \quad (1.2.7)$$

The treatment of the stress and strain tensors uses the nine variable formalism, defining strain  $\epsilon_{ij}$  as:

$$\epsilon_{ij} = \frac{1}{2} (v_{i,j} + v_{j,i}) \quad (i, j = 1, 3) \quad (1.2.8)$$

although there are only six independent components of strain. Except in Section 4.5 small strain theory is used throughout.

Compressive stresses and strains are taken as positive, and all stresses are effective stresses except in Sections 2.1, 3.5 and Appendix A where a dash notation is used to indicate effective stresses rather than the deviator of a tensor. *Chapters 6 and 7* The variable  $p'$  represents effective mean stress throughout.

Subscripts are used as qualifiers to quantities (e.g. plastic volumetric strain  $v_p$ ) but for tensorial quantities bracketed superscripts are used to avoid confusion with the indices (e.g. plastic strain  $\epsilon_{ij}^{(p)}$ ).

Certain words are used in an unusual or specialised sense, and in this case are usually italicised for emphasis; thus the word *force* is frequently used in the more general sense used in thermodynamics rather than with the more common meaning in mechanics.

### 1.3 Rate Independent Theories for Soils

Although both clays and sands exhibit creep under constant stress and stress relaxation at constant deformation, these would largely seem to be secondary effects, with the main response being rate independent rather than viscous in nature. Only rate independent theories for the soil skeleton will be treated in the rest of this work, but rate dependence due to consolidation effects (interaction of the soil skeleton and a viscous pore fluid) may still be accounted for. Several classes of rate independent theories have been used for soils, and these are characterised principally by the nature of the response which they predict on loading followed by unloading and subsequent reloading. Some of the more important types of theory are outlined below.

The simplest rate independent theory is that of elasticity, in which:

$$\sigma_{ij} = c_{ijkl} \epsilon_{kl} \quad (1.3.1)$$

If  $c_{ijkl}$  is variable then non-linear behaviour can be described, as in curve OA of Figure 1.1(a) which shows a typical one dimensional monotonic loading curve. On unloading, however, the curve would be retraced, which is an unrealistic description of a real material. Dilatancy on shearing cannot be accommodated within elasticity, since if the stiffness matrix predicts dilatancy for shearing in one direction it must predict compression on a reversed shearing. As long as attention is restricted solely to loading then elasticity may be useful; for instance the non-linear elastic model of Duncan and Chang (1970) (which includes some additional empirical features) has been extensively used in engineering calculations.

In order to obey the first law of thermodynamics for a non-dissipative system, elastic laws may be restricted to hyper-elasticity such that:

$$\sigma_{ij} = \frac{\partial W}{\partial \epsilon_{ij}} \quad (1.3.2)$$

where  $W$  is a function of strain. This class of materials is a subset

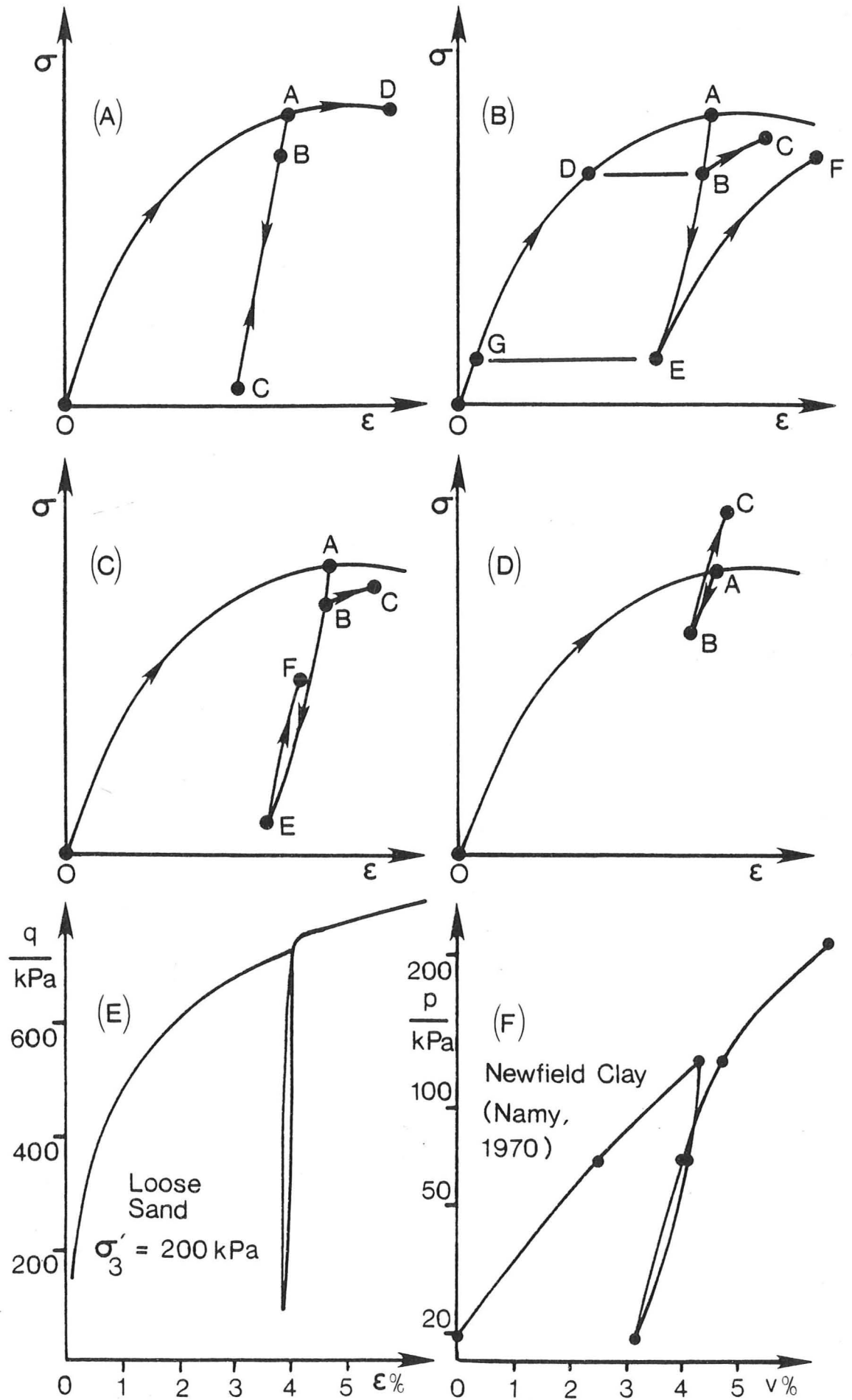


Figure 1.1 Forms of stress-strain curves given by different theoretical models

of the elastic materials.

A wider class of materials consists of those which are hypo-elastic, the simplest form being given by:

$$\dot{\sigma}_{ij} = c_{ijkl} \dot{\epsilon}_{kl} \quad (1.3.3)$$

These materials can accommodate the non-linear loading OA of Figure 1.1(b); if more complex first order terms are added to the right hand side of Equation (1.3.3) then unloading of the form ABE in Figure 1.1(b) can be achieved. Such a model is described by Gudehus and Kolymbas (1979), in which the stress rate is taken as a homogeneous but non-linear function of strain rate. The resulting model is *incrementally non-linear*, i.e. if it were to be reduced to the form of Equation (1.3.3) the stiffness  $c_{ijkl}$  would depend on the direction of the strain rate  $\dot{\epsilon}_{kl}$ . Although soils may in reality display incremental nonlinearity, this property is undesirable in a simple model since in calculations using methods such as finite element analysis an iterative procedure must be used in which the stiffness matrix must be re-formed according to the response calculated.

A further disadvantage is that in its present form the model of Gudehus and Kolymbas uses stress as the only structural parameter, so that on the reloading curves BC and EF the slopes are the same as for the sections of the initial loading curve at D and G in Figure 1.1(b) (see Kolymbas and Gudehus (1980)). Whilst the model may therefore be of use in primary loading and first unloading, and can accommodate dilatancy, the behaviour on reloading is unrealistic. An improvement could be achieved by including other structural parameters, for instance a preconsolidation pressure.

A more familiar approach to the loading-unloading behaviour than hypo-elasticity is plasticity theory. In this theory the strain is divided into two additive components. The elastic strain increment occurs for all changes of stress, and is usually restricted by hyperelasticity.

The plastic component only occurs if the stress point lies on the yield locus, which is a surface in stress space, and (for a hardening material) the stress increment is outward directed from the yield locus. The magnitude of the plastic strain increment is related to the movement of the yield locus by a hardening law, and the direction of the plastic strain increment is independent of the direction of the stress increment and is given by the normal to a plastic potential. The type of behaviour given by plasticity theory can describe the loading curve OA of Figure 1.1(a), and an unloading-reloading curve ABC. On reloading to A the initial curve is re-joined and the path AD followed. Plasticity theories are incrementally bilinear, that is the stiffness matrix can be reduced to the form of Equation (1.3.3) where the stiffness  $c_{ijkl}$  takes two values, one if plastic loading occurs and the other for elastic unloading. If a pointed yield locus is allowed the theory becomes incrementally nonlinear.

An alternative approach is that of endochronic theory, first introduced by Valanis (1971) for application to metals, and since extensively applied to concrete and soils, e.g. Bazant and Krizek (1976). The essential feature of the theory is the use of an *intrinsic time* which depends both on the real time and on the deformation of the material. For a rate independent material the intrinsic time does not depend on real time and is given by an expression of the form:

$$(\dot{\xi})^2 = D_{ijkl}^{(1)} \dot{\epsilon}_{ij} \dot{\epsilon}_{kl} \quad (1.3.4)$$

The incremental behaviour is then given by an expression of the form:

$$\dot{\sigma}_{ij} = D_{ijkl}^{(2)} \dot{\epsilon}_{ij} + D_{ijkl}^{(3)} \sigma_{kl} \dot{\xi} \quad (1.3.5)$$

Each of the tensors  $D_{ijkl}$  may depend on stress, strain and intrinsic time, so there is scope for considerable complexity of behaviour. Loading and unloading curves of the form OABE in Figure 1.1(c) are possible. On reloading from E a suitable choice of functions gives the realistic

behaviour EF, but on reloading after a small unloading the slope BC is approximately the same as the original loading slope at A. Recent modifications to the theory apparently eliminate this unrealistic behaviour, but at the expense of the equally unrealistic reloading curve of BC in Figure 1.1(d). Endochronic theory is closely related to hypo-elasticity, and the equations resulting from the theory are also incrementally nonlinear: they may be approximately linearised, however, for limited loading paths.

The behaviour of loose Leighton Buzzard sand in a drained triaxial compression test is shown in Figure 1.1(e) and of Newfield Clay in an isotropic consolidation test in Figure 1.1(f). In both of these tests the character of the overall loading, unloading and reloading cycle is most nearly described by plasticity theory rather than any of the alternatives described above. For these reasons, and because of ample other evidence of the usefulness of plasticity theory for soils, the remainder of this dissertation is concerned primarily with plasticity theories rather than any of the other rate independent theories discussed above.

#### 1.4 Plasticity Theories for Soils

In recent years the number of theoretical models for soils either using rigorous plasticity theory or based more loosely on the concepts of plasticity has increased enormously. Any review must necessarily be highly selective, and in the following most emphasis is placed on the developments related to the critical state models, on which attention at Cambridge has been principally focussed.

Plasticity theory was developed initially for the study of ductile metals, and first involved the use of *perfect plasticity* (e.g. Prager and Hodge (1951)) in which the yield locus is fixed in stress space and is therefore identical to the failure locus. Perfect plasticity has

found much application to the problem of the failure of soils, principally through the application of the upper and lower bound theorems. The theory is particularly useful in studying the undrained behaviour of clay (which may be treated as a purely cohesive material). Although the bound theorems are considerably weakened for a frictional material with a non-associated flow rule (Drucker (1954)), plasticity theory has also been applied with success to frictional materials (e.g. the stress field solutions developed by Sokolovskii (1965)).

Whilst useful in the study of the failure of a soil, perfect plasticity is not so suitable for the study of the development of displacements under working loads and before failure is reached. For this application a work hardening theory of plasticity is necessary. The application of a work hardening theory to soils was first qualitatively described by Drucker et al. (1957), who suggested an "extended Von Mises" conical yield locus closed by a spherical work hardening cap. Although several later models are qualitatively similar to this prototype, the model was incomplete and did not achieve a full synthesis of soil behaviour.

At about the same time Roscoe et al. (1958) successfully combined the ideas of a unique surface in  $(p', q, V)$  space for normally consolidated clays (introduced by Rendulic (1936)), the normalisation of clay behaviour with respect to preconsolidation pressure (following Hvorslev (1936)) and an extension of the idea of a critical voids ratio (Casagrande (1936)) to that of a critical state line in  $(p', q, V)$  space. (For definitions of  $p'$  and  $q$  see Schofield and Wroth (1968),  $V$  is specific volume.) The intersection of an "elastic wall" (which simply represents a statement of elastic isotropy) with the state boundary surface for normally consolidated clays (the Roscoe surface) was later identified as a yield locus (Calladine (1963)). Quite separately a work

equation similar in concept to that of Taylor (1948) may be integrated to give a plastic potential; adoption of Drucker's stability hypothesis allows this to be identified as a yield locus, which happens to be similar in shape to that given by the intersection of the elastic wall and the Roscoe surface.

Finally, expressed conveniently in terms of variables appropriate to the triaxial test, the Cam-Clay model of Schofield and Wroth (1968) achieved a synthesis of the above ideas. The "elastic wall" and work hardening law are specified by the consolidation behaviour (using a simple empirical relation); the work equation is integrated to give a plastic potential, and normality is assumed to give also the yield locus. The "Critical State" is automatically included and the yield surface is part of the "State Boundary Surface". The model goes far in not only fitting the behaviour of soft clays, but also in explaining that behaviour. The behaviour implied by the model is mainly qualitatively correct, for instance the variation of undrained strength with over-consolidation ratio is quite well described.

The slight change in the flow rule to give Modified Cam-Clay (Roscoe and Burland (1968)) and the addition of a shear modulus result in a model which is well suited to computation using the Finite Element Method. Whilst useful for modelling the loading of soft clays the critical state models are less suitable for overconsolidated materials, or for unloading or reversal of loading on soft materials.

The loading of stiff soils shows a work hardening behaviour apparently linked to a yield locus taking approximately the conical form used by Drucker et al. (1957). This has given rise to a series of "cap models" employing a combination of the conical locus and a consolidation "cap". The models are mainly empirical and that by Lade (1977) is a good example of the type. In the case of a sand the conical locus (in this example a distorted cone in stress space) assumes

greater importance than the consolidation behaviour. Lade's model is expressed entirely in terms of plasticity theory. In adopting a non-associated flow rule and non-conservative elastic behaviour it moves far from the simple theories where the uniqueness and bound theorems apply. Although the model may fit test data accurately the validity of any solutions to boundary value problems may therefore be questioned.

The Lade model, like the Cam-Clay models does not fit unloading behaviour well. Soils show hysteresis and nonlinear behaviour below the yield locus, and attempts to include these effects have been made in a variety of ways. Hueckel and Nova (1979) use for example a model related to the cap models, but incorporate a "paraelastic" strain in which the elastic compliance increases with the distance from the last stress reversal point so that hysteresis is introduced. The form of all unloading curves is similar, and no "shakedown" to elastic behaviour is possible.

The above model introduces hysteresis effects independently from the main plastic behaviour. An alternative is to link these effects specifically to plasticity. This is achieved by the model of Dafalias and Herrmann (1980), and a simplified version of the concepts involved is given here. For every stress point A in Figure 1.2 an image point B on a "Bounding Surface" is determined. The plastic strain in a conventional plasticity model with an associated flow rule and a yield locus  $f(\sigma_{ij}, \epsilon_{ij}^{(p)}) = 0$  is given by:

$$\dot{\epsilon}_{ij}^{(p)} = \frac{1}{h} \frac{\partial f}{\partial \sigma_{ij}} \frac{\partial f}{\partial \sigma_{kl}} \dot{\sigma}_{kl} \quad (1.4.1)$$

where  $h$  is a hardening modulus. In the bounding surface model  $f$  is interpreted as the bounding surface and  $\sigma_{ij}$  in Equation (1.4.1) as the stress at the image point. The value of  $h$  is then given by:

$$h = h_0 + h_1 \frac{\delta}{(p'_c - \delta)} \quad (1.4.2)$$

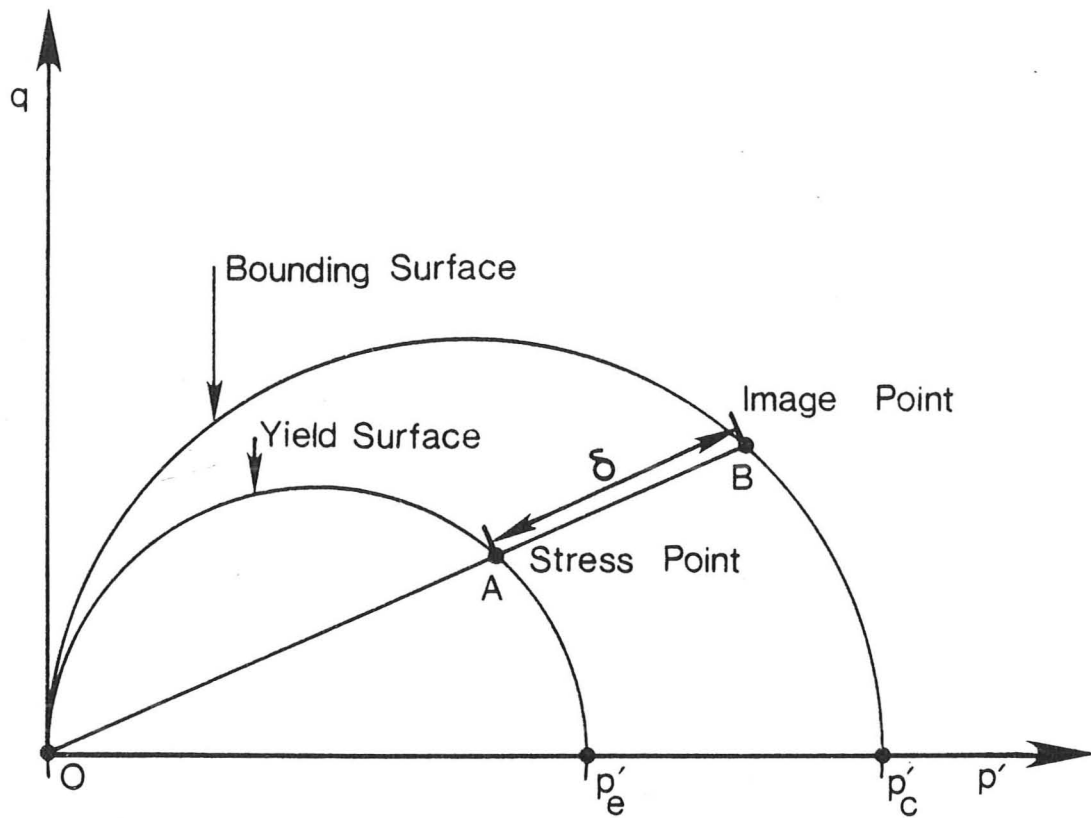


Figure 1.2 Yield and bounding surfaces for simplification of model of Dafalias and Herrmann (1980)

where  $\delta$  is as shown on Figure 1.2. The result is that when the stress point is on the bounding surface conventional plastic behaviour is given, inside the surface a reduced plastic strain occurs if the quantity  $p'_e$  is increasing. (A yield locus through the stress point and similar to the bounding surface may be imagined.) The model has several advantages: it is incrementally bilinear, models hysteresis and has a smooth transition from elastic to plastic behaviour. Whether the development of plastic strains after many cycles is in fact modelled accurately is as yet unknown.

An alternative arrangement which also produces hysteresis effects

involves the use of multiple yield loci. The model of Prevost (1979) uses this technique, with many yield loci of different sizes, all similar in shape to the Modified Cam-Clay yield locus but not fixed in stress space, nested together in stress space. Each locus has a simple linear hardening law associated with it which determines its contribution to the overall plastic strain. The yield loci are each translated independently by the stress point. These models are characterized principally by many material constants, but this is countered by the fact that they require no complex functions to be chosen. Although capable of fitting test data well their value for the solution of boundary value problems seems questionable.

Finally the "microstructural" model of Calladine (1971) may be mentioned. Although based on theories for the contact behaviour of planes in the material, calculations using the model also involve multiple yield loci, in this case each associated with a different plane. Computationally the problems are similar to those of the last model, although conceptually the models are very different. The distribution of yield loci in stress space is quite different in the two models, and the microstructural model does not require a large number of material constants.

The above models give some idea of the ways in which plasticity theory may be modified to accommodate many aspects of soil behaviour. Although some of the latter models are more accurate than the simple models they have the disadvantages of complexity. They are not pursued further here, where the emphasis is rather on the establishment of simple models on a theoretical basis which seems better suited to the description of soils than conventional plasticity theory.

### 1.5 The Contribution of Particulate Mechanics

An alternative to the continuum mechanics approach is to adopt an analysis paying specific regard to the particulate nature of soils. This work is usually based on assumptions of rounded particles with frictional contacts; the results are therefore more applicable to sands than clays, where the particles are predominantly plate or rod like in form and complex electrical interactions are frequently important. Although the particulate nature of soil is specifically acknowledged, the aim of the theories is to describe macroscopic behaviour and so their results may ultimately be very similar to those of continuum mechanics. The studies of particulate mechanics fall approximately into four fields:

- (a) The analysis of regular arrays of rigid frictional particles.
- (b) The analysis of irregular arrays paying special attention to stresses and strain increments on planes oblique to the principal stress directions.
- (c) Probabilistic analysis of irregular arrays.
- (d) Study of the contacts between particles.

Topic (b) may not involve an approach specifically taking into account the particulate nature of soil, but derives from the significance of certain planes in the analyses of type (a) and has led to some fruitful results.

The importance of the analysis of regular arrays lies entirely in the expectation that more complex irregular assemblies will behave in an analogous manner to the simple structures which are studied. This expectation may not be realised since regular arrays involve certain highly unrealistic features; for instance the fairly continuous creation and destruction of particle contacts in the deformation of an irregular array is replaced by the sudden change of whole sets of contacts. In spite of these problems the method has given some useful results, in particular the analysis of a regular array of spheres by Rowe (1962)

which led to the development of the stress-dilatancy theory. More recently Thornton and Blackburn (1980) have extended the analysis of assemblies of spheres to demonstrate the importance of an anisotropic structure on the initial yield locus of a soil. Although the study of regular arrays is mainly a theoretical exercise, the results may also be verified experimentally. The tests of Rowe (1962) demonstrate for instance the development of discrete shear bands in strain softening materials.

The analysis of soil behaviour placing particular emphasis on certain planes oblique to the principal stress directions dates from Coulomb's first contribution to the subject. That analysis was purely concerned with the strength of the material, but more recent analyses have also made many hypotheses about the flow. The stress-dilatancy theory of Rowe (1962) for instance results in a flow rule by considering sliding on planes for which an energy ratio is minimised (the validity of the energy ratio hypothesis is open to question). The inclusion of this approach amongst particle mechanics is because the planes of interest arise by analogy with certain important planes in the analysis of regular arrays.

More recently Matsuoka (1974) has focussed attention on the deformation of soil in relation to the "Mobilised Plane" (identical to Coulomb's critical plane), and also the "Spatially Mobilised Plane", a concept rather more difficult to interpret physically (Matsuoka (1976)). The analysis makes complex assumptions about particle movements related to the plane, the details of which are open to criticism. Some promising results have, however, been reported. The models are formulated in such a way that strains are calculated in response to stress changes, and may be difficult to use within continuum mechanics.

A deterministic approach to the deformation of irregular arrays of particles is prohibitively complex, but analyses using probabilistic techniques have been attempted. The initial work in the subject was

by Horne (1965) who, assuming no rotation of particles, derived from virtual work principles a complex expression for the ratio of the work input per unit volume  $\sigma_1 \dot{\epsilon}_1$  and output  $(\sigma_2 \dot{\epsilon}_2 + \sigma_3 \dot{\epsilon}_3)$  (assuming  $\dot{\epsilon}_2 < 0$ ) dependent on the orientation of the contacts on which sliding occurs. He adopts Rowe's assumption that the ratio takes its minimum value and derives the optimum sliding direction for this to occur. The result is the stress dilatancy expression in the form:

$$\frac{-\sigma_1 \dot{\epsilon}_1}{\sigma_2 \dot{\epsilon}_2 + \sigma_3 \dot{\epsilon}_3} = \tan^2 (\pi/4 + \phi_\mu/2) \quad (1.5.1)$$

Horne also introduced a measure of anisotropy, the "mean projected solid path" or "mpsp" which is the mean distance <sup>in</sup> a given direction traversed between two random contacts on a particle. The variation of "mpsp" with direction is a measure of the structure of a granular assembly and is related to the distribution of contact directions. Horne makes use of an arbitrary probability density function for the contact directions to derive the "mpsp" in terms of this function under certain assumptions. Using another probability density function for the proportion of particles sliding at a given velocity, and assuming no particle rotation, he also derives expressions for strain rates. With further simplifying assumptions Horne calculates the stress ratio for initial deformation of an isotropic assembly, the peak stress ratio and the stress ratio for deformation at constant volume (Horne (1969)). Further work (e.g. Oda (1974)) has been done using other fabric indices and assumptions, resulting mainly in slight modifications of the stress-dilatancy flow rule.

Although involving rather complex mathematics, all the above calculations are based on several arbitrary, and largely unverifiable, assumptions. Lagoni (1976) for instance questions an assumption by Oda (1974) which has a significant effect on his final result. Some assumptions have, however, been examined experimentally, and Oda has

supported his work with experiments on both two dimensional rod models and also sands. He has shown for instance (Oda (1972)) that in a triaxial test the predominant direction of contact normals is approximately the principal stress direction. He also finds the more surprising result that at any stress state there are a small number of contacts near the limiting friction condition, but that the proportion of such contacts increases little with stress ratio. This finding indicates that any change in stress ratio may be expected to cause irreversible strains. Information about the orientation of the contacts near critical would be relevant to Rowe's hypothesis of a critical angle for sliding contacts.

Some aspects of soil behaviour may be inferred from the study of particle contacts using Hertzian contact theory (see for example Mindin and Deresiewicz (1953)). The approach of two contacting rounded elastic bodies may be shown under certain assumptions to be proportional to the two thirds power of the normal force between them. Thus one may expect the elastic volumetric strain to be proportional to the two thirds power of the pressure. In practice a rather lower power law is observed, probably due to the angularity of contacts and the formation of new contacts.

If a shear force is applied between two spherical elastic frictional bodies, then an annulus of the contacting area must slip if the stress ratio increases. So, since a stress ratio change will in general increase the shear stress at some contacts, then dissipative (plastic) behaviour must be expected for any change of stress ratio (note that this is without gross slippage of particles). Allowing that an elastic stress change at constant stress ratio will slightly alter particle arrangements then any stress change may be expected to cause plastic deformation.

In the remainder of this dissertation soils will be described entirely in terms of continuum mechanics. The contributions described above must be borne in mind, however, as giving some indication of the type of behaviour which a continuum theory must accommodate.

## CHAPTER 2

## THEORETICAL BACKGROUND TO PLASTICITY THEORY FOR SOILS

In this Chapter some ideas from continuum mechanics are introduced as preliminaries to the thermomechanical analysis in the next Chapter. Kinematic variables and their conjugate forces are introduced, and a discussion of internal variables is given. The theoretical restrictions conventionally imposed on plasticity theory are described, and their over-restrictive nature for soils is noted.

2.1 Kinematic Variables and Conjugate Forces

Plasticity theory is expressed in terms of continuum mechanics, in which the real non-homogeneous material is replaced by the idealised mathematical concept of a homogeneous continuum. It is usual in continuum mechanics to assume that the current state of a material body may be described entirely by the history of its motion and temperature. Considering an infinitesimal homogeneous element of a material, its motion may be described by a properly defined strain tensor  $\epsilon_{ij}$  (measured from some arbitrary reference state) and its history; the temperature is not of interest in this study. Corresponding to the strain tensor is a stress tensor, which must be defined so that the product of the stress with the strain rate gives the rate of work input per unit volume to the material. For a single phase material this simply reduces to:

$$L = \sigma_{ij} \dot{\epsilon}_{ij} \quad (2.1.1)$$

For a single phase material it is straightforward to show that the conventional definitions used in small strain theory of stress as force per unit area and strain as deformation per unit length satisfy Equation (2.1.1). For a two phase material such as a saturated soil the position is, however, more complex. Assuming that the region under

consideration consists of sufficient grains for the concepts of an averaged stress, strain, pore pressure and voids ratio to be meaningful, then the deformation of the soil skeleton may be described by the conventionally defined strain: additional parameters must be introduced to describe the motion of the pore fluid. The correct stresses will be the *forces* which are conjugate to the kinematic variables, i.e. those quantities which when multiplied by the rate of change of the kinematic variables give the rate of work input per unit volume. The word *force* is used here in the generalised thermodynamic sense, and not in the narrower mechanical sense (the *forces* here have the dimension of stress, not of mechanical force).

In Appendix A (Houlsby (1979)) it is shown that, under the idealisation of incompressible grains and an incompressible pore fluid, the rate of work input per unit volume to a granular material is given by:

$$L = \sigma'_{ij} \dot{\epsilon}_{ij} - u'_{,i} w_{,i} \quad (2.1.2)$$

so that the stresses conjugate to the strains are the effective stresses defined by Terzaghi (1943). The motion of the pore fluid is described by the artificial seepage velocity, and the corresponding *force* is the (negative) excess pore pressure gradient. It is suggested in Appendix A that the uncoupling of the work input into two terms as in Equation (2.1.2) is related to the principle of effective stress. This idea is explored in greater detail in Section 3.5, but the above result is first extended to a more general case.

The idealisations under which Equation (2.1.2) was derived are most appropriate for a saturated soil. A better approximation is achieved if the pore fluid is regarded as compressible. In this case an additional kinematic parameter, the average volumetric strain in the pore fluid  $v^{(w)}$ , must be included. Using the definitions of Appendix A the compatibility condition is now written:

$$\int_A (nf_j + (1-n)v_j)v_j dA + \int_V n\dot{v}^{(w)} dV = 0 \quad (2.1.3)$$

in which the first integral is the outflow of material from the element and the second is the new term giving the compression of the pore fluid.

This equation may be rewritten (cf. Equation (8) of Appendix A):

$$w_{j,j} + v_{j,j} + n\dot{v}^{(w)} = 0 \quad (2.1.4)$$

The analysis then proceeds exactly as in Appendix A, except that on substitution of the compatibility condition into the power input expression the result is:

$$L = -u'_{,i}w_i - \sigma_{ij}v_{i,j} + uv_{j,j} + nu\dot{v}^{(w)} - \sigma_{ij,j}v_i + \rho g_i v_i \quad (2.1.5)$$

simplification then results in the final power input per unit volume as:

$$L = \sigma'_{ij}\dot{\epsilon}_{ij} - u'_{,i}w_i + nu\dot{v}^{(w)} \quad (2.1.6)$$

which shows that the *force* corresponding to the new kinematic variable is the quantity  $nu$ , the total pore pressure scaled by the porosity. The extreme case in which the pore fluid is highly compressible, e.g. as in the case of a dry soil, may now be considered. In this case the excess pore pressure gradient will usually be small and the second term in Equation (2.1.6) is not important. The magnitude of the total pore pressure is, however, not necessarily small; for instance the atmospheric pressure in a dry soil is often of comparable magnitude to the effective stress. The force corresponding to the skeleton strain is in each case the Terzaghi effective stress.

Although it is the conventional effective stress which corresponds to the skeleton strain for both a dry and a saturated soil, no analysis has been made of the unsaturated three phase material. Bishop (1959) suggests a definition for effective stress for an unsaturated material, depending on the different pore water and air pressures, which is equivalent to:

$$\sigma'_{ij} = \sigma_{ij} - [u^{(a)} + \chi(u^{(w)} - u^{(a)})] \delta_{ij} \quad (2.1.7)$$

where the parameter  $\chi$  depends on the porosity and must be determined experimentally. The difference between the pore water and pore air pressures can only arise as a result of surface tensions between the two fluid phases. When surface tensions are accounted for the analysis of Appendix A is considerably complicated, and it has not been established whether a definition of the form used by Bishop may be used to give the appropriate *effective stress* which is conjugate to the skeleton strain.

## 2.2 The Use of Internal Variables in Plasticity Theory

In the preceding Section it was stated that the state of a material could be described by the history of its motion. The forces on the body (which in the case of a continuum are the stresses) are regarded as the response to changes in the state of the material. In general the response to any particular change in state will depend not only on the current state, but on the whole history of the material. Thus the stress will depend not only on the current strain but on the strain history as well: the stress is said to be a *functional* of the history of strain, rather than a *function* of strain.

An alternative to the *functional* approach is the use of "internal variables". The internal variables are not directly observable quantities, but are convenient fictions which in some way summarise the history of the material. A simple example of an internal variable is the preconsolidation pressure for a clay. The whole of the previous consolidation history is summed up in a single previous maximum consolidation pressure, and the behaviour of a soil element depends both on its current stress and on the preconsolidation pressure.

Another useful form of an internal variable is the plastic strain, and in the following Chapters internal parameters will all be kinematic (strain like) parameters. In the simple example shown in Figure 2.1(a)

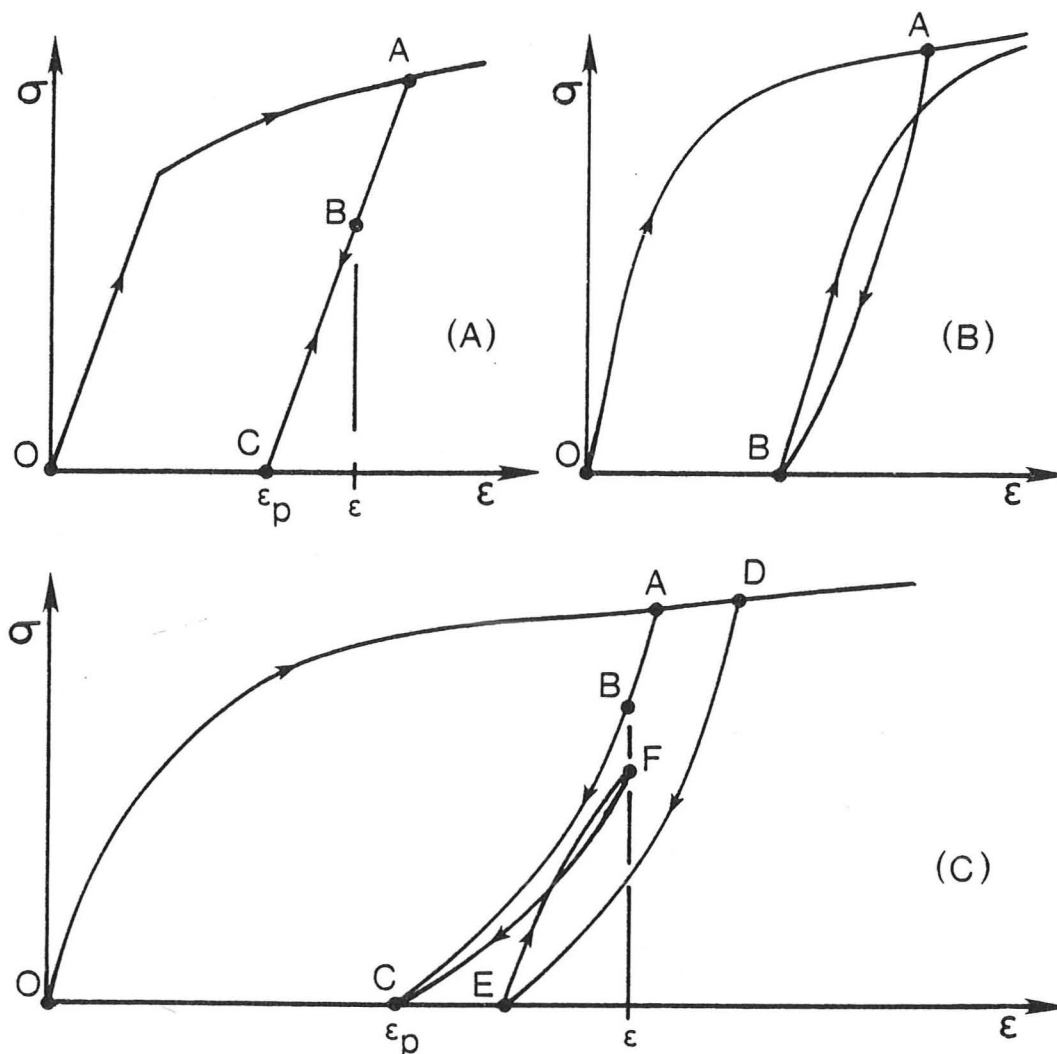


Figure 2.1 Unloading-reloading curves and internal variables

of an elastic-plastic material with non-linear work hardening the strain  $\epsilon$  and the plastic strain  $\epsilon_p$  at the point  $B$  are sufficient to determine both the stress and the response to all subsequent changes in strain. The strain alone would not be sufficient.

A real material will more probably behave as shown in Figure 2.1(b), showing hysteresis on unloading-reloading curves. In this case a single plastic strain is inadequate for the complete description of the material. Consider in Figure 2.1(c) samples of a hypothetical material loaded along  $OABC$  and  $OADEF C$  ( $D$  has been chosen so that both samples finally unload to  $C$ ). At  $B$  and  $F$  both are at the same strain and plastic strain (since both would end at  $C$  on unloading). The samples are, however,

at different stresses, so a single internal variable is insufficient to describe the material.

Although models using a single internal variable may describe some behaviour of the sort shown in Figure 2.1(b), this is only by requiring the hysteresis curves to take certain restricted forms. If a single internal variable is used the level of complexity of behaviour which can be described is essentially that shown in Figure 2.1(a). For each additional variable a further level of complexity may be added. In order to describe very complex loading histories an infinite number may be necessary in theory (with this leading back to the approach using *functionals*) but for all practical purposes a small number is adequate. Figure 2.1(a) reproduces many of the features of behaviour of a typical soil (see Figure 1.1(e) and (f)) and a single plastic strain tensor will allow this character of response to be described.

In the following Chapters attention will be restricted entirely to materials with a limited number of internal variables, resulting in distinct yield loci and elastic regions. The study does not include behaviour in which continuous curvature of unloading-reloading curves, and the consequent effects of hysteresis and accumulation of irreversible strains over many cycles are important. The models studied are for a small number of unload-reload cycles and not for the special behaviour after many (e.g. several thousand) cycles.

### 2.3 Theoretical Restrictions Imposed on Plasticity Theory

Elastic-plastic theories for the behaviour of soils may either be purely empirical, based on the curve fitting of tests on soils (e.g. the non-linear elastic theory of Duncan and Chang (1970)) or may be based on some more fundamental postulates which seek to explain the behaviour of the soil as well as to model it (e.g. the Cam-Clay flow rule, Schofield and Wroth (1968)). The two approaches are often combined,

and the theory of elastic-plastic materials is able to accommodate an almost limitless variety of models. Questions must arise, however, as to whether a model is internally consistent or whether additional limitations must be imposed on plasticity theory.

Certain self-evident conditions will not be dealt with in detail here. A model must for instance be complete and consistent in that it should determine a response for any specified stress or strain path; models properly formulated in terms of continuum mechanics usually satisfy this criterion. A second condition that is usually imposed is that of continuity: that infinitesimally differing applied paths result in infinitesimally differing responses. (This is not a fundamental law, but a condition imposed on the grounds of an intuitive approach to how materials are expected to behave.) The formulation of plasticity theory by Hill (1950) automatically satisfies continuity, but more elaborate models must be checked for this condition.

The laws of thermodynamics also impose certain limitations on the ways in which continuum theories may be expressed. The simplest example is that of elasticity; if a "strain energy function" does not exist, i.e. the stresses cannot be obtained by the differentiation of a potential function (Equation 1.3.2), then it is possible to extract energy continuously from the material over many cycles and the first law of thermodynamics is violated. Various attempts have been made to apply thermodynamics to limit the possible forms of plastic behaviour, with Drucker's stability postulate (Drucker (1951)) being perhaps the best known limitation of this type.

Drucker's postulate is not a statement of the second law of thermodynamics, although the two appear to be superficially similar; it is therefore regarded as a "quasi-thermodynamic" classification of materials. The postulate has been stated in a variety of equivalent ways, but represents the idea that if a material is in a given state of

stress, and an external agency applies additional stresses, then "The work done by the external agency on the displacements it produces must be positive or zero" (Drucker (1959)). If the external agency applies stresses  $\delta\sigma_{ij}$ , resulting in additional strains  $\delta\varepsilon_{ij}$  then the postulate is that:

$$\delta\sigma_{ij}\delta\varepsilon_{ij} \geq 0 \quad (2.3.1)$$

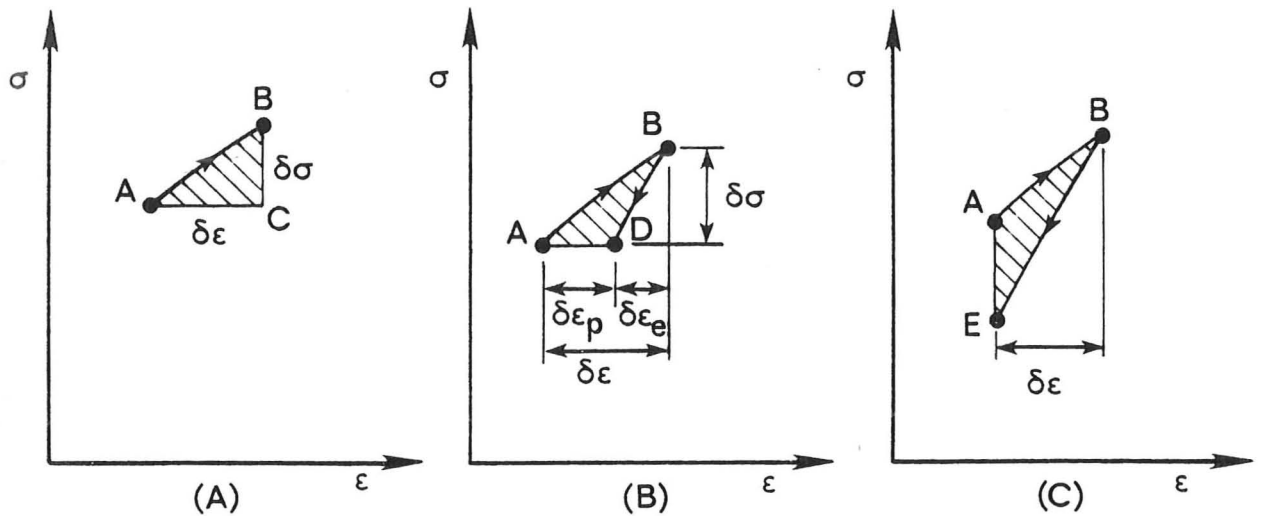


Figure 2.2 Stress and strain cycles for the postulates of Drucker and Il'iushin

In the one-dimensional case shown in Figure 2.2(a) the postulate states that the area ABC must be positive; strain softening behaviour is therefore excluded. If the external agency then removes the applied  $\delta\sigma_{ij}$ , and the remaining strains are  $\delta\varepsilon_{ij}^{(p)}$ , it also follows that:

$$\delta\sigma_{ij}\delta\varepsilon_{ij}^{(p)} \geq 0 \quad (2.3.2)$$

i.e. in the one dimensional case in Figure 2.2(b) the area ABD must be positive. From this fact it can be shown that if the elastic properties do not depend on the plastic deformation then (making also the conventional assumptions of plasticity theory) the yield locus is convex and identical to the plastic potential for plastic strain. If the elastic behaviour does depend on the plastic deformation (elastic-plastic coupling) these results are only slightly modified. In this

case careful attention must be paid to the precise definition of plastic strain.

An alternative restriction is the "Postulate of Elasticity", of Il'iushin (1961) which states that the work done during a cycle of strain must be positive or zero. In the one dimensional case shown in Figure 2.2(c) the area ABE must be positive. This hypothesis is again superficially similar to a statement of the second law of thermodynamics, and has frequently been misinterpreted as such. It is less restrictive than Drucker's postulate, and allows for instance strain softening behaviour. In the absence of elastic-plastic coupling the convexity of the yield surface and normality of the plastic strain increment to the yield surface also follow from this postulate.

#### 2.4 The Need for a Less Restrictive Approach

The main results of either Drucker's or Il'iushin's postulates are convexity of the yield locus and normality of the plastic strain increment. Although there is no strong experimental evidence against convexity, there is a major deviation from the normality condition for some materials, notably coarse granular materials (e.g. Poorooshasb et al. (1966)). The obvious microscopic non-homogeneity of such materials may seem to make a continuum approach to their modelling invalid, but all materials are non-homogeneous when viewed on a sufficiently small scale. It should be possible to produce a continuum theory which adequately models granular materials when a sufficiently large region is considered for a continuum approach to be applicable.

The criteria of both Drucker and Il'iushin are over-restrictive; they are thought to be sufficient conditions to ensure that the second law of thermodynamics is obeyed, but are not necessary. A strain cycle need not, for instance, be a cycle in the thermodynamic sense, but may involve changes to the internal structure of the material. For certain

changes it may be possible for the material to release energy. The usefulness of the postulates lies not, however, in the mere compliance with thermodynamics, but in some important corollaries.

From Drucker's postulate it is possible to prove the uniqueness of incremental response for the stress and strain rates of an elastic-plastic material under given changes in applied boundary forces and displacements (Drucker (1956)). The importance of a single solution existing for a given problem is obvious. Other corollaries are the upper and lower bound theorems which allow the exact solution for the ultimate loads on perfectly plastic materials to be closely bracketed by simple methods. If a non-associated flow rule is allowed the theorems are so much weakened as to render them virtually useless in many cases (Drucker (1954)).

The major motivation in seeking a new approach to theoretical restrictions on plasticity theory is to establish a formulation which satisfies the laws of thermodynamics, but also allows the non-associated flow observed in soils. In the conventional approach plasticity theory is developed from a series of assumptions (e.g. the existence of a yield locus) and the limitations discussed above then applied to the theory. In the following Chapter an alternative approach is made in that a formulation is derived starting from the laws of thermodynamics and therefore including them as an integral part. In its form for rate independent materials the new formulation gives rise to theories of the elastic-plastic type. The new approach can, however, accommodate non-associated flow.

By founding the formulation on a few simple assumptions it is hoped that it will lead to theorems such as that of uniqueness of incremental response and modified forms of the bound theorems. As first steps in this direction some corollaries of the formulation are presented, e.g. the existence of a yield locus.

## CHAPTER 3

## A THERMOMECHANICAL FORMULATION OF PLASTICITY THEORY

In this Chapter a new formalism for the expression of plasticity theories is given; using a method of description of materials based on thermodynamics. Some implications for rate independent materials are studied; and in particular the existence of a yield locus is examined. Specific examples of some elastic-plastic models are given, and the inclusion of the effects of a pore fluid are discussed with reference to the principle of effective stress.

### 3.1 Introduction to Thermomechanical Methods

The method of analysis used in this Chapter is based on a simple extension of classical equilibrium thermodynamics as a field theory to processes which need not be infinitesimally slow, i.e. may be in non-equilibrium. The approach used is that of the so-called "generalised" thermodynamics. Most of the following derivation is uncontroversial, and a discussion of the rigour of the thermodynamic methods would be inappropriate here. The method used employs, however, an extremum principle (the *orthogonality condition*) the validity of which has been questioned. A defence of the principle will not be given; but it may be noted that since it represents a stronger statement than the second law of thermodynamics it may in any case be regarded as a classification of a restricted set of materials rather than a law of nature. Those materials which comply with the orthogonality condition will be thermodynamically admissible.

The first assumption of the thermomechanical method is that the state of a material (in a thermodynamic sense) may be entirely described by a suitable number of kinematic parameters and temperature. Although

there is a view that an infinite number of parameters may be needed to describe even a single homogeneous element, the view is taken here that for all practical purposes a limited number may be used (as discussed in the preceding Chapter). The kinematic parameters are divided into two sets:

- (a) The strains  $\epsilon_{ij}$  .
- (b) Internal parameters  $\alpha_{ij}^{(n)}$  .

The internal parameters need not take the form of symmetric second order tensors, but by comparison with the strains it is convenient to consider the cases where they do take this form. In conventional elastic-plastic theories the internal parameters are strain-like quantities, for instance the "plastic strain"  $\epsilon_{ij}^{(p)}$  . The internal parameters may be thought of as representing a record of the history of deformation of the material, and some examples of this role of the internal parameters are given later.

Note that the stresses are not included as parameters describing the state of the material, but are regarded as a response to changes in strain; this may be contrasted with the notion that stress is an independently observable property whereas strain is merely a quantity measured from an arbitrary reference state. The method has certain advantages, however, in that it avoids any ambiguity in the consideration of both hardening and softening behaviour (both of which are of engineering importance). Types of behaviour in which certain strain paths are not possible (either locking or sub-critical softening) are less easy to accommodate, but seem of little practical importance. It is also found that although strain is measured from some arbitrary state the mechanical behaviour of a material may still be expressed in such a way that it is independent of the reference state; the problem

that strain is not an independently observable property may therefore be resolved.

### 3.2 Ziegler's Thermomechanical Formulation

The restrictions of thermomechanics on material behaviour are now developed. The analysis follows that of Ziegler (1977) and is at first developed for a system and then later specialised for a continuum. It is hypothesised that a state of a system may be entirely described by a set of independent kinematic parameters  $a_k$  and the temperature  $\theta$ . Forces  $A_k$  corresponding to the kinematic parameters are defined such that the work done on the system is given by:

$$dW = A_k da_k \quad (3.2.1)$$

If  $dQ$  is the heat supply then the First Law of Thermodynamics states that there is a property (a function of the state) called the internal energy ( $U = U(a_k, \theta)$ ) such that:

$$dU = dW + dQ \quad (3.2.2)$$

$$dU = A_k da_k + dQ \quad (3.2.3)$$

The Second Law of Thermodynamics states that there is a property called entropy ( $S = S(a_k, \theta)$ ) such that:

$$\theta dS \geq dQ \quad (3.2.4)$$

where the equality holds only for reversible processes. If one defines:

$$dS = (dS)^{(i)} + (dS)^{(r)} \quad (3.2.5)$$

$$\theta (dS)^{(r)} = dQ \quad (3.2.6)$$

where  $(dS)^{(i)}$  and  $(dS)^{(r)}$  are the "irreversible" and "reversible"

changes in entropy, then the two laws may be rewritten as:

$$dW = dU - \theta dS + \theta (dS)^{(i)} \quad (3.2.7)$$

$$(dS)^{(i)} \geq 0 \quad (3.2.8)$$

Expanding  $dU - \theta dS$  in terms of partial derivatives with respect to  $\theta$  and  $a_k$  and considering a process of pure heating only (i.e.  $dW = da_k = 0$ ) it follows that for the second equation to be valid for both heating and cooling:

$$\frac{\partial U}{\partial \theta} - \theta \frac{\partial S}{\partial \theta} = 0 \quad (3.2.9)$$

It follows that:

$$A_k da_k = \left( \frac{\partial U}{\partial a_k} - \theta \frac{\partial S}{\partial a_k} \right) da_k + \theta (dS)^{(i)} \quad (3.2.10)$$

The expression  $\theta (dS)^{(i)}$  therefore has the form of a work term and, if it is assumed that the irreversible entropy changes depend linearly on the changes of state, may be written as  $A_k^{(d)} da_k$  where  $A_k^{(d)}$  are the dissipative forces defined by:

$$A_k^{(d)} = A_k - \frac{\partial U}{\partial a_k} + \theta \frac{\partial S}{\partial a_k} \quad (3.2.11)$$

Similarly  $\left( \frac{\partial U}{\partial a_k} - \theta \frac{\partial S}{\partial a_k} \right)$  may be termed the quasiconservative forces and written as  $A_k^{(q)}$ , thus

$$A_k = A_k^{(d)} + A_k^{(q)} \quad (3.2.12)$$

By defining another property, the free energy ( $\Psi$ ) as  $(U - \theta S)$  one may readily show that:

$$A_k^{(q)} = \frac{\partial \Psi}{\partial a_k} \quad (3.2.13)$$

Rewriting in terms of rates rather than infinitesimals one can write:

$$\begin{aligned}\dot{W} &= A_k \dot{a}_k = A_k^{(q)} \dot{a}_k + A_k^{(d)} \dot{a}_k \\ &= A_k^{(q)} \dot{a}_k + \theta \dot{S}^{(i)} \\ &= A_k^{(q)} \dot{a}_k + \Phi\end{aligned}\quad (3.2.14)$$

where  $\Phi = A_k^{(d)} \dot{a}_k = \theta \dot{S}^{(i)} \geq 0$  is termed the dissipation function and may depend on both state and rate of change of state, i.e.

$$\Phi = \Phi(a_k, \theta, \dot{a}_k, \dot{\theta}) \quad (3.2.15)$$

Consider now the problem of determining the dissipative forces  $A_k^{(d)}$  for a given single set of velocities  $\dot{a}_k$ . The definition of the dissipation function gives one equation:

$$\Phi = A_k^{(d)} \dot{a}_k \quad (3.2.16)$$

which will determine the absolute magnitudes of  $A_k^{(d)}$  for given  $\dot{a}_k$  provided the relative magnitudes of the various components of  $A_k^{(d)}$  are known: the problem therefore resolves into that of establishing the relative magnitudes of  $A_k^{(d)}$ , i.e. the direction of the  $A_k^{(d)}$  vector. Assuming then that  $\Phi$  is an analytic function of  $\dot{a}_k$  then so will be  $A_k^{(d)}$ ; it may therefore be assumed that  $A_k^{(d)}$  is a function of  $\Phi$  and its derivatives with respect to  $\dot{a}_k$ ; however, the only one of these which is a vector is  $\frac{\partial \Phi}{\partial \dot{a}_k}$ , and so  $A_k^{(d)}$  (a vector) must be in the direction of this vector since this is the only term which can determine the direction of  $A_k^{(d)}$ , i.e.

$$A_k^{(d)} = v \frac{\partial \Phi}{\partial \dot{a}_k} \quad (3.2.17)$$

where  $v$  is a multiplier which may be determined by:

$$v = \Phi / \left( \frac{\partial \Phi}{\partial \dot{a}_k} \dot{a}_k \right) \quad (3.2.18)$$

(The above argument differs only in detail from Ziegler's. For a rigorous mathematical proof of the above result the fact that general (rather than Cartesian) tensors may be used must be included; contracted products of higher order differentials cannot then take the form of a vector of appropriate dimensions.)

The function  $\Phi$  may be represented in velocity ( $\dot{a}_k$ ) space by surfaces where  $\Phi = \Phi_0 = \text{constant}$ . It can be shown that the above equations represent a condition of orthogonality of the dissipative force vector to the  $\Phi = \Phi_0$  surfaces (see Figure 3.1). This condition (and its corollaries) can be used to show that such surfaces must be

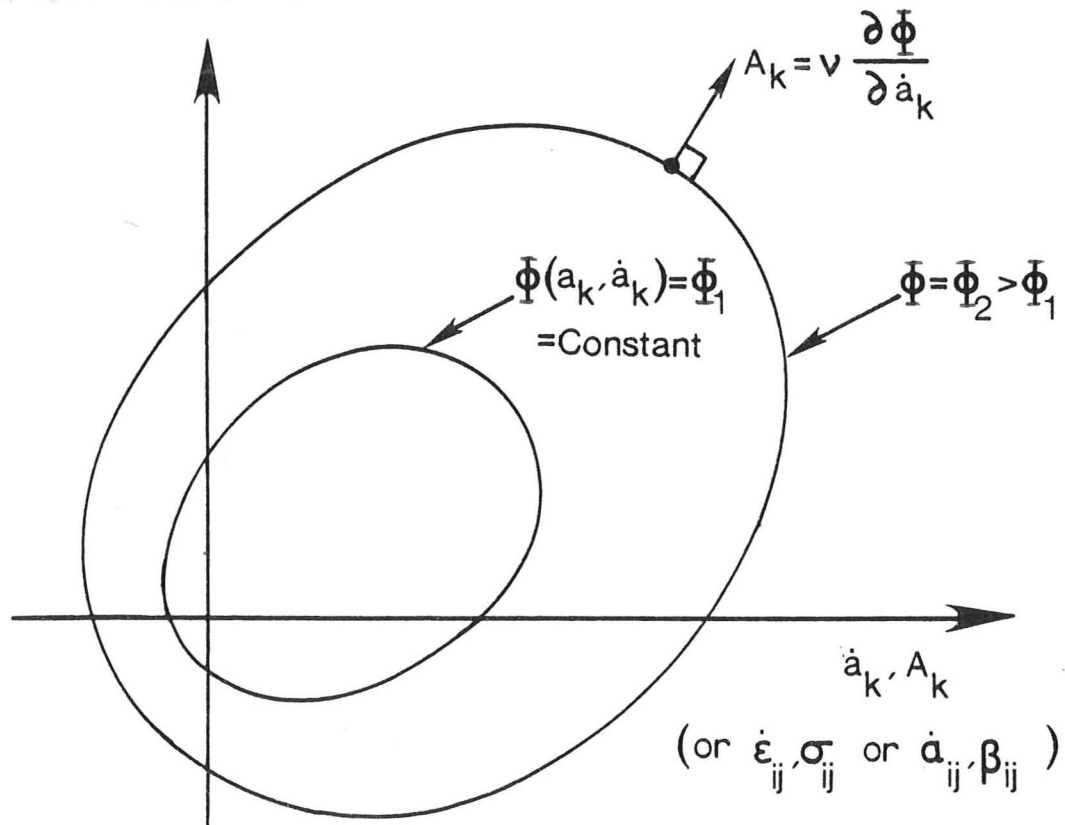


Figure 3.1 Orthogonality of the dissipative force to  $\Phi = \text{constant}$  surface in velocity space

convex and nested about the origin, and that  $\Phi$  must increase at least linearly with distance from the origin in velocity space.

The orthogonality condition has been proven by Ziegler for the case of a single velocity tensor (under certain conditions not examined in detail here). The result cannot be proven when the dissipation is a function of several tensors, except for certain special cases. If the dissipation function is a homogeneous function of any given degree in the velocities of several tensors then the condition may be proven; in particular for the case where  $\Phi$  is a homogeneous first order function of the velocities the multiplier  $\nu$  is equal to unity and:

$$A_k^{(d)} = \frac{\partial \Phi}{\partial \dot{a}_k} \quad (3.2.19)$$

which represents the rate independent case since  $A_k^{(d)}$  is of zeroth order in velocity. This is also the limiting case where  $\Phi$  increases linearly with velocity.

Although the orthogonality condition remains unproven for the more complex cases, it is suggested by Ziegler as a fundamental principle of maximum dissipation rate.

Having established the thermomechanical basis of the orthogonality principle, this may now be applied to continuum mechanics. The strains  $\epsilon_{ij}$  will replace the kinematic parameters  $a_k$ , along with the internal variables  $\alpha_{ij}^{(n)}$  (for simplicity only a single internal variable tensor will be considered and the superscript (n) dropped). The thermodynamic forces corresponding to the strains are the stresses  $\sigma_{ij}$ , and those corresponding to the internal parameters will be termed internal forces  $\beta_{ij}$ . The specific values of the free energy and the dissipation function will now be used:

convex and nested about the origin, and that  $\Phi$  must increase at least linearly with distance from the origin in velocity space.

The orthogonality condition has been proven by Ziegler for the case of a single velocity tensor (under certain conditions not examined in detail here). The result cannot be proven when the dissipation is a function of several tensors, except for certain special cases. If the dissipation function is a homogeneous function of any given degree in the velocities of several tensors then the condition may be proven; in particular for the case where  $\Phi$  is a homogeneous first order function of the velocities the multiplier  $\nu$  is equal to unity and:

$$A_k^{(d)} = \frac{\partial \Phi}{\partial \dot{a}_k} \quad (3.2.19)$$

which represents the rate independent case since  $A_k^{(d)}$  is of zeroth order in velocity. This is also the limiting case where  $\Phi$  increases linearly with velocity.

Although the orthogonality condition remains unproven for the more complex cases, it is suggested by Ziegler as a fundamental principle of maximum dissipation rate.

Having established the thermomechanical basis of the orthogonality principle, this may now be applied to continuum mechanics. The strains  $\epsilon_{ij}$  will replace the kinematic parameters  $a_k$ , along with the internal variables  $\alpha_{ij}^{(n)}$  (for simplicity only a single internal variable tensor will be considered and the superscript (n) dropped). The thermodynamic forces corresponding to the strains are the stresses  $\sigma_{ij}$ , and those corresponding to the internal parameters will be termed internal forces  $\beta_{ij}$ . The specific values of the free energy and the dissipation function will now be used:

$$\psi = \psi(\epsilon_{ij}, \alpha_{ij}) \quad (3.2.20)$$

$$\phi = \phi(\epsilon_{ij}, \alpha_{ij}, \dot{\epsilon}_{ij}, \dot{\alpha}_{ij}) \quad (3.2.21)$$

the latter being of the first order in velocities since only rate independent behaviour is considered here. The forces are now given by:

$$\sigma_{ij} = \sigma_{ij}^{(q)} + \sigma_{ij}^{(d)}, \quad \sigma_{ij}^{(q)} = \rho \frac{\partial \psi}{\partial \epsilon_{ij}}, \quad \sigma_{ij}^{(d)} = \rho \frac{\partial \phi}{\partial \dot{\epsilon}_{ij}} \quad (3.2.22)$$

$$\beta_{ij} = \beta_{ij}^{(q)} + \beta_{ij}^{(d)}, \quad \beta_{ij}^{(q)} = \rho \frac{\partial \psi}{\partial \alpha_{ij}}, \quad \beta_{ij}^{(d)} = \rho \frac{\partial \phi}{\partial \dot{\alpha}_{ij}} \quad (3.2.23)$$

where  $\rho$  is the density. Noting then that

$$dW = \sigma_{ij} d\epsilon_{ij} + \beta_{ij} d\alpha_{ij} = \sigma_{ij} d\epsilon_{ij} \quad (3.2.24)$$

which must hold for all  $d\alpha_{ij}$ , it follows that:

$$\beta_{ij} = \beta_{ij}^{(q)} + \beta_{ij}^{(d)} = 0 \quad (3.2.25)$$

The problem of deriving material response from the governing functions is now formally solved in that if the functions  $\phi$  and  $\psi$  are specified it is possible to derive the values of the stresses for any given values of the internal parameters, strains and strain rates. The variation of the internal parameters is also determined. The use of this method in which the behaviour of a dissipative material is derived from potentials is an extension of the derivation of the behaviour of elastic materials from an elastic potential. The equivalence between the two methods is illustrated in Table 3.1.

$$\psi = \psi(\epsilon_{ij}, \alpha_{ij}) \quad (3.2.20)$$

$$\phi = \phi(\epsilon_{ij}, \alpha_{ij}, \dot{\epsilon}_{ij}, \dot{\alpha}_{ij}) \quad (3.2.21)$$

the latter being of the first order in velocities since only rate independent behaviour is considered here. The forces are now given by:

$$\sigma_{ij} = \sigma_{ij}^{(q)} + \sigma_{ij}^{(d)}, \quad \sigma_{ij}^{(q)} = \rho \frac{\partial \psi}{\partial \epsilon_{ij}}, \quad \sigma_{ij}^{(d)} = \rho \frac{\partial \phi}{\partial \dot{\epsilon}_{ij}} \quad (3.2.22)$$

$$\beta_{ij} = \beta_{ij}^{(q)} + \beta_{ij}^{(d)}, \quad \beta_{ij}^{(q)} = \rho \frac{\partial \psi}{\partial \alpha_{ij}}, \quad \beta_{ij}^{(d)} = \rho \frac{\partial \phi}{\partial \dot{\alpha}_{ij}} \quad (3.2.23)$$

where  $\rho$  is the density. Noting then that

$$dW = \sigma_{ij} d\epsilon_{ij} + \beta_{ij} d\alpha_{ij} = \sigma_{ij} d\epsilon_{ij} \quad (3.2.24)$$

which must hold for all  $d\alpha_{ij}$ , it follows that:

$$\beta_{ij} = \beta_{ij}^{(q)} + \beta_{ij}^{(d)} = 0 \quad (3.2.25)$$

The problem of deriving material response from the governing functions is now formally solved in that if the functions  $\phi$  and  $\psi$  are specified it is possible to derive the values of the stresses for any given values of the internal parameters, strains and strain rates. The variation of the internal parameters is also determined. The use of this method in which the behaviour of a dissipative material is derived from potentials is an extension of the derivation of the behaviour of elastic materials from an elastic potential. The equivalence between the two methods is illustrated in Table 3.1.

	Conservative (Elastic)	Dissipative (Plastic)
Kinematic variables	$\epsilon_{ij}$	$\epsilon_{ij} \quad \alpha_{ij}^{(n)}$
Functions specified	$\psi(\epsilon_{ij})$	$\psi(\epsilon_{ij}, \alpha_{ij})$ $\phi(\epsilon_{ij}, \alpha_{ij}^{(n)}, \dot{\epsilon}_{ij}, \dot{\alpha}_{ij}^{(n)})$ (1 <sup>st</sup> order in $\dot{\epsilon}_{ij}, \dot{\alpha}_{ij}^{(n)}$ )
Response	$\sigma_{ij} = \rho \frac{\partial \psi}{\partial \epsilon_{ij}}$	$\sigma_{ij} = \rho \frac{\partial \psi}{\partial \epsilon_{ij}} + \rho \frac{\partial \phi}{\partial \dot{\epsilon}_{ij}}$ $0 = \rho \frac{\partial \psi}{\partial \alpha_{ij}^{(n)}} + \rho \frac{\partial \phi}{\partial \dot{\alpha}_{ij}^{(n)}}$

Table 3.1 Comparison of thermomechanical formulation for conservative and dissipative rate independent materials

### 3.3 Some Implications of Ziegler's Formulation for Conventional Plasticity Theory

Conventional plasticity theory is founded on the hypothesis of a yield locus, enclosing a purely elastic region, and of a flow rule. Neither of these is adopted as a fundamental hypothesis in Ziegler's formulation, but both arise as consequences in the case of rate independent materials. In the following analysis the existence of a yield locus in stress space for a dissipative rate independent material with a finite number of internal parameters is proven. The flow rule is often strongly linked to the yield locus through the normality principle: although Ziegler (1977) states that the normality principle follows directly from the orthogonality condition, this is found to be true only for "cohesive" materials in which the dissipation does not depend on the strain state.

A proof is first made of the existence of a yield locus and of a limited normality criterion for a simple rigid-perfectly plastic

material. It is convenient in this case to describe the stresses by a series of six quantities  $\sigma_i$ , and the corresponding strain rates by  $\dot{\epsilon}_i$  such that:

$$L = \sigma_i \dot{\epsilon}_i \quad i = 1, 6 \quad (3.3.1)$$

where  $L$  is the rate of work input per unit volume and the summation convention over a repeated index is used. Consider now the case where some of the strains may only be zero:

$$\dot{\epsilon}_j = 0 \quad j = p, 6 \quad (3.3.2)$$

where the ordering of the stresses and strains has been chosen such that Equation (3.3.1) applies. It follows that the corresponding stresses  $\sigma_j$  are reactions and may be arbitrarily specified. The dissipation may be a function of the remaining strain rates  $\dot{\epsilon}_k$  ( $k = 1, p - 1$ ) and of the arbitrary  $\sigma_j$ :

$$D = D(\dot{\epsilon}_k, \sigma_j) \quad (3.3.3)$$

where  $D$  is the dissipation per unit volume and is a first order function of the strain rates. (It is convenient to use the quantity  $D = \rho \phi$  here.) The case of a simple rigid-plastic material in which the free energy is constant is considered, so that the stresses  $\sigma_k$  are given solely by the orthogonality principle by:

$$\sigma_k = \frac{\partial D}{\partial \dot{\epsilon}_k} \quad (3.3.4)$$

It follows that (subject to certain limitations on the form of  $D$ ) a partial Legendre transformation with respect to  $\dot{\epsilon}_k$  and  $\sigma_k$  may be carried out and there exists a potential  $E(\sigma_k, \sigma_j)$  given by:

$$E = \sigma_k \dot{\epsilon}_k - D \quad (3.3.5)$$

such that:

$$\dot{\epsilon}_k = \frac{\partial E}{\partial \sigma_k} \quad (3.3.6)$$

and further that:

$$\frac{\partial E}{\partial \sigma_j} + \frac{\partial D}{\partial \sigma_j} = 0 \quad (3.3.7)$$

Since  $D$  is first order in  $\dot{\epsilon}_k$  it follows that

$$D = \frac{\partial D}{\partial \dot{\epsilon}_k} \dot{\epsilon}_k = \sigma_k \dot{\epsilon}_k \quad (3.3.8)$$

so that  $E = 0$  and the existence of a yield locus is proven since  $E(\sigma_k, \sigma_j) = E(\sigma_i) = 0$  is a relation between the stresses which must be satisfied when straining occurs. Equation (3.3.6) represents a limited normality criterion in the subspace  $\sigma_k$ . If the stresses  $\sigma_j$  are further divided into those which do and do not appear in the function  $D$ :

$$D = D(\dot{\epsilon}_k, \sigma_\ell) \quad \ell = q, 6 \quad (3.3.9)$$

and  $\sigma_m$  ( $m = p, q-1$ ) are those stresses which are reactions but do not appear in  $D$ , it follows that also:

$$\frac{\partial E}{\partial \sigma_m} = - \frac{\partial D}{\partial \sigma_m} = 0 = \dot{\epsilon}_m \quad (3.3.10)$$

So that the normality condition holds in the extended subspace  $\sigma_n$  ( $n = 1, q-1$ ), but not in  $\sigma_\ell$  for which  $\dot{\epsilon}_\ell = 0$  and the dissipation depends on  $\sigma_\ell$  and:

$$\frac{\partial E}{\partial \sigma_\ell} = - \frac{\partial D}{\partial \sigma_\ell} \neq 0 \quad (3.3.11)$$

This result is expressed diagrammatically in Figure 3.2.

Examining now the more general case of elastic plastic materials, it is useful first to re-state the formulation for a general rate independent material with a single internal variable. The results of Section 3.2 may be concisely written:

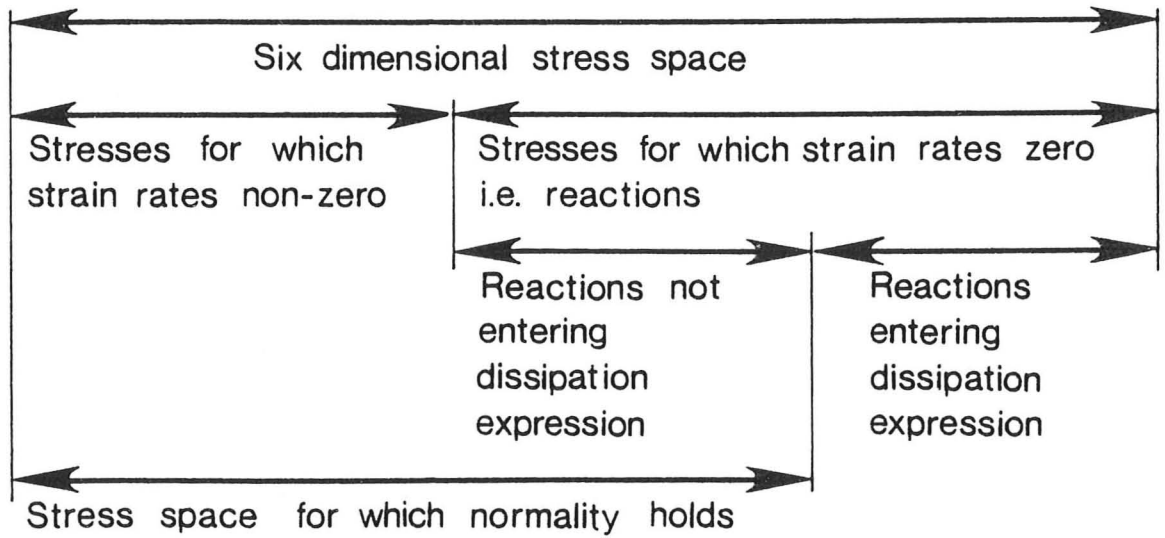


Figure 3.2 Schematic diagram showing the stress space for which the normality rule for a rigid-plastic material will apply

$$\psi = \psi(\epsilon_{ij}, \alpha_{ij}) \quad (3.3.12)$$

$$\phi = \phi(\epsilon_{ij}, \alpha_{ij}, \dot{\epsilon}_{ij}, \dot{\alpha}_{ij}) \quad (3.3.13)$$

$$\sigma_{ij} = \rho \frac{\partial \psi}{\partial \epsilon_{ij}} + \rho \frac{\partial \phi}{\partial \dot{\epsilon}_{ij}} \quad (3.3.14)$$

$$0 = \rho \frac{\partial \psi}{\partial \alpha_{ij}} + \rho \frac{\partial \phi}{\partial \dot{\alpha}_{ij}} \quad (3.3.15)$$

It is of interest to re-formulate these expressions in terms more familiar in plasticity theory in order to establish some common ground between the two approaches. It is convenient to choose the plastic strain as the internal variable and the assumption of plasticity theory is that the dissipation depends only on the plastic strain rate, thus  $\phi$  is not a function of  $\dot{\epsilon}_{ij}$ . Making the substitutions:

$$\epsilon_{ij}^{(p)} = \alpha_{ij}, \quad \epsilon_{ij}^{(e)} = \epsilon_{ij} - \alpha_{ij} \quad (3.3.16)$$

where the latter is the usual division of strain in elastic-plastic theory, one may re-write:

$$\psi = \psi^*(\epsilon_{ij}^{(e)}, \epsilon_{ij}^{(p)}) \quad (3.3.17)$$

$$\phi = \phi^*(\epsilon_{ij}^{(e)}, \epsilon_{ij}^{(p)}, \dot{\epsilon}_{ij}^{(p)}) \quad (3.3.18)$$

The stress and internal force expressions become (noting  $\partial\phi/\partial\dot{\epsilon}_{ij}^{(p)} = 0$ ):

$$\sigma_{ij} = \rho \frac{\partial\psi}{\partial\epsilon_{ij}} = \rho \frac{\partial\psi^*}{\partial\epsilon_{kl}^{(e)}} \frac{\partial\epsilon_{kl}}{\partial\epsilon_{ij}} + \rho \frac{\partial\psi^*}{\partial\epsilon_{kl}^{(p)}} \frac{\partial\epsilon_{kl}}{\partial\epsilon_{ij}} \quad (3.3.19)$$

$$0 = \rho \frac{\partial\psi}{\partial\alpha_{ij}} + \rho \frac{\partial\phi}{\partial\dot{\alpha}_{ij}} = \rho \frac{\partial\psi^*}{\partial\epsilon_{kl}^{(e)}} \frac{\partial\epsilon_{kl}}{\partial\alpha_{ij}} + \rho \frac{\partial\psi^*}{\partial\epsilon_{kl}^{(p)}} \frac{\partial\epsilon_{kl}}{\partial\alpha_{ij}} + \rho \frac{\partial\phi}{\partial\dot{\alpha}_{ij}} \quad (3.3.20)$$

Substitution of the differentials obtained from Equation (3.3.16) and noting that  $\partial\phi/\partial\dot{\alpha}_{ij} = \partial\phi^*/\partial\dot{\epsilon}_{ij}^{(p)}$  allows simplification to:

$$\sigma_{ij} = \rho \frac{\partial\psi^*}{\partial\epsilon_{ij}^{(e)}} \quad (3.3.21)$$

$$\sigma_{ij} = \rho \frac{\partial\psi^*}{\partial\epsilon_{ij}^{(p)}} + \rho \frac{\partial\phi^*}{\partial\dot{\epsilon}_{ij}^{(p)}} \quad (3.3.22)$$

The significance of these equations may be interpreted as follows. The function  $\phi^*$  is of first order in  $\dot{\epsilon}_{ij}^{(p)}$ , so that  $\partial\phi^*/\partial\dot{\epsilon}_{ij}^{(p)}$  is of zeroth order, and contains only ratios between the components of  $\dot{\epsilon}_{ij}^{(p)}$ . If all these components are zero there is no dissipation and Equation (3.3.22) becomes indeterminate: the material behaves elastically and the stress is determined by Equation (3.3.21).

If, however,  $\dot{\epsilon}_{ij}^{(p)}$  is non-zero, i.e. dissipation occurs, then Equations (3.3.21) and (3.3.22) give two separate expressions for  $\sigma_{ij}$  which will take the form  $\sigma_{ij} = \sigma_{ij}(\epsilon_{kl}^{(e)}, \epsilon_{kl}^{(p)})$  and  $\sigma_{ij} = \sigma_{ij}(\epsilon_{kl}^{(e)}, \epsilon_{kl}^{(p)}, \dot{\epsilon}_{kl}^{(p)})$  respectively. Clearly these 18 equations

allow in principle a solution for  $\dot{\epsilon}_{ij}^{(e)}$  and  $\dot{\epsilon}_{ij}^{(p)}$  if  $\dot{\sigma}_{ij}$  is specified and the current state known. The general form of the incremental solution has not been derived, but it has been empirically observed that functions of the form described above may be manipulated to give models which always involve a yield locus for plastic deformation and also result in a specific flow rule.

The precise definition of the flow rule has not been achieved, but the existence of a yield locus for the elastic-plastic model may be proven. Defining the quantity  $x_{ij} = \sigma_{ij} - \rho \frac{\partial \psi^*}{\partial \epsilon_{ij}^{(p)}}$  it follows from Equation (3.3.22) under certain restrictions on  $\phi^*$  that there exists a function  $E$  such that:

$$E = E(x_{ij}, \epsilon_{ij}^{(e)}, \epsilon_{ij}^{(p)}) = x_{ij} \dot{\epsilon}_{ij}^{(p)} - \rho \phi \quad (3.3.23)$$

And further that  $E = 0$  since  $\phi$  is of first order in  $\dot{\epsilon}_{ij}^{(p)}$ . Noting that  $x_{ij}$  is a function of  $\epsilon_{ij}^{(e)}$  and  $\epsilon_{ij}^{(p)}$  only, and that in principle it is possible from Equation (3.3.21) to express  $\epsilon_{ij}^{(e)}$  as a function of  $\sigma_{ij}$  and  $\epsilon_{ij}^{(p)}$  it is therefore possible to express:

$$E = E^*(\sigma_{ij}, \epsilon_{ij}^{(p)}) = 0 \quad (3.3.24)$$

which is the equation of a yield locus in stress space, dependent on the state of plastic deformation. It has therefore been proven that the forms of function in Equations (3.3.17) and (3.3.18) will give rise to a yield locus, although a general scheme for determining it is not presented.

Although the above form for plasticity theories is equally valid, the original formulation of Equations (3.3.12) and (3.3.13) will be preferred in the following Chapters. In the next Section some specific examples of elastic-plastic theories derived from this formulation are given.

### 3.4 Derivation of Specific Elastic-Plastic Models from Thermomechanics

The use of a free energy function to derive elastic behaviour is well established (see for example Love (1927)) and an isotropic elastic material can for instance be described by:

$$\rho\psi = \frac{\lambda}{2} \epsilon_{ii} \epsilon_{jj} + \mu \epsilon_{ij} \epsilon_{ij} \quad (3.4.1)$$

$$\rho\phi = 0 \quad (3.4.2)$$

where  $\lambda$  and  $\mu$  are Lamé's constants. Carrying out the differentiation gives:

$$\sigma_{ij} = \lambda \epsilon_{kk} \delta_{ij} + 2\mu \epsilon_{ij} \quad (3.4.3)$$

Ziegler (1977) studies the rigid-cohesive and elastic-cohesive materials, but rather than following the strict formalism outlined in Section 3.2 he presents the familiar results of additive elastic and plastic strains, a yield locus and an associated flow rule. Although he links these ideas with those outlined above he does not give a formal derivation of the behaviour of an elastic-plastic material from the two functions  $\psi$  and  $\phi$ .

The appropriate functions for an isotropic elastic-perfectly plastic material with a von Mises yield surface and associated flow rule are:

$$\rho\psi = \left(\frac{\lambda}{2} + \frac{\mu}{3}\right) \epsilon_{ii} \epsilon_{jj} + \mu (\epsilon'_{ij} - \epsilon'_{ij}{}^{(p)}) (\epsilon'_{ij} - \epsilon'_{ij}{}^{(p)}) \quad (3.4.4)$$

$$\rho\phi = \sqrt{2} c (\dot{\epsilon}'_{ij}{}^{(p)} \dot{\epsilon}'_{ij}{}^{(p)})^{\frac{1}{2}} \quad (3.4.5)$$

where  $\epsilon'_{ij}{}^{(p)}$  is an internal variable which will be seen to play the role of a conventional plastic strain and a dash notation indicates the deviator of a tensor. Differentiating as in Equations (3.3.14) and (3.3.15) gives:

$$\sigma_{ij} = \left(\lambda + \frac{2\mu}{3}\right) \epsilon_{kk} \delta_{ij} + 2\mu(\epsilon'_{ij} - \epsilon'^{(p)}_{ij}) \quad (3.4.6)$$

$$0 = -2\mu(\epsilon'_{ij} - \epsilon'^{(p)}_{ij}) + \sqrt{2} c \dot{\epsilon}'_{ij} / (\dot{\epsilon}'_{kl} \dot{\epsilon}'_{kl})^{\frac{1}{2}} \quad (3.4.7)$$

The first of these equations yields the value of the mean stress:

$$\frac{\sigma_{kk}}{3} = \left(\lambda + \frac{2\mu}{3}\right) \epsilon_{kk} \quad (3.4.8)$$

and combination of the equations then gives:

$$\sigma'_{ij} = \sqrt{2} c \dot{\epsilon}'_{ij} / (\dot{\epsilon}'_{kl} \dot{\epsilon}'_{kl})^{\frac{1}{2}} \quad (3.4.9)$$

which confirms directly the flow rule in which the plastic strain components are proportional to the components of the stress deviator. Equation (3.4.9) also gives the relationship between the stresses:

$$\sigma'_{ij} \sigma'_{ij} = 2c^2 \quad (3.4.10)$$

which is the von Mises yield condition which must be satisfied by the stresses if  $\dot{\epsilon}'_{ij}^{(p)}$  is non-zero. Equation (3.4.9) also confirms the fact that  $\dot{\epsilon}'_{kk}^{(p)} = 0$ , i.e. there is no plastic volumetric strain in this model.

If  $\dot{\epsilon}'_{ij}^{(p)}$  is identically zero, then the stresses are undetermined, but the differentiation of Equation (3.4.6) then gives:

$$\dot{\sigma}_{ij} = \lambda \dot{\epsilon}'_{kk} \delta_{ij} + 2\mu \dot{\epsilon}'_{ij} \quad (3.4.11)$$

so that the material behaves elastically under these conditions. When  $\dot{\epsilon}'_{ij}^{(p)}$  is non-zero the incremental response may be written:

$$\dot{\sigma}_{ij} = \left(\lambda + \frac{2}{3} \mu\right) \dot{\epsilon}'_{kk} \delta_{ij} + 2\mu(\dot{\epsilon}'_{ij} - \dot{\epsilon}'^{(p)}_{ij}) \quad (3.4.12)$$

which may be re-arranged to give:

$$\dot{\epsilon}'_{ij} = \dot{\epsilon}'^{(p)}_{ij} + \frac{\dot{\sigma}'_{ij}}{2\mu} \quad (3.4.13)$$

Noting that  $\dot{\epsilon}'_{ij}{}^{(p)} = \dot{\epsilon}_{ij}{}^{(p)}$  this confirms that the change in the internal variable  $\epsilon_{ij}{}^{(p)}$  simply represents an additional term to the strain deviator when dissipation occurs, i.e. that  $\epsilon_{ij}{}^{(p)}$  corresponds to the conventional plastic strain.

The above derivation shows how an elastic-plastic material may be derived from Ziegler's formulation without introducing in addition the conventional hypotheses of a yield locus, flow rule, compliance matrix and the summation of independent elastic and plastic strain components. It is emphasised that although the final material behaviour derived is identical, the hypotheses in the conventional and thermomechanical formulations are completely different.

As was stated in the last Chapter, one of the main motivations in examining a new approach to plasticity theory is the derivation of plasticity models with non-associated flow rules. Both the stability criterion of Drucker (1951) and the postulate of plasticity of Il'iushin (1961) lead to the normality condition; but it was shown in the last Section that the orthogonality condition leads to normality only in a limited stress space for a rigid-plastic material. An example of an elastic-plastic material with a non-associated flow rule will now be given.

Consider for instance the following functions:

$$\rho\psi = \left(\frac{\lambda}{2} + \frac{\mu}{3}\right) \epsilon_{ii} \epsilon_{jj} + 2\mu (\epsilon'_{ij} - \epsilon'_{ij}{}^{(p)}) (\epsilon'_{ij} - \epsilon'_{ij}{}^{(p)}) \quad (3.4.14)$$

$$\rho\phi = \frac{2}{3} M \left(\lambda + \frac{2\mu}{3}\right) \epsilon_{kk} (\dot{\epsilon}'_{ij}{}^{(p)} \dot{\epsilon}'_{ij}{}^{(p)})^{\frac{1}{2}} \quad (3.4.15)$$

in which the cohesion has been replaced by a term proportional to the mean normal stress. The elastic properties of this model are exactly as for the cohesive one, and during plastic deformation there is again no plastic volumetric strain, with the plastic strain components being in the same proportions as the components of the stress deviator.

However, the yield locus is derived as:

$$\sigma'_{ij}\sigma'_{ij} = \frac{2M^2}{27} \sigma_{ii}\sigma_{jj} \quad (3.4.16)$$

which is a conical locus in principal stress space sometimes termed the 'extended von Mises' locus. The constant  $M$  is related to a friction angle, and is equivalent to the same parameter used in critical state soil mechanics. Although there is still association of the yield locus and flow rule in the octahedral plane the plastic strain increment is no longer normal to the yield locus in the isotropic-deviatoric plane. There is ample experimental evidence that such behaviour occurs in granular materials. The above model does not include the effects of plastic dilation, which occurs in real soils, but this may also be included; it has been shown, however, that this formulation can accommodate non-associated behaviour.

### 3.5 Effective Stress Models for Soils

The models described in the preceding Section were all single phase models, in which the stress is simply derived as the thermodynamic force conjugate to the strain. If the models are applied to a two phase soil and the strain interpreted as the skeleton strain, then as shown in Section 2.1 the derived stress will be the effective stress. No terms are present in the free energy and dissipation expressions containing the kinematic parameters describing the pore fluid:  $v^{(w)}$  and  $w_i$ . All differentials with respect to these quantities are therefore zero, and so their conjugate forces  $n_u$  and  $u'_{,i}$  are zero. There is no pore pressure or pore pressure gradient: the pore fluid is equivalent to a vacuum.

A pore fluid of stiffness  $K^{(w)}$  may be introduced to the elastic model by modifying Equation (3.4.1) to give:

$$\rho\psi = \frac{\lambda}{2} \epsilon_{ii}\epsilon_{jj} + \mu\epsilon_{ij}\epsilon_{ij} + \frac{nK^{(w)}}{2} v^{(w)2} \quad (3.5.1)$$

with the final term clearly representing an additional elastic strain energy due to compression of the pore fluid. The stresses are derived exactly as before, and now interpreted as effective stresses, and the force corresponding to  $v^{(w)}$  given by:

$$n\nu = \rho \frac{\partial\psi}{\partial v^{(w)}} = nK^{(w)} v^{(w)} \quad (3.5.2)$$

so that the pore pressure is related to the volumetric strain in the pore fluid through the bulk stiffness  $K^{(w)}$ . The factor  $n$  in Equation (3.5.1) was introduced because the pore fluid only occupies a fraction  $n$  of the total volume of the element.

The above model obeys the principle of effective stress: the deformation of the soil skeleton is related only to the Terzaghi effective stress and not to the pore pressure. This is due to the fact that there is no coupling of terms between the strain  $\epsilon_{ij}$  and the pore fluid compression  $v^{(w)}$  in Equation (3.5.1). It was suggested in Appendix A that the principle of effective stress was closely related to an uncoupling of these terms. This may now be clarified by differentiating Equation (3.5.1) for a non-dissipative material, and equating this change of free energy to the work input:

$$\sigma'_{ij} \dot{\epsilon}_{ij} + n\nu \dot{v}^{(w)} = \lambda \epsilon_{ii} \dot{\epsilon}_{jj} + 2\mu \epsilon_{ij} \dot{\epsilon}_{ij} + nK^{(w)} v^{(w)} \dot{v}^{(w)} \quad (3.5.3)$$

where  $\sigma'_{ij}$  represents effective stress (not the deviator of stress) and it has been assumed that pore pressure gradients do not exist. The proof of Section 2.1 shows that there is no coupling between the effective stress / skeleton strain and pore pressure / pore fluid compression terms on the left hand side of Equation (3.5.3). It is only because the free energy has been chosen so that there is similarly no coupling on the right hand side that this model exhibits the

principle of effective stress: the skeleton strains depend only on the Terzaghi stress.

This analysis may be extended to an elastic soil with a compressible viscous pore fluid by including a dissipation term in the artificial seepage velocity:

$$\rho \dot{\phi} = k \gamma^{(w)} w_i w_i \quad (3.5.4)$$

(Note that  $w_i$  is the rate of change of the kinematic variable, as shown in Equation (2.1.6); the actual kinematic variable, which corresponds to a pore fluid displacement, has not been defined.)

The effective stress and pore pressure are defined as before, but in addition there is now a term defining the pore pressure gradient:

$$-u'_{,i} = \frac{1}{2} \rho \frac{\partial \dot{\phi}}{\partial w_i} = k \gamma^{(w)} w_i \quad (3.5.5)$$

which simply represents Darcy's law. Note that the factor of  $1/2$  appears in Equation (3.5.5) because the dissipation function is of second order in the velocity  $w_i$  and so  $v$  defined by Equation (3.2.18) is not unity. It is unfamiliar to consider the pore pressure gradient derived as a *force* in exactly the same way as the effective stress or pore pressure; this result arises, however, simply from the choice of the kinematic variables chosen to represent the state of the material. It represents exactly the same idea as the conventional thermodynamic idea of the temperature gradient being the *force* corresponding to the heat flow.

Although coupling of  $\epsilon_{ij}$  and  $v^{(w)}$  terms in Equation (3.5.1) would result in a model which did not obey the principle of effective stress, certain forms of coupling between the skeleton and pore fluid behaviour are possible without violating the principle. For instance in Equation (3.5.4) the permeability  $k$  could be a function of the

skeleton volumetric strain, and there is evidence that this is indeed the case. In this case the pore fluid behaviour would depend on the state of the soil skeleton, but since the dissipation function would still not contain terms in the rate of strain the effective stress expression would be unaltered: the skeleton strains will still depend solely on the effective stress.

A model in which the principle of effective stress is not obeyed could also be expressed within the thermodynamic framework. For instance, if the free energy expression included terms involving products between the skeleton strain and pore fluid compression, e.g.

$$\rho\psi = \frac{\lambda}{2} \epsilon_{ii} \epsilon_{jj} + \mu \epsilon_{ij} \epsilon_{ij} + A \epsilon_{ii} v^{(w)} \quad (3.5.6)$$

then the equivalent to Equation (3.5.3) would read:

$$\sigma'_{ij} \dot{\epsilon}_{ij} + n u \dot{v}^{(w)} = \lambda \epsilon_{ii} \dot{\epsilon}_{jj} + \mu \epsilon_{ij} \dot{\epsilon}_{ij} + A v^{(w)} \dot{\epsilon}_{ii} + A \epsilon_{ii} \dot{v}^{(w)} \quad (3.5.7)$$

The presence of  $v^{(w)}$  in the third term on the right hand side of Equation (3.5.7) means that the effective stress (as defined by Terzaghi) can be altered by a change in pore fluid strain with no accompanying skeleton strain. In conventional terms the principle of effective stress is not obeyed. The fact that models not exhibiting the effective stress principle involve somewhat unlikely product terms may offer some explanation as to why soils are observed as obeying the principle.

The above examples only include cases where the skeleton itself behaves elastically. If dissipation occurs in the skeleton then the dissipation function may contain both first and second order terms in velocities; for instance in the case of an extended von Mises material Equation (3.4.15) would be modified to:

$$\rho\phi = \frac{2}{3} M \left( \lambda + \frac{2\mu}{3} \right) \epsilon_{kk} \left( \dot{\epsilon}_{ij}^{(p)} \dot{\epsilon}_{ij}^{(p)} \right)^{\frac{1}{2}} + k \gamma^{(w)} w_i w_i \quad (3.5.8)$$

This is an example of a non-homogeneous dissipation function which is *complex* in the sense that it depends on two different sets of velocities (Ziegler (1977)). Ziegler offers no proof that in general the orthogonality principle will apply in complex processes, but suggests tentatively that it will apply. However, in this particular case the process is *compound* in that the dissipation is made up from two separate terms in the two velocities. For this case the orthogonality condition may be applied separately to each of the terms in turn and the forces derived in the usual way.

In this Chapter the thermodynamic formalism of Ziegler (1977) has been outlined and its application to plasticity theory discussed. As well as some general implications of the approach some specific elastic-plastic models have been described. With an appropriate choice of variables effective stress models may be described; including the behaviour of the pore fluid within the same framework as that of the soil skeleton. All the models discussed in the remainder of this dissertation are effective stress models. It is emphasised that the assumptions included in the formalism may be over-restrictive in enforcing a stronger principle than the second law of thermodynamics.

Both in this Chapter and in the remainder of this dissertation it is assumed that each element of soil deforms homogeneously. The possibility of describing the onset of non-homogeneous deformation is discussed in Appendix B.

CHAPTER 4  
DERIVATION OF THE MODIFIED CAM-CLAY MODEL  
FROM THERMOMECHANICS

The Cam-Clay family of models is introduced and a new derivation of Modified Cam-Clay, using the thermomechanical method outlined in the last Chapter, is described. Comparisons are made with other energy theories for clays. The model is extended to general stress states, and the application of large strain theory is studied.

#### 4.1 The Cam-Clay Models

The "Cam-Clay" theoretical model for soil behaviour was described by Schofield and Wroth (1968). The model is expressed in the theory of plasticity and is based on simple hypotheses for the storage and dissipation of energy, the concept of "stability" as defined by Drucker (1959) and an empirical relation for the pressure-specific volume behaviour of a soft clay. The model successfully combines the consolidation and shearing behaviour of clays within a single framework, but it is not entirely satisfactory in all its predictions. One notable defect is the prediction of excessively large shear strains for consolidation at small stress ratios, with this effect being due to the pointed shape of the yield locus. This effect was eliminated by the introduction of a slightly different hypothesis for the dissipation of energy by Roscoe and Burland (1968), resulting in the "Modified Cam-Clay" model.

Although Modified Cam-Clay too is not completely satisfactory, it successfully models many of the features of the behaviour of soft clays. The predictions for clays with an overconsolidation ratio greater than about two are less good, with strength usually over-predicted; and too stiff a response on load reversal is predicted

for most cases. Modified Cam-Clay in its original form involved no elastic shear strain; the resulting underprediction of shear strains at low stress ratios is in part improved by including a constant elastic shear modulus, and this has frequently been done in numerical computations using the model.

Although some comparisons with experimental data will be made, a systematic presentation of evidence to justify the applicability of the Modified Cam-Clay model to soils or to assess the accuracy of its predictions will not be presented. The successful use of the model has been demonstrated elsewhere (e.g. the use of a very similar model in the prediction of the behaviour of an embankment by Wroth (1977)). In this Chapter it will be demonstrated how the model may be derived from a thermomechanical basis, and in the next Chapter some modifications to the model will be made within the same framework.

#### 4.2 Derivation of the Modified Cam-Clay Model from Thermomechanics

In the spirit of the thermomechanical approach, the behaviour of the model will not be stated at this stage, but the two functions required (the specific free energy and specific dissipation) will first be introduced. The behaviour will then be derived from these functions, and the links with conventional plasticity theory noted. This approach should be contrasted with the conventional technique in which the final behaviour of the model (e.g. the shape of the yield locus) is specified from the outset. For a simple model there is apparently no advantage in the new approach, which in fact appears to be rather less direct. However, in more complex cases the new method offers certain advantages, which will be illustrated by considering some simple modifications to the two governing functions, and studying the effect on the resulting model.

Although the model will later be extended to more general stress states, it is first presented here in terms of the simplified stress and strain parameters used by Schofield and Wroth (1968) for the description of the triaxial test. For mathematical convenience the logarithmic (Hencky) definition of strain is used; this is indistinguishable from the Cauchy strain for the small strain analysis of Sections 4.2 to 4.4. Two internal variables  $v_p$  and  $\epsilon_p$  are used; their significance will be discussed later.

The specific free energy and dissipation functions are stated as:

$$\psi = [p_r \kappa^* \exp((v-v_p)/\kappa^*) + 3G(\epsilon-\epsilon_p)^2/2 + p_r (\lambda^*-\kappa^*) \exp((\ln(\Gamma/V_o)+v_p)/(\lambda^*-\kappa^*))]/\rho \quad (4.2.1)$$

$$\phi = [p_r \exp((\ln(\Gamma/V_o)+v_p)/(\lambda^*-\kappa^*))] (\dot{v}_p^2 + M^2 \dot{\epsilon}_p^2)^{1/2} / \rho \quad (4.2.2)$$

where  $p_r$  is a reference quantity with the dimensions of stress which is necessary to establish dimensional consistency. For all numerical calculations  $p_r$  is simply taken as 1.0 kPa .

Direct differentiation of these expressions, using the method outlined in Section 3.2 results in the equations for the stresses:

$$p' = \rho \frac{\partial \psi}{\partial v} + \rho \frac{\partial \phi}{\partial \dot{v}} = p_r \exp((v-v_p)/\kappa^*) \quad (4.2.3)$$

$$q = \rho \frac{\partial \psi}{\partial \epsilon} + \rho \frac{\partial \phi}{\partial \dot{\epsilon}} = 3G(\epsilon-\epsilon_p) \quad (4.2.4)$$

and for the internal forces:

$$0 = \rho \frac{\partial \psi}{\partial v_p} + \rho \frac{\partial \phi}{\partial \dot{v}_p} = -p_r \exp((v-v_p)/\kappa^*) + p_r \exp((\ln(\Gamma/V_o)+v_p)/(\lambda^*-\kappa^*)) + p_r \exp((\ln(\Gamma/V_o)+v_p)/(\lambda^*-\kappa^*)) \dot{v}_p (\dot{v}_p^2 + M^2 \dot{\epsilon}_p^2)^{-1/2} \quad (4.2.5)$$

$$0 = \rho \frac{\partial \psi}{\partial \varepsilon_p} + \rho \frac{\partial \phi}{\partial \dot{\varepsilon}_p} = -3G(\varepsilon - \varepsilon_p) + p_r \exp((\ln(\Gamma/V_o) + v_p)/(\lambda^* - \kappa^*)) M^2 \dot{\varepsilon}_p (\dot{v}_p^2 + M^2 \dot{\varepsilon}_p^2)^{-\frac{1}{2}} \quad (4.2.6)$$

The latter two equations may be rewritten by substituting the values of the stresses and introducing the definition:

$$p'_x = p_r \exp((\ln(\Gamma/V_o) + v_p)/(\lambda^* - \kappa^*)) \quad (4.2.7)$$

to give:

$$(p' - p'_x) = p'_x \dot{v}_p (\dot{v}_p^2 + M^2 \dot{\varepsilon}_p^2)^{-\frac{1}{2}} \quad (4.2.8)$$

$$q = p'_x M^2 \dot{\varepsilon}_p (\dot{v}_p^2 + M^2 \dot{\varepsilon}_p^2)^{-\frac{1}{2}} \quad (4.2.9)$$

Returning to the expressions for the stresses, their differentials with respect to time are given by:

$$\dot{p}' = p_r \exp((v - v_p)/\kappa^*) (\dot{v} - \dot{v}_p)/\kappa^* \quad (4.2.10)$$

$$\dot{q} = 3G(\dot{\varepsilon} - \dot{\varepsilon}_p) \quad (4.2.11)$$

which may be rearranged to give:

$$\dot{v} = \kappa^* \dot{p}'/p' + \dot{v}_p \quad (4.2.12)$$

$$\dot{\varepsilon} = \dot{q}/3G + \dot{\varepsilon}_p \quad (4.2.13)$$

Noting that no dissipation occurs (i.e.  $\phi = 0$ ) only when  $\dot{v}_p$  and  $\dot{\varepsilon}_p$  are both zero, it is clear that in the case of no dissipation the above equations simply represent the incremental behaviour of an elastic material with a constant shear modulus  $G$  and a bulk modulus proportional to the mean effective stress and equal to  $p'/\kappa^*$ . The elastic shear strain, although not included in the original Modified Cam-Clay, is a straightforward addition which has frequently been used in more recent versions of the model adapted for computational

purposes. The bulk modulus in the original model was equal to  $p'V/\kappa$ , where  $V$  is the specific volume, with the dependence on specific volume being a result of the choice of elastic swelling lines as straight in  $(\ln p', V)$  space. The form of the model derived here results in straight swelling lines in  $(\ln p', \ln V)$  space, and the parameter  $\kappa^*$  will take a different numerical value from the parameter  $\kappa$  in the original model by a factor of approximately  $1/V$ . The advantages of the use of plotting in  $(\ln p', \ln V)$  space are discussed by Butterfield (1979), and this minor alteration to the original model seems slightly advantageous overall. A particular gain is that the incremental stress strain relations are independent of the parameter  $\Gamma$ , which serves only to locate the consolidation lines in  $(\ln p', \ln V)$  space. Within the constraints of small strain theory the two forms are identical. The swelling lines may be derived as:

$$\ln V = \ln \Gamma - \lambda^* \ln(p'_x/p'_r) - \kappa^* \ln(p'/p'_x) \quad (4.2.14)$$

In the case where dissipation occurs the total strain is made up of two components: the strain which would have occurred if the same stress component had been applied and the process had been non-dissipative, plus an additional term given by the rate of change of the appropriate internal variable. In plasticity these are conventionally called the "elastic" and "plastic" strains, but it should be noted that this simple division is only possible because  $\psi$  and  $\phi$  in this case take a certain form. The internal variables for this model happen to correspond exactly to the conventionally defined plastic strains.

If no dissipation occurs Equations (4.2.8) and (4.2.9) are both indeterminate, but in the case of dissipation (at least one of  $\dot{v}_p$  and  $\dot{\epsilon}_p$  non-zero) they may be combined to give:

$$(p' - p'_x)^2 + q^2/M^2 = p'_x{}^2 \quad (4.2.15)$$

$$\dot{\epsilon}_p / \dot{v}_p = q/[M^2(p' - p'_x)] \quad (4.2.16)$$

These equations impose additional restrictions which ultimately allow  $\dot{v}_p$  and  $\dot{\epsilon}_p$  to be eliminated and a direct incremental relationship to be established between stress and strain. The first restriction is that for any value of  $p'_x$ , and hence of  $v_p$ , there is a relationship between the stresses such that the stress point lies on a given surface. Clearly this is the yield surface of conventional plasticity. It is important to note that the shape of the yield surface, and indeed its very existence, is a result of the choice of the dissipation function; the bounding surface to the elastic region was not introduced as a hypothesis.

In this model the yield locus is an ellipse centred on the point  $(p'_x, 0)$  in  $(p', q)$  space and passing through the origin. The parameter  $p'_x$  is related to the isotropic consolidation pressure  $p'_c$  by  $p'_c = 2p'_x$ . This locus is exactly as used by Roscoe and Burland (1968). The dependence of the size of the yield locus on one of the internal variables  $v_p$  represents the process of work hardening. The yield locus can only be altered by a dissipative process ( $\dot{v}_p \neq 0$ ), and remains fixed during any elastic deformation.

Equation (4.2.16) establishes the ratio between the rates of the internal variables (identical to the conventional plastic strain rates); and this ratio depends on the current stress state. This is clearly the flow rule of plasticity theory, and it may readily be verified that Equation (4.2.16) represents an associated flow rule in that the  $(\dot{v}_p, \dot{\epsilon}_p)$  vector is normal to the yield surface at the stress point in a space with superimposed  $(p', q)$  and  $(\dot{v}_p, \dot{\epsilon}_p)$  axes. The flow rule is therefore identical to that of Modified Cam-Clay and

correctly predicts hardening, softening, and a critical state. The critical state occurs when  $\dot{v}_p = 0$  and  $\dot{\epsilon}_p$  is non-zero, hence  $p' = p'_x$  and  $q = \pm Mp'$ , showing that  $M$  corresponds to the usual critical state parameter. Although in this model the flow rule is associated, this is not always the case for plasticity models derived using the thermomechanical method, see for example Section 3.4.

The final component of the Modified Cam-Clay model is the hardening law, which historically has been derived from the experimental fact that the states of plastically deforming soft clays all lie on a unique surface in  $(p', q, V)$  space. This surface may be derived by eliminating  $v_p$ ,  $p'_x$  and  $v$  from Equations (4.2.3) and (4.2.14), making use of the definition of  $p'_x$  (Equation (4.2.7)) and of volumetric strain  $v = \ln(V_0/V)$ . Finally substitution of  $\eta = q/p'$  results in:

$$\ln V = \ln \Gamma - \lambda^* \ln(p'/p_r) - (\lambda^* - \kappa^*) \ln[(1 + \eta^2/M^2)/2] \quad (4.2.17)$$

which is the equation of the so-called "State Boundary Surface". The projections of consolidation lines at constant stress ratio  $\eta$  are straight lines of slope  $-\lambda^*$  in  $(\ln p', \ln V)$  space, with this minor alteration from the original model being similar to the case of the swelling lines.

Outline diagrams of the model in  $(p', q)$  and  $(\ln p', \ln V)$  space are shown in Figures 4.1 and 4.2, with these being a convenient way of representing a Cam-Clay type model.

It has been demonstrated that a soil model, almost identical to Modified Cam-Clay, may be derived entirely from specific forms of the functions  $\psi$  and  $\phi$  and the thermomechanical formalism. It is useful at this state to take the analysis slightly further to show how this formulation could be used in practical problems. Most important is the

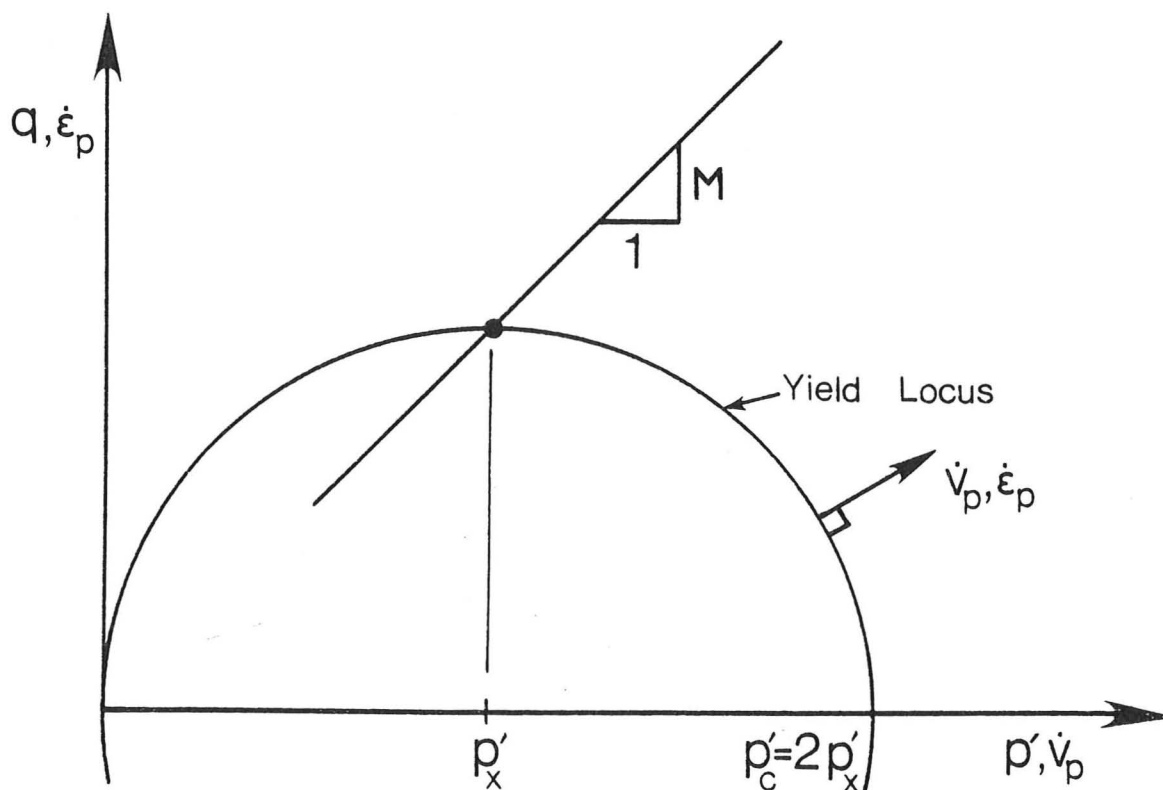


Figure 4.1 Modified Cam-Clay yield locus in triaxial stress space, flow rule

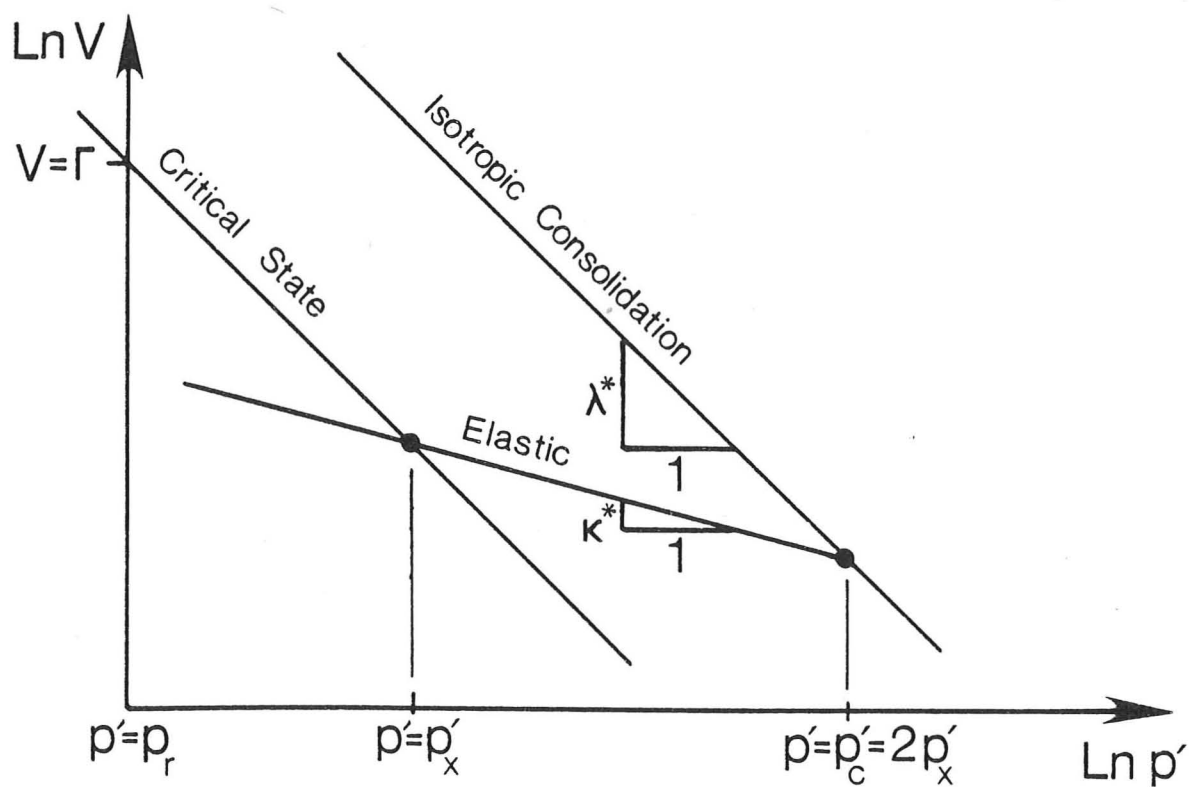


Figure 4.2 Consolidation and swelling lines for Modified Cam-Clay

derivation of the incremental stress-strain response which allows the model to be implemented using the Finite Element Method.

For the elastic case  $\dot{v}_p = \dot{\epsilon}_p = 0$  and Equations (4.2.12) and (4.2.13) reduce to give the stiffness matrix:

$$\begin{bmatrix} \dot{p}' \\ \dot{q} \end{bmatrix} = \begin{bmatrix} p'/\kappa^* & 0 \\ 0 & 3G \end{bmatrix} \begin{bmatrix} \dot{v} \\ \dot{\epsilon} \end{bmatrix} \quad (4.2.18)$$

In order to establish the incremental plastic response an additional equation to the three incremental equations (4.2.12), (4.2.13) and (4.2.16) is required in order to eliminate both  $\dot{v}_p$  and  $\dot{\epsilon}_p$ . This equation is supplied by differentiating the equation for the yield locus Equation (4.2.15), to give:

$$(p' - p'_x) \dot{p}' - p' \dot{p}'_x + q \dot{q} / M^2 = 0 \quad (4.2.19)$$

and noting that:

$$\dot{p}'_x = p'_x \dot{v}_p / (\lambda^* - \kappa^*) \quad (4.2.20)$$

The solutions for  $\dot{v}_p$  and  $\dot{\epsilon}_p$  are:

$$\dot{v}_p = \frac{(\lambda^* - \kappa^*)}{(M^2 p'^2 + q^2)} \left( \frac{\dot{p}'}{p'} (M^2 p'^2 - q^2) + 2q \dot{q} \right) \quad (4.2.21)$$

$$\dot{\epsilon}_p = \frac{(\lambda^* - \kappa^*) 2qp'}{(M^4 p'^4 - q^4)} \left( \frac{\dot{p}'}{p'} (M^2 p'^2 - q^2) + 2q \dot{q} \right) \quad (4.2.22)$$

which may be combined with Equations (4.2.12) and (4.2.13) to give the compliance relation:

$$\begin{bmatrix} \dot{v} \\ \dot{\epsilon} \end{bmatrix} = \begin{bmatrix} \kappa^*/p' & 0 \\ 0 & 1/3G \end{bmatrix} \begin{bmatrix} \dot{p}' \\ \dot{q} \end{bmatrix} + \frac{\lambda^* - \kappa^*}{M^2 p'^2 + q^2} \begin{bmatrix} \frac{M^2 p'^2 - q^2}{p'} & 2q \\ 2q & \frac{4q^2 p'}{M^2 p'^2 - q^2} \end{bmatrix} \begin{bmatrix} \dot{p}' \\ \dot{q} \end{bmatrix} \quad (4.2.23)$$

"Elastic"

"Plastic"

This relation may readily be inverted to give the stiffness matrix,

which is symmetric, as is always the case for an elastic-plastic model with an associated flow rule. Note that the parameter  $\Gamma$  enters neither the elastic nor plastic incremental stress-strain relations, but serves only to locate the consolidation and swelling lines in  $(\ln p', \ln V)$  space, being the value of specific volume  $V$  at the reference pressure  $p_r$ .

In addition to the incremental form of the stress-strain relations a criterion must be established to determine whether the response to any specified stress or strain increment will be elastic or plastic. The criterion adopted here is that the material adopts the response which minimises the free energy for a given strain increment. Since no discontinuous stress changes can occur ( $p'$  and  $q$  are continuous and single valued functions of the kinematic variables) it follows that for a given strain increment from a given stress state the input work is fixed. The orthogonality principle may be considered as a principle of maximal energy dissipation, so for a fixed work input this corresponds to a principle of minimal energy storage. The minimum free energy criterion is therefore closely linked to the orthogonality principle.

In order to minimise free energy, plastic behaviour (i.e. dissipation) will occur whenever the constraints of the model allow it. The first constraint is that the stress point must be on the yield locus. The second is that Equation (4.2.8) requires that  $\dot{v}_p$  is positive if  $p' > p'_x$  and negative if  $p' < p'_x$ . From Equation (4.2.21) it can be shown that  $\dot{v}_p$  is positive when  $p' > p'_x$  if the stress increment vector is directed outward from the yield locus. Thus the minimal free energy criterion corresponds exactly to the conventional plastic loading criterion for this case. On the softening side of the critical state,  $p' < p'_x$ , the loading criterion cannot be expressed in

stress space, since all strain increments result in a stress vector directed inward from the yield locus. This problem exists in both the conventional and new approaches, but can be avoided in conventional theory by making use of a yield locus in strain space. In the present theory the inversion of Equation (4.2.23) is used with Equation (4.2.21) to establish directly the loading criterion in terms of strain increments if  $p' < p'_x$ .

In studying the above derivation of the Modified Cam-Clay model there is little apparent advantage over the conventional approach to plasticity theory, although it is emphasised that the two methods involve completely different sets of hypotheses. In the next Chapter several small changes are made to the simple model, and in these the benefits of the new approach are illustrated. The changes to the model also allow some familiarity to be established with the significance of certain forms of  $\psi$  and  $\phi$ . Not only does this allow functions then to be chosen with particular properties, but it also gives some understanding of the underlying mechanisms which are the cause of these properties.

#### 4.3 Comparisons with Alternative Energy Theories for Clays

The original Cam-Clay model is based on a simple energy theory for the behaviour of a clay. The state of the clay was considered as defined by its location in  $(p', q, V)$  space, and the stored and dissipated energy per unit volume ( $\dot{W}_s$  and  $\dot{W}_d$ ) were given by:

$$\dot{W}_s = \kappa \dot{p}' / V \quad (4.3.1)$$

$$\dot{W}_d = Mp' |\dot{\epsilon}| \quad (4.3.2)$$

These two expressions do not completely define the material, and so additional assumptions from conventional plasticity theory were

also made. The first assumption was that the total strain was made up of additive elastic and plastic strains, the second that the change in stored energy  $\dot{W}_s$  could be equated to the quantity  $(p'\dot{v}_e + q\dot{\epsilon}_e)$ . This leads directly to the result that there is zero recoverable shear strain and that the bulk modulus is equal to  $p'V/\kappa$ .

The dissipated energy is then equal to the remaining quantity  $(p'\dot{v}_p + q\dot{\epsilon}_p)$ , and when substituted into Equation (4.3.2) this gives a flow rule. The assumption of normality allows integration to give a yield locus. The value of the integration constant is equivalent to a preconsolidation pressure, and governs the size of the yield locus. The expansion of the locus was then linked to the volumetric plastic strain by the empirically observed relation that consolidation lines are approximately straight in  $(\ln p', V)$  space. This then provides the hardening law.

The final assumption in the model, which is not usually stated explicitly, is that  $\dot{\epsilon} > 0$  for  $q > 0$  and  $\dot{\epsilon} < 0$  for  $q < 0$ . Because of the modulus sign in Equation (4.3.2) two families of yield loci are given according to the sign of  $\dot{\epsilon}$ . The final assumption is required to select the appropriate yield locus, and results in the characteristic bullet shape symmetrical about the  $p'$ -axis.

The only change introduced in Modified Cam-Clay was to alter Equation (4.3.2) to

$$\dot{W}_d = p' (\dot{v}_p^2 + M^2 \dot{\epsilon}^2)^{\frac{1}{2}} \quad (4.3.3)$$

with the result that the yield locus becomes an ellipse, and the final assumption is no longer required.

In order to compare the above functions with those used in the thermomechanical method, the latter will first be re-stated in terms of stresses rather than strains. Substitution of the expressions for

the stresses and  $p'_x$  into Equations (4.2.1) and (4.2.2) yields the free energy and dissipation per unit volume as:

$$\rho\psi = \kappa^* p'_x + q^2/6G + (\lambda^* - \kappa^*) p'_x \quad (4.3.4)$$

$$\rho\phi = p'_x (\dot{v}_p^2 + M^2 \dot{\epsilon}_p^2)^{\frac{1}{2}} \quad (4.3.5)$$

The first term of Equation (4.3.4) is directly comparable to Equation (4.3.1), the difference simply resulting in a bulk modulus of  $p'/\kappa^*$  instead of  $pV/\kappa$ . The second term represents the additional energy stored on shearing, and results in a constant elastic shear modulus  $G$ . The third term is of a different character, and represents an additional free energy as a result of plastic compression.

The presence of the last term is a result of the different definitions of "stored energy". In the thermomechanical formulation Equation (4.3.4) gives the *free energy*, whereas Equation (4.3.1) gives a more loosely defined recoverable power. The comparison of Equation (4.3.3) and Equation (4.3.5) is also linked to the definitions for the energy expressions. Equation (4.3.5) gives the thermomechanical dissipation as proportional to preconsolidation pressure, and Equation (4.3.3) a dissipated quantity proportional to pressure.

The use of different energy functions is familiar in thermodynamics, where as well as the *internal energy*  $U$ , defined by Equation (3.2.2), the *free energy*  $\psi$ , the *enthalpy* and other energy like quantities are used. Each of these new quantities is given by the Legendre transformation of the internal energy, expressed as a function of the *extensive* parameters for the system, in which some of the independent variables are replaced by *intensive* parameters (see for instance Callen (1960)). For instance the free energy is the transformation in which temperature replaces entropy as the independent variable.

In the use of elastic strain energy potentials the system studied

is conservative and the entropy undefined, so that the distinction between free and internal energy is unnecessary. The extension of such ideas to dissipative systems needs, however, this distinction to be made. If Equation (4.3.1) is interpreted as the internal energy, then an expression for the entropy may be derived as:

$$s = -(\lambda^* - \kappa^*) p'_x / \theta \quad (4.3.6)$$

suggesting that the entropy is reduced as the sample is consolidated: in thermodynamic terms the clay is achieving a more ordered state.

From considerations of statistical mechanics, Jowitt and Munro (1975) suggest that the entropy of an assembly of rigid particles is related directly to the porosity and, although the mathematical expression is different, this idea is similar to that expressed in Equation (4.3.6).

A graphical understanding of the magnitude of the free energy may be made in the following way. The free energy is first divided into parts arising from isotropic and deviatoric deformation, with the deviatoric part being simply the linear elastic shear strain energy  $3G(\epsilon - \epsilon_p)^2/2$  which is the area below an unloading-reloading line in  $q - \epsilon$  space. The remaining isotropic part may be written as:

$$\rho\psi^{(iso)} = \lambda^* p'_x + \kappa^* (p' - p'_x) \quad (4.3.7)$$

The equation of the critical state line may be derived as:

$$p'_x = p_r \exp((\ln(\Gamma/V_0) + v)/\lambda^*) \quad (4.3.8)$$

so that the area in a consolidation plot between the  $v$ -axis and the critical state line at a  $p'_x$  value of  $p'_{x1}$  (i.e. the area between the  $v$ -axis, critical state line and AB in Figure 4.3) is given by:

$$\int_{-\infty}^{v_{x1}} p'_x dv = p_r \lambda^* \exp((\ln(\Gamma/V_0) + v_{x1})/\lambda^*) = \lambda^* p'_{x1} \quad (4.3.9)$$

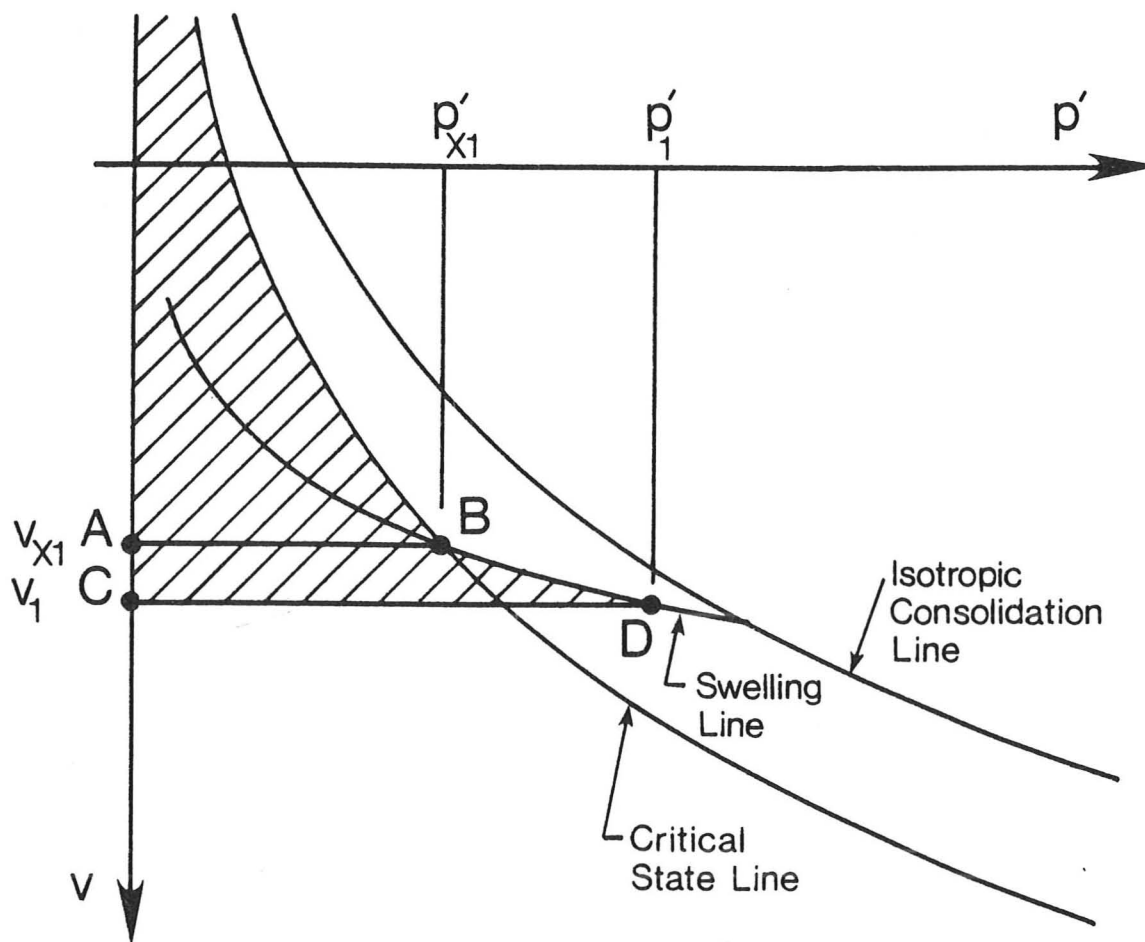


Figure 4.3 Consolidation plot of volumetric strain against pressure for the interpretation of the free energy function

Similarly the equation of a swelling line with  $p'_x = p'_{x1}$  may be written:

$$p' = p_r \exp((\ln(\Gamma/V_0) - (\lambda^* - \kappa^*) \ln(p'_{x1}) + v)/\kappa^*) \quad (4.3.10)$$

and the area ABDC in Figure 4.3 determined as:

$$\int_{v_{x1}}^{v_1} p' dv = \kappa^* (p'_{x1} - p'_x) \quad (4.3.11)$$

The isotropic part of the free energy function may be equated to the sum of these two areas, and is shown as the shaded region in Figure 4.3. This result may be compared with the approach of Palmer (1967) who adopted as a hypothesis that the internal energy of a

saturated clay was given by this area, attributing the first part of the area to energy change due to plastic deformation and the second part to elasticity. Whilst Palmer justifies this choice on grounds of physical reasoning about the balance between external loads and the forces between particles, no such argument is attempted here.

Palmer equates the dissipative part of the work input to the product of the shear strain rate and a quantity  $q^*$ , thus

$$\dot{W} = \dot{W}_s + q^* \dot{\epsilon} \quad (4.3.12)$$

No elastic shear strain is assumed, so that the total and plastic shear strains are identical. Palmer finds experimental evidence that  $q^*$  depends strongly on voids ratio, but to a much lesser extent on the actual pressure (cf. the assumption  $q^* = Mp'$  in the original Cam-Clay model, using also a different expression for  $W_s$ ). The equivalent term to  $q^*$  for the thermomechanical version of Modified Cam-Clay may be established as:

$$q_{mcc}^* = p'_x (M^2 - \eta^2) / 2\eta \quad (4.3.13)$$

Using Palmer's parameters  $\bar{p}'$  and  $\bar{q}^*$  (which are  $p'$  and  $q^*$  normalised by dividing by the  $p'$  and  $q$  values on the critical state line at the same specific volume) this may be used to derive the expression

$$\bar{q}_{mcc}^* = M / \left[ \bar{p}'^{(\lambda^* + \kappa^*) / (\lambda^* - \kappa^*)} \left( 2\bar{p}'^{(-\lambda^* / (\lambda^* - \kappa^*))} - 1 \right)^{\frac{1}{2}} \right] \quad (4.3.14)$$

Making use of Palmer's values of  $M$  and  $\kappa/\lambda$  this relation is plotted as the heavy line on Figure 4.4, which also shows Palmer's interpretation of triaxial tests on Kaolin by Thurairajah (1961). Although the exact trends are not fitted the agreement with the experimentally derived  $\bar{q}^*$  is quite good, particularly near  $\bar{p}' = 1.0$ ,

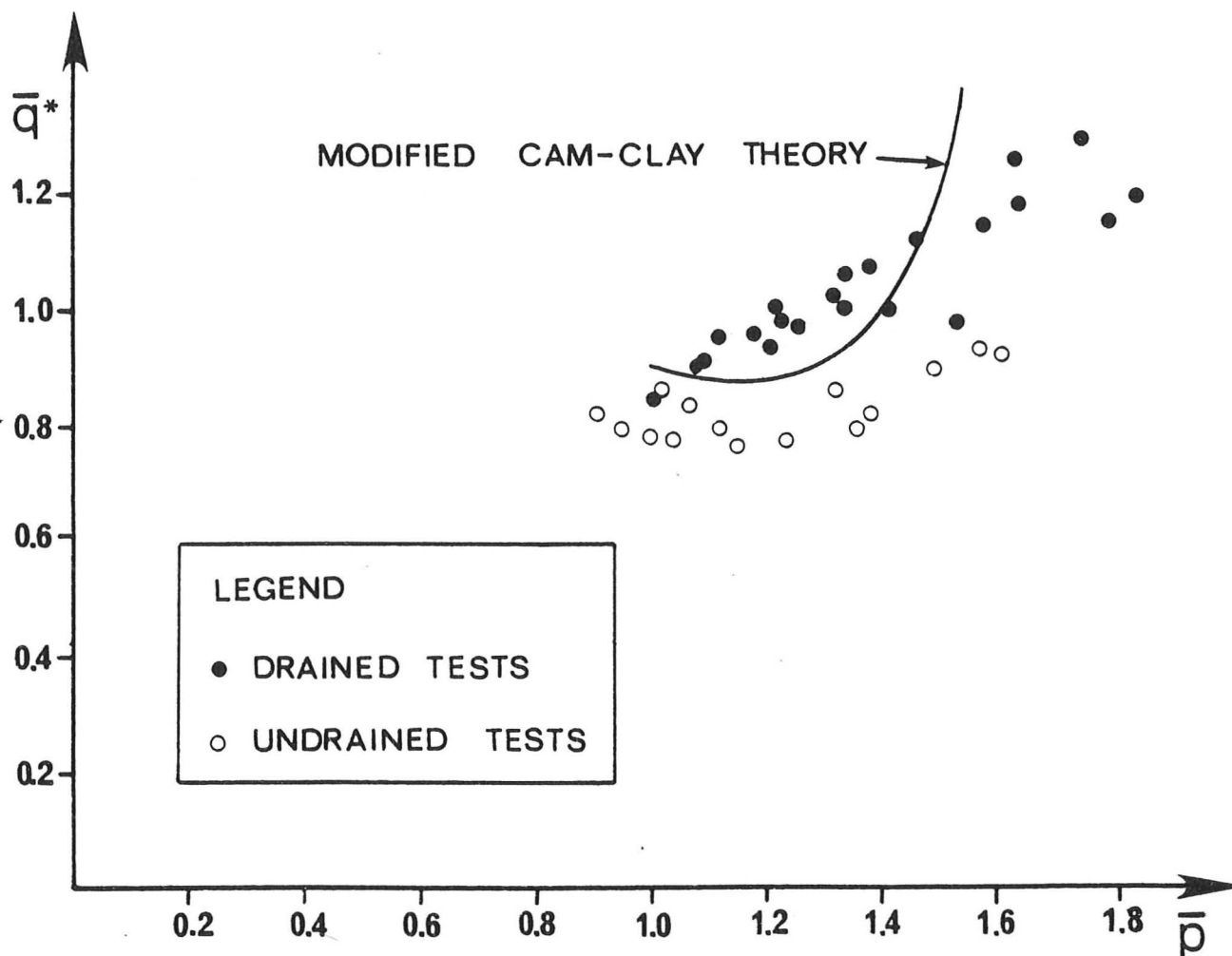


Figure 4.4 Variation of normalised  $q^*$  parameter with pressure (after Palmer (1967), triaxial data from Thurairajah (1961))

for which the data may be regarded as most reliable as the critical state is approached. The presence of elasticity in shear causes the  $q^*$  calculated by Palmer to be an underestimate, particularly at low stress ratios. The inclusion of an elastic shear modulus may therefore bring the derived points of Figure 4.4(b) closer to the theoretical curve.

Comparing the energy functions used in the classical plasticity and thermomechanical approaches to Modified Cam-Clay has shown that the two methods can be reconciled, provided that the stored energy in the plasticity approach is not equated with the free energy. An alternative

stored energy hypothesis used by Palmer proves to be very similar to that in the thermomechanical approach.

#### 4.4 Extension of the Modified Cam-Clay Model to General Stress States

The model so far described is expressed in terms of parameters which are applicable only to the stress states which occur in the triaxial test. It may be extended to general stress states by replacing the functions of  $v$ ,  $\epsilon$ ,  $v_p$  and  $\epsilon_p$  by functions of the invariants of the strain and plastic strain tensors.

It is convenient to define a quantity, equivalent to the conventional elastic shear strain:

$$\epsilon_{ij}^{(e)} = \epsilon_{ij} - \epsilon_{ij}^{(p)} \quad (4.4.1)$$

where  $\epsilon_{ij}^{(p)}$  will be used as the internal variable.

It then follows that, for any function  $x$ , expressed alternatively as a function of  $\epsilon_{ij}$  and  $\epsilon_{ij}^{(p)}$  or of  $\epsilon_{ij}^{(e)}$  and  $\epsilon_{ij}^{(p)}$ :

$$\frac{\partial x(\epsilon_{ij}, \epsilon_{ij}^{(p)})}{\partial \epsilon_{ij}} = \frac{\partial x(\epsilon_{ij}^{(e)}, \epsilon_{ij}^{(p)})}{\partial \epsilon_{ij}^{(p)}} \quad (4.4.2)$$

$$\frac{\partial x(\epsilon_{ij}, \epsilon_{ij}^{(p)})}{\partial \epsilon_{ij}^{(p)}} = \frac{\partial x(\epsilon_{ij}^{(e)}, \epsilon_{ij}^{(p)})}{\partial \epsilon_{ij}^{(p)}} - \frac{\partial x(\epsilon_{ij}^{(e)}, \epsilon_{ij}^{(p)})}{\partial \epsilon_{ij}^{(e)}} \quad (4.4.3)$$

The free energy and dissipation functions for the Modified Cam-Clay model may now be written in terms of invariants as:

$$\begin{aligned} \psi = & [p_r \kappa^* \exp(\epsilon_{(1)}^{(e)}/\kappa^*) + 2G\epsilon_{(2)}^{(e)} + \\ & + p_r (\lambda^* - \kappa^*) \exp((\ln(\Gamma/V_o) + \epsilon_{(1)}^{(p)})/(\lambda^* - \kappa^*))] / \rho \end{aligned} \quad (4.4.4)$$

$$\phi = p_r \exp((\ln(\Gamma/V_o) + \epsilon_{(1)}^{(p)})/(\lambda^* - \kappa^*)) (\dot{\epsilon}_{(1)}^{(p)})^2 + \frac{4M^2}{3} \epsilon_{(2)}^{(p)} / \rho \quad (4.4.5)$$

which reduce to the expressions in triaxial variables with the

appropriate substitutions. Making use of Equation (4.4.2) these may be differentiated to give the stress:

$$\sigma_{ij} = p_r \exp(\varepsilon_{(1)}^{(e)}/\kappa^*) \delta_{ij} + 2G\varepsilon_{ij}^{(e)} \quad (4.4.6)$$

(Since only effective stress behaviour is considered the usual dash notation is omitted to avoid confusion with the notation for a deviator.)

The internal forces may be obtained, using Equation (4.4.3):

$$\begin{aligned} 0 = & -p_r \exp(\varepsilon_{(1)}^{(e)}/\kappa^*) \delta_{ij} - 2G\varepsilon_{ij}^{(e)} \\ & + p_r \exp((\ln(\Gamma/V_o) + \varepsilon_{(1)}^{(p)})/(\lambda^* - \kappa^*)) \delta_{ij} \\ & + p_r \exp((\ln(\Gamma/V_o) + \varepsilon_{(1)}^{(p)})/(\lambda^* - \kappa^*)) \frac{\dot{\varepsilon}_{(1)}^{(p)} \delta_{ij} + \frac{2M^2}{3} \varepsilon_{ij}^{(p)}}{(\dot{\varepsilon}_{(1)}^{(p)2} + \frac{4M^2}{3} \dot{\varepsilon}_{(2)}^{(p)})^{\frac{1}{2}}} \end{aligned} \quad (4.4.7)$$

Equation (4.4.6) may be further differentiated to yield the incremental relation:

$$\dot{\sigma}_{ij} = \frac{\sigma_{kk}}{\kappa^*} \dot{\varepsilon}_{\ell\ell}^{(e)} \delta_{ij} + 2G\dot{\varepsilon}_{ij}^{(e)} \quad (4.4.8)$$

which is the generalisation of elastic behaviour with a constant shear modulus and bulk modulus proportional to mean effective stress.

It is convenient to split Equation (4.4.7) into its isotropic and deviatoric parts, and to substitute values for the stresses to give:

$$\sigma_{(1)}/3 - p_x = p_x \dot{\varepsilon}_{(1)}^{(p)} / (\dot{\varepsilon}_{(1)}^{(p)2} + \frac{4M^2}{3} \dot{\varepsilon}_{(2)}^{(p)})^{\frac{1}{2}} \quad (4.4.9)$$

$$\sigma_{ij}^{(p)} = p_x \frac{2M^2}{3} \dot{\varepsilon}_{ij}^{(p)} / (\dot{\varepsilon}_{(1)}^{(p)2} + \frac{4M^2}{3} \dot{\varepsilon}_{(2)}^{(p)})^{\frac{1}{2}} \quad (4.4.10)$$

where  $p_x = p_r \exp((\ln(\Gamma/V_o) + \varepsilon_{(1)}^{(p)})/(\lambda^* - \kappa^*))$  has also been substituted.

As in the case of the triaxial variables these may be re-arranged to give the yield locus and flow rule:

$$\left(\frac{\sigma_{(1)}}{3} - p_x\right)^2 + \frac{3\sigma'_{(2)}}{M^2} = p_x^2 \quad (4.7.11)$$

$$\left(\frac{\sigma_{(1)}}{3} - p_x\right) \frac{2M^2}{3} \dot{\epsilon}'_{ij}(p) = \sigma'_{ij} \dot{\epsilon}_{(1)} \quad (4.7.12)$$

The full incremental elastic and plastic response may be derived in exactly the same way as for the triaxial case.

Note that in principal stress space a section of the yield locus is circular in the octahedral plane. This is the case in models where the dissipation depends only on the first two invariants of the plastic strain rate tensor. A more realistic shape for the yield locus for a soil is a curvilinear triangle in the deviatoric plane; such an effect could be achieved by a dependence also on the third invariant of the tensor.

#### 4.5 Extension to Large Strain Theory

The above models are all based on small strain theory, for which the approximation that the density is constant is valid. Under this approximation the specific volume only varies by a small quantity, and so no distinction is made between  $\dot{V}/V$  and  $\dot{V}/V_0$ ; hence the original Modified Cam-Clay and the model described in this paper in which consolidation lines are straight in  $(\ln p', \ln V)$  rather than  $(\ln p', V)$  space are essentially identical. In large strain theory, where density changes are accounted for, this distinction is necessary.

The following discussion will be limited to the case of the triaxial test, and the extension to more general stress states is not as straightforward as for the small strain case. The Hencky logarithmic strain and the Euler stress will be used. Neither of these variables is convenient for an extension of the theory to general stresses, for which a Lagrangian approach using Green's strain and the Kirchoff

stress tensor is more appropriate. The mathematics of the triaxial case is, however, simpler in the terms used here.

Using strains and stresses defined in this way it follows that the work input per unit mass to the soil skeleton is given by:

$$\frac{\dot{W}}{\rho} = \frac{1}{\rho} (p' \dot{v} + q \dot{\epsilon}) \quad (4.5.1)$$

where  $\rho$  is the density in the current state. It follows that:

$$p' = \rho \left( \frac{\partial \psi}{\partial v} + \frac{\partial \phi}{\partial \dot{v}} \right) \quad (4.5.2)$$

$$q = \rho \left( \frac{\partial \psi}{\partial \epsilon} + \frac{\partial \phi}{\partial \dot{\epsilon}} \right) \quad (4.5.3)$$

Since  $\rho$  must now be treated as a variable, distinction must be made as to whether  $\rho$  in Equations (4.2.1) and (4.2.2) is to be interpreted as the initial or the current density. Either interpretation is allowable, the choice simply representing two possible hypotheses for the forms of the functions  $\psi$  and  $\phi$ . If  $\rho$  is considered as the initial density ( $\rho_0$ ), then the bracketed expressions in Equations (4.2.1) and (4.2.2) simply represent the free energy and dissipation per unit mass, scaled by a constant factor  $\rho_0$ . Alternatively if  $\rho$  is considered as the current density the bracketed expressions are equal respectively to  $\rho\psi$  and  $\rho\phi$ , the free energy and dissipation per unit volume. In this latter case, since  $\rho$  depends on the volumetric strain it must first be replaced using the identity

$$\rho = \rho_0 \exp(v) \quad (4.5.4)$$

before the differentiation is carried out.

Examining first the assumption that the expressions apply for unit mass, the stresses are derived as:

$$p' = (\rho/\rho_0) p_r \exp((v-v_p)/\kappa^*) = p_r \exp(v(1+\kappa^*)/\kappa^*) \exp(-v_p/\kappa^*) \quad (4.5.5)$$

$$q = \rho/\rho_0 \ 3G(\varepsilon-\varepsilon_p) = \exp(v) 3G(\varepsilon-\varepsilon_p) \quad (4.5.6)$$

The incremental expressions for the stresses are:

$$\dot{p} = p\dot{v}(1+\kappa^*)/\kappa^* - p\dot{v}_p/\kappa^* \quad (4.5.7)$$

$$\dot{q} = q\dot{v} + 3G \exp(v) (\dot{\varepsilon}-\dot{\varepsilon}_p) \quad (4.5.8)$$

Equation (4.5.7) shows that elastic swelling lines are now of slope  $-\kappa^*/(1+\kappa^*)$  in  $(\ln p', \ln V)$  space, and that  $\dot{v}_p$  no longer represents the conventionally defined plastic strain, which would be given by  $v_i$  where:

$$v_i = v_p/(1+\kappa^*) \quad (4.5.9)$$

The slight dependence of the shear modulus on the density results in curved constant shear strain contours of the form:

$$q = A p' \left( \frac{\kappa^*}{1+\kappa^*} \right) \quad (4.5.10)$$

The state boundary surface may be derived as:

$$(1+\lambda^*) \ln V = \ln \Gamma + \lambda^* \ln V_0 - \lambda^* \ln \left( \frac{p'}{p_r} \right) - (\lambda^*-\kappa^*) \ln \left( \frac{\eta^2/M^2+1}{2} \right) \quad (4.5.11)$$

so that the slope of consolidation lines is now  $\frac{-\lambda}{1+\lambda}$  in  $(\ln p', \ln V)$  space. In order to restore  $\lambda^*$ ,  $\kappa^*$  and  $\ln \Gamma$  to their original meanings they must be replaced by  $\lambda'/(1-\lambda')$ ,  $\kappa'/(1-\kappa')$  and  $(\ln \Gamma' - \lambda' \ln V_0)/(1-\lambda')$  respectively in the free energy and dissipation expressions (the dashed parameters having the original meaning). If this substitution is made the state boundary surface becomes:

$$\ln V = \ln \Gamma' - \lambda' \ln \left( \frac{p'}{p_r} \right) - \frac{(\lambda'-\kappa')}{(1-\kappa')} \ln \left( \frac{\eta^2/M^2+1}{2} \right) \quad (4.5.12)$$

so that the separation of the normal consolidation and critical state lines is slightly altered from the original model. This is due to the fact that the yield locus is slightly changed from that of the original model, and may be expressed in the form:

$$p'^2 - (2p'_x)^{(1-\kappa')} p'^{(1+\kappa')} + \frac{q^2}{M^2} = 0 \quad (4.5.13)$$

The flow rule is also altered by a small amount.

In the alternative approach in which the expressions for  $\psi$  and  $\phi$  are interpreted as applying to unit volume (as opposed to unit mass) the substitution of Equation (4.5.4) before differentiation results in the stress expressions:

$$p' = p_r \exp((v-v_p)/\kappa^*) - [p_r \kappa^* \exp((v-v_p)/\kappa^* + 3G(\varepsilon-\varepsilon_p)^2/2 + p_r (\lambda^*-\kappa^*) \exp((\ln(\Gamma/V_o) + v_p)/(\lambda^*-\kappa^*)))] \quad (4.5.14)$$

$$q = 3G(\varepsilon-\varepsilon_p) \quad (4.5.15)$$

The main result of this is to alter the yield locus to:

$$\left( \frac{(p' + \frac{q^2}{6G} + (\lambda^*-\kappa^*)p'_x)}{1 - \kappa^*} - p'_x \right)^2 + q^2/M^2 = p'_x{}^2 \quad (4.5.16)$$

with intercepts at  $-p'_x(\lambda^*-\kappa^*)$  and  $p'_x(2-\lambda^*-\kappa^*)$  on the  $q = 0$  axis.

Undrained stress paths take the form of parabolas:

$$p' = p'_1 - \frac{q^2}{6G} \quad (4.5.17)$$

where  $p'_1$  is the intercept on the isotropic axis. The flow rule and incremental stress strain relations are more complicated than for the small strain analysis, and are not given in detail here.

The functions used in large strain analysis are considerably more complex than those for the case where strain is small. If the analysis

is extended to general stress systems an even greater complexity is introduced. It is worthwhile therefore to assess the significance of the change to large strain analysis, and determine if it is necessary for routine soil mechanics problems.

The magnitude of the difference for the two analyses depends on the values of  $\lambda^*$  and  $\kappa^*$ , and will be illustrated using values based on those used by Randolph et al. (1979) for Boston Blue Clay and given in Table 4.1, which also includes information which will be referred to at a later stage. These parameters are obtained from the material tested at pressures in the region of  $p' = 200$  kPa .

Parameter	Boston Blue Clay	Speswhite Kaolin	Champlain Sea Clay	Llyn Brianne Slate Dust
References	Randolph et al. (1979)	Unpublished data	Yong and Silvestri (1977)	Lewin and Burland (1970)
M	1.2	0.88	1.2	1.044
$\lambda^*$	0.075	0.117	0.2	0.052
$\kappa^*$	0.015	0.027	0.005	0.007
G/MPa	10.0	13.5	2.07	33.1
$\Gamma$	2.7	3.3	4.3	-
$\alpha$	80.0	75.0	-	-
$\beta$	50.0	65.0	-	-

Table 4.1 Values of Modified Cam-Clay Parameters

If large strain analysis is taken into account the constant shear strain contours for the model where the functions are considered as referring to unit mass are of the shape shown in Figure 4.5. Clearly the effect of the large strain analysis is very small in that, except at very low pressures, the contour is essentially a line at constant deviator stress. Similarly the separation of the isotropic and

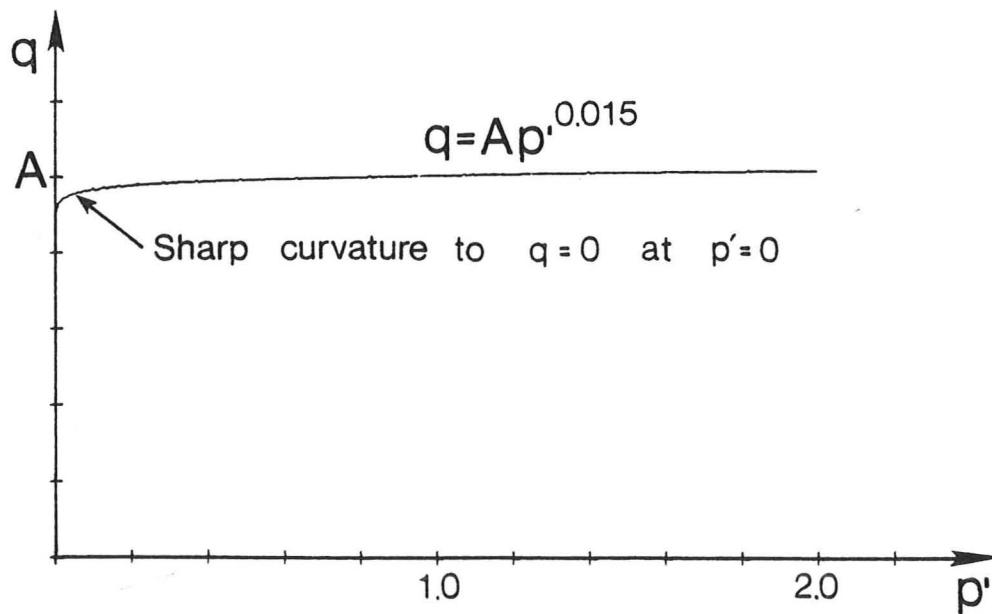


Figure 4.5 Elastic shear strain contour from large strain theory

critical state lines on a consolidation plot changes in the ratio 0.985 : 1.0, an undetectable amount. The alteration of the shape of the yield locus is therefore very small.

If the alternative form of the functions for large strain analysis is used, it may be noted that at  $p' = 200$  kPa the maximum value of  $q$  may be 240 kPa and  $\frac{q^2}{6G} = 0.96$ , so that the paraboloid form of the undrained stress paths given by Equation (4.5.17) represents a negligible deviation from the small strain analysis. The alteration of the shape of the yield locus is slightly more significant, and in particular the possibility of negative mean effective stress of up to  $-0.06 p'_x$  may be important.

For a clay in which  $\lambda^*$  and  $\kappa^*$  are not large, however, it appears that large strain analysis gives results differing by only a very small amount from the conventional small strain analysis. The additional complexity is therefore unnecessary in most cases, although

it may be of importance for some highly compressible clays.

In this Chapter the derivation of the Modified Cam-Clay model from a thermomechanical approach has been given, arriving at a complete elastic-plastic model using a different set of initial hypotheses from those used in conventional plasticity theory. The model has been generalised from triaxial to general stress states, and some implications of using large strain theory explored. In the next Chapter the application of the thermomechanical approach will be demonstrated further by changing the free energy and dissipation functions slightly to result in modified forms of the model.

## CHAPTER 5

VARIATIONS ON MODIFIED CAM-CLAY AND COMPARISONS  
WITH EXPERIMENTAL DATA

A computer program for studying models of the Modified Cam-Clay type is first briefly described. Three alterations of the simple Modified Cam-Clay model are then discussed: the first involves a change in the yield locus shape and the latter two both involve a variable shear modulus. Computations using the models are compared with the results of a series of triaxial tests on Kaolin.

### 5.1 Numerical Calculations Using Modified Cam-Clay Models

In the last Chapter the Modified Cam-Clay model was derived from a thermomechanical approach, offering perhaps little advantage over the more conventional expression in terms of plasticity theory. In this Chapter the free energy and dissipation terms will be altered slightly, allowing some insight into how forms of the functions are related to material behaviour. The thermomechanical approach reveals links between different aspects of behaviour which could not be anticipated in plasticity theory.

For many stress paths it is not possible to obtain closed form solutions for the strains computed from the various theoretical models which are to be discussed, so that numerical methods must be used. The models are therefore implemented in a *Single Element Analysis* program in which the calculation is carried out incrementally in exactly the same way as in *Finite Element Analysis*. Before moving on to the description of more complex models this program will be briefly described.

The program allows the incremental calculation of the response of

a model to any combination of stress or strain control, and so models may be tested and proven for different types of stress path. The routines used for each model could then be used directly in a Finite Element Analysis. Each model could be studied separately by changing a subroutine in the Single Element Program.

For each increment of the calculation the compliance matrix is calculated according to the current state of the sample. If the stress path is specified the strain increments are calculated directly; if a combination of stress and strain control is used the response is obtained by some simple matrix manipulation which is not elaborated here. Calculations are carried out using four independent stresses (three direct stresses and one shear stress) so that the limitation of one of the principal stresses being in a fixed direction has been imposed. This limited case is sufficient for the analysis of many soil mechanics problems, for instance all problems of plane stress, plane strain or axi-symmetry. Drained and undrained behaviour is correctly accounted for by augmenting the effective compliance matrix:

$$\begin{bmatrix} \dot{\epsilon}_1 \\ \dot{\epsilon}_2 \\ \dot{\epsilon}_3 \end{bmatrix} = \begin{bmatrix} c_1 & c_2 & c_3 \\ c_4 & c_5 & c_6 \\ c_7 & c_8 & c_9 \end{bmatrix} \begin{bmatrix} \dot{\sigma}'_1 \\ \dot{\sigma}'_2 \\ \dot{\sigma}'_3 \end{bmatrix} \quad (5.1.1)$$

to give a compliance matrix in terms of total stresses:

$$\begin{bmatrix} \dot{\epsilon}_1 \\ \dot{\epsilon}_2 \\ \dot{\epsilon}_3 \\ \dot{v}_f \end{bmatrix} = \begin{bmatrix} c_1 & c_2 & c_3 & -c_1-c_2-c_3 \\ c_4 & c_5 & c_6 & -c_4-c_5-c_6 \\ c_7 & c_8 & c_9 & -c_7-c_8-c_9 \\ c_1+c_4+c_7 & c_2+c_5+c_8 & c_3+c_6+c_9 & \left\{ \begin{array}{l} -c_1-c_2 \dots -c_9 \\ -\frac{(V-1)}{VK_w} \end{array} \right\} \end{bmatrix} \begin{bmatrix} \dot{\sigma}_1 \\ \dot{\sigma}_2 \\ \dot{\sigma}_3 \\ \dot{u} \end{bmatrix} \quad (5.1.2)$$

The first three lines of the above equation arise directly from the definition of effective stress. The final line gives an expression for  $\dot{v}_f$ , which is the volumetric strain which would be deduced from measurements of flow of the pore fluid into or out of a sample. The quantity  $\dot{v}_f$  is equal to the sum of the principal strain rates, modified by a term which corrects for the compression of the pore fluid due to pore pressure changes ( $K_w$  is the pore fluid bulk modulus). An undrained test would be specified by requiring  $\dot{v}_f = 0$ , but for this case the sum of the principal strains will not be identically zero because of pore fluid compressibility.

In order to prove the program before using it to study more complex models it was first checked against closed form solutions for some simple cases. Table 5.1 shows the results for calculations of a drained test on normally consolidated clay using the Modified Cam-Clay

q	v %				ε %			
	Number of increments			Closed form	Number of increments			Closed form
	10	100	1000		10	100	1000	
0.0	0.000	0.000	0.000	0.000	0.000	0.000	0.000	0.000
2.0	0.167	0.206	0.209	0.210	0.067	0.090	0.092	0.092
4.0	0.412	0.473	0.478	0.479	0.191	0.249	0.255	0.256
6.0	0.700	0.769	0.775	0.776	0.396	0.495	0.505	0.507
8.0	1.003	1.073	1.079	1.080	0.694	0.839	0.854	0.856
10.0	1.306	1.372	1.378	1.379	1.096	1.294	1.315	1.317
12.0	1.599	1.660	1.665	1.666	1.622	1.889	1.917	1.920
14.0	1.879	1.933	1.938	1.938	2.311	2.680	2.719	2.724
16.0	2.144	2.191	2.194	2.195	3.251	3.805	3.865	3.872
18.0	2.393	2.433	2.436	2.436	4.669	5.697	5.819	5.832
20.0	2.627	2.661	2.663	2.663	7.487	13.878	20.274	∞

$M = 1.2, \lambda^* = 0.025, \kappa^* = 0.005, G = 1000.0, \Gamma = 2.0, K_w = 2.0 \times 10^6, \sigma_3' = 10.0$   
 (Arbitrary units of stress)

Table 5.1 Calculations Using the Modified Cam-Clay Model for a Drained Triaxial Test on Normally Consolidated Clay

model with 10, 100 and 1000 stress increments to the critical state. Comparison with the closed form solution shows that the correct solution is approached as the number of increments is increased. The very large shear strains as the critical state is approached are the most difficult to calculate accurately.

When shown graphically the results for 100 and 1000 increments and the closed form solution are almost indistinguishable; and this was also found to be the case for other types of test. Of the order of 100 increments were used for most of the following calculations. Although trivial in the case of the Single Element Analysis it is important to minimise the calculation steps in Finite Element Analysis for economic reasons.

## 5.2 A Change in the Dissipation Function

The fact that the yield locus for Modified Cam-Clay passes through the origin in stress space is apparently arbitrary, and arises because of the appearance of the term  $p_r \exp((\ln(\Gamma/V_o) + v_p)/(\lambda^* - \kappa^*))$  in both the free energy and the dissipation expressions. If either of these terms is multiplied by a constant the yield locus no longer passes through the origin. The most convenient way of achieving this is to multiply the term  $\dot{v}_p$  in the dissipation function by a factor  $N$ , where  $N$  is a new material parameter. The dissipation expression becomes:

$$\phi = \frac{1}{\rho} \left( p_r \exp((\ln(\Gamma/V_o)/(\lambda^* - \kappa^*)) (N^2 \dot{v}_p^2 + M^2 \dot{\epsilon}_p^2)^{\frac{1}{2}} \right) \quad (5.2.1)$$

Carrying out the differentiations as before shows that the elastic properties remain unchanged. The yield locus is altered to:

$$(p' - p'_x)^2/N^2 + q^2/M^2 = p'_x{}^2 \quad (5.2.2)$$

and the flow rule is associated to the new locus, still giving the

critical state at  $\eta = M$ .

If  $N > 1$  this apparently results in a small region within the yield locus where negative mean effective stress can occur (Figure 5.1)

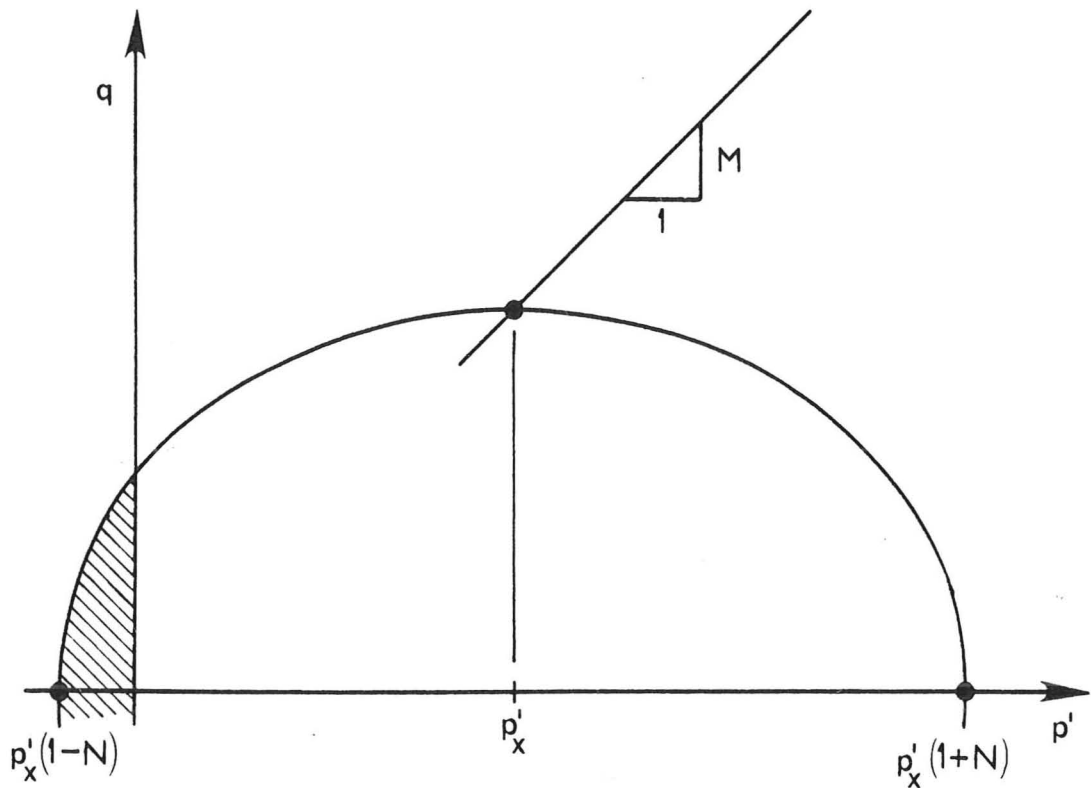


Figure 5.1 Yield locus for material with  $N > 1$  (see Equation (5.2.1))

but in fact this region cannot be reached since infinite elastic volumetric expansion is predicted as the mean effective stress falls to zero. A similar change to the yield locus was introduced by Van Eekelen and Potts (1978) in a model for Drammen Clay based on Modified Cam-Clay.

If  $N < 1$  the effect is to introduce a maximum stress ratio of:

$$\eta_m = M/(1 - N^2)^{\frac{1}{2}} \quad (5.2.3)$$

as shown in Figure 5.2. Overconsolidation ratio may be defined as  $p'_c/p'$ , where  $p'_c$  is the larger pressure at which the yield locus cuts the isotropic axis, i.e.  $p'_c = p'_x(1+N)$ . For a sample which undergoes isotropic consolidation and swelling, plastic swelling will occur when an overconsolidation ratio of  $(1+N)/(1-N)$  is reached, resulting in the modified consolidation plot of Figure 5.3. The elastic region is entirely confined between the isotropic consolidation and isotropic

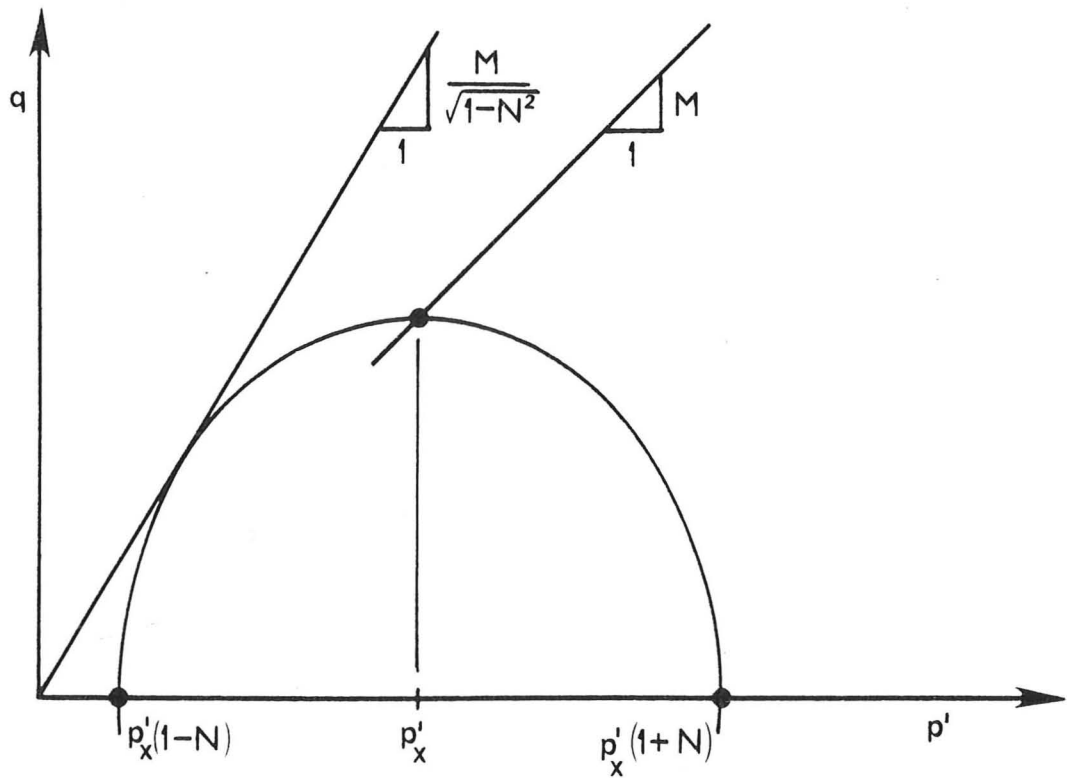


Figure 5.2 Yield locus for material with  $N < 1$  (see Equation (5.2.1))

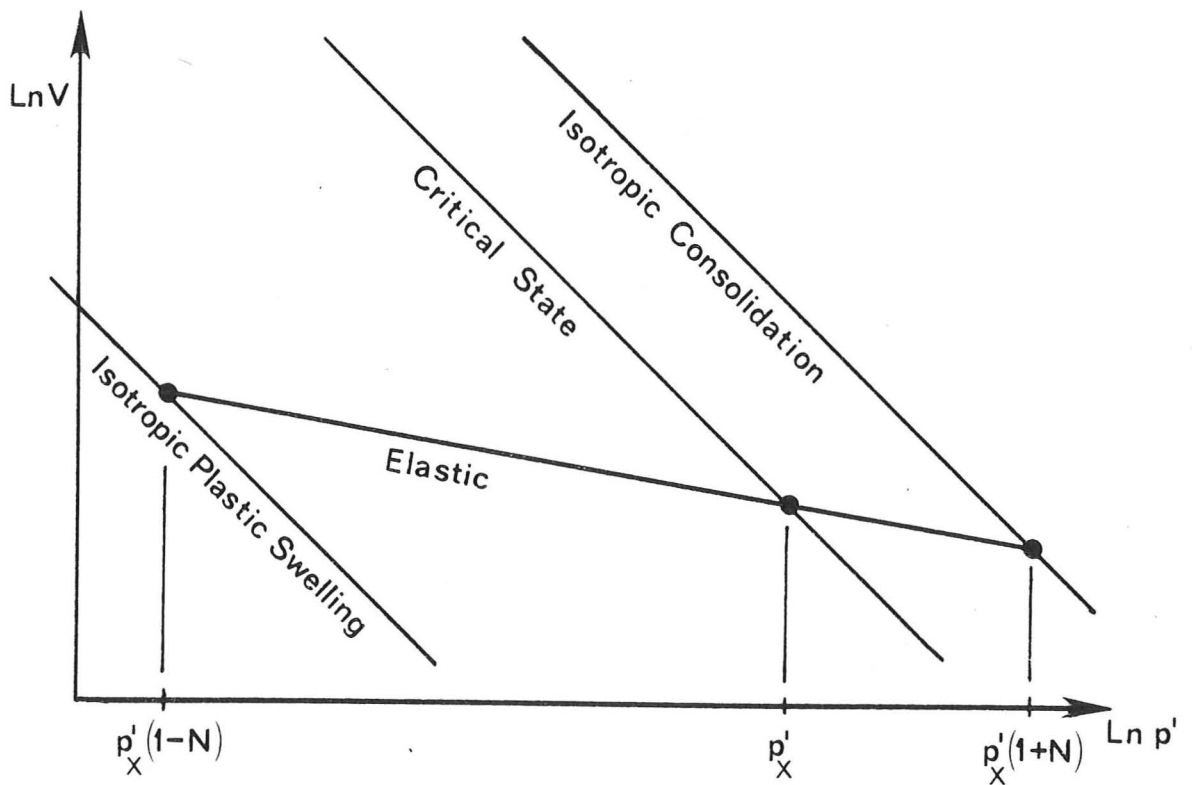


Figure 5.3 Consolidation and swelling lines for material with  $N < 1$  (see Equation (5.2.1))

plastic swelling lines. The idea of a plastic swelling curve was suggested by Parry (1965) from consideration of a simple mechanistic approach based on intergranular forces, and further evidence of plastic swelling is given by Parry and Amerasinge<sup>h</sup> (1973).

In plasticity models the assumption is often made that the rate of plastic work should be non-negative, i.e.:

$$\sigma_{ij} \dot{\epsilon}_{ij}^{(p)} \geq 0 \quad (5.2.4)$$

The assumption is introduced on "thermodynamic" grounds, and is indeed proven by Molenkamp (1980) from thermodynamics under certain restrictive assumptions. A corollary of the assumption is that the yield locus must include the origin in stress space. This condition is clearly violated by the model described above, since non-negative plastic work is not a requirement of the formulation. The requirement only applies to models derived from Ziegler's formulation under the following additional conditions:

(a) A single internal variable tensor, denoted by  $\epsilon_{ij}^{(p)}$  exists. It is then convenient to define  $\epsilon_{ij}^{(e)}$  by:

$$\epsilon_{ij}^{(e)} = \epsilon_{ij} - \epsilon_{ij}^{(p)} \quad (5.2.5)$$

(b) Dissipation depends only on changes in the internal variable, and not on the strain rate, i.e.:

$$\phi = \phi(\epsilon_{ij}, \epsilon_{ij}^{(p)}, \dot{\epsilon}_{ij}^{(p)}) \quad (5.2.6)$$

(The further restriction that  $\phi$  is homogeneous of first order in  $\dot{\epsilon}_{ij}^{(p)}$  is of course necessary for a rate independent material.)

(c) The free energy depends only on the so-called "elastic" strain, i.e.:

$$\psi = \psi(\epsilon_{ij}^{(e)}) = \psi(\epsilon_{ij} - \epsilon_{ij}^{(p)}) \quad (5.2.7)$$

The first assumption simply restricts attention to a class of

materials of limited complexity: very little attention has been given to materials with multiple internal variables. The second then represents the usual assumption of plasticity theory that only changes in the plastic strain cause dissipation. Denoting the internal force corresponding to  $\varepsilon_{ij}^{(p)}$  by  $\sigma_{ij}^{(p)}$  this restricted form of the dissipation function results in:

$$\phi = \frac{1}{\rho} \sigma_{ij}^{(pd)} \dot{\varepsilon}_{ij}^{(p)} \geq 0 \quad (5.2.8)$$

It is the third assumption which is most restrictive, in that it eliminates the possibility of elastic-plastic coupling and of certain types of hardening behaviour. The limited form of  $\psi$  results in:

$$\sigma_{ij}^{(pq)} = \rho \frac{\partial \psi}{\partial \varepsilon_{ij}^{(p)}} = -\rho \frac{\partial \psi}{\partial \varepsilon_{ij}} = -\sigma_{ij} \quad (5.2.9)$$

Noting that  $\sigma_{ij}^{(pq)} + \sigma_{ij}^{(pd)} = 0$  it follows that, combining Equations (5.2.8) and (5.2.9) and noting that the density is always positive

$$\sigma_{ij} \varepsilon_{ij}^{(p)} \geq 0 \quad (5.2.4, \text{bis})$$

The restrictive assumptions introduced here correspond exactly to those under which Molenkamp (1980) derived the same result, but are interpreted as defining the limited class of elastic-plastic materials for which Equation (5.2.4) holds rather than general assumptions for all elastic-plastic materials.

One of the main effects of the introduction of the additional parameter  $N$  is the alteration of the shape of undrained stress paths, particularly for heavily overconsolidated soils. Figure 5.4 shows the undrained stress paths calculated using Modified Cam-Clay for a series of tests at a single preconsolidation pressure; the parameters used are those for Speswhite Kaolin given in Table 4.1. Figure 5.5 shows the same tests if the parameter  $N = 0.8$  is introduced. The alteration of the yield locus shape has a relatively small effect on the wet side of

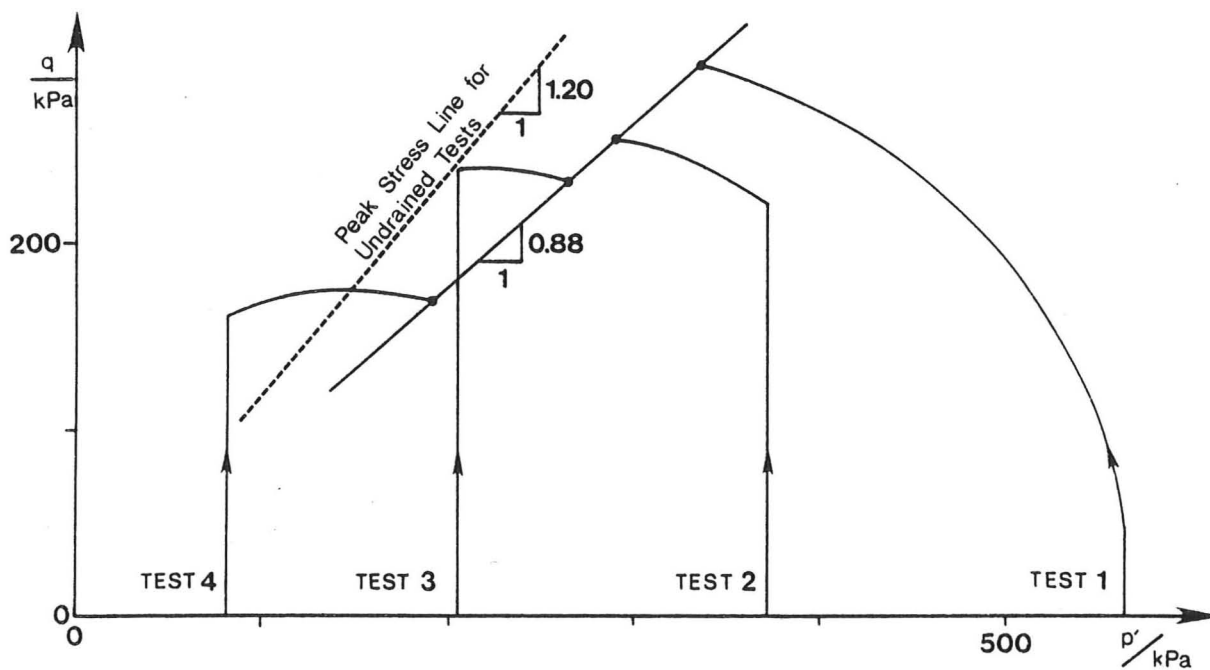


Figure 5.4 Undrained stress paths for tests 1-4 on Kaolin, modelled by Modified Cam-Clay

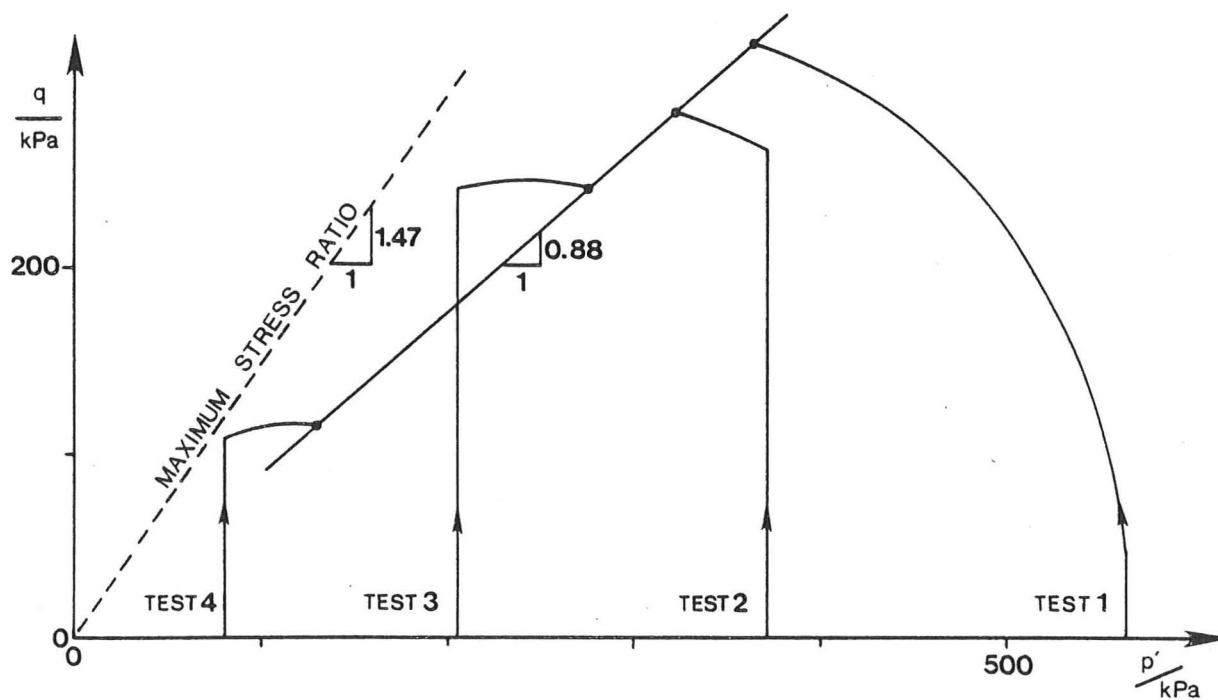


Figure 5.5 Undrained stress paths for tests 1-4 on Kaolin, modelled by material with  $N = 0.8$

critical, but causes a more noticeable effect on the dry side, giving comparatively lower strengths. At even higher overconsolidation ratios the stress paths become more curved and tangential to the maximum stress ratio line at  $\eta = M/(1-N^2)^{\frac{1}{2}}$ .

### 5.3 A Pressure Dependent Shear Modulus

The behaviour of real soils indicates that the shear modulus is not constant, but is a function of the mean effective stress, and an extensive discussion of the variation is given by Wroth et al. (1979). Zytynski et al. (1978) show that it is thermodynamically inadmissible for the shear modulus to depend on pressure unless the bulk modulus conversely depends on the shear stress. Experimental results of Namy (1970) indicate, however, that a shear modulus proportional to pressure might be appropriate. In an attempt to introduce this effect the shear modulus in Equation (4.2.1) is replaced by a term proportional to the pressure, which is given by  $\exp((v-v_p)/\kappa^*)$  :

$$\psi = \frac{1}{\rho} \left( \kappa p_r \exp((v-v_p)/\kappa^*) + \frac{3\alpha p_r}{2} \exp((v-v_p)/\kappa^*) (\epsilon - \epsilon_p)^2 + (\lambda^* - \kappa^*) p_r \exp((\ln(\Gamma/V_o) + v_p)/(\lambda^* - \kappa^*)) \right) \quad (5.3.1)$$

Clearly the more complex expression will introduce extra terms on differentiation, thus:

$$p' = p_r \exp((v-v_p)/\kappa^*) + \frac{3\alpha p_r}{2\kappa^*} \exp((v-v_p)/\kappa^*) (\epsilon - \epsilon_p)^2 \quad (5.3.2)$$

$$q = 3\alpha p_r \exp((v-v_p)/\kappa^*) (\epsilon - \epsilon_p) \quad (5.3.3)$$

It follows that:

$$\eta = \frac{3\alpha(\epsilon - \epsilon_p)}{1 + \frac{3\alpha}{2\kappa^*} (\epsilon - \epsilon_p)^2} \quad (5.3.4)$$

$$p' = p_r \exp((v-v_p)/\kappa^*) + q^2 / (6\alpha\kappa^* p_r \exp((v-v_p)/\kappa^*)) \quad (5.3.5)$$

So that contours of elastic shear strain ( $\epsilon - \epsilon_p$ ) are constant stress ratio lines, and contours of elastic volumetric strain ( $v - v_p$ ) are parabolas of the form:

$$q = 6\alpha\kappa^* p_1' (p' - p_1') \quad (5.3.6)$$

where  $p_1'$  is the intercept on the  $p'$  axis. The latter curves represent the undrained stress paths of overconsolidated samples. The contours are illustrated in Figure 5.6 together with the yield locus which is unchanged from the simple model. Note that maximum stress

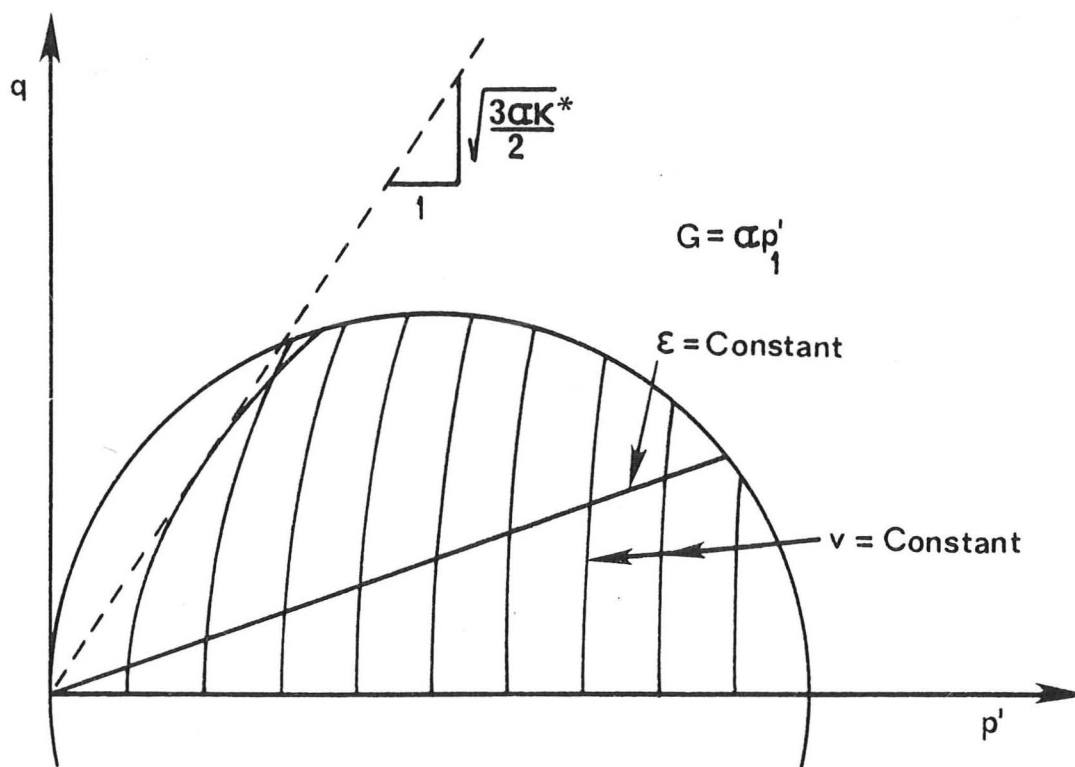


Figure 5.6 Contours of shear and volumetric strain for elastic behaviour of material with shear modulus proportional to pressure

ratio which can be achieved is  $(\frac{3\alpha\kappa^*}{2})^{\frac{1}{2}}$  and that increased shearing then reduces the stress ratio. Linked to this is the fact that the curvature of the undrained stress paths causes them to cross. These secondary effects, caused by the expected interaction between shear and volumetric behaviour, are thought to be unrealistic. Figure 5.7 shows the calculations for the same family of undrained tests as in Figure 5.4,

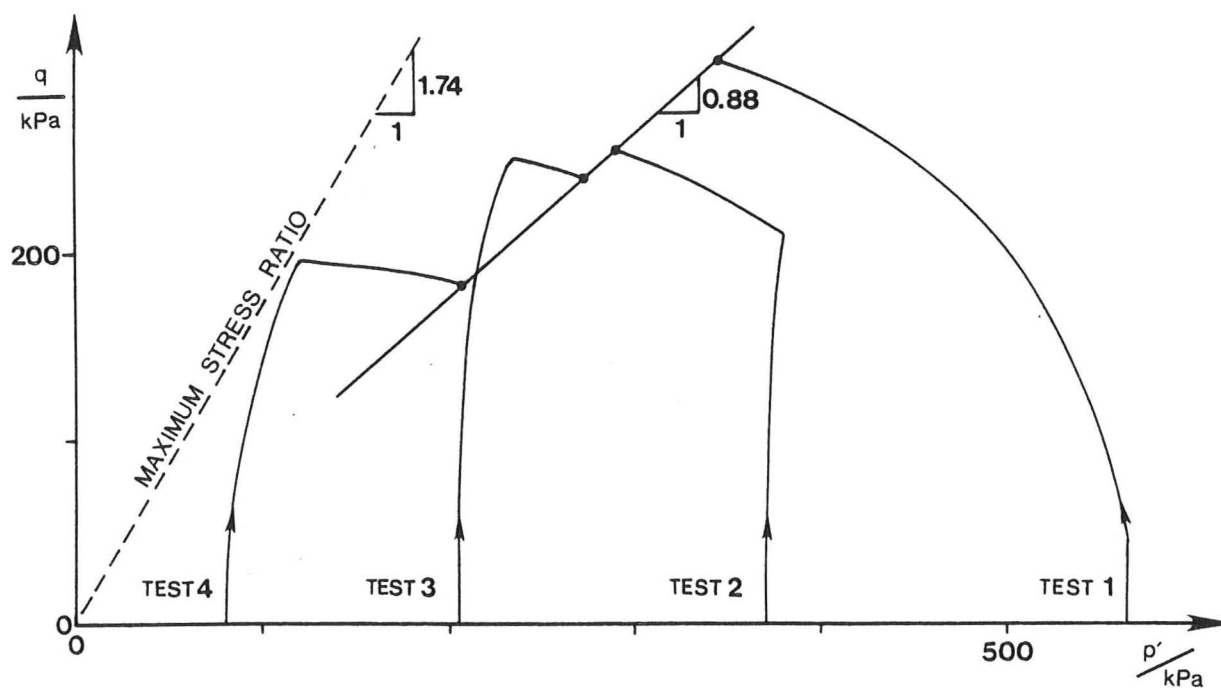


Figure 5.7 Undrained stress paths for tests 1-4, modelled with shear modulus proportional to pressure

but using a shear modulus proportional to pressure with an  $\alpha$  value of 75. The curvature of undrained stress paths is most noticeable at high overconsolidation ratios. For tests at higher overconsolidation ratios than those shown the calculation must be terminated when the maximum stress ratio is reached since the subsequent predicted behaviour is not thought to be realistic.

It is useful to note that the quantity  $\alpha\kappa^*$  represents the ratio  $G/K$  on the isotropic axis, and is related to the apparent Poisson's ratio on this axis by  $\nu = (3 - \alpha\kappa^*) / (6 + 2\alpha\kappa^*)$ .

#### 5.4 Elastic-Plastic Coupling

Although the analysis of the previous section could have been achieved using only the simpler thermodynamic concept of an elastic potential, the following results can only be obtained by making use of the new formulation. An alternative to the use of a shear modulus

proportional to pressure is to make the modulus proportional to preconsolidation pressure. This has the advantage of restoring the non-dimensionalization of all behaviour at a given overconsolidation ratio with respect to pressure, which is central to both Critical State Soil Mechanics and also the SHANSEP analysis and design procedure (Ladd and Foott (1974)). This scaling does not hold completely for a material with constant shear modulus, and, as shown in the last section, can only be introduced by a pressure dependent shear modulus at the expense of unrealistic side effects.

The model with shear modulus dependent on preconsolidation pressure represents an example of elastic-plastic coupling, in which the elastic properties are altered during plastic deformation. Thus the effect of a shear test on a lightly overconsolidated sample would show the pattern shown in Figure 5.8 on load reversal. The model is achieved by replacing the shear modulus by a term proportional to the parameter  $p'_x$  (i.e.

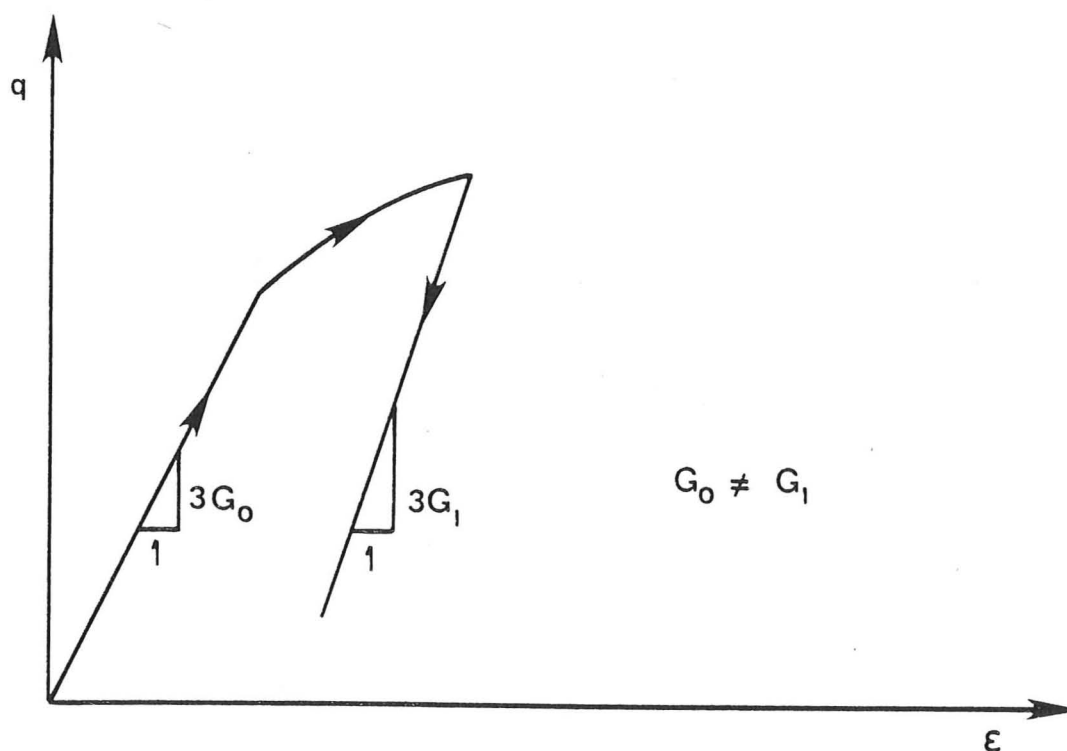


Figure 5.8 Loading and unloading of material with elastic-plastic coupling

proportional to preconsolidation pressure). The  $p'_x$  term cannot be included directly in the free energy expression, but must be expressed in terms of the kinematic parameter  $v_p$  (see Equation 4.2.7) to give the free energy expression:

$$\psi = \frac{1}{\rho} [\kappa^* p_r \exp((v-v_p)/\kappa^*) + 3\beta p_r \exp((\ln(\Gamma/V_o)+v_p)/(\lambda^*-\kappa^*))(\epsilon-\epsilon_p)^2/2 + (\lambda^*-\kappa^*) p_r \exp((\ln(\Gamma/V_o)+v_p)/(\lambda^*-\kappa^*))] \quad (5.4.1)$$

which leads to the following stress and internal force equations:

$$p' = p_r \exp((v-v_p)/\kappa^*) \quad (5.4.2)$$

$$q = 3\beta p_r \exp((\ln(\Gamma/V_o)+v_p)/(\lambda^*-\kappa^*))(\epsilon-\epsilon_p) \quad (5.4.3)$$

$$0 = -p_r \exp((v-v_p)/\kappa^*) + p_r \exp((\ln(\Gamma/V_o)+v_p)/(\lambda^*-\kappa^*)) \left(1 + \frac{3\beta(\epsilon-\epsilon_p)^2}{2(\lambda^*-\kappa^*)}\right) + p_r \exp((\ln(\Gamma/V_o)+v_p)/(\lambda^*-\kappa^*)) \dot{v}_p (\dot{v}_p + M^2 \dot{\epsilon}_p^2)^{-\frac{1}{2}} \quad (5.4.4)$$

$$0 = -3\beta p_r \exp((\ln(\Gamma/V_o)+v_p)/(\lambda^*-\kappa^*))(\epsilon-\epsilon_p) + p_r \exp((\ln(\Gamma/V_o)+v_p)/(\lambda^*-\kappa^*)) M^2 \dot{\epsilon}_p (\dot{v}_p^2 + M^2 \dot{\epsilon}_p^2)^{-\frac{1}{2}} \quad (5.4.5)$$

The incremental response may be derived as:

$$\dot{v} = \kappa^* \dot{p}/p + \dot{v}_p \quad (5.4.6)$$

$$\dot{\epsilon} = \frac{\dot{q}}{3\beta p'_x} + \dot{\epsilon}_p - \frac{q \dot{v}_p}{3\beta(\lambda^*-\kappa^*) p'_x} \quad (5.4.7)$$

The elastic response is exactly as was intended, but it is clear that  $\dot{\epsilon}_p$  is no longer the plastic strain as it is conventionally defined. The additional shear strain to the elastic component during an infinitesimal increment of plastic deformation is given by:

$$\dot{\epsilon}_i = \dot{\epsilon}_p - \frac{q \dot{v}_p}{3\beta(\lambda^*-\kappa^*) p'_x} \quad (5.4.8)$$

Since this expression cannot be integrated to give  $\epsilon_i$  in terms of the other kinematic parameters it follows that it is not possible to

re-formulate this model in an alternative way in order that the conventional plastic strain may play the role of an internal parameter.

When Equations (5.4.4) and (5.4.5) are combined to give the yield locus the result is:

$$\left(p' - p'_x - \frac{q^2}{6\beta(\lambda^* - \kappa^*)p'_x}\right)^2 + q^2/M^2 = p'^2_x \quad (5.4.9)$$

which is no longer an ellipse, but represents a slight distortion of the original shape, as illustrated in Figure 5.9. If the value of

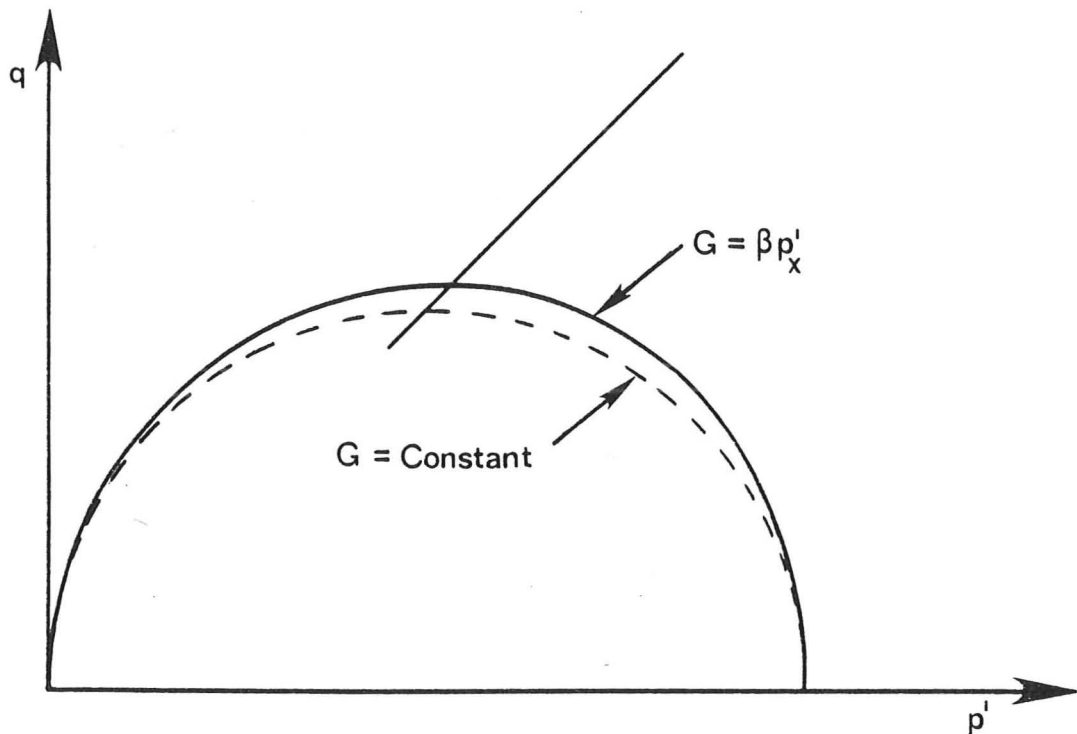


Figure 5.9 Yield locus of material with elastic-plastic coupling

$\beta(\lambda^* - \kappa^*)$  takes a sufficiently small value, the yield locus may become locally concave. Such a local concavity was anticipated by Drucker (1964) as allowable in a material satisfying his stability criterion, if there was a sufficiently strong coupling between elastic parameters and plastic deformation.

The flow rule may be derived as:

$$\dot{\epsilon}_p / \dot{v}_p = q / \left( M^2 \left( p' - p'_x - \frac{q^2}{6\beta(\lambda^* - \kappa^*)p'_x} \right) \right) \quad (5.4.10)$$

and it may be shown that although the  $(\dot{v}_p, \dot{\epsilon}_p)$  vector is no longer

normal to the yield locus the  $(\dot{v}_p, \dot{\epsilon}_i)$  vector is normal to the new locus. Thus normality of the conventionally defined plastic strain is retained. The material still obeys Drucker's stability postulate (in the hardening region) which results in the normality of conventional plastic strain increment even for the coupled case, as derived by Drucker (1964). This approach may be contrasted with the formulation of Maier and Hueckel (1977) in which it is assumed a priori that for an associated material the normality condition would apply to the quantity analogous to the  $(\dot{v}_p, \dot{\epsilon}_i)$  vector.

Noting that the critical state occurs when  $\dot{v}_p = 0$ , this occurs at a stress ratio of:

$$\eta_{cs} = M / \left( 1 + \frac{M^2}{6\beta(\lambda - \kappa)} \right) \quad (5.4.11)$$

and so the meaning of the parameter  $M$  is slightly altered in this model.

Figure 5.10 shows the undrained tests of Figure 5.4 modelled by the coupled elastic-plastic model. The only effect is a very slight change

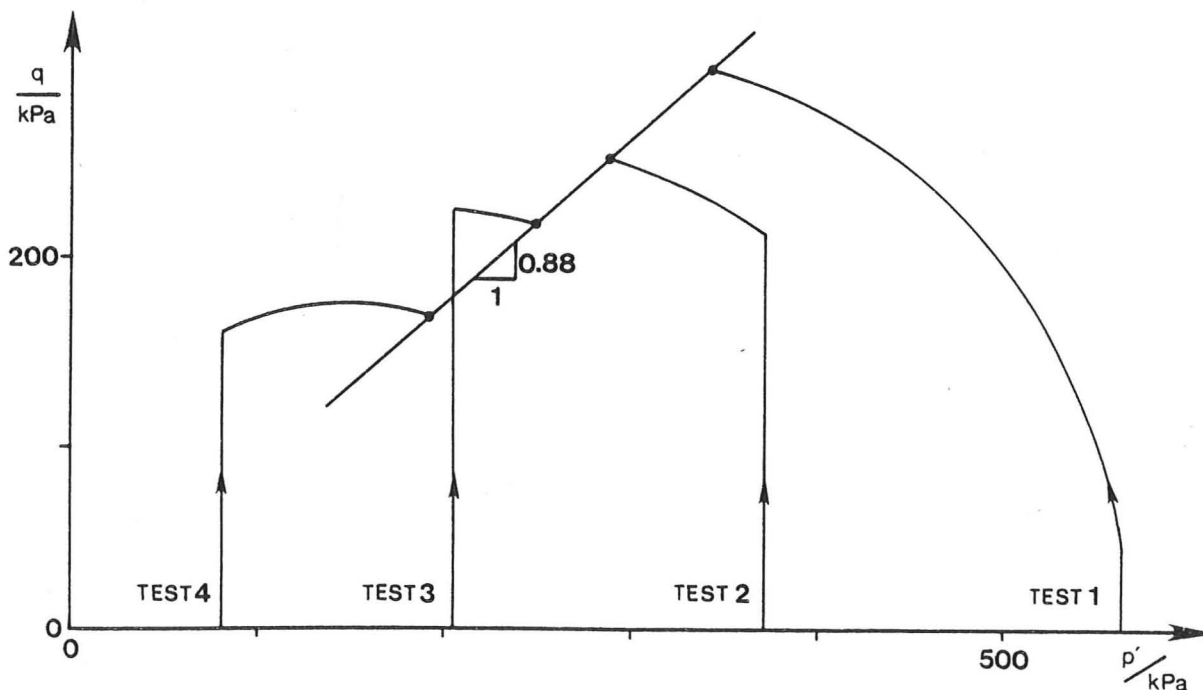


Figure 5.10 Undrained stress paths for tests 1-4, modelled by material with shear modulus proportional to preconsolidation pressure

normal to the yield locus the  $(\dot{v}_p, \dot{\epsilon}_i)$  vector is normal to the new locus. Thus normality of the conventionally defined plastic strain is retained. The material still obeys Drucker's stability postulate (in the hardening region) which results in the normality of conventional plastic strain increment even for the coupled case, as derived by Drucker (1964). This approach may be contrasted with the formulation of Maier and Hueckel (1977) in which it is assumed a priori that for an associated material the normality condition would apply to the quantity analogous to the  $(\dot{v}_p, \dot{\epsilon}_p)$  vector.

Noting that the critical state occurs when  $\dot{v}_p = 0$ , this occurs at a stress ratio of:

$$\eta_{cs} = M / \left( 1 + \frac{M^2}{6\beta(\lambda - \kappa)} \right) \quad (5.4.11)$$

and so the meaning of the parameter  $M$  is slightly altered in this model.

Figure 5.10 shows the undrained tests of Figure 5.4 modelled by the coupled elastic-plastic model. The only effect is a very slight change

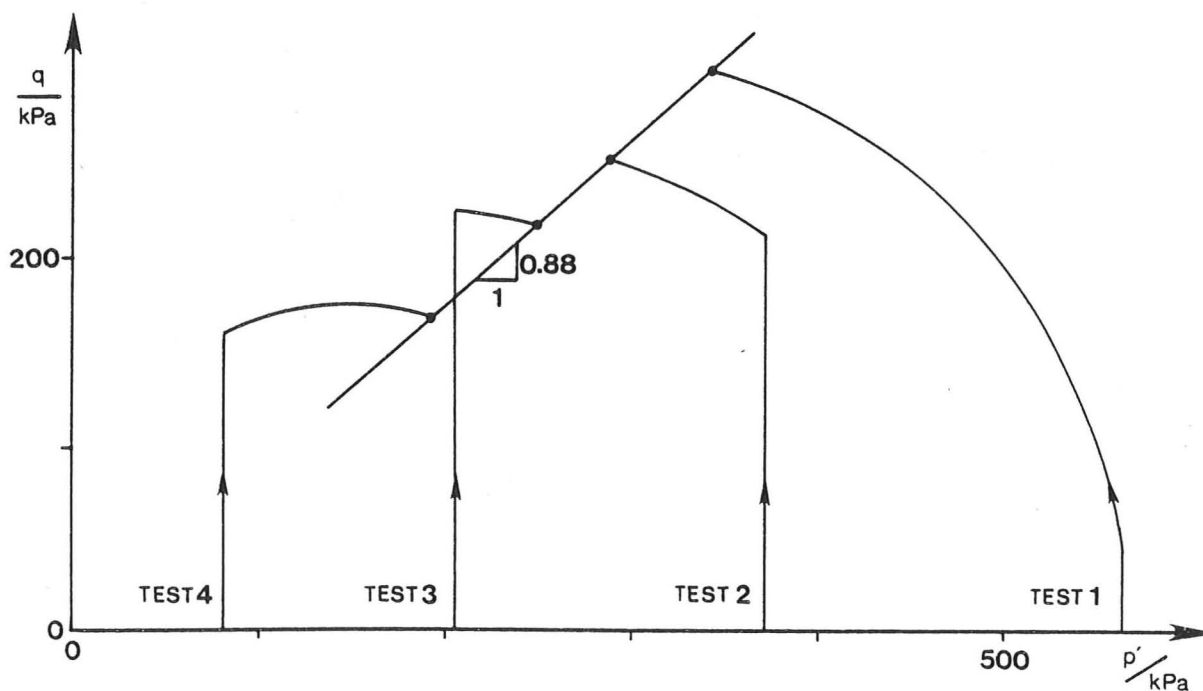


Figure 5.10 Undrained stress paths for tests 1-4, modelled by material with shear modulus proportional to preconsolidation pressure

in the plastic parts of the paths, due to the alteration of the shape of the yield locus. The effect of elastic-plastic coupling is less dramatic than the introduction of a pressure dependent shear modulus.

Although the introduction of elastic-plastic coupling has resulted in a change from the Modified Cam-Clay elliptical yield locus, it is not suggested that the use of a coupled model and the elliptical locus would necessarily be unacceptable thermodynamically. It may be possible by the use of more complex free energy and dissipation functions to generate a model which retains the elliptical locus whilst introducing coupling.

#### 5.5 Experimental Data on the Variation of the Shear Modulus of a Clay

It has been usual in the past to use either a fixed shear modulus or fixed Poisson's ratio for calculations using Modified Cam-Clay (Wroth and Zytynski (1977)), although it is recognised that the first is unrealistic and the second is theoretically unacceptable. In introducing a variable shear modulus, proportional either to pressure or preconsolidation pressure, within a rigorous thermomechanical framework it was found that the simple model was also altered by certain secondary effects. These effects depend on the form of the variation of the modulus, and their magnitude varies directly with the modulus magnitude.

The variation of the shear modulus for a clay is of importance in many practical problems. The effect of this parameter on the performance of driven piles is for instance significant, and is discussed by Randolph et al. (1979). In particular the details of the variation of the modulus with other engineering parameters are of importance. The review of Wroth et al. (1979), based on data from many materials, concludes that the ratio  $G/c_u$  (and hence  $G/p'_o$ ) is approximately constant for a normally consolidated clay, suggesting either of the

models with  $G$  proportional to  $p'$  or  $p'_c$ . The form of variation of shear modulus with overconsolidation ratio  $R$  is given in the same review as:

$$G/p'_0 = (G/p'_0)_{n.c.} (1 + C \ln R) \quad (5.5.1)$$

where  $C$  is a constant. This is not entirely consistent with either of the models, but suggests that  $G/p'$  increases with overconsolidation ratio, as would be given by a constant  $G/p'_c$  value. In this Section a series of tests are described which were specifically made to study the problem of the variation of the modulus, in order to assess which model may be most valuable.

A series of tests on Speswhite Kaolin were made at a variety of pressures and preconsolidation histories. Full details of the tests are given by Davidson (1980). Undrained triaxial compression tests were carried out at isotropic consolidation pressures of 100, 200, 400 and 570 kPa. For each of these preconsolidation pressures tests were carried out at a range of overconsolidation ratios. The results of the ten tests are summarised in Table 5.2.

The clay was one dimensionally consolidated from a slurry to  $\sigma'_v \approx 100$  kPa and cylindrical samples taken with oiled thin walled tubes of 50 mm internal diameter. After storage the samples were extruded and trimmed to 100 mm length and mounted in a conventional triaxial cell. The end plates were rough, with drainage from both ends through filter paper and a porous disc. Rotation of the top cap was prevented. The samples were isotropically consolidated in the cell and allowed to swell to the appropriate cell pressure, a back pressure of 100 kPa maintaining saturation throughout. Consolidation and swelling was in stages each of about 12 hours, with a minimum of 24 hours at the final point before shearing. Taking  $c_v = 0.18$  mm<sup>2</sup>/sec, 90% consolidation is expected in about 4 hours.

Test Number	$\frac{p'_c}{\text{kPa}}$	$\frac{p'_o}{\text{kPa}}$	$\frac{G}{\text{kPa}}$	$G/p'$	$G/p'_x$	$\frac{c_u}{\text{kPa}}$
1	570	564	30200	75.5	87.3	144
2	554	372	18600	59.2	61.0	112
3	596	205	12200	55.9	40.9	94
4	567	81	9500	105.5	33.5	65
5	408	408	16700	60.7	65.6	94
6	410	206	11800	60.8	57.6	71
7	410	102	13200	117.8	64.4	59
8	205	205	9300	71.5	70.2	45
9	205	105	7900	76.0	76.7	40
10	112	112	5200	66.6	75.7	27
Mean			13500	75.0	63.3	
Standard Deviation			7100	20.7	16.3	

Table 5.2 Undrained Triaxial Tests on Kaolin (data from Davidson(1980))

Shearing was at a constant rate of approximately 5% axial strain per hour, the load being measured by a proving ring, and a rotating bushing eliminating ram friction. Axial strain was measured by a dial gauge and corrected for apparatus stiffness, cell pressure measured by a Bourdon gauge and back pressure by an electrical transducer. During undrained shear the stress ratio  $\eta$  was continuously monitored and an unload-reload cycle executed between  $\eta = 0.6$  and  $\eta = 0.2$  in order to measure the shear modulus under standardised conditions. (Because the clay behaves in a much more complex way than the simple model the modulus varies with the magnitude of the cycle used for its determination.) A typical stress-strain curve for one of the tests is shown in Figure 5.11.

The shear modulus was defined by the slope of the line between the end points of the hysteresis loop (see Figure 5.11) and the measured values are given in Table 5.2. Also given in Table 5.2 are the values of  $G/p'$  using the mean  $p'$  value for the unload-reload cycle and of

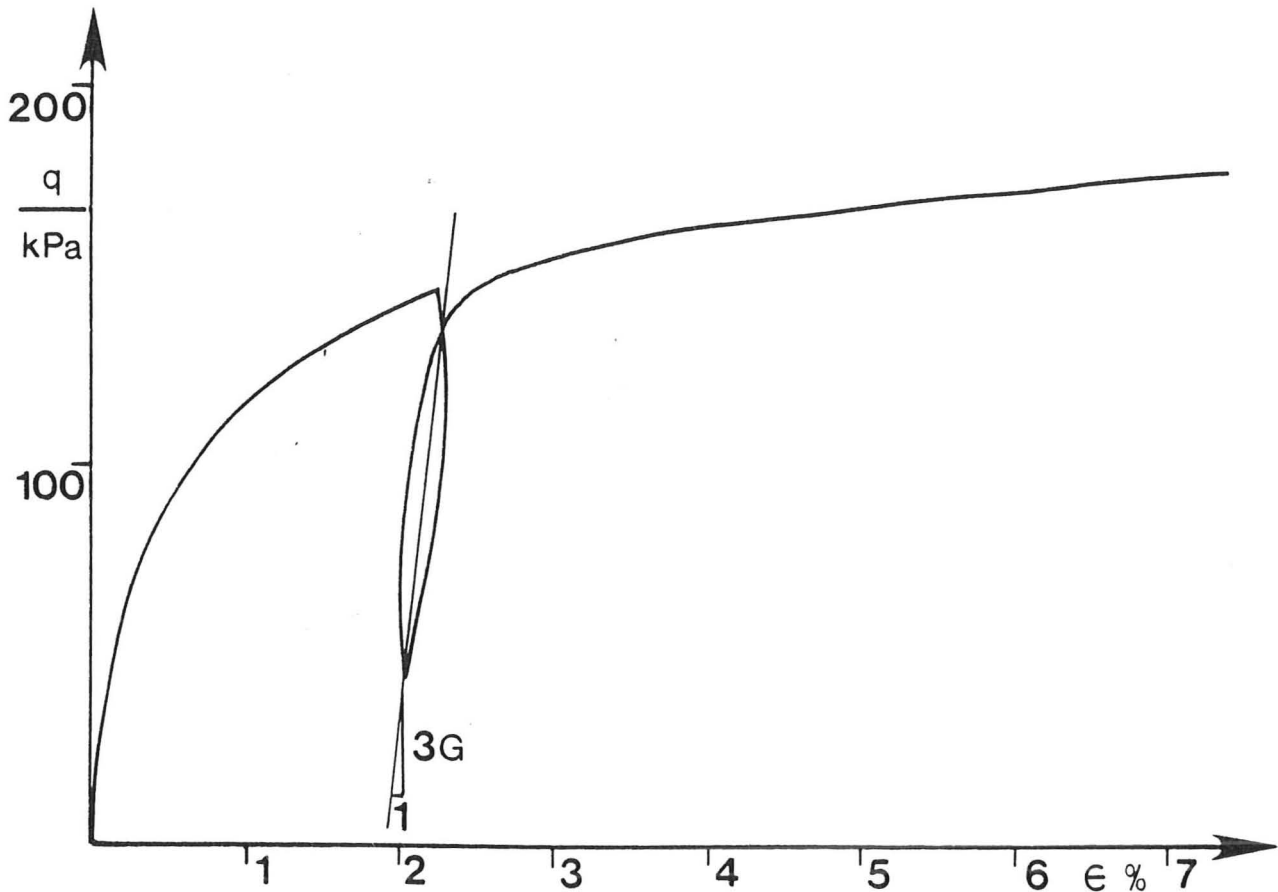


Figure 5.11 Shear stress - shear strain curve for test 3 on Speswhite Kaolin (data from Davidson (1980))

$G/p'_x$ , where  $p'_x$  is given by  $p'_c/2$  for samples with an overconsolidation ratio greater than 2. A correction is made to the  $p'_c$  value using conventional Modified Cam-Clay theory for the additional consolidation on shearing of the samples on the wet side of critical.

Examining the mean and standard deviation values of  $G$ ,  $G/p'$  and  $G/p'_x$  shows that a shear modulus proportional either to pressure or preconsolidation pressure provides a much better fit to the data than a constant shear modulus. Although the set of tests 1-4 at  $p'_c \approx 570$  kPa would seem to indicate that the modulus proportional to pressure would be more appropriate, the data do not distinguish between the two possibilities of  $G \propto p'$  or  $G \propto p'_c$ . Clearly the modulus depends on both parameters, and a Modified Cam-Clay model with both effects could be introduced. This degree of sophistication would seem unwarranted

until more detailed data are available, and may be unnecessary since the shear behaviour on unloading is not truly represented by elasticity. There is a clear indication, however, that either of the models with a variable modulus would be better than the conventional approach, and the choice may depend on the problem in hand.

The magnitude of the secondary effects of a variable shear modulus was apparent in the shapes of the undrained stress paths, and Figure 5.12 shows the experimental data for the four tests with  $p'_c \approx 570$  kPa. The shapes of the curves for the tests on the wet side of critical are as expected from conventional critical state theory, with the unload-reload section showing elastic behaviour at almost constant  $p'$  and a very distinct yield point. Comparison with calculations using Modified Cam-Clay (Figure 5.4) with the parameters for Speswhite Kaolin given in Table 4.1 shows good agreement for the normally consolidated sample but an overprediction of the strength of the overconsolidated samples.

Although it has not been derived from a thermomechanical approach, it is worthwhile also comparing the results with calculations from the original Cam-Clay model. Strength predictions for the overconsolidated samples are much better, but the undrained stress path for the normally consolidated sample is incorrect (see Figure 5.13).

Computations for the tests on Kaolin were also made using the model with a modified dissipation function incorporating the additional parameter  $N$ . There are insufficient data in this case to make an accurate estimate of the best value of  $N$ , so a value of 0.8 was arbitrarily chosen for the calculations shown in Figure 5.5. Although the effect of introducing a peak stress ratio of 1.47 is to make the behaviour in the most heavily overconsolidated case more realistic, with a lower strength, the effect of the taller, narrower elliptical yield locus is to increase the predicted strengths of the intermediate samples unrealistically.

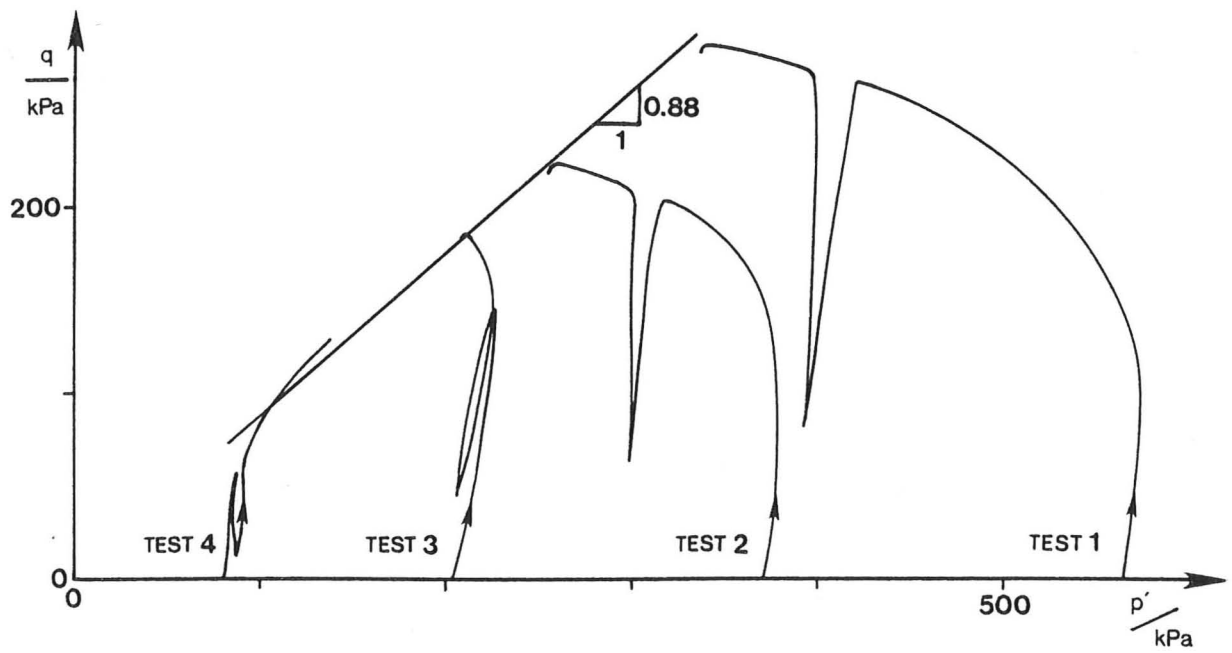


Figure 5.12 Undrained stress paths for tests 1-4 on Speswhite Kaolin

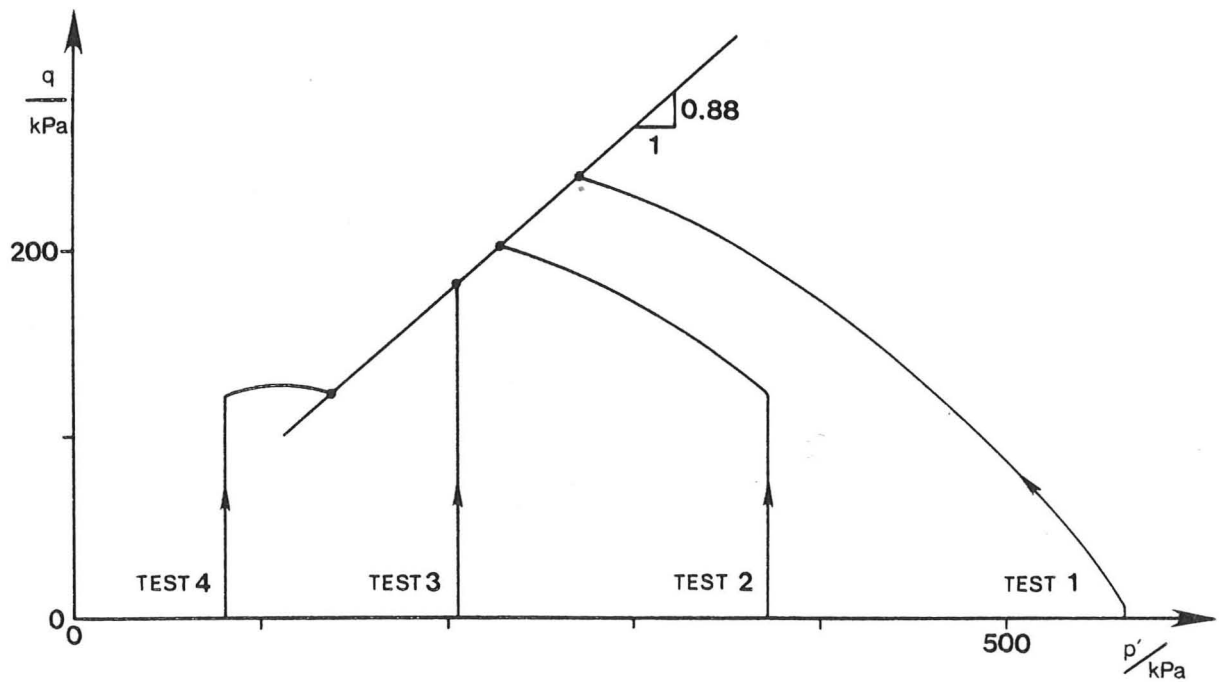


Figure 5.13 Undrained stress paths for tests 1-4, modelled by Cam-Clay

The model with a shear modulus proportional to pressure gave the curves shown in Figure 5.7. Once again the prediction for the normally consolidated sample is good. The curvature of the undrained paths is only slight, and would agree with the experimental data in which the unload-reload loops are at approximately constant  $p'$ . For the heavily overconsolidated sample the curvature results in the undrained path intersecting the yield locus at a higher point, giving a larger strength than for the simple model. The value of the quantity  $\alpha\kappa^*$  used in the modelling of the tests implies a Poisson's ratio on the isotropic line of  $-0.104$ , which is unrealistic. It should be borne in mind, however, that the model with a constant shear modulus always implies a negative Poisson's ratio at  $p'$  values less than  $G\kappa^*/1.5$  (135.0 kPa using the parameters for Speswhite Kaolin) and that with shear modulus proportional to preconsolidation pressure gives a negative value for  $p'/p'_c$  less than  $\beta\kappa^*/3$ .

Finally the curves for the model with shear modulus proportional to preconsolidation pressure are almost identical to those for Modified Cam-Clay; the secondary effects due to change in shape of the yield locus are very small (see Figure 5.10).

In summary, although the various modified models differ in detail, they generally all provide a reasonable modelling of undrained stress paths for the normally consolidated samples. For the overconsolidated samples the strengths are generally overpredicted. The variation of strength with overconsolidation ratio for Modified Cam-Clay is given by:

$$c_u/p'_o = (p'_c/p'_o) \frac{M}{2^{\Lambda+1}} \quad (5.5.2)$$

where  $\Lambda = (\lambda^* - \kappa^*)/\lambda^*$ , for samples on the wet side of critical. For samples on the dry side the peak  $q$  occurs before the critical state (on the broken line in Figure 5.4) and this results in a small increase in  $c_u$  from Equation (5.5.2): only a 3.5% increase is given for

$\Lambda = 0.77$  , the value used for Speswhite Kaolin.

Figure 5.14 shows the variation of  $c_u/p'_0$  with overconsolidation ratio, showing a straight line correlation in agreement with Equation (5.5.1). The best fit to the data would be given by  $\Lambda = 0.64$  and  $M = 0.73$ , as compared with  $\Lambda = 0.77$  which is derived from consolidation data on Speswhite Kaolin from other sources and  $M = 0.88$  which was derived from the final stress ratios in the tests on normally consolidated samples. A better overall fit to the shapes of the undrained paths and the strength values could have been achieved using the alternative parameters, but this would yield an unjustifiably favourable impression of the models since it is making use of information which may not be directly available to an engineer: in practice  $M$  and  $\Lambda$  would be determined as in this case.

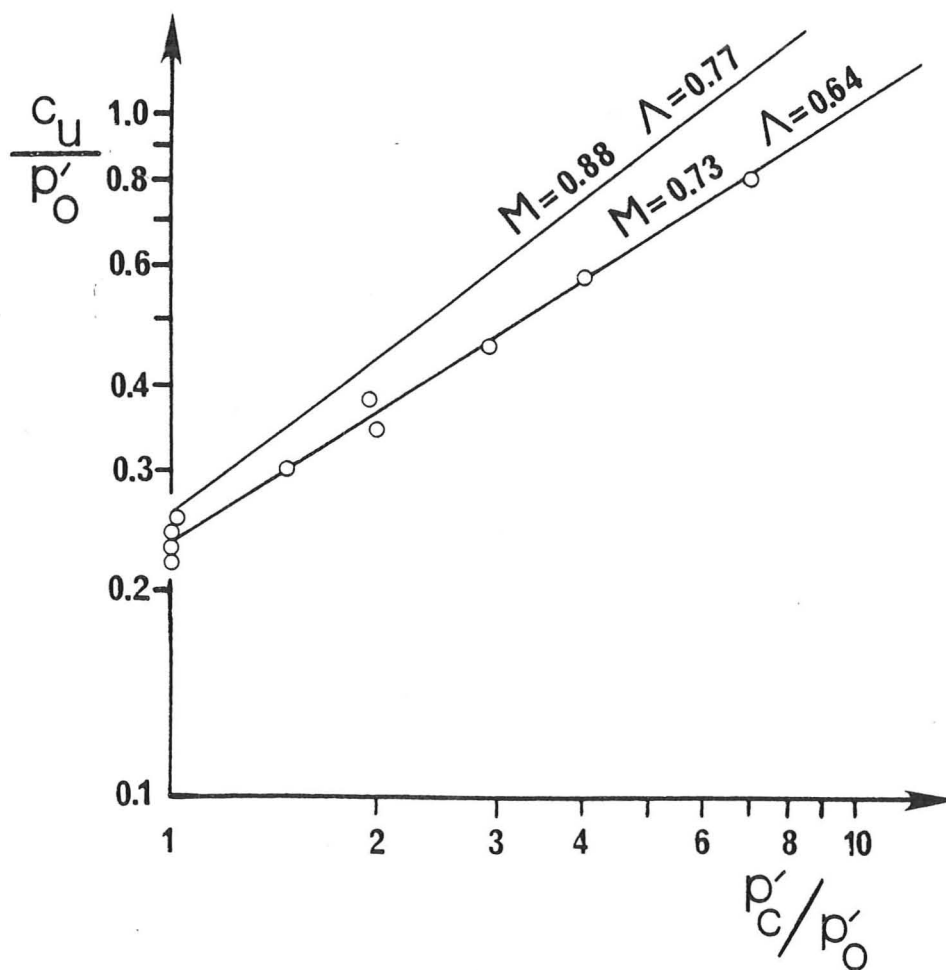


Figure 5.14 Variation of normalised undrained shear strength with overconsolidation ratio, Speswhite Kaolin

Allied to the problem of overestimation of the strength of overconsolidated samples is the overestimation of their stiffness. All the models imply an initial purely elastic response, usually to peak strength. Figure 5.15 for instance shows the modelling using Modified Cam-Clay of tests 1-4, which may be compared with Figure 5.11 for test 3. In practice overconsolidated samples yield much earlier than the models predict.

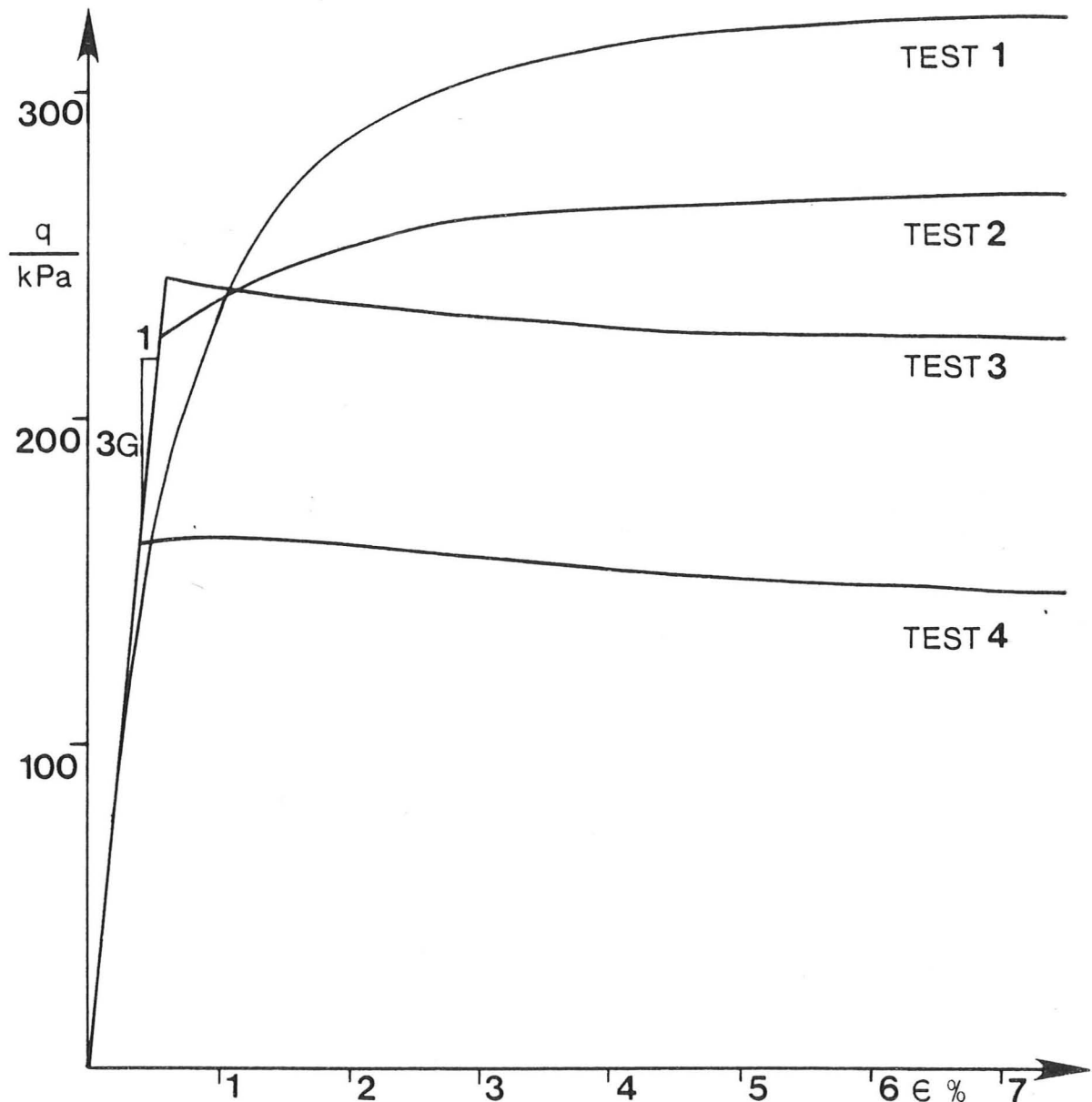


Figure 5.15 Shear stress - shear strain curves for tests 1-4, modelled by Modified Cam-Clay

The Cam-Clay family of theoretical models are known to fit the broad behaviour of soft clays well. In this Chapter it has been shown that although certain aspects of clay behaviour may be modelled well

within a rigorous thermomechanical framework, there are many aspects of clay behaviour which are not included even in the more sophisticated models. In the next Chapter further features of clay behaviour which are not accommodated in the present thermomechanical approach will be examined.

## CHAPTER 6

## FURTHER ASPECTS OF THE BEHAVIOUR OF CLAYS

There are aspects of soil behaviour with important practical significance which have not yet been accommodated within the thermomechanical framework used in the last three Chapters. Two of these topics are, however, considered as too important to omit, and are therefore discussed here in terms of conventional plasticity theory. The first topic is that of the generalisation of yield loci to stress states not accessible in the triaxial test, and the second is the development of plastic anisotropy and its dependence on stress history.

6.1 Generalisation of Yield Loci in the Octahedral Plane

The models which have been described in the previous Chapters have all been based on data derived from the triaxial test, and so refer only to the limited stress conditions which may be attained in this test. In Section 4.4 a generalisation of Modified Cam-Clay to fully general stress states was given, with this simply being derived by substituting appropriate invariant functions of the strains and internal variables in the isotropic and deviatoric terms in the original triaxial model. This generalisation is not, however, unique: several different general models could all reduce to the same model in the triaxial plane. In this Section some alternative generalisations will be discussed.

One way of representing the generalisation of a plasticity model to states other than those in the triaxial test is by the shape of a section of the yield locus in principal stress space ( $\sigma'_1, \sigma'_2, \sigma'_3$ ) at constant mean pressure  $p'$ . The shape is usually shown projected onto the "octahedral plane", which is the plane in principal stress space perpendicular to the space diagonal  $\sigma'_1 = \sigma'_2 = \sigma'_3$ . In this plane the three principal stress axes are seen as  $120^\circ$  apart (Figure 6.1). The generalisation used in Section 4.4 gives a circular section, as does the Von Mises yield locus. The failure points of soils tested at intermediate values of  $\sigma'_2$  between

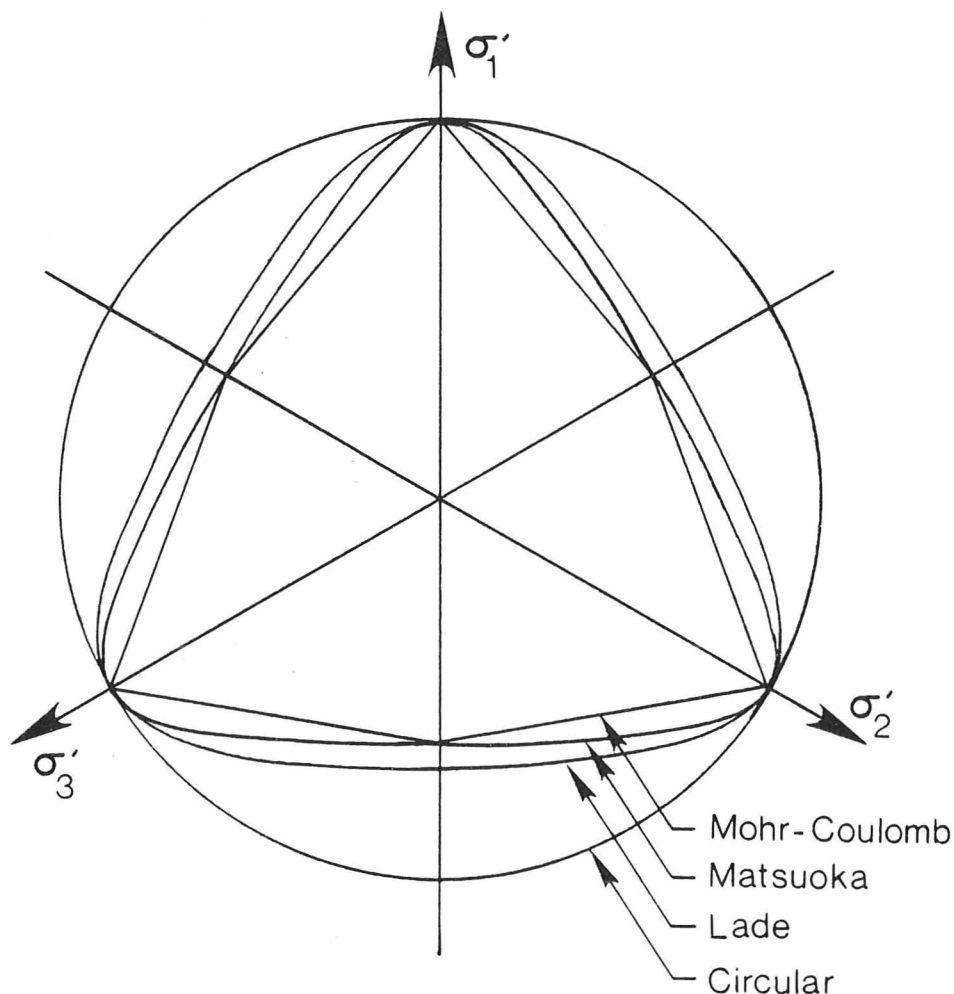


Figure 6.1 Generalisation of failure criteria in the octahedral plane for  $\phi' = 40^\circ$  in triaxial compression

triaxial compression and extension show a variation which approximates more closely to the Mohr-Coulomb criterion (an irregular hexagon in the octahedral plane) than the circular section (see e.g. Pearce (1970)). A curvilinear triangle, approximating to the Mohr-Coulomb hexagon, but passing outside it at intermediate  $\sigma'_2$  values if chosen to coincide at triaxial compression would seem to offer the best overall approximation.

It may be expected that the shape of the yield locus will be similar to that of the failure envelope, and so the alternative shapes will first be introduced as failure criteria. The envelope of failure points for a cohesionless granular material plots on an approximately conical or pyramidal surface in principal stress space, the section of the cone specifying the octahedral generalisation. The "extended" Von Mises

criterion for instance gives a circular cone and may be expressed in terms of stress invariants as:

$$\sigma'_{(2)}/\sigma'^2_{(1)} = \text{Constant} \quad (6.1.1)$$

Many authors have suggested different shapes for such a curve, but the simplest and potentially most useful are those due to Lade and Duncan (1975) and Matsuoka and Nakai (1974). Lade's criterion, which he has also used as a yield surface, may be expressed as the function:

$$\sigma'_{(3)}/\sigma'^3_{(1)} = \text{Constant} \quad (6.1.2)$$

For low equivalent friction angles the section approximates to a circle, and at very high angles it approaches an equilateral triangle. The curve for a given friction angle in triaxial compression passes slightly outside the Mohr-Coulomb hexagon in triaxial extension (see Figure 6.1).

The Matsuoka generalisation is based on reasoning about the significance of the "Spatially Mobilised Plane", a concept which is not discussed further here. It results in a failure surface of the form:

$$\sigma'_{(3)}/(\sigma'_{(1)}\sigma'_{(2)}) = \text{Constant} \quad (6.1.3)$$

which is found to bear exactly the same mathematical relationship to the Mohr-Coulomb cohesionless criterion as the Von Mises surface to the Tresca; i.e. it may be represented as a curve passing through the apices of the irregular Mohr-Coulomb hexagon (see Figure 6.1).

As a brief excursion from the main theme of this Section, this observation leads to the suggestion of a more general form of failure criterion, expressed most conveniently in terms of principal stresses as:

$$\frac{(\sigma'_1 - \sigma'_2)^2}{(c + \sigma'_1 \tan \phi)(c + \sigma'_2 \tan \phi)} + \frac{(\sigma'_2 - \sigma'_3)^2}{(c + \sigma'_2 \tan \phi)(c + \sigma'_3 \tan \phi)} + \frac{(\sigma'_3 - \sigma'_1)^2}{(c + \sigma'_3 \tan \phi)(c + \sigma'_1 \tan \phi)} = 8 \quad (6.1.4)$$

which may be compared with the Mohr-Coulomb criterion with friction and

cohesion which may be written for  $\sigma'_1 > \sigma'_2 > \sigma'_3$  as:

$$\frac{(\sigma'_1 - \sigma'_3)^2}{(c + \sigma'_1 \tan \phi)(c + \sigma'_3 \tan \phi)} = 4 \quad (6.1.5)$$

If  $\phi = 0$  is inserted in Equations (6.1.4) and (6.1.5) the Von Mises and Tresca conditions are given; if  $c = 0$  is substituted the Matsuoka and cohesionless Mohr-Coulomb criteria result.

The main difference between the shapes suggested by Lade and Matsuoka is that whilst Matsuoka's gives the same equivalent angle of friction at both triaxial compression and extension, Lade's gives a slightly higher angle in extension. Evidence in favour of both has been obtained, and it is likely that neither is capable of modelling the failure of all soils. Both give a considerably better approximation than the circular generalisation and both give a slightly higher angle of friction at intermediate  $\sigma'_2$  values (e.g. under plane strain conditions) than at triaxial compression.

Although the non-circular generalisations have not been studied in the context of the thermomechanical method, the Matsuoka criterion may be derived from the thermomechanical approach, and it is worthwhile examining the functions which lead to it. In terms of principal strains the Von Mises criterion results from a dissipation function:

$$\rho \phi = \frac{2\sqrt{2}}{3} c ((\dot{\epsilon}_1^P - \dot{\epsilon}_2^P)^2 + (\dot{\epsilon}_2^P - \dot{\epsilon}_3^P)^2 + (\dot{\epsilon}_3^P - \dot{\epsilon}_1^P)^2)^{\frac{1}{2}} \quad (6.1.6)$$

The simplest extension to a frictional type of behaviour involves replacing  $c$  with a term proportional to pressure, and after substitution of the stresses into the dissipation expression the "extended Von Mises" criterion may be derived from a function of the form:

$$\rho \phi = \frac{\sqrt{2}M}{9} (\sigma'_1 + \sigma'_2 + \sigma'_3) ((\dot{\epsilon}_1^P - \dot{\epsilon}_2^P)^2 + (\dot{\epsilon}_2^P - \dot{\epsilon}_3^P)^2 + (\dot{\epsilon}_3^P - \dot{\epsilon}_1^P)^2)^{\frac{1}{2}} \quad (6.1.7)$$

It may be expected, however, that each of the dissipation components of the form  $(\dot{\epsilon}_1^P - \dot{\epsilon}_2^P)^2$  may depend on the stresses in a different way rather than simply a uniform multiplication by the pressure. In particular

the  $(\dot{\epsilon}_1^P - \dot{\epsilon}_2^P)^2$  term may be expected to depend on  $\sigma_1'$  and  $\sigma_2'$  but not  $\sigma_3'$  (following similar reasoning to that used in derivation of the Mohr-Coulomb criterion). The Matsuoka criterion may be derived from a dissipation function of the form:

$$\rho\phi = \frac{2\sqrt{2}}{3} \text{Tan}\phi (\sigma_1'\sigma_2'(\dot{\epsilon}_1^P - \dot{\epsilon}_2^P)^2 + \sigma_2'\sigma_3'(\dot{\epsilon}_2^P - \dot{\epsilon}_3^P)^2 + \sigma_3'\sigma_1'(\dot{\epsilon}_3^P - \dot{\epsilon}_1^P)^2)^{\frac{1}{2}} \quad (6.1.8)$$

which suggests that the reason that soils exhibit the non-circular failure criterion may be connected to the fact that the rate of dissipation on individual sliding planes is related directly to the stresses on the planes and not simply to the mean pressure.

Since the failure conditions for clays (and sands) are known to be better represented by the above curves, it is worthwhile exploring whether these may be combined with the Modified Cam-Clay model to achieve better modelling of clays. The combination has not been achieved within the framework of the thermomechanical method, but has been made in terms of conventional plasticity theory. Since the models involve associated flow rules it is not thought that any thermodynamic principle is violated.

The yield locus in the triaxial plane ( $\sigma_2' = \sigma_3'$ ) may be extended by non-circular shapes in one of two ways. The curvilinear triangle may be determined for a particular friction angle (e.g. the critical state angle) and the whole of the locus generalised by taking every constant  $p'$  section as this shape. The alternative is to generalise each point on the triaxial compression locus by the shape appropriate to the stress ratio at that point. The latter possibility is not only less arbitrary but also has the advantage that it preserves *isotropy* (in the sense defined by Il'iushin (1960)) near the isotropic axis; a result supported by the evidence of Pearce (1970).

If any of the stresses become tensile then both the Matsuoka and Lade shapes are unrealistic in that the loci become concave. The Modified Cam-Clay locus cannot therefore be generalised directly using

the second method above if this problem is to be avoided. (In the region in triaxial compression where the stress ratio  $\eta$  is greater than 3.0 the minor stress is tensile). It is therefore convenient first to modify the locus to eliminate a tensile region, this may be achieved by altering the Modified Cam-Clay ellipse so that it becomes tangential to a line of slope 3.0 at the origin in stress space (Figure 6.2). The resulting

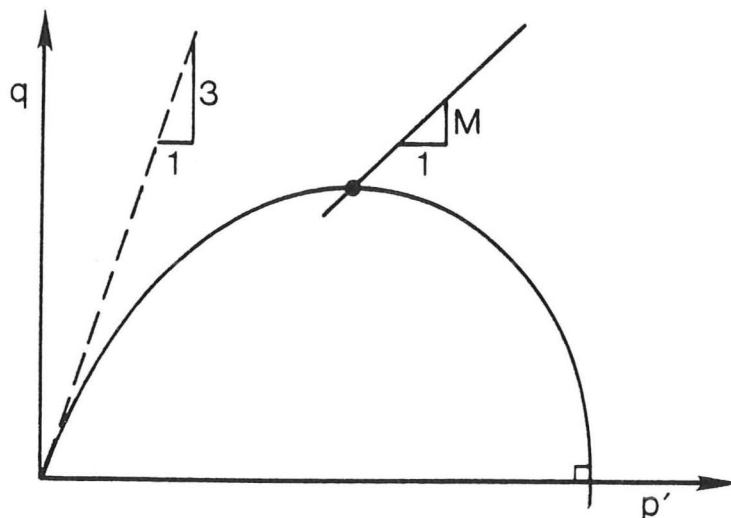


Figure 6.2 The No-Tension Ellipse yield Locus

locus, which is a part of an ellipse in the compression side of the triaxial plane, will be referred to as the No Tension Ellipse.

A flatter slope than 3.0 could be chosen, but that of 3.0 keeps the new models closest to the original. Support for a plastic potential tangential to the tensile region at very low stress comes from two sources. The first is from the integration of the stress-dilatancy flow rule (Rowe (1962)) which fits the behaviour of dense granular materials well, and gives a plastic potential tangential to the tensile region as  $p'$  approaches zero. The second source is experimental data for the flow of soft rocks correlated by Gerogiannopoulos and Brown (1978). Soft rocks may be expected to behave very like heavily overconsolidated clays, and excluding two intact marbles from the list of eleven materials studied by Gerogiannopoulos and Brown, the average slope of the plastic potential at the origin was 3.10 (range 2.76 - 3.94).

The No Tension Ellipse has been generalised by the circular, Lade and Matsuoka shapes and implemented using the program described in Section 5.1. In each case no extra parameters are required, the yield locus shape being entirely defined by the critical state parameter  $M$ . Apart from the change in the shape of the yield locus (and its associated plastic potential) the models are exactly the same as Modified Cam-Clay.

The effect of the change in the shape of the yield locus in the octahedral plane is twofold. The first, and most obvious, result is the variation of shear strength with the parameter  $b$  (defined as  $(\sigma_2 - \sigma_3)/(\sigma_1 - \sigma_3)$  and ranging from 0.0 in triaxial compression to 1.0 in extension). The failure points for a series of tests at different  $b$  values and three pressures on Champlain Sea Clay (Yong and Silvestri (1977)) are shown on Figure 6.3. Modelling of the tests using Modified Cam-Clay and the properties given in Table 4.1, together with

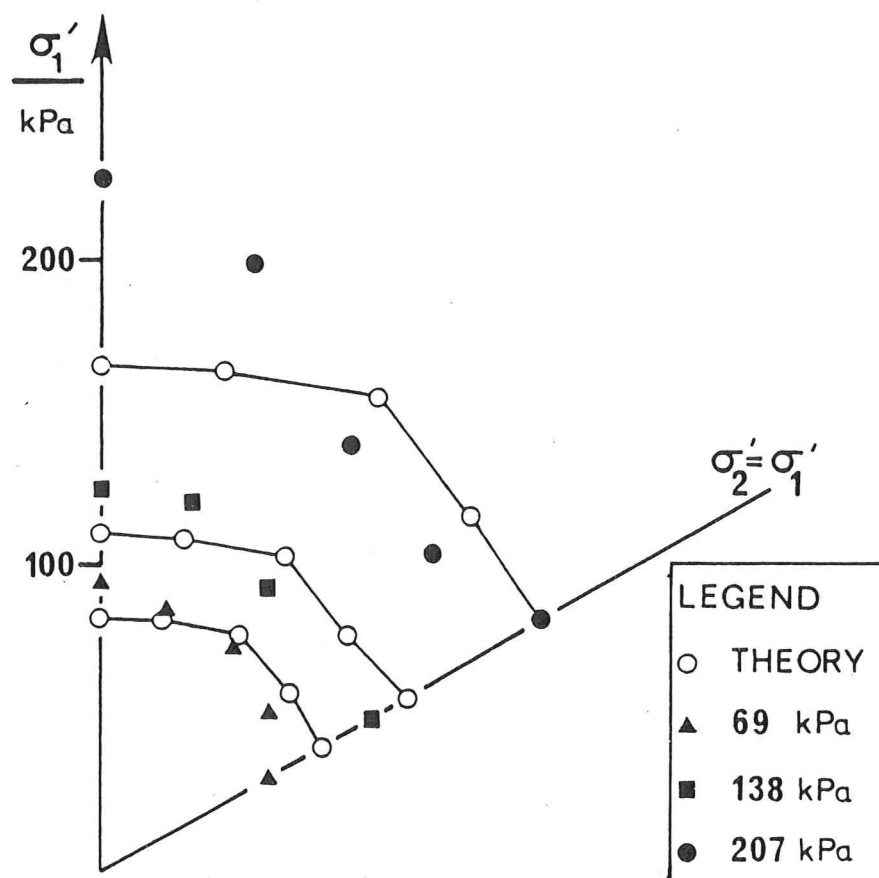


Figure 6.3 Failure points for Champlain Sea Clay, modelled by Modified Cam-Clay

$p'_c = 152$  kPa (Wroth and Houlsby (1980)) fits the average strength at each pressure well, but does not give the correct variation with  $b$ . Figure 6.4 shows modelling of the same tests with the No Tension Ellipse and Matsuoka generalisation (using  $M = 1.4$  and  $p'_c = 124$  kPa); the

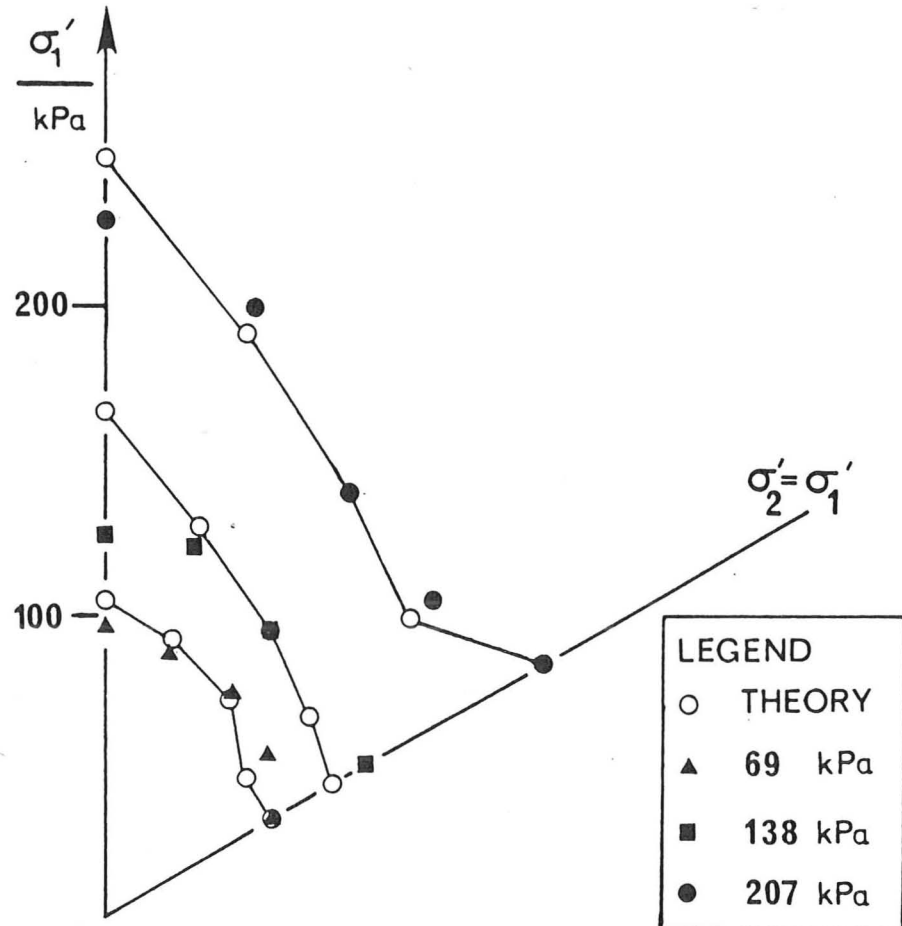


Figure 6.4 Failure points for Champlain Sea Clay, modelled by No Tension Ellipse (Matsuoka generalisation)

variation of strength with  $b$  value is much better fitted by this model. (The irregular pattern of strength variation arises because the tests were made using large loading increments, which were also modelled in the theoretical calculations.) A sufficiently accurate modelling of this variation is important since strengths measured in triaxial compression tests are frequently used in the analysis of problems involving plane strain or other shearing modes.

The second effect of the change of the generalisation is to alter the flow rule, giving different ratios between the plastic strain

components on shearing at any given  $b$  value. A converse effect is that when strain rate ratios are fixed, for instance under  $\sigma_1 = \sigma_3$  plane strain conditions, the flow rule affects the stress ratios. A series of undrained plane strain tests on Boston Blue Clay were reported by Ladd et al. (1971). The samples were one dimensionally consolidated to a maximum pressure of  $\sigma'_{1\max} \approx 400$  kPa, then allowed to swell to over-consolidation ratios  $(\sigma'_{1\max} / \sigma'_1)$  of 1, 2 and 4 before shearing. Figure 6.5 shows the stress paths in  $(s', t)$  space for tests A-6 (OCR = 1), A-8 (OCR = 2) and P-10 (OCR = 1). The last test, which was sheared by

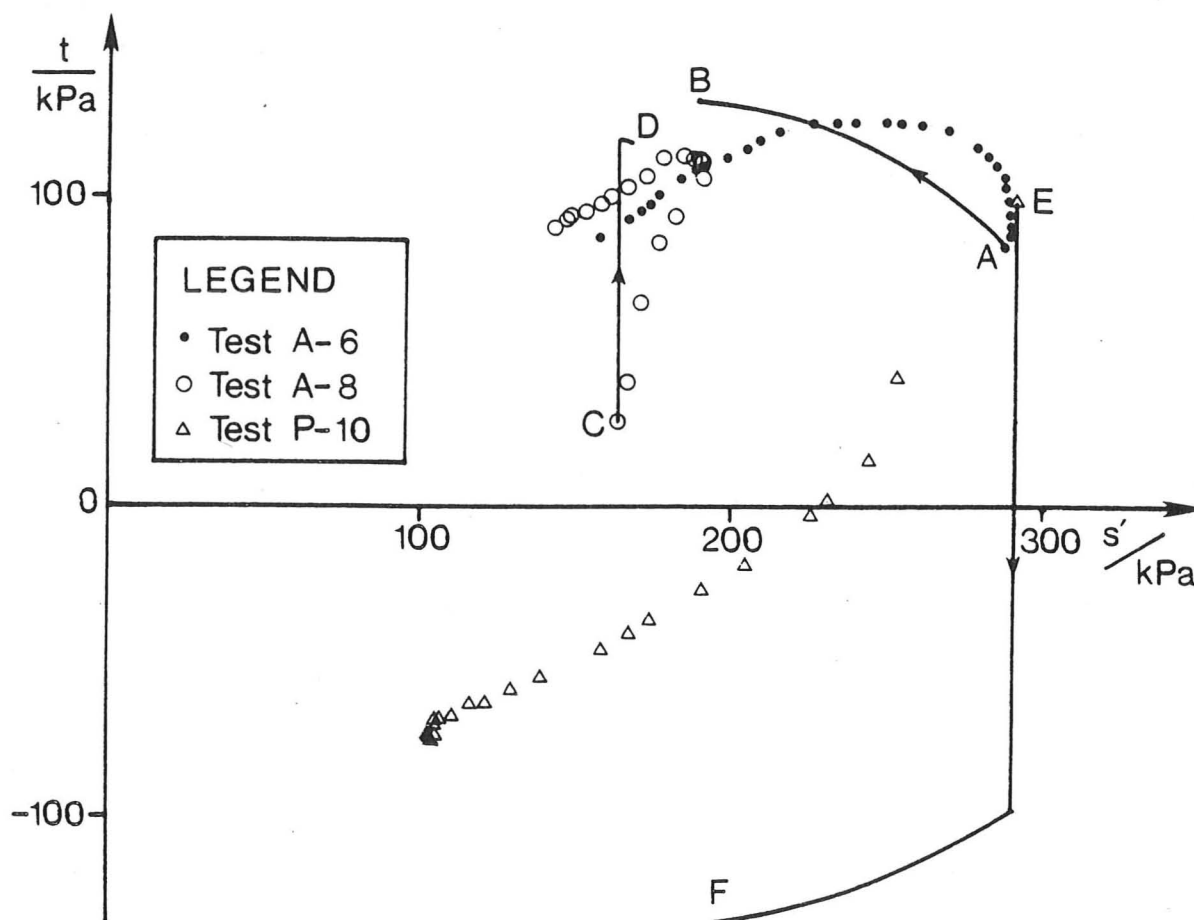


Figure 6.5 Stress paths for plane strain undrained tests on Boston Blue Clay (data from Ladd et al. (1974))

reduction of  $\sigma'_1$ , will be discussed later. The stress paths modelled by Modified Cam-Clay are also shown in Figure 6.5, giving a reasonable fit for tests A-6 and A-8, except for the overestimation of strength due to the use of the circular generalisation with parameters derived from



G to E, also terminating at too high a value of  $b$ . In each case the final  $b$  value is 0.5, i.e.  $\sigma_2' = (\sigma_1' + \sigma_3')/2$ , and this is true for all models with circular generalisations as the critical state is approached. In practice the  $\sigma_2'$  value is rather lower: the Lade generalisation of the No Tension Ellipse (path AF for test A-6 and CHF for test A-8) predicts the development of the  $\sigma_2'$  value more accurately, with a  $b$  value of approximately 0.22 at the end of the tests.

## 6.2 Anisotropy and the Effect of Stress History

The modelling of test P-10 (see Figure 6.5) by Modified Cam-Clay is grossly in error, in that the predicted elastic stress path at constant  $p'$  is quite unlike the actual curved stress path, which is more characteristic of a plastically deforming material on the wet side of critical. This behaviour is typical of a one dimensionally consolidated material, and is also observed in triaxial tests. The conclusion is that the yield locus for a one dimensionally consolidated soil is anisotropic, i.e. not centred on the  $p'$  axis. Tests reported by Mitchell (1970) indicate for instance a yield locus for a natural clay as an approximately ellipsoidal shape rotated so that it is more nearly centred on the  $K_0$  line rather than the isotropic axis.

As well as affecting the yield locus, the consolidation history also affects the plastic potential. Lewin (1973) carried out a series of tests on slate dust with various types of consolidation history. The first series of tests involved consolidation at various constant  $\eta$  values; ignoring the small elastic strains the strain rate ratios imply a plastic potential similar to (but less pointed than) the Modified Cam-Clay ellipse. A second series involved an initial constant  $\eta$  consolidation at  $\eta = -0.369, 0.0$  or  $0.546$  (cf.  $\eta$  at the critical state of 1.044) followed by a change of stress ratio and a further consolidation at the new  $\eta$  value. In each case the strain rate ratios

during the second consolidation phase imply an approximately ellipsoidal plastic potential centred on the first constant stress ratio line. The rotation was sufficient that in some cases a negative plastic shear strain could occur at a positive stress ratio (less than the stress ratio for the first consolidation). Clearly the plastic potential depends on the stress history.

The type of behaviour described above involves a combination of isotropic and kinematic hardening which allows anisotropy to change and develop with stress history. It is not obvious how this may best be accommodated within the thermomechanical framework, and in particular quantitative information is lacking. The following explanation in terms of the Cam-Clay model offers, however, some explanation of the process which must be described.

The Cam-Clay locus consists of two parts which are obtained by integrating a work equation for the cases  $\dot{\epsilon} > 0$  and  $\dot{\epsilon} < 0$ . The conventional model is obtained by assuming that  $\dot{\epsilon} > 0$  applies for  $q > 0$  and  $\dot{\epsilon} < 0$  for  $q < 0$ , resulting in the bullet shaped locus centred on the isotropic axis (Figure 6.7(a)). Ohta and Wroth (1976)

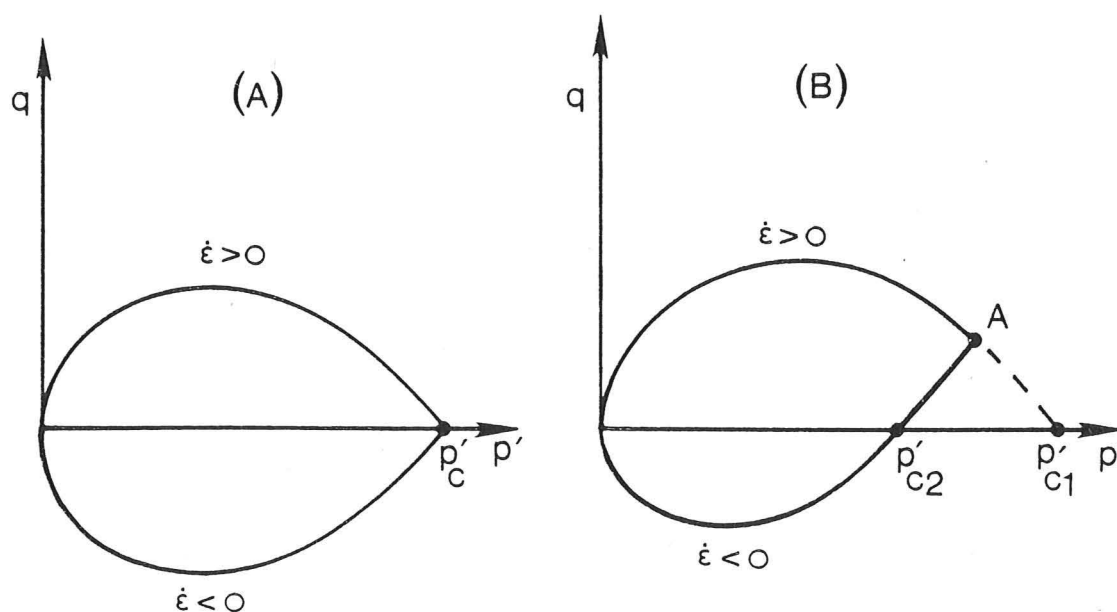


Figure 6.7 Isotropic and anisotropic Cam-Clay yield loci

describe a similar model in which the locus is centred on the one dimensional consolidation line, by assuming  $\dot{\epsilon} < 0$  for  $\sigma'_3/\sigma'_1 > K_0$  (see Figure 6.7(b)). No suggestion is made, however, as to how the anisotropy could develop with subsequent loading. If the compression and extension loci are treated as independent loci with preconsolidation pressures  $p'_{c1}$  and  $p'_{c2}$  on Figure 6.7(b), then any constant  $\eta$  consolidation (e.g. to A) will result in a pointed yield locus centred on that constant  $\eta$  line. The trend of behaviour given by this simple model is the same as that observed by Lewin, but in detail the model is not correct. The alteration of the flow rule is not as dramatic as suggested by the sudden change from the compression to the extension locus.

The above model raises the question as to whether a particular stress history may cause a pointed yield locus to develop. The undrained tests A-6 and P-10 on Boston Blue Clay suggest a pointed locus in that both compression and extension result in plastic strain. This question may be partly resolved by a series of tests on slate dust reported by Lewin and Burland (1970). Four series of samples were consolidated at constant stress ratio to four  $\eta$  values, all at  $p' = 142$  kPa. Each sample in each series was then subjected to a different small stress probe of fixed length in stress space. (Stress probe tests are discussed in detail in the next Chapter.) The strains were measured during the probes and are shown in Figure 6.8 plotted against the direction of the probe in stress space.

For a range of increment directions the strains are very small, indicating a very stiff elastic response. If the yield locus is smooth, then larger plastic strains will be measured over a range of stress increment directions of  $180^\circ$  (Figure 6.9(a)), if it is pointed the large strains will occur for a larger angle. <sup>(Figure 6.9(b))</sup> The four curves on each of the plots in Figure 6.8 show the calculated response, using Modified Cam-Clay with the parameters for Slate Dust given in Table 4.1, for each of the

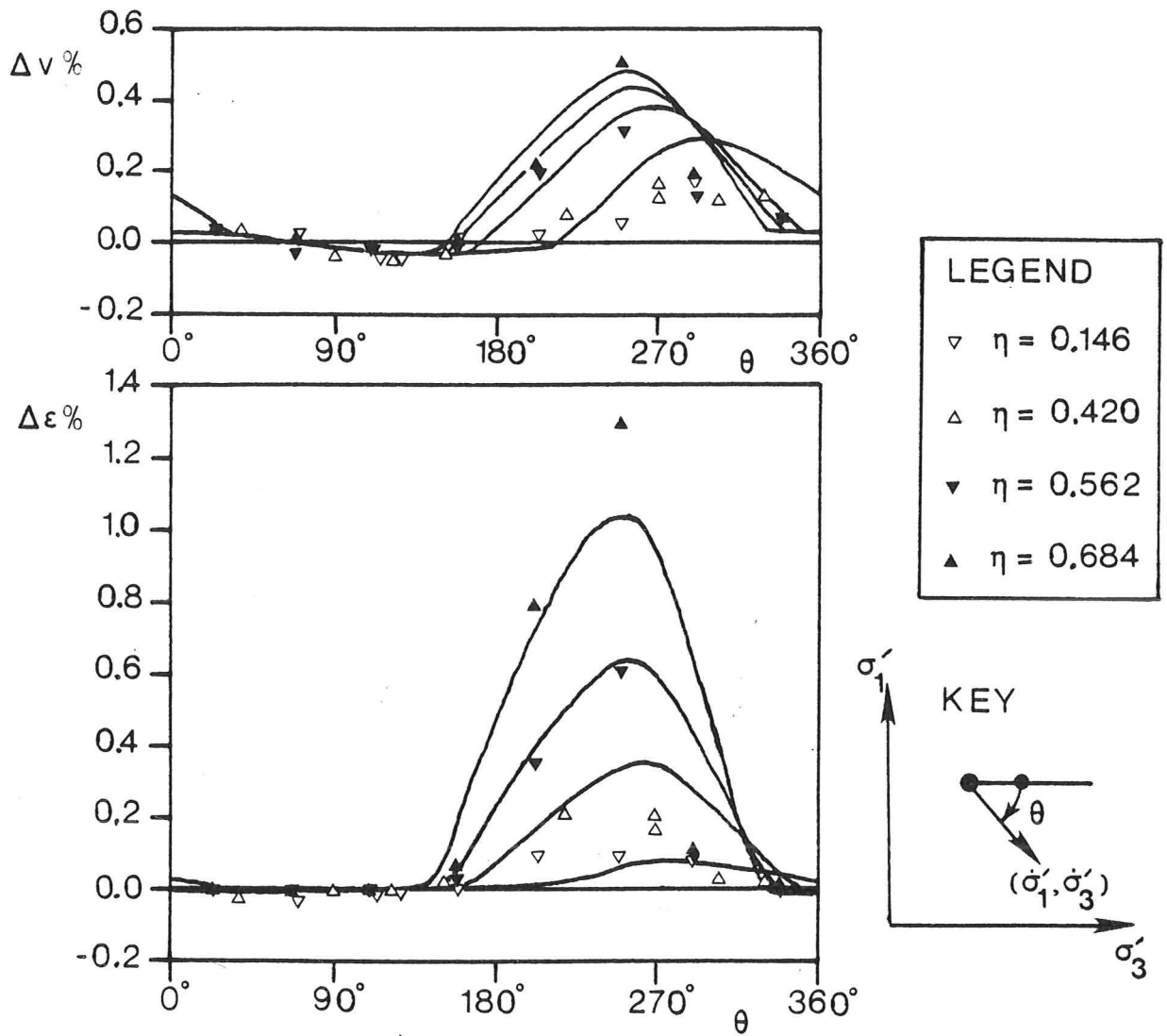


Figure 6.8 Stress probe response and fit using Modified Cam Clay (data from Lewin (1970))

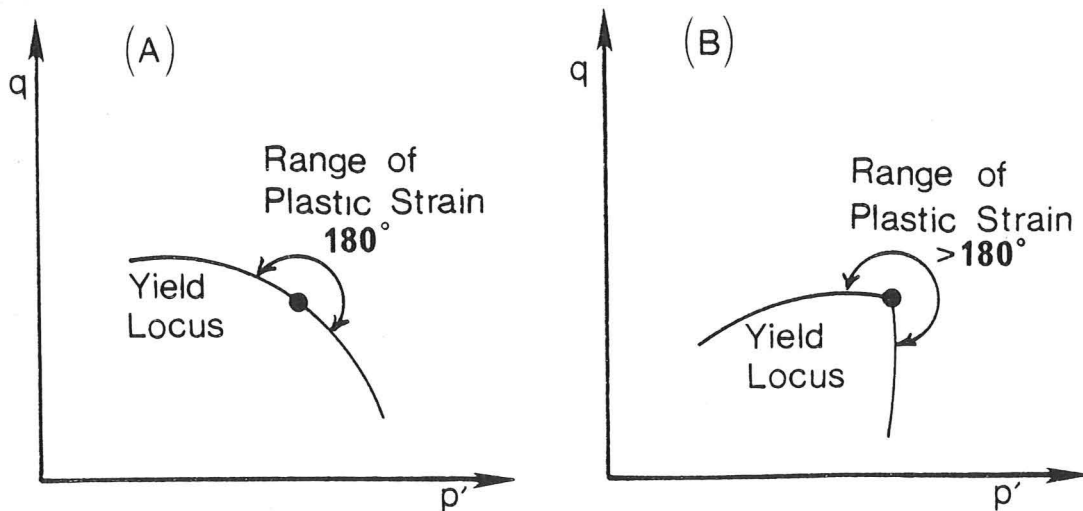


Figure 6.9 Ranges of plastic strain for smooth and pointed yield loci

four series of tests (the largest shear and volumetric strains referring to the tests at the highest stress ratio). The  $180^\circ$  range of plastic strains can clearly be seen for this model with a single smooth yield surface. The model fits the character of the response well, although in detail it does not predict the marked decline in volumetric strain at low stress ratio. A model with a smooth yield locus is adequate, however, to describe these tests which are an extremely severe check on the applicability of plasticity theory. If the model with a pointed yield locus (formed by independent compression and extension loci) is used, then large plastic strains are predicted unrealistically in the region where only the extension locus is active.

The same tests also provide a check on the uniqueness of the flow rule for samples with one particular stress history. The use of a smooth plastic potential would require that the plastic strain vectors for each set of tests should be in a fixed direction, the addition of the very small elastic strains will have only a small effect on this result. Figure 6.10 shows the strain increments for the series of tests at  $\eta = 0.562$ , compared with the strain increment direction predicted by Modified Cam Clay. Clearly the strain increments do not lie on a unique line, indicating that the plastic potential is not unique but that the plastic strain increment direction depends slightly on the stress increment direction. The Modified Cam Clay flow rule does, however, give a reasonable approximation to the observed flow.

Summarising the evidence for the variation of the flow rule, the two series of tests by Lewin indicate that the flow rule for a clay depends both on the consolidation history and on the stress increment direction. The first effect requires an anisotropic plastic potential, and the second (which appears to be fairly minor) a pointed plastic potential. Turning to the evidence about the yield locus, the plane strain tests on the Boston Blue Clay indicate that the yield locus is also anisotropic after one dimensional consolidation. Evidence for a

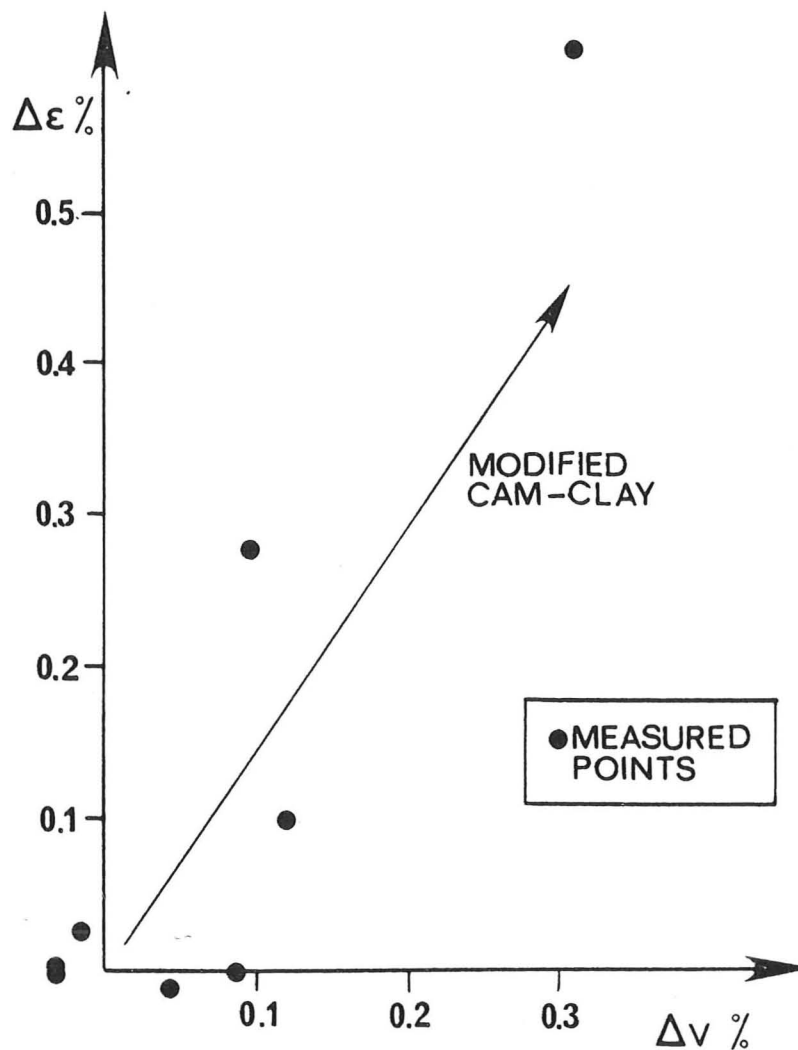


Figure 6.10 Strain response to stress probes at  $\eta = 0.562$  on Slate Dust (data from Lewin (1970))

pointed yield locus is conflicting, the Boston Blue Clay tests hint at a pointed locus, but the range of stress probes giving a small strain response in Lewin's tests indicates that the locus may be smooth.

Whilst acknowledging the importance of anisotropy, a satisfactory method of incorporating it into Modified Cam-Clay models has not been found. The tests described in this Section have highlighted the problems of plastic anisotropy, but in spite of this it has been found that the Modified Cam-Clay isotropic model performs reasonably well provided that the direction of subsequent loading is not far removed from the original consolidation direction. Until a satisfactory inclusion of anisotropy can be made the applicability of the models is

restricted to this range.

The discussion above relates entirely to the problem of plastic anisotropy. There are no theoretical problems in the introduction of elastic anisotropy to a Modified Cam-Clay model, the only restriction being the necessity that elastic behaviour should be derived from a potential. At present there seem to be insufficient data on the variation of elastic moduli with stress history to warrant the formulation of complex models. If the elastic properties are to depend on stress history as well as current stress then elastic-plastic coupling must be introduced, and the problems discussed in Section 5.4 will arise.

## CHAPTER 7

## THE EXPERIMENTAL PROGRAMME

The material for experimental study, fine Leighton Buzzard sand, is described. The types of tests of plasticity theory for soils are discussed and stress cycle tests (similar to stress probe tests) are proposed. A programme of investigation into the effects of stress and of stress history on the behaviour of dense sand is given.

### 7.1 The Choice of Material for Experimental Study

The object of the tests described in the following Sections is to study the fundamental behaviour of the simplest of granular materials. In a sand the interaction between particles is expected to be purely mechanical, rather than electrochemical as in clay, and so sands may be expected to correspond most nearly to an ideal granular material. Most sands encountered in civil engineering practice are relatively dense, so all tests were on a sand at a single high density. At the opposite end of soil behaviour an investigation of the local state of soft clays has already been made by Lewin (1970). The choice of sand for investigation has the further advantages that the stress cycle tests (which must be drained) may be carried out quite quickly, and that creep becomes of less importance.

In tests involving changes in cell pressure an important contributor to the measured volume change of the sample is the effect of the change of pressure on the penetration of the grains into the sample membrane. This effect reduces with particle size, so a fine sand was used for the tests. Fine sands also have the advantage that by increasing the ratio of sample size to particle size a more continuous response is observed, with smaller jumps due to movements of small groups of particles.

The sand chosen was an almost single sized 0.2 mm quartz grained sand from Leighton Buzzard. The specific gravity of the grains is 2.65 and the grading passing between the British Standard No.60 and No.100 sieves is shown in Figure 7.1. The grains, micrographs of which are given in Figure 7.2, are rounded to sub-angular. A single sized material was chosen for ease of preparation of a uniform sample. The mean specific volume of the samples was 1.623, giving a saturated bulk unit weight of  $19.8 \text{ kN/m}^3$ .

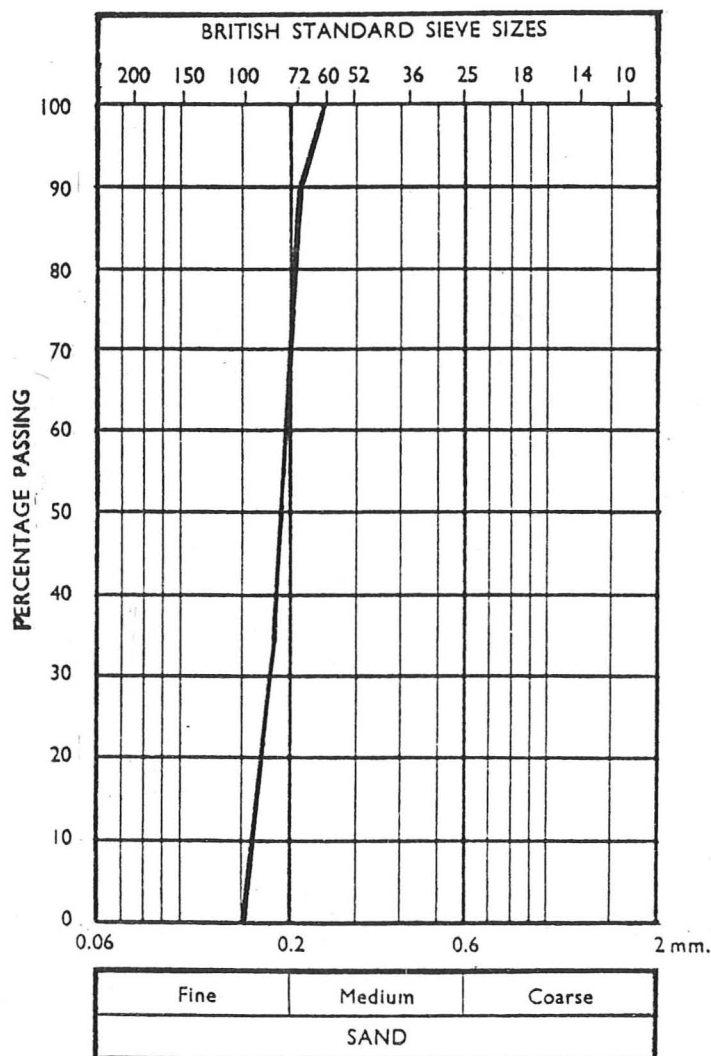


Figure 7.1 Grading curve of Leighton Buzzard sand (dry sieving)

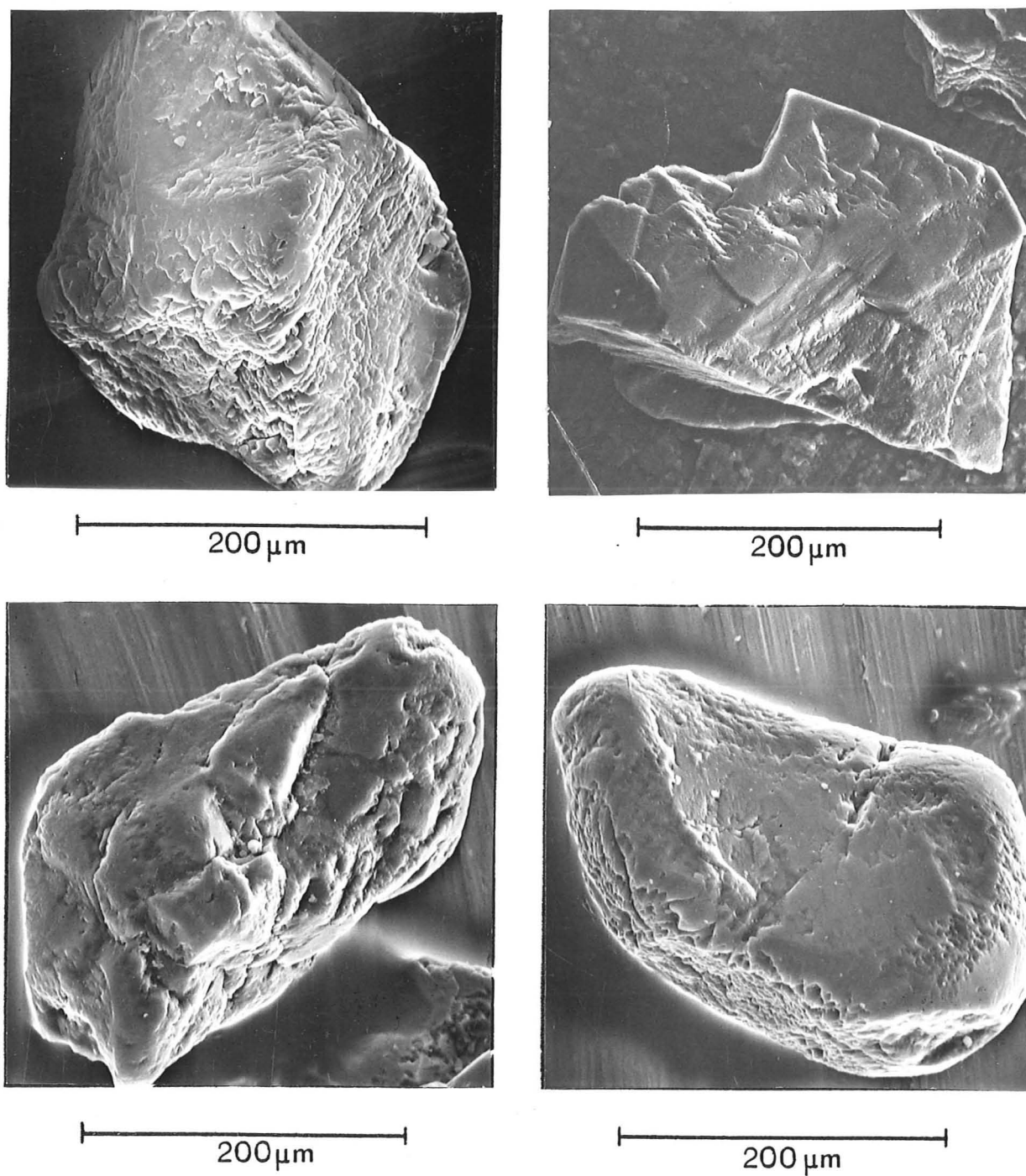


Figure 7.2 Micrographs of Leighton Buzzard sand grains

The results of a conventional drained triaxial compression test at  $\sigma'_3 \approx 260$  kPa are shown in Figure 7.3, showing a typical response for a dense sand with an initially stiff response followed by a fairly flat peak in the stress ratio - shear strain curve. The initial compression

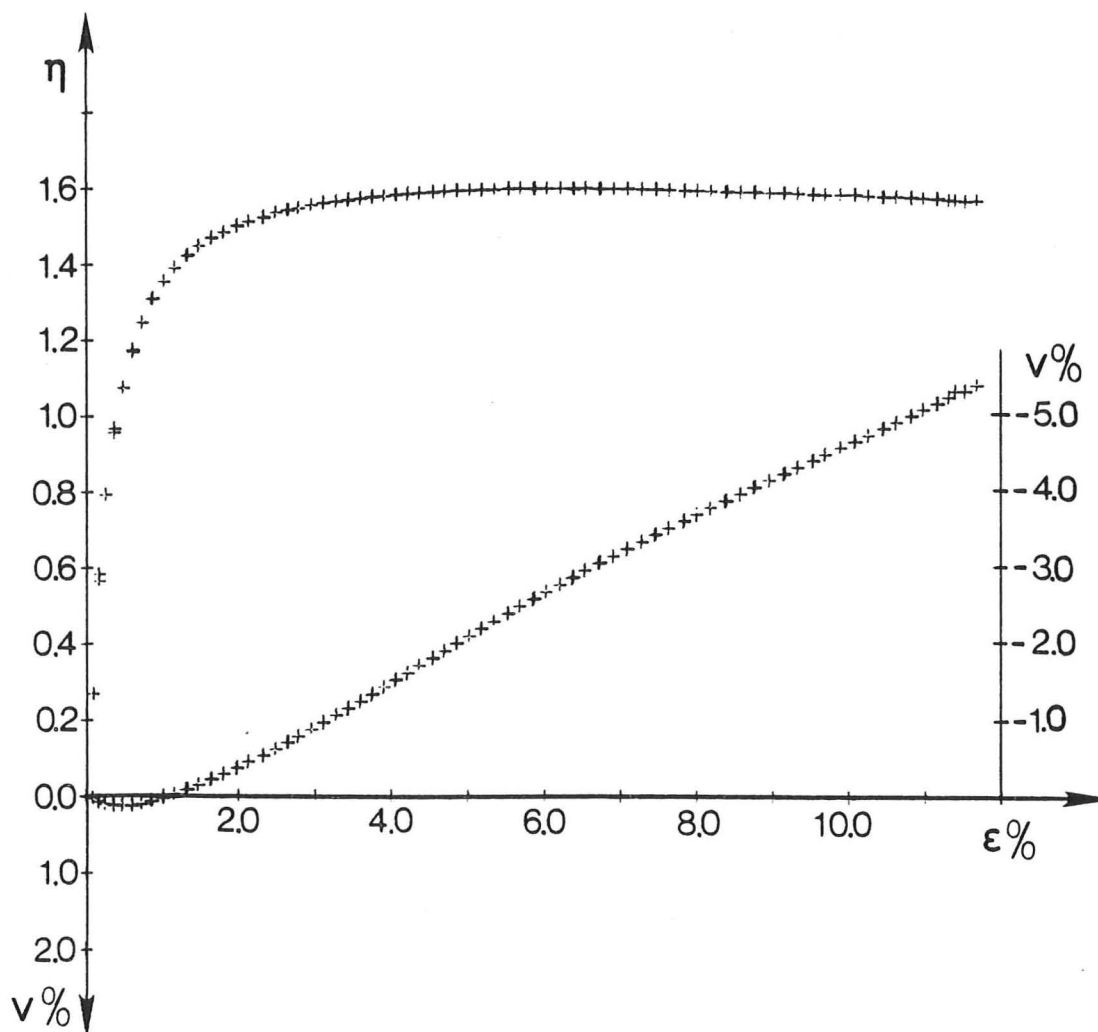


Figure 7.3 Conventional drained triaxial test 2072 on Leighton Buzzard sand,  $\sigma'_3 \approx 260$  kPa

is followed by a large dilation. A plot of  $R = \sigma'_1/\sigma'_3$  against  $D = -2\dot{\epsilon}_3/\dot{\epsilon}_1$ , Figure 7.4, shows that the stress-dilatancy flow rule  $R = KD$  (Rowe (1962)) is quite closely followed, with a value of  $K = 2.57$ , corresponding to  $\phi_{cv} = 26.1^\circ$ . The peak stress ratio corresponds to  $\phi_p = 39.1^\circ$ .

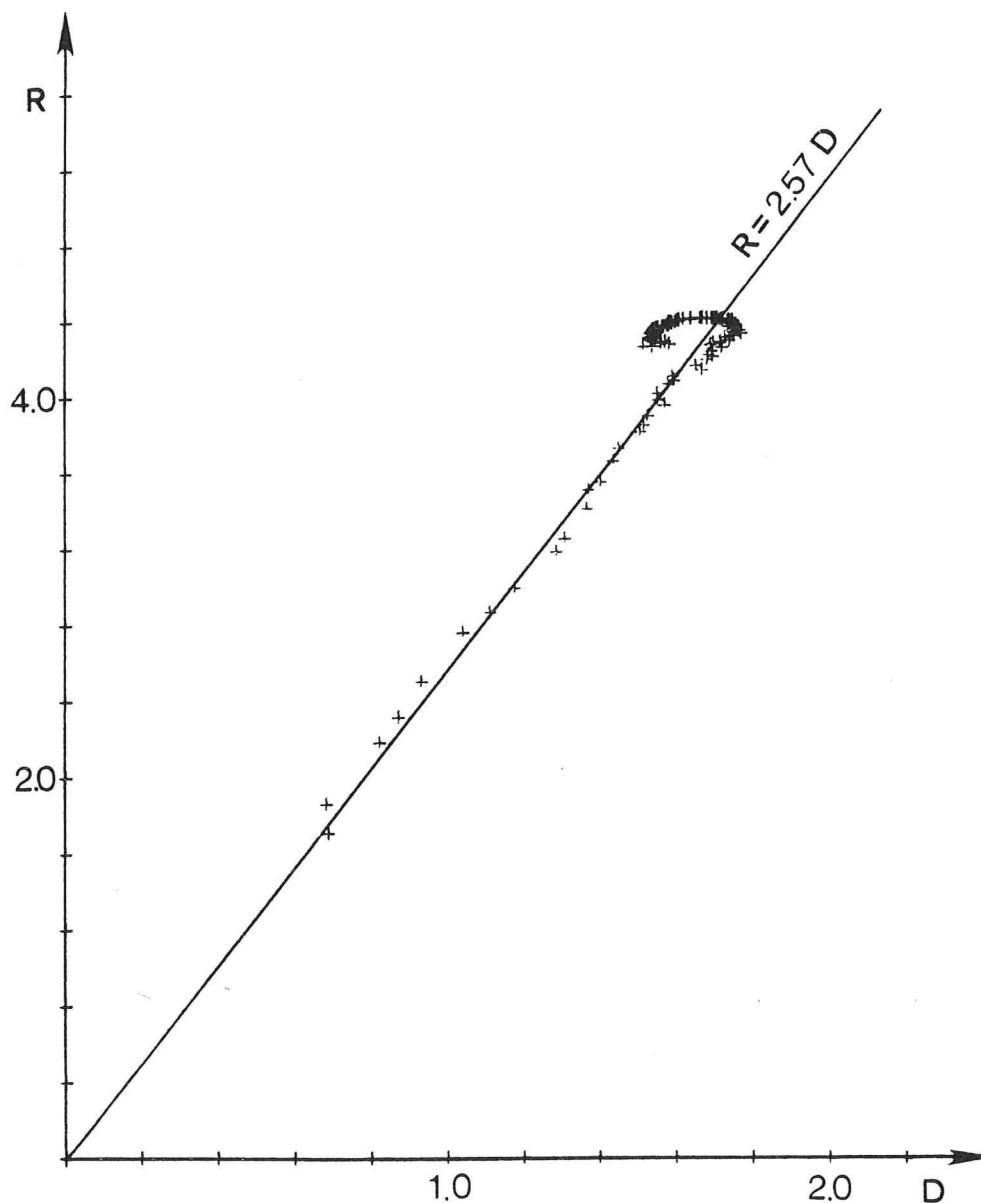


Figure 7.4 Stress-dilatancy plot for conventional drained triaxial test 2072

## 7.2 Experimental Testing of Plasticity Theory

The tests described in the following Sections are not those which might be carried out as part of routine experiments to determine the properties of specific soils, but are those which are used to establish more rigorously whether plasticity theories form an appropriate framework to describe soils. Having established the validity of a particular theory, much simpler tests may then provide the necessary parameters.

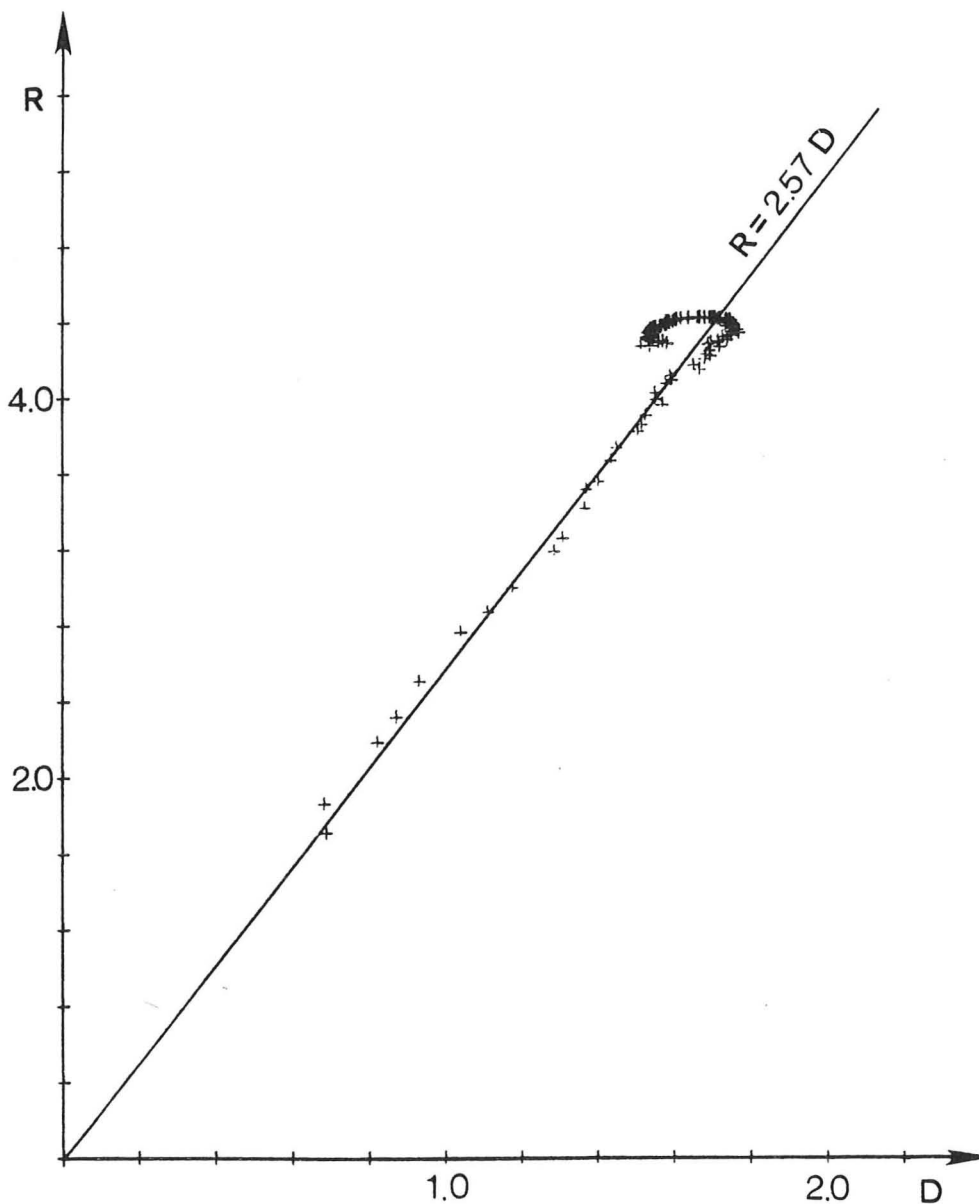


Figure 7.4 Stress-dilatancy plot for conventional drained triaxial test 2072

## 7.2 Experimental Testing of Plasticity Theory

The tests described in the following Sections are not those which might be carried out as part of routine experiments to determine the properties of specific soils, but are those which are used to establish more rigorously whether plasticity theories form an appropriate framework to describe soils. Having established the validity of a particular theory, much simpler tests may then provide the necessary parameters.

Many routine tests concentrate principally on the failure of a material, but the concern here is with the deformation of the material, recoverable and irrecoverable, at working loads below failure.

The first and simplest tests of plasticity theory are experiments in which the soil is loaded monotonically, unloaded and reloaded, and the character of the response observed. Such tests might be either consolidation tests or shear tests. Under these conditions the response of a soil is essentially of the type predicted by plasticity theory, as shown in Figure 1.1(e) and (f). These tests provide, however, only limited information about the more general applicability of the theory. The limitations are:

- (a) It must be assumed that the response on the unloading-reloading line (assuming hysteresis is small) is of an elastic rather than plastic character: the information available in a test restricted to a single line in stress space is insufficient to derive the entire incremental stress-strain matrix, and so the different form of an elastic rather than a plastic matrix cannot be determined.
- (b) In a test restricted to a single line in stress space the previous maximum stress point may be determined as a yield point, but no information is given about the shape of the yield surface.
- (c) The strains on unloading may be assumed to be elastic and subtracted from the total strains to determine the plastic strains. The orientation of the plastic potential can be inferred, but there is no indication as to whether this is unique or depends on the stress path.
- (d) Only limited information on the hardening of the material is available.
- (e) No information is provided about the stiffness of the material on the so-called "loading to the side", i.e. when the stress path has a sharp change in direction.

In spite of these limitations, tests of this sort have provided extensive information about plasticity theories for soils, for instance the good experimental evidence for the stress-dilatancy flow rule for monotonic loading of sands (Rowe (1962)) and the detailed knowledge of the consolidation and swelling of clays.

By carrying out families of similar tests much more information may be obtained, for instance on the variation of elastic properties. Carrying out two or more types of test provides even more detail, e.g. the unique specific volume contours for a normally consolidated clay in triaxial stress space located by Rendulic (1936). More recently the use of simple shear and true triaxial devices has extended this type of information to a much wider variety of stress conditions.

Although sets of tests on different samples provide information about plasticity theory, they do not check the form of the yield locus which is established for a single specimen on loading; the yield locus must be inferred directly. Tatsuoka and Ishihara (1974) report triaxial tests of the form shown in Figure 7.5 in order to establish the yield locus for a sand. A sample is first loaded along AB then unloaded to C. After changing the cell pressure the sample is reloaded along DE, and the shape of the stress-strain curve allows a yield point to be identified at F. The yield locus is assumed to pass through B and F. The investigation is continued with further probes. This sort of investigation gives a more detailed picture in that the yield locus is identified at two points for the same sample, independently of the study of the flow rule. (The tests are, however, complicated by the hardening of the material since the yield locus expands during the path FE.) Since the tests involve crossing the yield locus in approximately the same direction in each case it does not fully explore the effect of loading to the side.

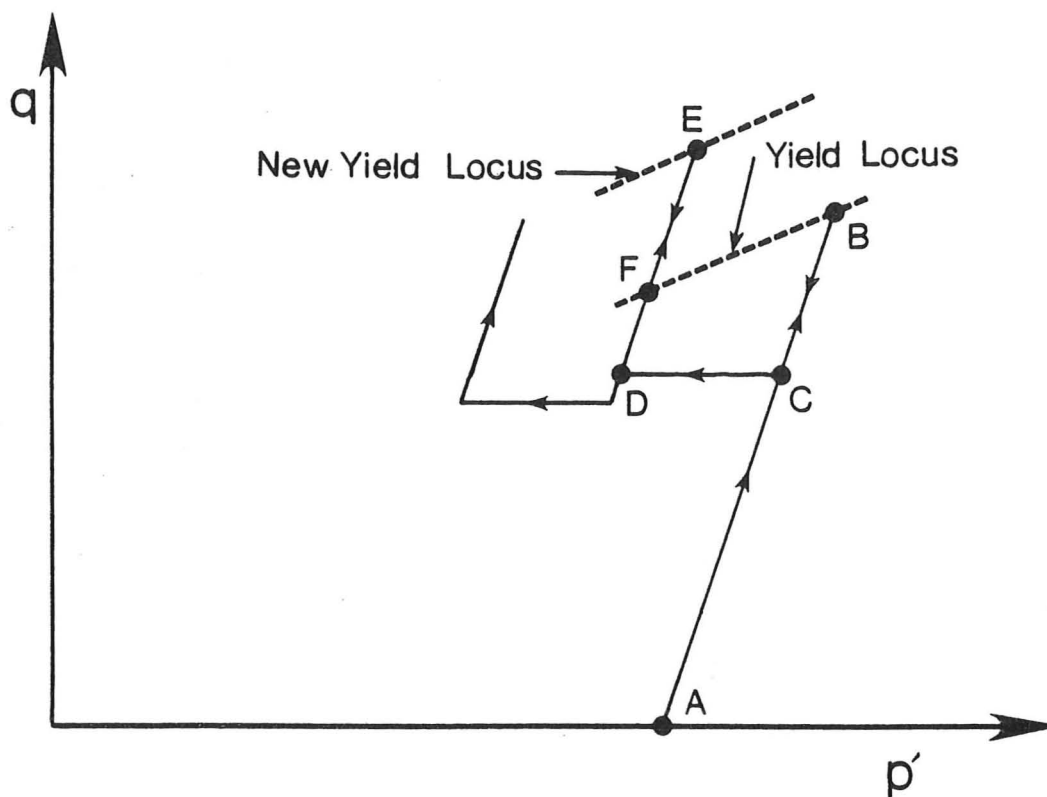


Figure 7.5 Test to locate the yield locus in the triaxial plane

Tatsuoka and Ishihara found that the yield loci for sands were not constant stress ratio lines but were curved towards lower stress ratios at higher pressures. The curves were not as marked however as in the Cam-Clay yield locus. The investigation of the behaviour of dense sand described in the following Chapters *produced an indication of the* orientation of the yield locus as well as independent measurements of other elastic and plastic properties. The form of the yield locus found is consistent with Tatsuoka and Ishihara's findings.

### 7.3 Stress Probe and Stress Cycle Tests

All the tests described above involve relatively large stress changes from which certain of the ideas of plasticity theory may be checked. An alternative is to investigate in detail the response of a material at a particular stress point, deduce the entire incremental stress-strain behaviour at that point and compare it to plasticity theory. Such an investigation was made by Lewin and Burland (1970), who reported a series of stress probe tests on normally consolidated clay.

In Lewin's tests samples were subjected to identical stress histories, and then subjected to a series of small stress probe tests (Fig.7.6(a)) in which the probe was made in a different direction for each test. The stress changes in each set of probes were small (5%) compared to the total stresses so that the investigation was truly of the 'local' state of the material. The strain response to the probes

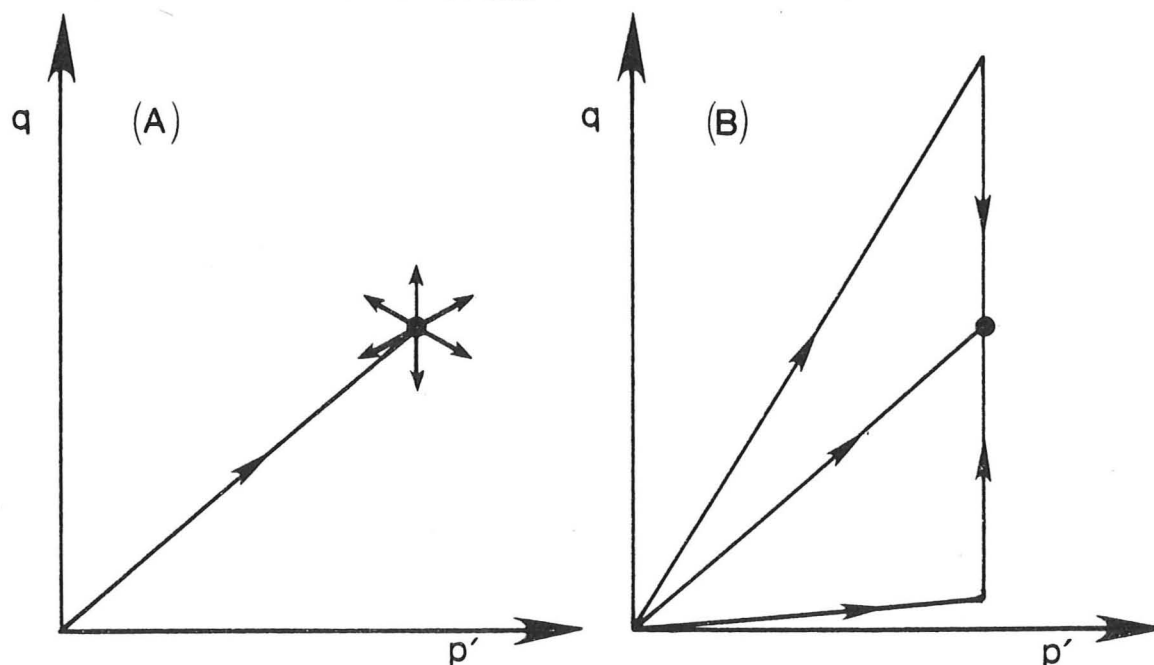


Figure 7.6 (a) Investigation of incremental response after fixed stress history, and  
(b) effect of stress history

gives detailed information about the elastic and plastic properties. Sets of stress probes at different stress ratios show the variation of behaviour with stress. (Reference to Figure 7.6(b) will be made later.)

The main disadvantage of stress probe tests is that they rely on the preparation of several identical samples. The inherent variability between samples introduces an uncertainty into the interpretation of the results. A very large number of samples is also required if an investigation into the effect of stress and of stress history is to be made. In the following it will be described how these problems may be partly overcome.

If a series of stress probes with loading and unloading were carried out on an elastic material, the response will be of the form shown in Figure 7.7(a). The end points of probes lying on a square in stress space map onto a parallelogram in strain space (Figure 7.7(b)).

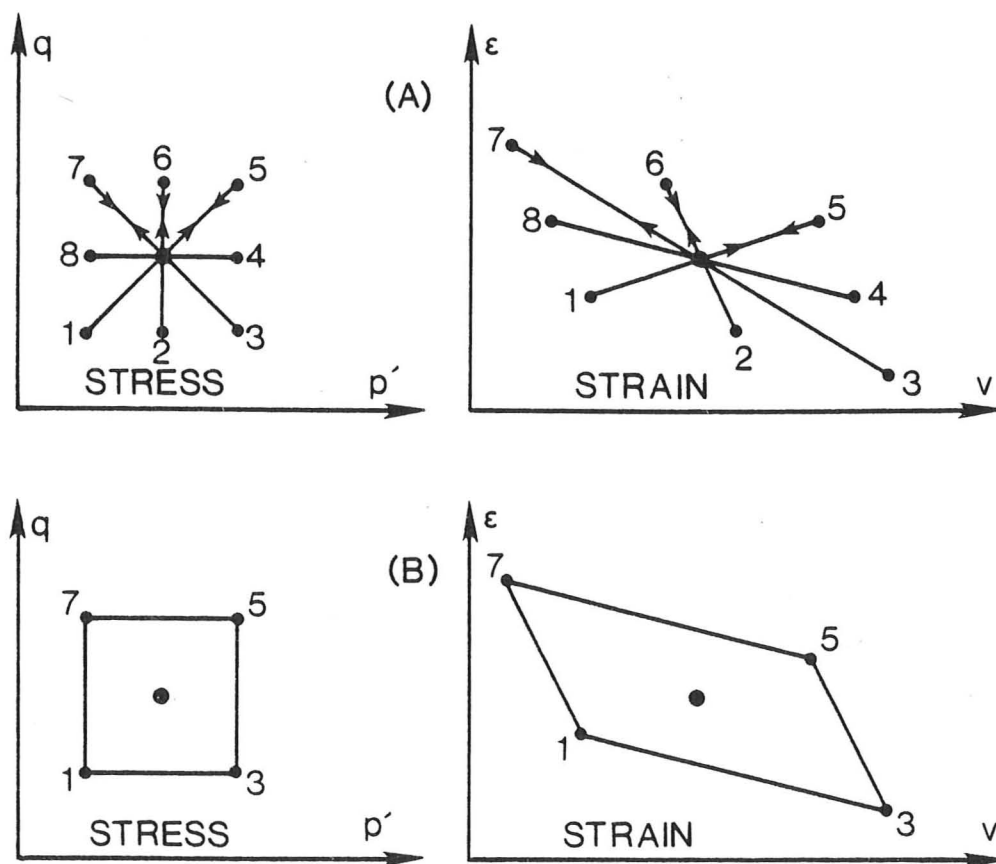


Figure 7.7 Stress probes and response, elastic material

If the probes are carried out on an elastic-plastic material the response will be of the type shown in Figure 7.8(a). Some of the probes involve a fully elastic response and some involve plastic loading and elastic unloading; the final points OABCD lie on a line oriented in the direction of the flow rule. It is possible to deduce the location of the original yield locus from the distribution of the final points, but the process is indirect.

Clearly all those tests which produce a purely elastic response could be carried out on a single element and would yield the same results; and indeed if all the tests were carried out on the same elastic-plastic sample (in order 1-8) the result would be as shown in Figure 7.8(b) in which much of the information from the original set of eight probes is retained in a single test. Note the break point P on the loading of segment 5 as the new yield locus established by probe 4 is crossed; and the purely elastic response to probes 6, 7 and 8 after the yield locus has been expanded to its maximum extent. The end points of probes 1, 2, 3, 4 and 5 are the same as in the tests on separate samples. The test may finally be simplified by omitting the return to the central point 0 between probes, resulting in the stress cycle test shown in Figure 7.8(c). The end points of all the probes 1-8 are obtained as the same in both Figure 7.8(b) and Figure 7.8(c). In addition, the stress cycle test shows a break at point Q as the yield locus is passed; this point can only be inferred indirectly from the stress probe results. Although the entire elastic-plastic response may be deduced from a single stress cycle test, more detailed information is given if both clockwise and anticlockwise tests are carried out on separate samples.

A real material will probably not behave exactly as the elastic-plastic idealisation; and in the case for instance of a material with

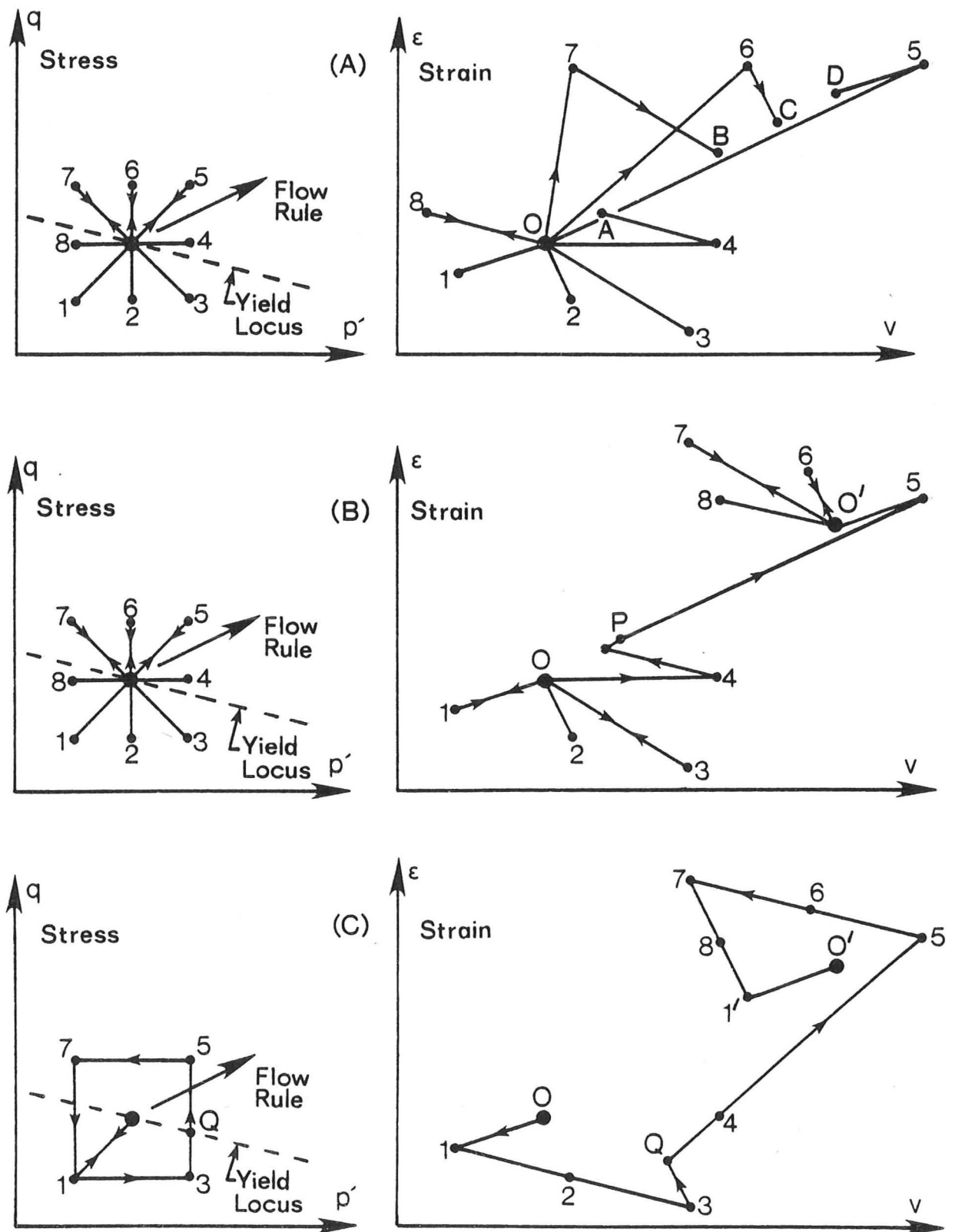


Figure 7.8 Stress probes, stress cycles and response, elastic-plastic material

two independent yield loci with different flow rules the final points of the stress probe response would not lie on the unique line of Figure 7.8(a). Such a result was in fact obtained by Lewin and Burland (1970) (see Section 6.2). Since the probes provide only a few discrete points on the final curve it is in practice difficult to interpret the data in terms of double yield loci, and the interpretation of tests in any more complex way than a single locus would be unrealistic for stress probe tests with any experimental scatter.

The stress cycle tests, which contain essentially the same information as the probe tests, must similarly be analysed assuming a single smooth yield locus. Several soil models use two loci, either of which may dominate during certain types of stress path. The cycle tests may therefore detect each locus separately.

Comparing the two methods for local investigation of material state, the cycle tests have the advantage that fewer tests are needed. If continuous monitoring is made all round the cycle they contain essentially the same information as many probe tests ending at each data point. The probe tests are more rigorous in that the incremental response of identical samples is found directly, but variation between samples may be a problem. In practice both must be interpreted using only a simple theory, and in this case provide the same information.

#### 7.4 The Effect of Stress and of Stress History

The behaviour of the sand varies with the stress state, so stress cycle tests were carried out at a variety of stress points in triaxial compression. The two most important effects are thought to be that of stress ratio and of pressure, so a grid of nine stress points at three pressures (267, 427 and 693 kPa) and three stress ratios (values of  $\eta$  of 0.75, 1.09 and 1.43) was chosen for investigation. The

pressures were chosen to represent realistic stress levels for civil engineering problems (400 kPa represents approximately 40 m of overburden in a saturated material) and the ratios may be compared with the critical state value of 1.03 and the peak at  $p' \approx 550$  kPa of 1.60. Although a wider range of stress levels would be desirable, it is difficult to achieve using a single apparatus if a consistent accuracy from the recording devices is required.

As well as dependence on the current state of stress, it is well known that the plastic behaviour of a soil produces a response which is strongly dependent on the primary loading history. Thus the behaviour of a clay depends on its preconsolidation pressure, and sands show a distinct change in stiffness at (approximately) the previous maximum stress ratio. Secondary effects do, however, also occur and the behaviour may depend on history even for primary loading. For instance Lewin (1973) presented data for a clay on the variation of the flow rule according to stress history, even for samples currently at their maximum stress ratio. This investigation was made by subjecting samples with different histories to identical subsequent stress paths (Figure 7.6(b)).

In order to investigate the effects of stress history, stress paths are first classified into different types. The simplest case is that in which both stress magnitude and ratio are increasing and at their maximum values (AB in Figure 7.9(a)). Paths with  $\eta$  increasing may also involve  $p'$  constant (CD in Figure 7.9(b)) or decreasing (EF in Figure 7.9(c)). Similarly  $\eta$  may be decreasing below some maximum previous value whilst  $p'$  is increasing (HI in Figure 7.9(d)), constant (KL in Figure 7.9(e)) or decreasing (NO in Figure 7.9(f)). Clearly many considerably more complex stress paths could also be studied, but attention is here restricted to primary loading and a

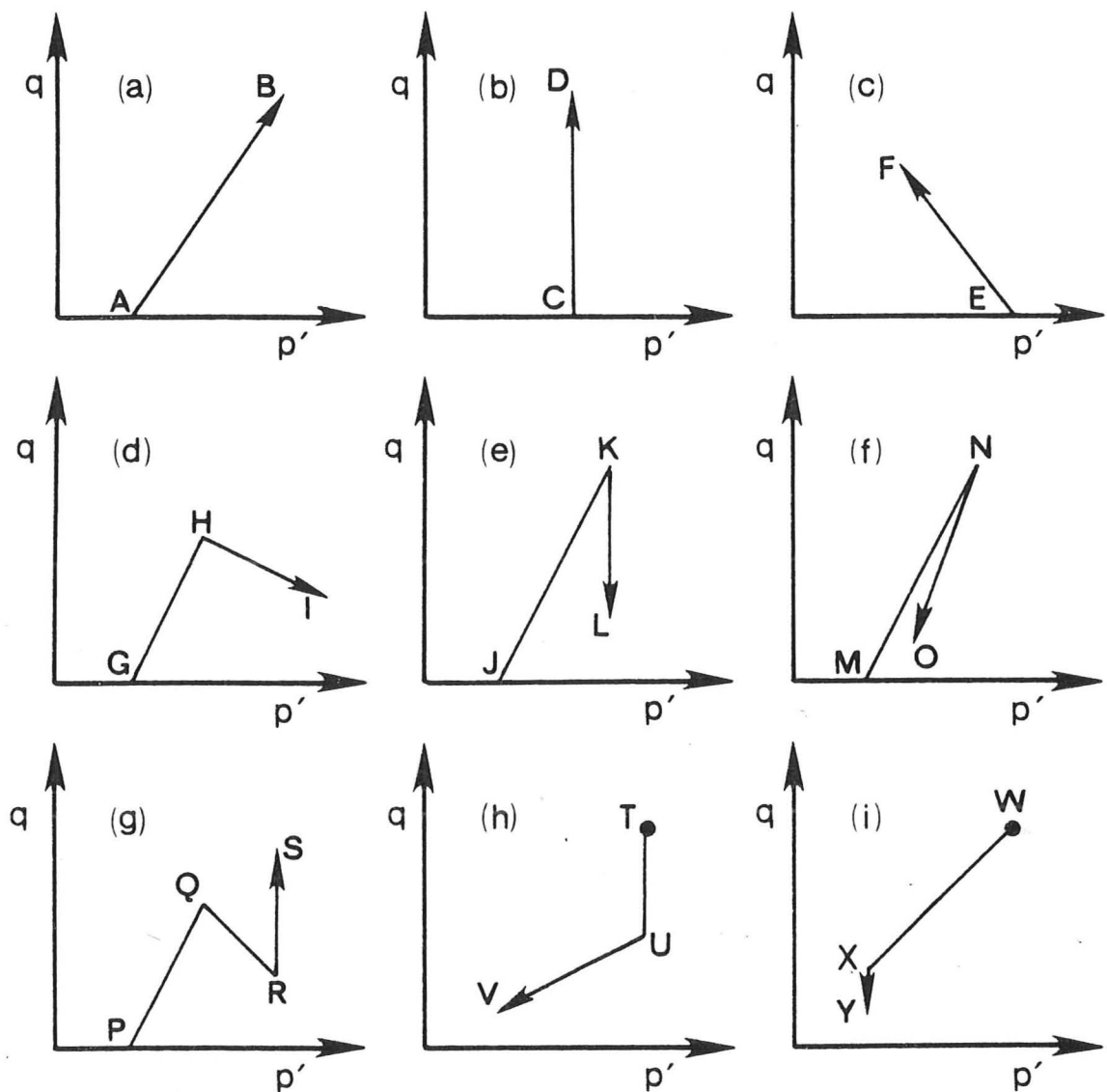


Figure 7.9 Classification of loading history in triaxial compression

first unloading. The path PQRS in Figure 7.9(g) will, however, also be studied where  $\eta$  increases on RS at a value below its maximum past value, but at a pressure higher than that at which the maximum was established. Under these conditions  $\sigma'_1$  may be at its largest value and so this path may be classed amongst those of primary loading.

On primary loading it will be assumed that if  $\eta$  and  $p'$  are both at their maximum values the behaviour will not depend on the previous stress path (as reported by Lade and Duncan (1976) for sand, but in

contrast to the findings of Lewin (1973) for clay). On unloading of both  $\eta$  and  $p'$  the case shown in Figure 7.9(f) will be divided into the two cases where first  $\eta$  then  $p'$  are reduced (TUV in Figure 7.9(h)) and vice versa (WXY in Figure 7.9(i)). On these paths secondary plastic strains occur which are path dependent; but these effects are masked by the large path independent plastic strains on primary loading.

To study the effects of stress and stress history several stress cycles were carried out in each test, with different sequences through the nine main stress points giving different classes of history. Up to nine cycles were carried out on a single sample. Each of the cycles is in the form of a parallelogram centred on the required stress point, with sides at constant pressure and at approximately constant stress ratio. The size of the parallelogram is scaled with stress magnitude so that the maximum stress change is approximately 10% of the current stress. The number of parallelograms and their spacing were largely determined by this criterion and various conditions of non-overlap of cycles.

In addition to the nine main stress points for investigation further points were defined for the standardisation of previous stress history; all the points are shown on Figure 7.10. Table 7.1 lists the tests with the sequence of stress points as given in Figure 7.10. In the tests with an odd code number the stress cycles were executed clockwise and those with an even number anticlockwise. The path from the central point for the cycle to the first corner was chosen so that it should be as nearly as possible elastic, i.e. approximately reversing the immediate past stress path.

In order to carry out the stress cycle tests a machine capable of simultaneously varying cell pressure and axial load in a triaxial test is required. Such a machine, using an automatic control and datalogging system, is described in the next Chapter.

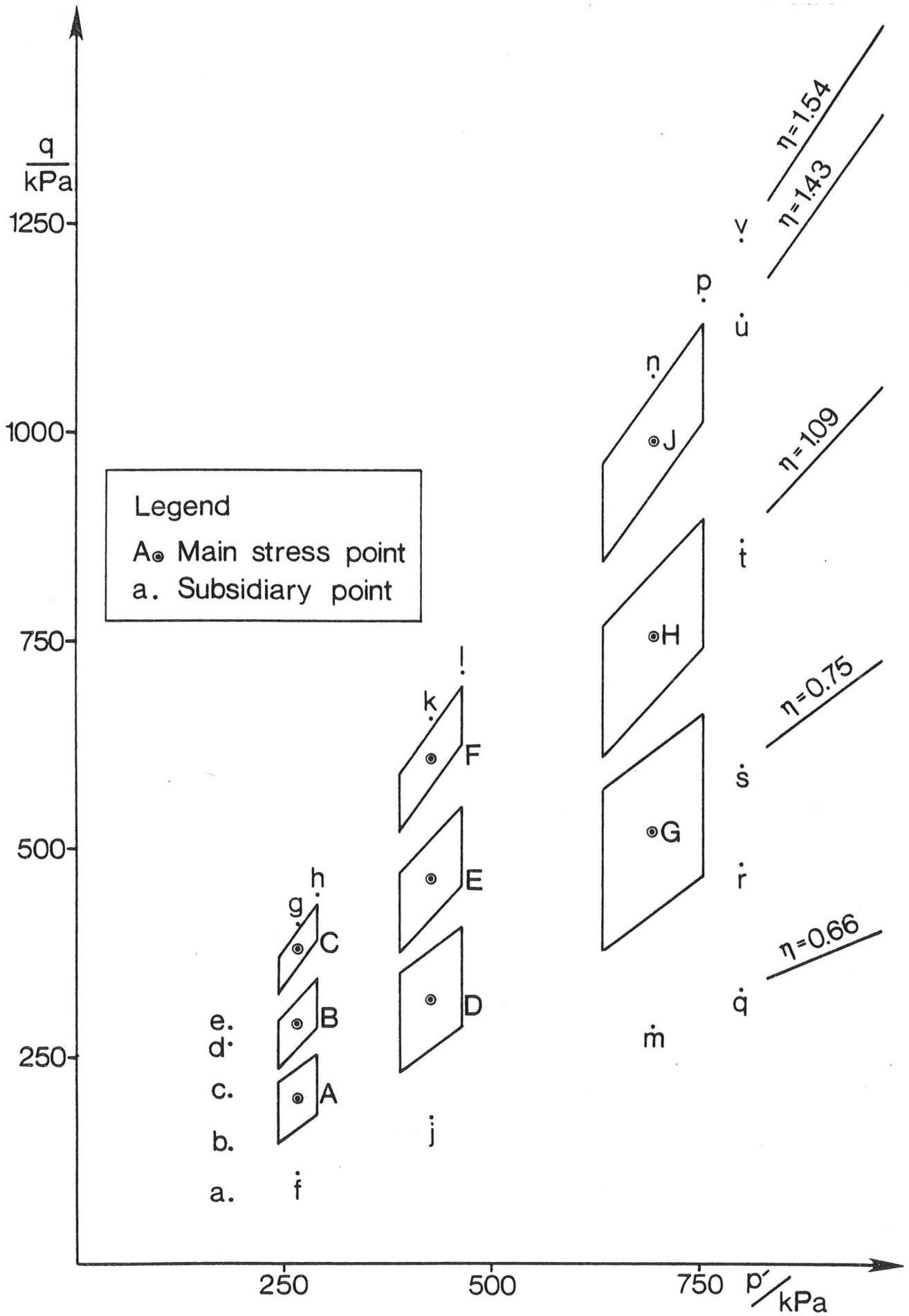


Figure 7.10 Standard stress points for stress cycle tests on dense sand

Specimen	Initial Specific Volume	Stress Path (see Figure 7.10)
1002	1.623	Constant $\sigma_3$ test, $\sigma_3 \approx 275$ kPa
1034	1.623	rGEC
2010	1.627	Special consolidation test, $\eta$ increasing
2012	1.622	AE (test discontinued)
2013	1.641	AEJvuJtHsGDA
2014	1.634	AEJvuJtHsGDA
2021	1.639	DEFvuJkFgCBA
2022	1.614	DEFvuJkFgCBA
2033	1.617	rGEC
2044	1.616	eCEG
2045	1.607	eCEG
2051	1.614	efABCgjDEFkmGHJ
2052	1.631	efABCgjDEFkmGHJ
2061	1.623	hCBA $\Delta$ FEDpJHG
2062	1.620	hCBA $\Delta$ FEDpJHG
2071	1.614	Special consolidation test, $\eta$ decreasing
2072	1.623	Constant $\sigma_3$ test, $\sigma_3 \approx 260$ kPa
Mean	1.623	
Standard deviation	0.009	

Table 7.1 Details of tests on dense sand

## CHAPTER 8

## A TRIAXIAL APPARATUS FOR STRESS CYCLE TESTS

A computer controlled triaxial machine is described, together with details of the electronic datalogging system and its calibration. A program for controlling the progress of tests by continuous adjustment of motor speeds is outlined. Details of the sample preparation are given, and the necessary calculations and corrections discussed.

### 8.1 A Computer Controlled Triaxial Machine

A schematic diagram of the triaxial apparatus is shown in Figure 8.1. In order to follow the complex stress paths necessary to conduct the stress cycle tests a fully automatic machine capable of following a predetermined stress path and logging all data automatically was necessary. This was achieved by linking a conventional triaxial cell, with all measurements made electronically, to a PDP-8E computer. The stress paths to be followed during given time intervals were specified on a control tape, and the computer controlled the speeds of two stepping motors to achieve the required stress path.

The triaxial machine (see Figures 8.2 and 8.3) consists of a Geonor triaxial cell mounted on a modified base plate in a Wykeham Farrance 1 tonne loading frame. The cell is fitted with a rotating top bushing to minimise the axial frictional force on the loading ram. The cell was modified by the fitting of 90 mm diameter end platens and a longer loading ram to accommodate the 70 mm high by 70 mm diameter cylindrical samples. Base fittings of the cell were also modified to allow fixing to the base plate in the loading frame.

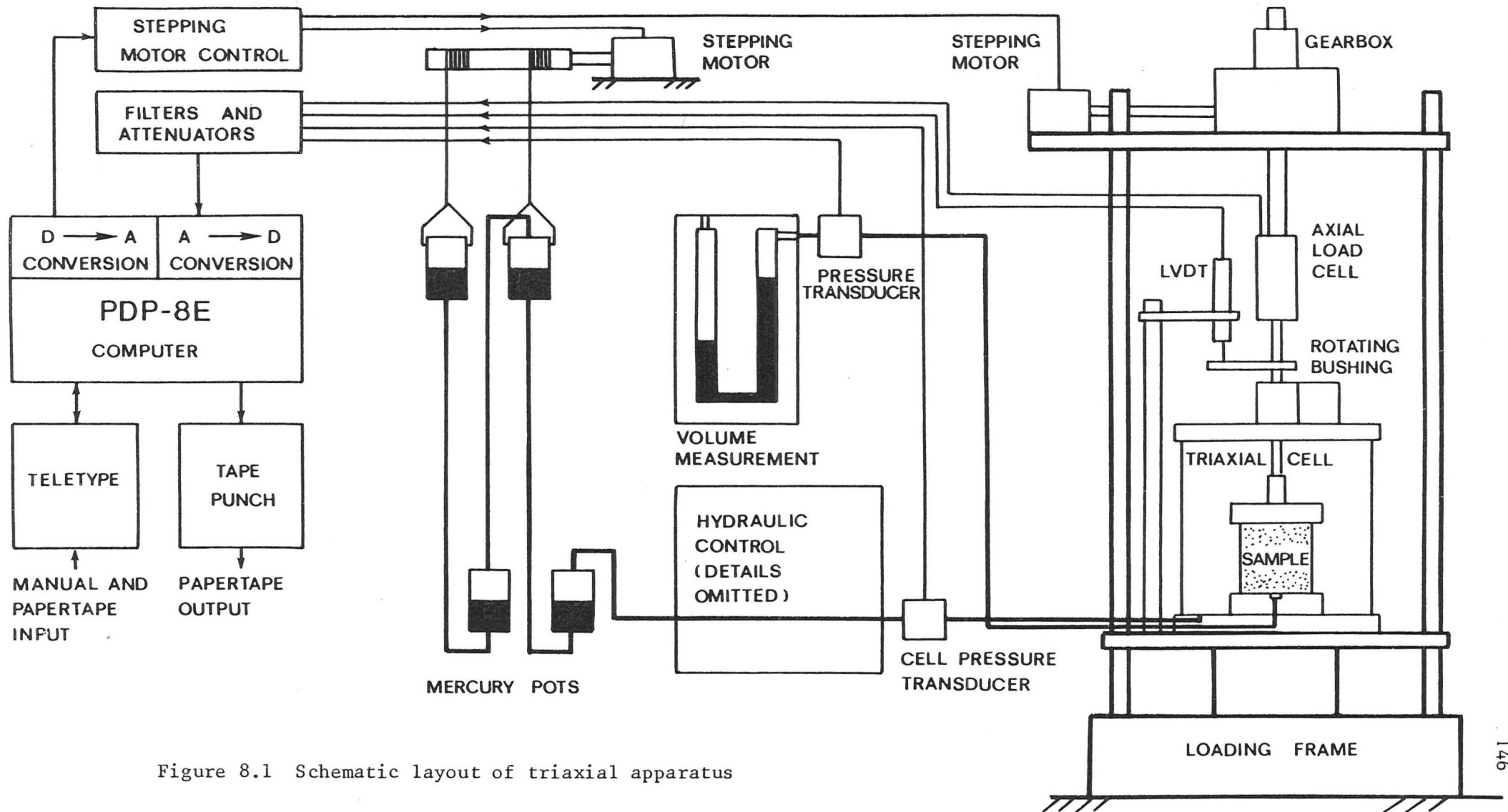


Figure 8.1 Schematic layout of triaxial apparatus

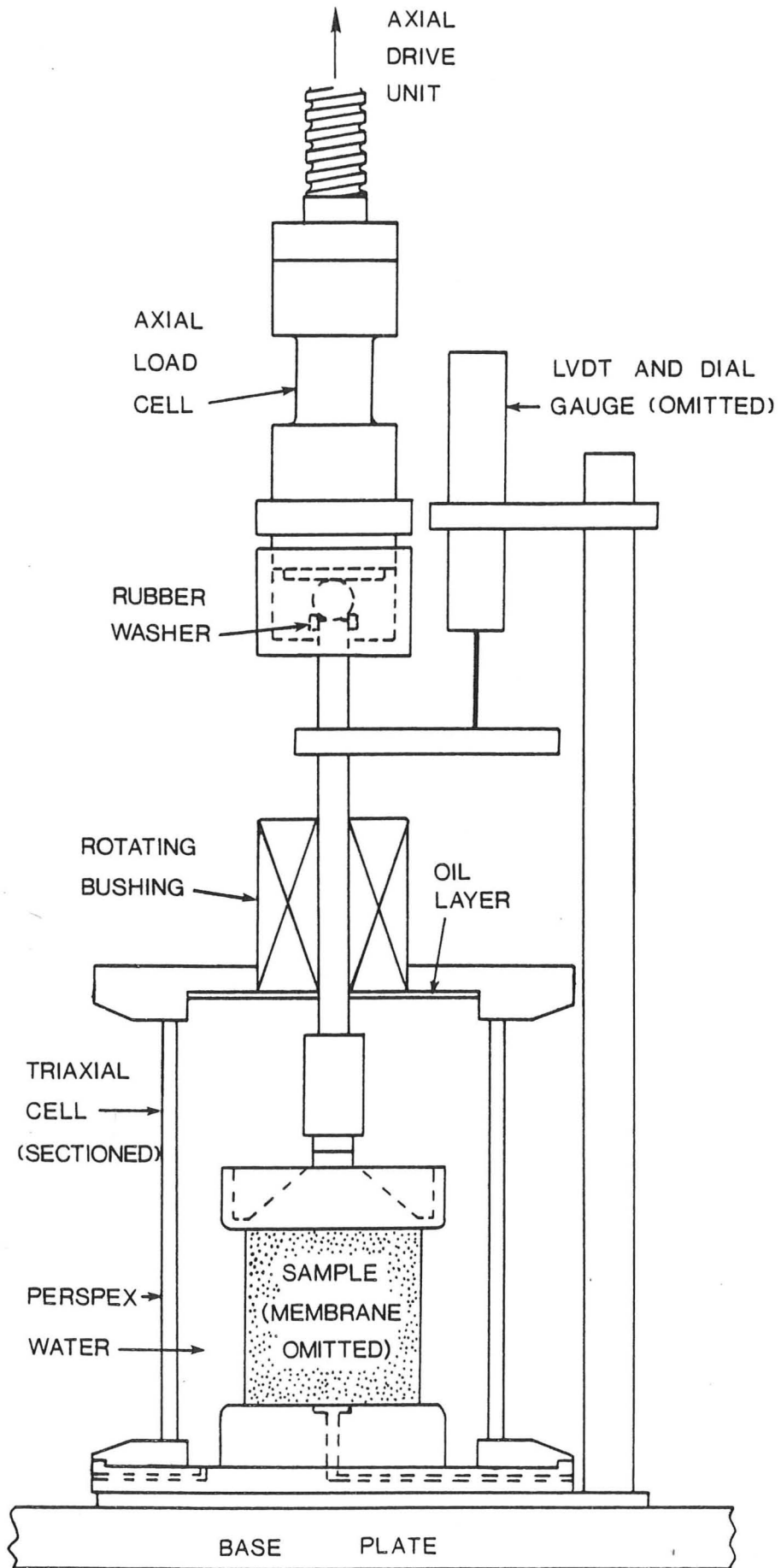


Figure 8.2 Triaxial cell and fittings (details omitted)

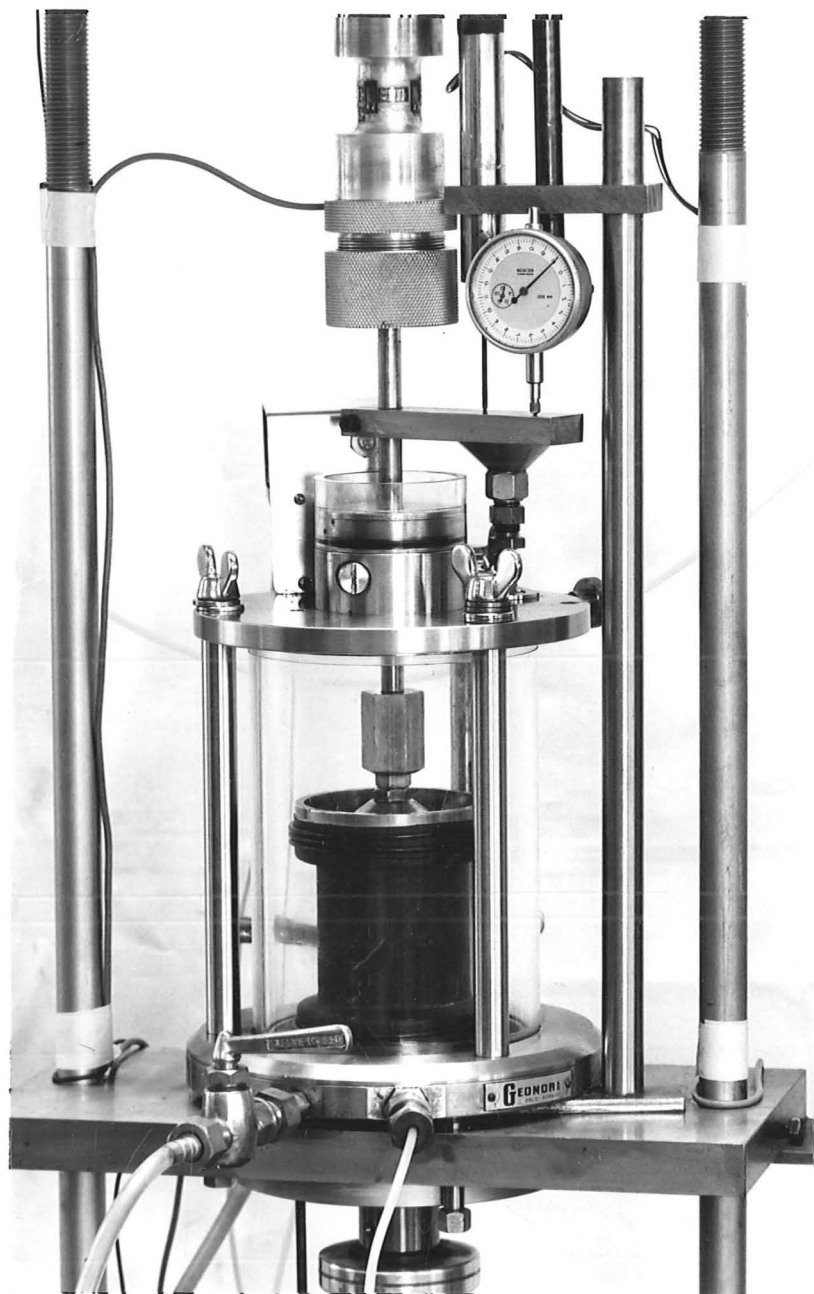


Figure 8.3 Triaxial cell in loading frame

The crosshead of the loading frame was replaced by the axial drive unit, mounted on a heavy plate. The drive consists of a stepping motor and a 200 : 1 reduction gearbox driving a 0.2 inch pitch ball screw through a further 25 : 1 worm and wheel reduction gearbox. At a maximum stepping rate of 200 steps/second a drive rate of 15 mm/hour is achieved. The ball screw runs on two nuts preloaded against each other so that backlash is eliminated if the load on the ram is reversed.

The axial drive of the Wykeham Farrance loading frame was not used during the tests.

The cell pressure is provided by a double system of mercury pots running on vertical rails. The height of the pots was controlled by a winding system driven by an identical stepping motor to the axial drive. At maximum stepping speed the full range of 0 - 600 kPa could be traversed in approximately 20 minutes. By simultaneously controlling the speeds of the two stepping motors any stress path within the region shown in Figure 8.4 is possible.

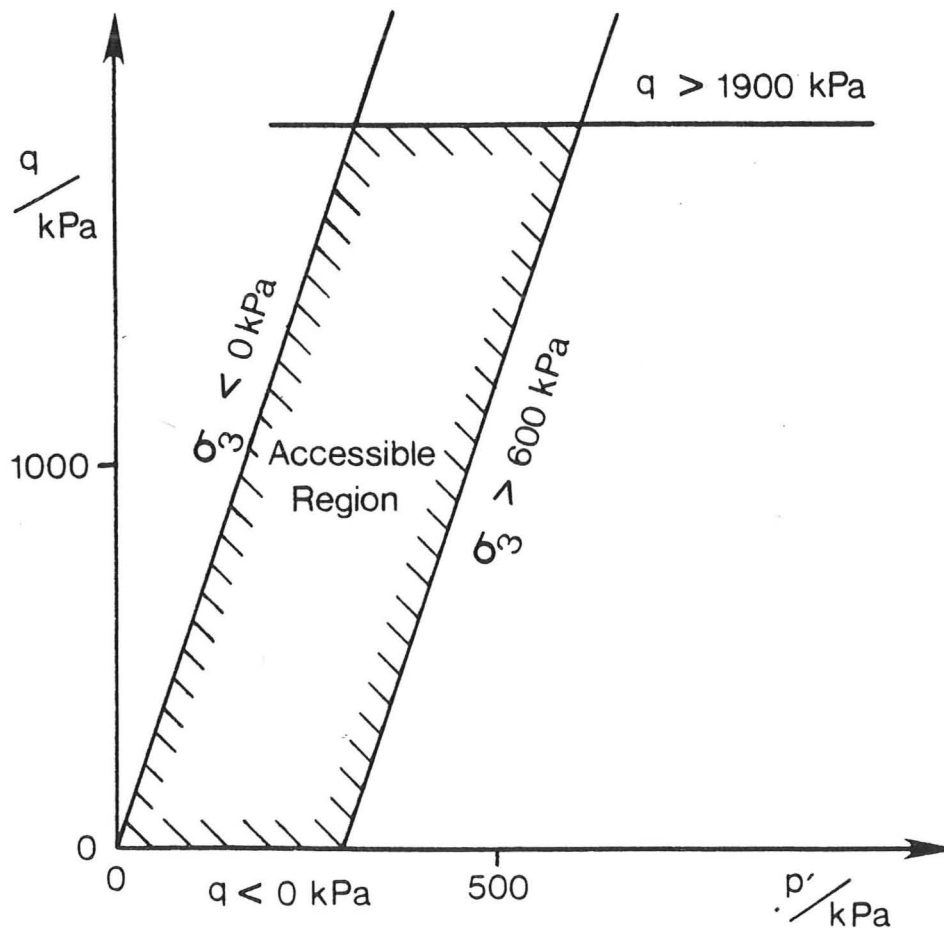


Figure 8.4 Region of stress space accessible with the triaxial apparatus

Although the physical control on the specimen was essentially stress control for the lateral direction (through the mercury pot system) and deformation control for the axial direction (through gearbox and ram),

the feedback system was arranged to allow stress control in both directions. Alternative systems using an axial load control device consisting of a double acting hydraulic ram, supported on rolling diaphragms and pressurised by mercury pots, and a lateral deformation control using a motorised piston controlling the cell fluid volume were both found to be less satisfactory.

## 8.2 The Transducers and Their Calibration

All information about the state of the sample is measured electronically by four transducers:

(a) The axial load is measured by a load cell consisting of a strain gauged hollow Dural column (Figure 8.5). The gauges (numbered

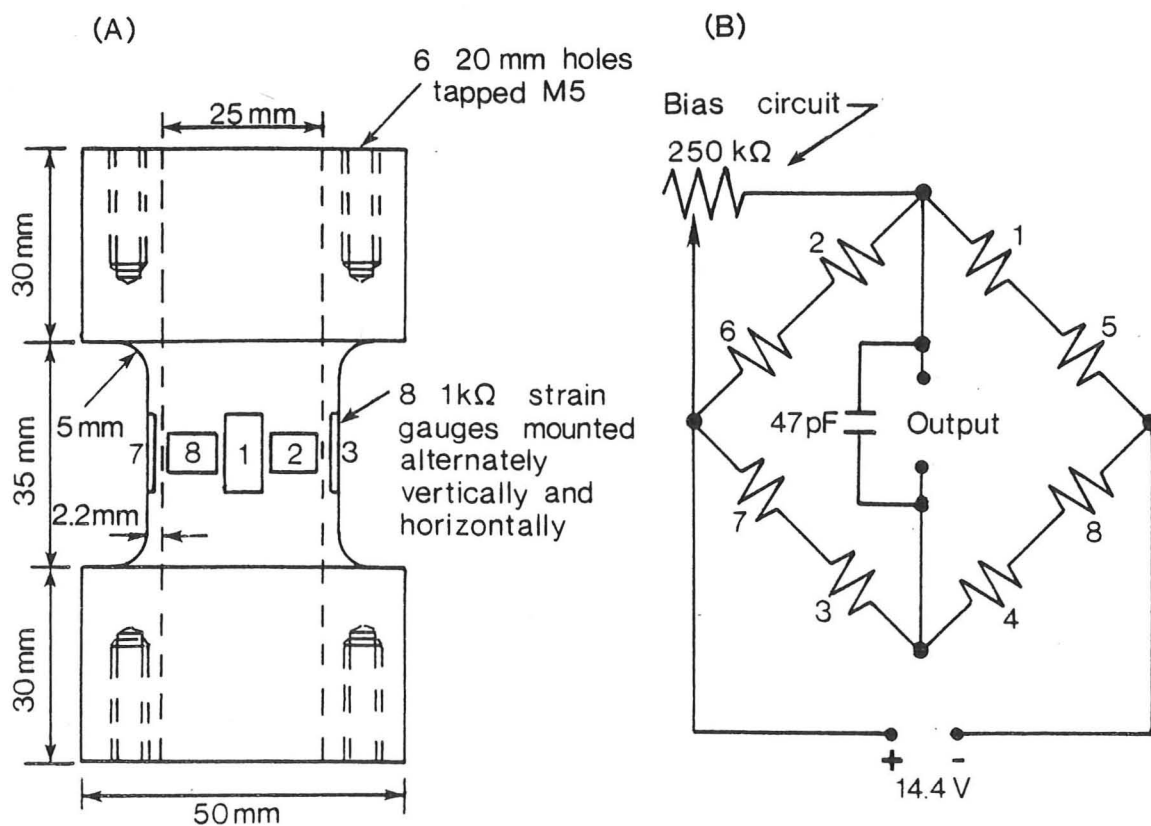


Figure 8.5 Axial load cell (a) elevation, (b) connection diagram

consecutively around the cylinder as shown on Figure 8.5) are wired to eliminate sensitivity to bending, and lateral dummy gauges are used both to compensate for temperature effects and to increase sensitivity due to the Poisson's ratio effect. With an energising voltage of 14.2 V and a biasing circuit introduced in the system an output of -5 mV to 5 mV gives a range of approximately 0 - 7.35 kN . On a 70 mm diameter sample this represents a range of deviator stress  $q$  of 0 - 1900 kPa .

Prior to calibration the load cell was loaded to approximately twice full scale load for two weeks, and cycled several thousand times in a fatigue device to a similar load in order to reduce creep and shakedown effects. Tests using deadweight loading indicated a maximum deviation from linearity of response equivalent to 8 N and a hysteresis not exceeding about 5 N . The cell was calibrated against a 1600 lb range proving ring mounted in the triaxial load frame. The calibration was carried out by manual control of reading of the transducer at specific proving ring readings, using the computerised measurement system described in the next Section. In order to simulate as closely as possible the conditions during the actual tests this was carried out whilst the computer was continuously reading all four transducers.

(b) The cell pressure is measured by a Bell and Howell transducer with a range of 150 psi . A biasing and voltage reduction circuit gives a range of 0 - 730 kPa with an excitation voltage of 4 V . The transducer was calibrated against a Bourdon gauge in a similar manner to the axial load cell.

(c) The axial deformation is measured by a Linear Variable Differential Transformer (LVDT) with a maximum range of 25 mm and output of 6 V . A filtering and voltage reduction circuit allows

switching between two ranges of 25 mm and 2.5 mm, both with an output of  $-5$  mV to  $5$  mV. A variable bias is provided so that the smaller range can be used at any point within the large range (see Figure 8.6).

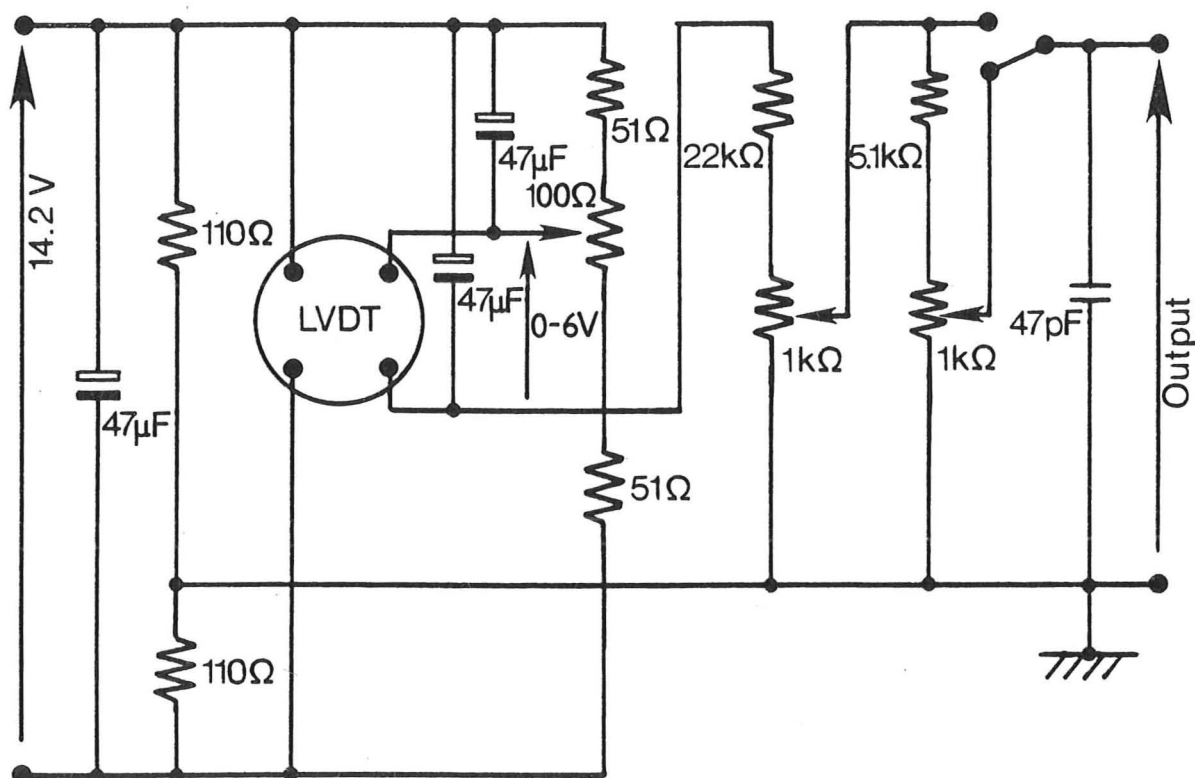


Figure 8.6 Variable attenuation and offset control for LVDT

The LVDT was calibrated against a micrometer; the response being highly linear and virtually free of hysteresis. The calibration constant for the fine range varies with location within the coarse range and is fitted closely by a quadratic function. Account of this variation is made automatically when the fine range is selected.

The measurements of very small deformations were subject to an apparently random fluctuation of the equivalent of a few microns. This was in part due to a slight tilting of the load ram with the rotation of the top bushing of the triaxial cell. The effect was

minimised by placing the LVDT as close as possible to the axis of the cell, but the alternative of a non-rotating bushing would have provided an unacceptable (and unknown) friction between the sample and the axial load cell.

(d) Both the volume change of the sample and the back pressure are measured by a sensitive Druck pressure transducer arranged as in Figure 8.7. The transducer measures the back pressure directly, and

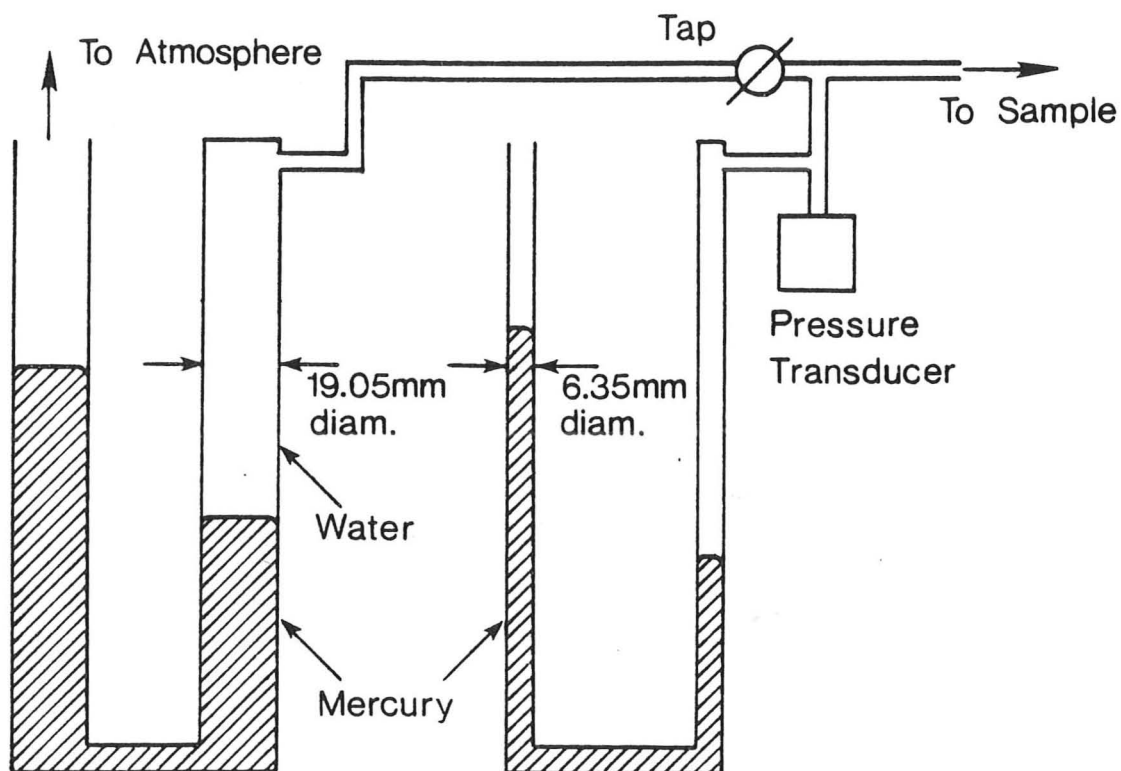


Figure 8.7 Schematic diagram of volume change measurement device

as the sample changes volume the change in mercury level in the U-tubes causes a small back pressure change. The maximum range of the device is 22.0 cc, for which a back pressure change of 18.2 kPa occurs. The range may be decreased (and sensitivity increased) tenfold by shutting off the larger of the U-tubes. The complete volume measurement device is shown in Figure 8.8.

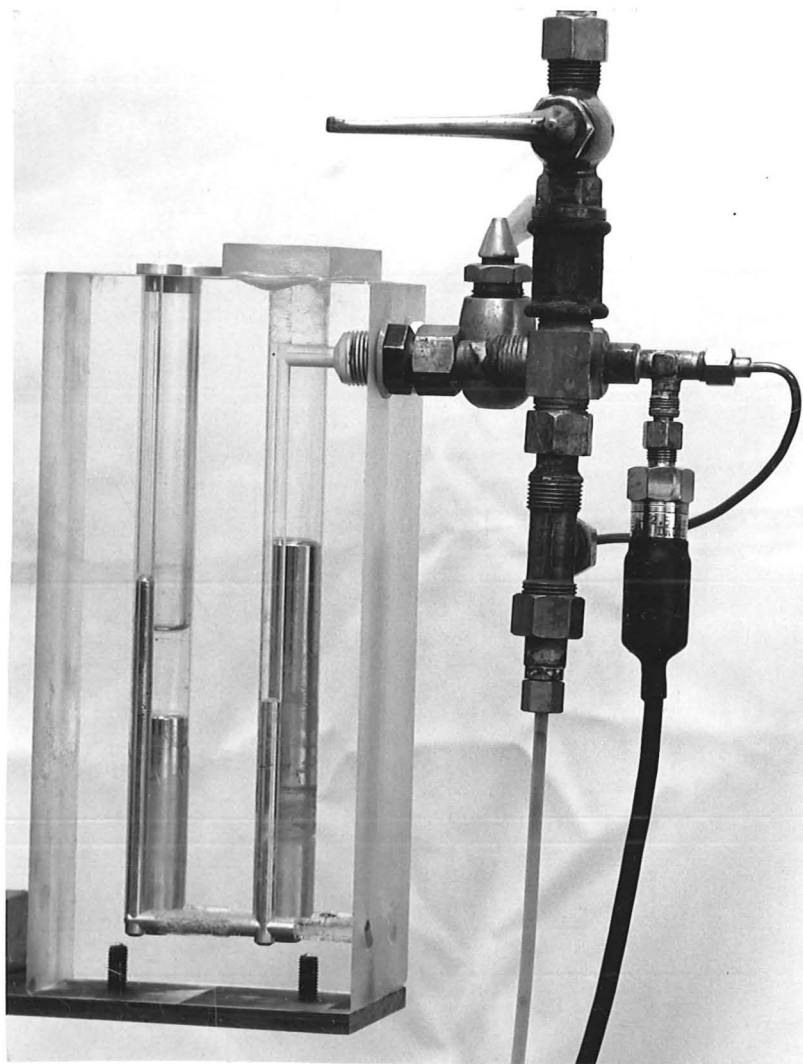


Figure 8.8 Volume change measurement device

The automatic measurement of volume change has been attempted by many workers using a variety of ingenious devices. The above device is relatively simple and has proved to be reliable and sensitive; it has the disadvantage that it causes a change in the back pressure, which can be accounted for in the automatic feedback system used here. The system could not be used where a large back pressure was necessary.

The device was calibrated by connecting it directly to a piston of 38.1 mm diameter, the travel of the piston being measured by a

dial gauge. It was impossible to make a sufficiently small measured volume change to assess hysteresis of the device, which may be expected due to any surface tension effects as the direction of travel is reversed. An upper limit of about  $5 \text{ mm}^3$  could, however, be put on any possible hysteresis. The linear response of the device is shown in Figure 8.9. Although a distinction has been made in plotting the measured points for different flow directions, the points are almost indistinguishable at the scale used, showing that hysteresis in the device is very small. The calibration for the secondary effect of back pressure variation was deduced directly from the known area of the U-tubes, the density of mercury and the volumetric calibration.

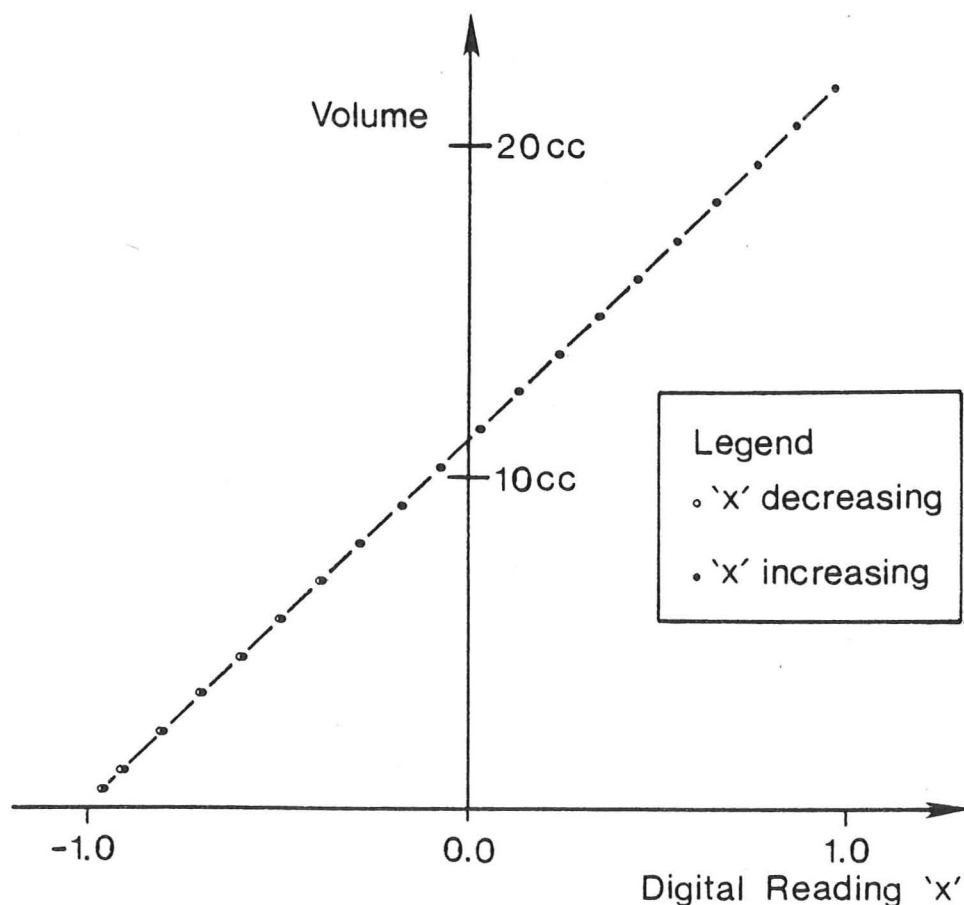


Figure 8.9 Calibration of volume change measurement device

### 8.3 Automatic Datalogging and Motor Control by the PDP-8E Computer

All the transducers are arranged to give an output in the range -5 mV to 5 mV, which is then amplified and converted to a digital value using the system described by Wood (1974). Each selected transducer is first connected to the logging system for 8 ms to allow the reading to settle to a steady value. The analogue to digital converter is then read a total of 512 times during a period of 40 ms in order to reduce the effects of noise and variation during the mains cycle, and all the readings added. Although each analogue to digital conversion is only to twelve bit accuracy, the addition produces a 21 bit value which is then used directly (i.e. without truncation to 12 bits) in the subsequent calculation. It is therefore possible to achieve a logging accuracy slightly better than 12 bits, with the fractional part being due to statistical variation. All transducer readings are subtracted from a fifth dummy reading in order to eliminate the effects of amplifier drift.

Assuming an accuracy to 12 bits represents a resolution of one part in four thousand, which with the range of the transducers converts to a resolution of stress and strain measurements on a 70 mm by 70 mm sample of:

Cell pressure	0.18 kPa
Deviator stress	0.48 kPa
Axial Strain	0.009% (coarse range), 0.001% (fine range)
Volumetric Strain	0.002% (coarse range), 0.0002% (fine range)

Numerical calculations in the PDP-8E are carried out using three word floating point arithmetic (two twelve bit word mantissa and one word exponent). The two words used for storage of the summed transducer readings are used as the mantissa and the exponent always taken as zero.

This results in the range  $-5$  mV to  $5$  mV being converted arbitrarily to numerical values  $-1.0$  to  $1.0$ . All the necessary calibration constants to convert the readings to stress and strain values are stored permanently in the computer.

As well as making use of the transducer readings, which are continuously monitored during the test, to calculate the current state of the sample, the readings were also recorded by punching on a high speed papertape punch at intervals which could be specified on the control tape for the test. Each set of punched data includes the time of reading and the two word mantissa for each of the four transducers. The complete tape for each test also includes an identifying code, records of the initial dimensions of the sample and a series of control characters specifying any changes made to the control system, e.g. changing of the range of one of the transducers. The output tape was subsequently processed on the C.U.E.D. Sigma-6 computer.

After calculation of the required motor speeds (details of the control program are given in the next Section) the speeds were expressed as single twelve bit words and each converted to a voltage in the range  $0$  V to  $5$  V by digital to analogue converters as described by Wood (1974). These voltages were used to control the speeds of the stepping motors in the range  $0$  to  $200$  steps per second by an Impex EM127 driving system. The drive directions of the two motors were determined separately and output to the EM127 by a purpose built logic device on the PDP-8E. Stepping motors were chosen for the main drive units because of this simplicity of control over a wide range of speeds. The EM127 device also allows manual control of the motors.

#### 8.4 The Triaxial Testing Control Program

The control program for the PDP-8E is intended to provide the maximum of versatility and ease of usage within the constraints of the 4 k of 12 bit words of memory available. Approximately 1.5 k words were used for storage of the binary loading system, a floating point arithmetic package and an alphanumeric typing routine for the teletype. The use of these routines, particularly the floating point arithmetic, considerably simplified the remainder of the programming. The program was written in MACRO-8, a simple assembler language consisting of mnemonics for machine code operations, enhanced by the use of several additional commands peculiar to the particular system.

A simplified block diagram of the monitor and control programs is given in Figure 8.10. The monitor program provides the facility to make small alterations to the program system from the keyboard without re-compiling the programs, or to read or alter the calibration constants stored in the system. It also allows manual output of the transducer readings, control of the motors and various routine operations such as entry to the main program.

At the start of a test the main control program is first used to record the dimensions of the sample and burette readings for the pore fluid volume, which are input from the keyboard, and to read the reference values for the transducers. This operation is carried out under manual control, with the program providing prompts for the data required. For all important transducer readings such as the initial values the transducers are read twice; if agreement is not achieved to one part in 4000 the operation is repeated. The test may then be carried out under manual control with the computer serving merely as a datalogger, or the automatic control routine entered.

The computer reads from papertape, input through the teletype,

## MONITOR PROGRAM

Allows alteration of program or data, manual control of output, entry to control program etc.

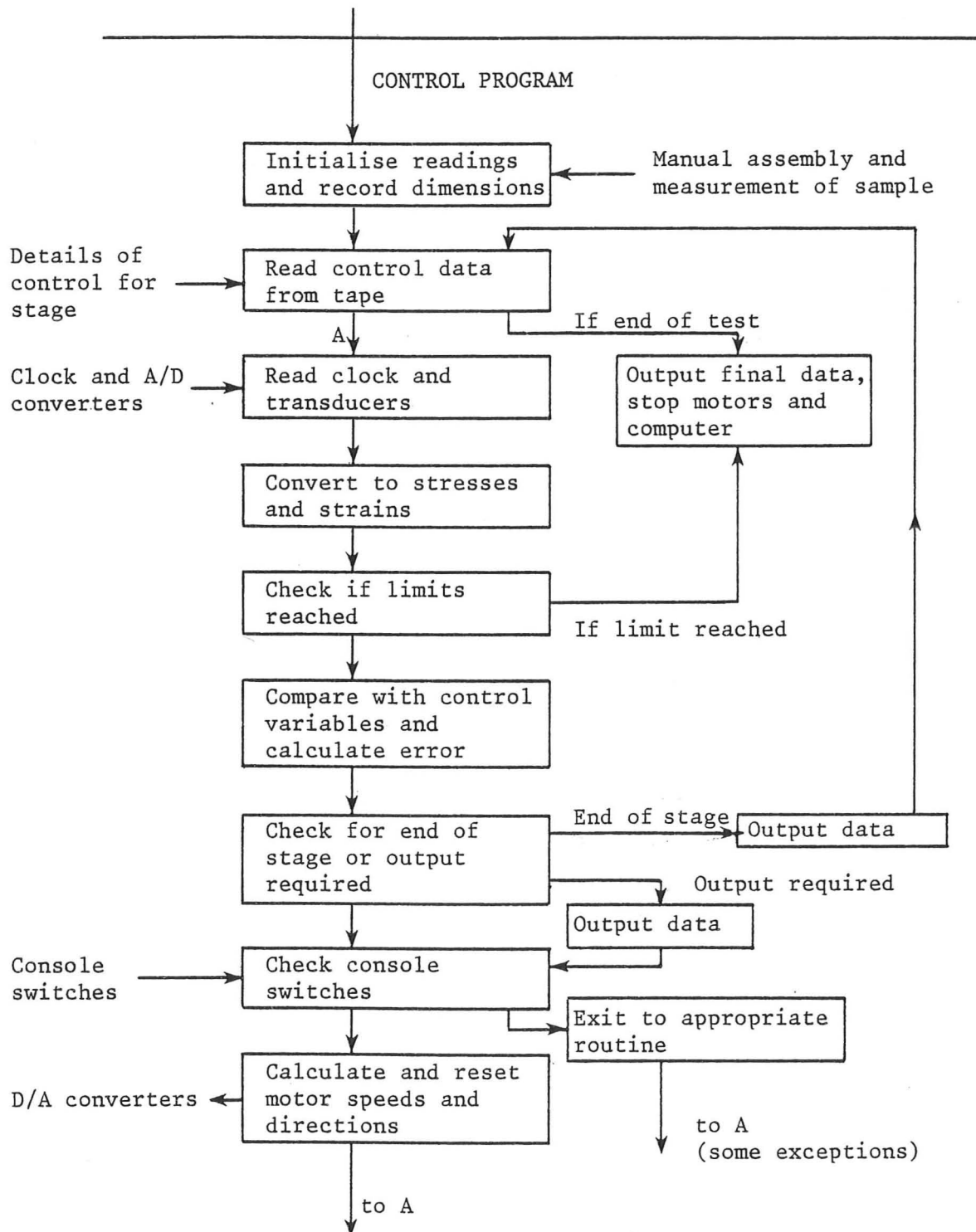


Figure 8.10 Block diagram of the control program for triaxial tests

the length of time the first stage of the test is to take and the nature of the control (either stress control or strain control may be specified in each of the axial and radial directions, although in practice only stress control has been used). It also reads the target values of stress or strain to be achieved by the end of the stage and the number of sets of output on papertape and on the teletype required for the stage. Throughout the stage the required value of the control variable will be calculated to give a linear variation with time from the value read experimentally at the beginning of the stage to the target value for the end. In subsequent stages the variation is between the previous and current target values. The output of data is given at equal time intervals throughout the stage.

The program then enters the main control cycle (at A in Figure 8.10), the time and transducer readings are read and the stresses and strains calculated. If any of the calculated quantities exceed pre-set limit values the test is automatically stopped. A hardware safety cut-out system is also provided by microswitches at the end of the travel of both the axial drive and of the mercury pot carriages. The stress or strain variables for control are compared with the required values and the current errors calculated. The time is checked and either high speed papertape output or teletype output of the stresses and strains is given if required. Since the output of data temporarily interrupts the control of the test the use of the slower teletype is kept to a minimum in automatic tests. If the end of the stage has been reached (the criterion being time rather than the values of the control parameters) then the data are output and the information for the next stage is read as for the first, and the whole process repeated. A special code is used to cause the end of a test.

If the control cycle is not interrupted by one of the above operations a check is made on the positions of the twelve switches on the computer console. These are used to alter the operation of the test in progress. The main use is to interrupt the program so that the range of the LVDT may be altered, or so that either the LVDT or the volume change measuring device may be changed from the coarse to fine range of accuracy. These operations must be carried out manually, with the control being later transferred back to the program. The control routine may be re-entered directly, or for some options the program first automatically changes the calibration constants to account for the change in transducer ranges. The console switches may also be used to provide a certain degree of manual control during the test, including provision of extra data output.

The final stage of the control cycle consists of the recalculation of the motor speeds. For both the axial and radial directions the current error in the control variable is both integrated and differentiated with respect to time, assuming a linear change with time since the last control cycle. For this purpose a software clock is used: the computer is fitted with a peripheral device which can be set to provide an *interrupt* signal every 20 ms. These signals are counted by a simple routine and may be converted to time by multiplying by a constant; the main program is automatically re-entered at the point from which the *interrupt* occurred.

An error factor is calculated on the basis:

$$E = a_1 \frac{de}{dt} + a_2 e + a_3 \int_{\text{Start of stage}}^{\text{Present}} e dt \quad (8.4.1)$$

where  $e$  is the current error and  $E$  the error factor. The constants  $a_1$ ,  $a_2$  and  $a_3$  were determined experimentally prior to the main test series to provide the most efficient following of the required path

without drift or hunting about the correct value. It was found impossible to eliminate hunting completely, but it could be maintained within acceptable limits. For all the tests the value of  $a_3$  used was zero as the use of this term did not improve the performance of the system.

The error factor is added to the previous motor speed, provided that this does not result in the maximum or minimum value being exceeded, in which case the limit value is simply used. The digital to analogue converters are then used to re-set the motor speeds, which are then held constant automatically until the end of the next control cycle.

The entire control is then re-entered, with the whole process being completed about three times per second, provided that none of the interruption routines is entered. About 80% of the time is taken in reading the transducers, calculation taking the remaining 20%. Since a typical stage of a test takes 30 minutes, about 500 control cycles are executed per stage, allowing close following of stress paths, e.g. as shown in Figure 8.11. The solid line shows the input stress path required and the open squares the stress points measured by the PDP-8E computer; the two paths are in very close agreement. After the full analysis of the control tape and more precise corrections the points shown as solid squares are given. These deviate slightly from the original intended path, with the whole cycle being shifted by an approximately constant amount.

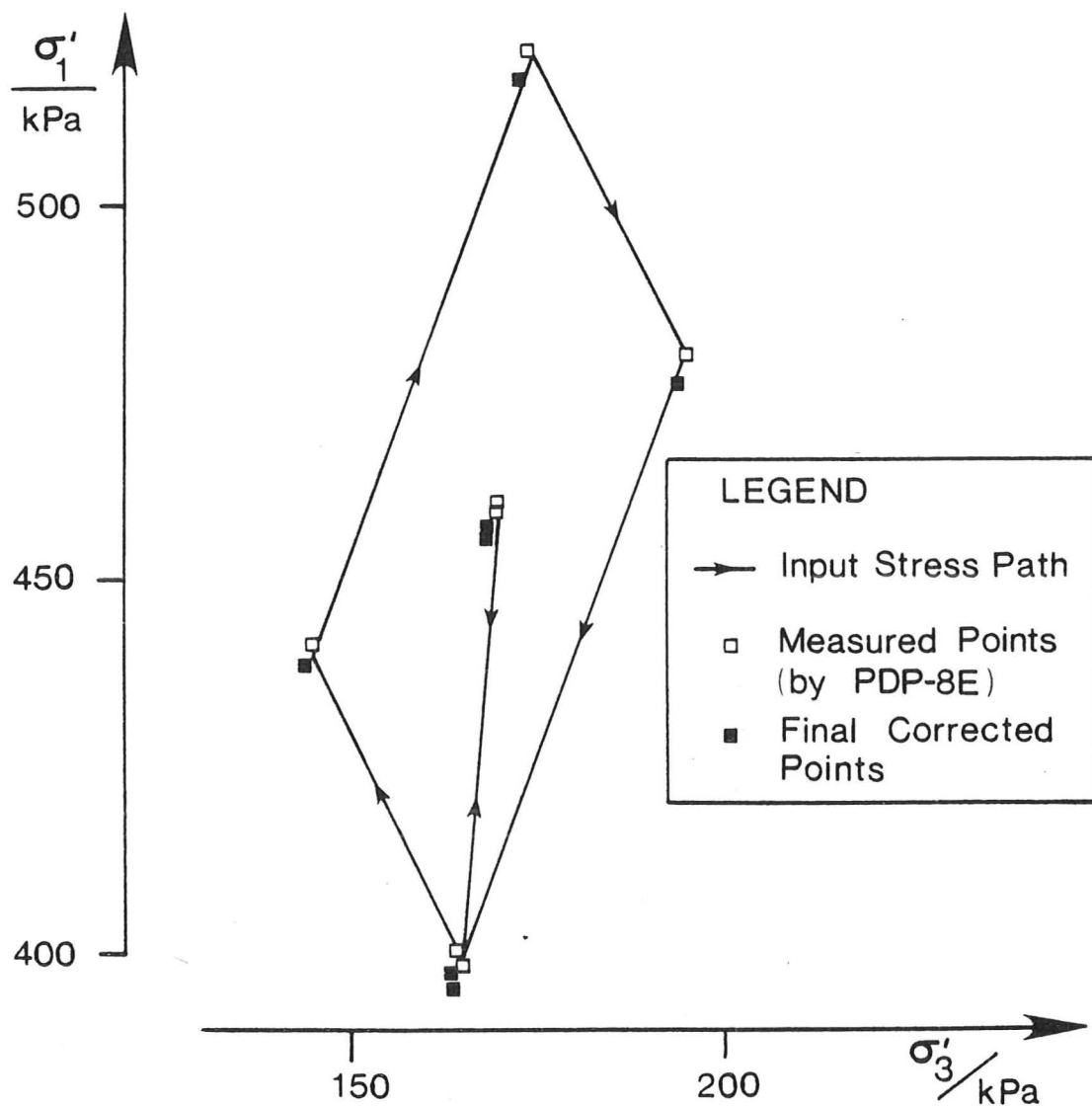


Figure 8.11 Following of a stress path in the triaxial apparatus, test 2051, cycle 2

### 8.5 Sample Preparation

Before use in the tests the sand was sieved and weighed in the air dry state, then saturated with de-aired water, boiled for approximately 15 minutes and allowed to cool. A split former for the cylindrical 70 mm  $\times$  70 mm sample was assembled on the base plate of the triaxial cell as shown in Figure 8.12, in which all fixing bolts have been omitted for clarity, and in Figure 8.13.

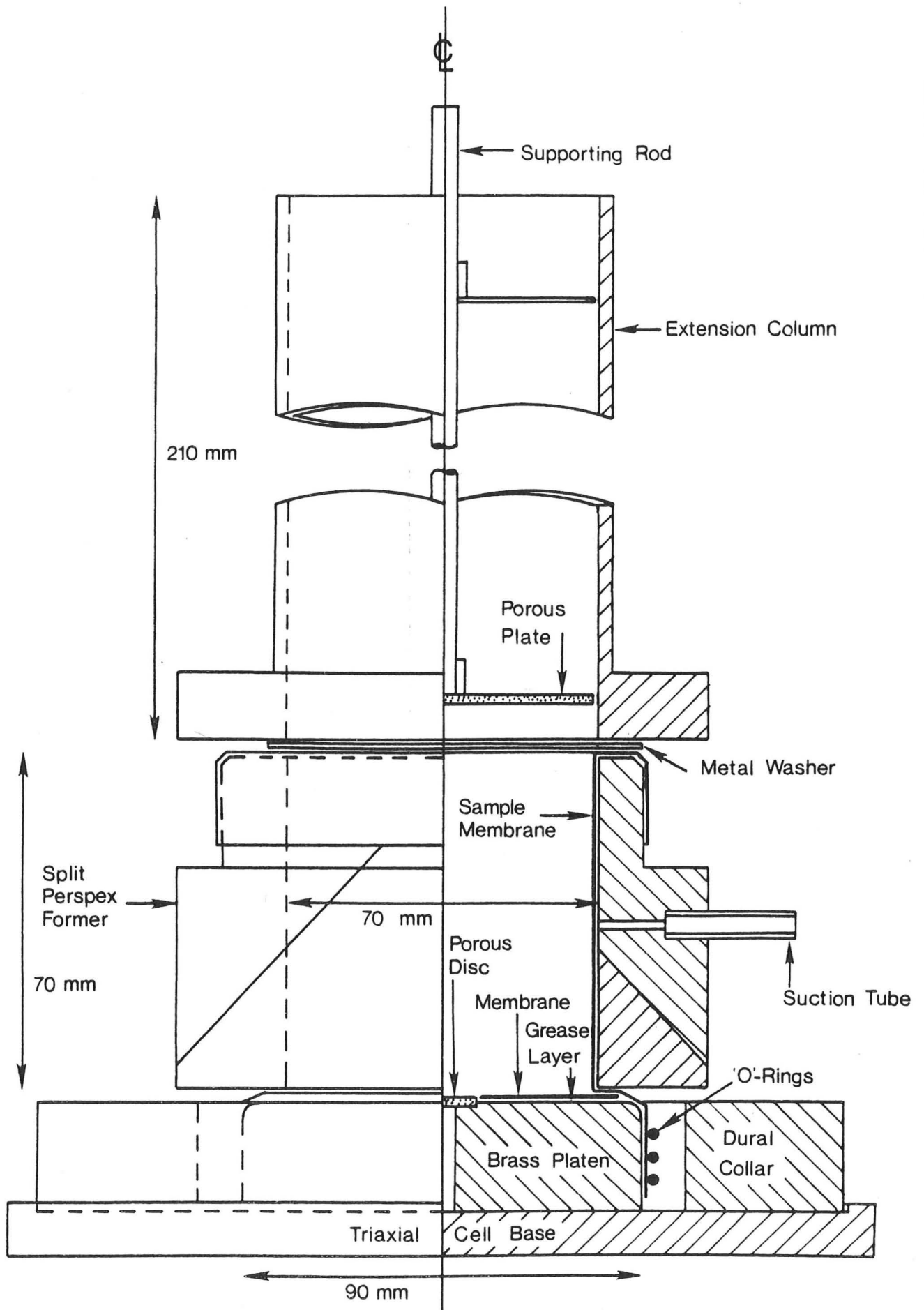


Figure 8.12 Sample preparation assembly (details of fixing bolts omitted)

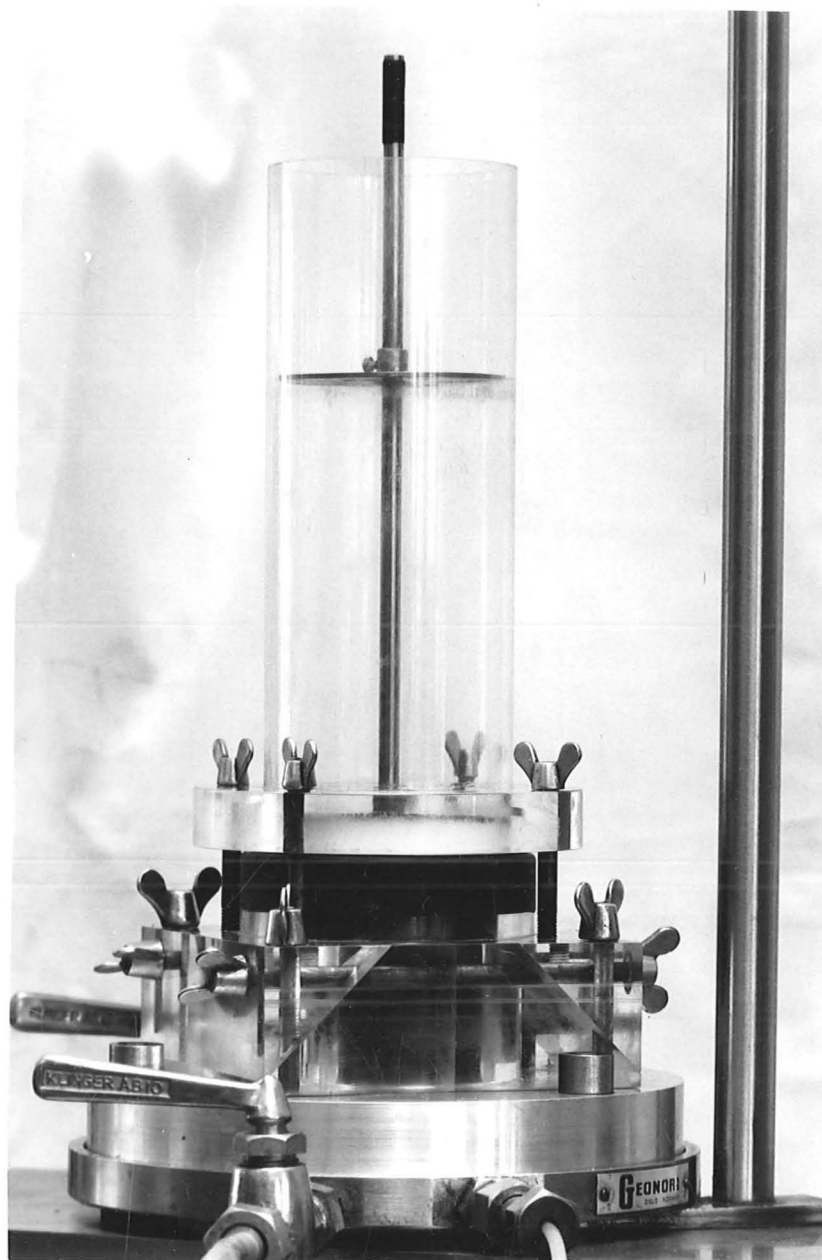


Figure 8.13 Sample preparation assembly

In the centre of the base platen is a drainage hole capped by a 15 mm diameter sintered metal disc. The remainder of the polished brass base platen is coated with a thin layer of silicone grease (Molykote 33M) and a 0.35 mm thick latex rubber membrane. The 0.42 mm thick latex rubber membrane surrounding the sample is moulded to fit the 90 mm diameter end caps, which are larger than the sample diameter to accommodate lateral expansion during the test. The membrane was sealed

to the base platen with three O-rings and held against the sample former by suction.

The former was extended vertically by a 210 mm high perspex column of 70 mm internal diameter, and both the sample space and column filled with de-aired water. The sand was then slowly spooned into the top of the column and allowed to settle. The weight of sand was chosen so that in the loose state achieved there was a surplus of about 10 mm height of sand above the top of the former. A porous metal disc of diameter slightly less than the extension column was then gently lowered onto the surface of the sand, and the whole of the base plate and former assembly vibrated using a pneumatic hammer.

A total of approximately one minute of vibration was necessary to bring the sample to the densest possible state using this method, and the height of a mark on the supporting rod for the porous disc was measured in order to check on the density achieved. The supporting rod was then removed and the water drained from the extension column. The extension column and the porous disc could then be removed gently, leaving the surface of the sand about 1 mm above the metal washer capping the sample former. The sand remained saturated at this stage due to surface tension. The top of the sand was formed to a flat surface by cutting a palette knife across the top of the metal washer. At this stage some loosening of the top layer of grains must have occurred, but this disadvantage is offset by the necessity of an exactly flat surface on the top of the sand before the placing of the top cap.

The metal washer capping the former was removed and a slight meniscus raised above the top of the sample by allowing a slow upward flow through the sample from the drainage hole. The polished brass top cap, with the face covered with a thin layer of silicone grease and

a membrane (as for the base platen) was then carefully lowered onto the top of the sample, the water meniscus allowing exclusion of air bubbles. The membrane was then raised and sealed to the top cap with three O-rings and a suction of approximately 10 kPa applied to the pore fluid through the drainage line to a burette. The split former could then be removed from the sample, the oblique cuts avoiding interference with the end platens. The height and diameter of the sample were measured and a burette reading taken to provide datum values for the dimensions of the sample. The triaxial cell was then assembled and transferred to the loading frame.

The cell was filled with water, with some heavy oil introduced at the top of the cell to prevent leakage past the rotating bushing. The loading ram was then attached to the axial drive, the LVDT positioned and reference values for the transducers read. Datum values for the cell pressure transducer and the pressure transducer on the volume change device were taken whilst both transducers were connected to an identical head of about 10 kPa, so that all subsequent pressure measurements truly represent the pressure difference across the sample membrane. The axial load was zeroed with the cell bushing rotating and the ram not in contact with the sample. A cell pressure of about 30 kPa was then applied and the volume change of the sample noted from the change in burette reading. Finally the pore water connection was transferred from the burette to the automatic volume measuring device, the ram brought into contact with the top cap and the zero reading for the axial strain taken. Transfer to automatic control was then made.

At the end of the test a much simplified reverse procedure was followed, with the sand from the sample being collected and oven dried before weighing to provide a check on the sample density. Values of

the initial specific volumes for the specimens reported here are given in Table 7.1.

The stresses and strains calculated for the samples were corrected to account for the compressibility of the loading ram, the membrane stiffness and the penetration of the membrane. Full details of these calculations are given in Appendix C.

In this Chapter the mechanical details of the triaxial apparatus, the system used in the control program and the procedure for assembling a triaxial sample have been described, together with details of the calibration of the measurement system. In the next Chapter the results of the stress cycle tests carried out in the triaxial apparatus are described.

## CHAPTER 9

## STRESS CYCLE TESTS ON DENSE SAND

The method of analysis for the stress cycle tests using a routine for optimising the fit of the elastic and plastic properties is described. The results of the tests are presented and the variation of elastic properties with stress and with stress history is discussed. Plastic behaviour is found to depend strongly on the stress history.

### 9.1 Analysis of Stress Cycle Tests

The analysis of the stress cycle tests on dense sand was carried out in four stages. The first stage was simply the processing of the output tape from the PDP-8E using the full corrections described in Appendix C to give a series of approximately 1000 stress and strain points for a typical test. The stress path was plotted out to provide a check on the intended path, and in each case the input stress path had been closely followed in the actual test. The data usually included a few isolated points representing clearly erroneous values, presumably as a result of interference on the datalogging system, and these points were deleted for the purposes of subsequent analysis.

The second stage of analysis involved the extraction of the data for each stress cycle from the information for the whole test, and plotting of this data in a standard format. The format used presents the data on four graphs with axes  $(p',q)$ ,  $(\epsilon,q)$ ,  $(p',v)$  and  $(\epsilon,v)$  as shown in Figure 9.1. The mapping of a line AB in these stress strain diagrams is also shown on the Figure. Diagram (a) gives the stress path, (b) the shear stress - shear strain response, (c) the pressure - volumetric strain response, and (d) and strain path. False origins are used for all the plots. Figure 9.2 shows a typical set of data, the small inset sketches showing the approximate path for each diagram. An assessment of the general character of the response to the stress cycle can be made from

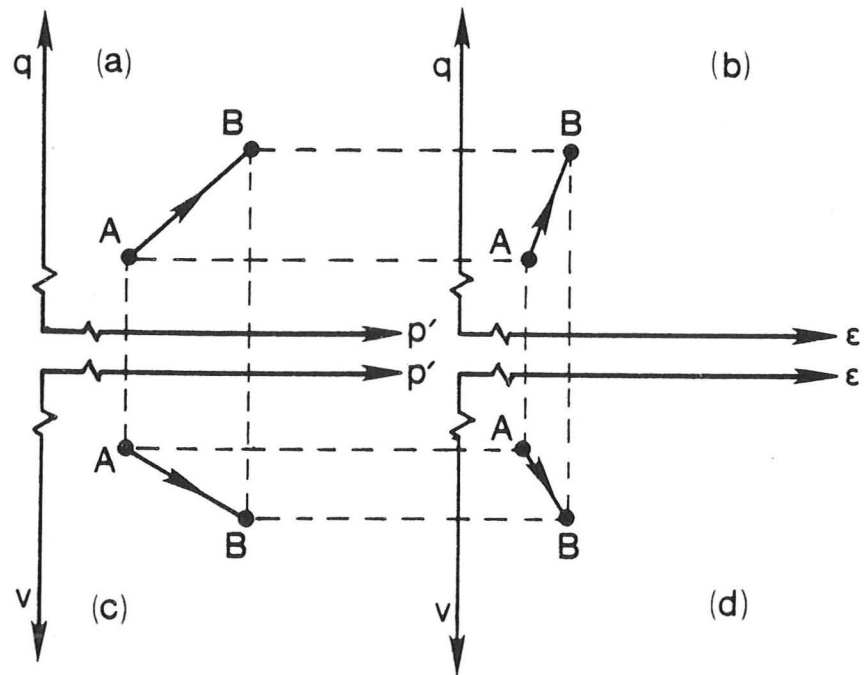


Figure 9.1 Stress and strain diagrams for presentation of stress cycle tests

this diagram. In this case the substantially elastic response gives a mapping of the parallelogram in stress space into a similar shape in strain space (Figure 9.2(a) and (d)). A plastic response gives much larger strains in a fixed direction in strain space (as a result of the flow rule) and a permanent strain at the end of the cycle (Figure 9.3). In many tests, however, it was not possible to distinguish a definite elastic and plastic response, with both effects being of comparable magnitude (Figure 9.4).

In all tests there was, however, evidence of a phase of recoverable behaviour, suggesting that an elastic-plastic type of response was occurring. The analysis of even the elastic part is, however, complicated by the possibility of anisotropy. For an isotropic elastic material the stiffness matrix in triaxial parameters is given by:

$$\begin{bmatrix} \dot{p}' \\ \dot{q} \end{bmatrix} = \begin{bmatrix} K & 0 \\ 0 & 3G \end{bmatrix} \begin{bmatrix} \dot{v}_e \\ \dot{\epsilon}_e \end{bmatrix} \quad (9.1.1)$$

so that there is no link between the  $p'$ - $v$  and  $q$ - $\epsilon$  responses, both being given by unique straight lines. In Figure 9.2 the response is

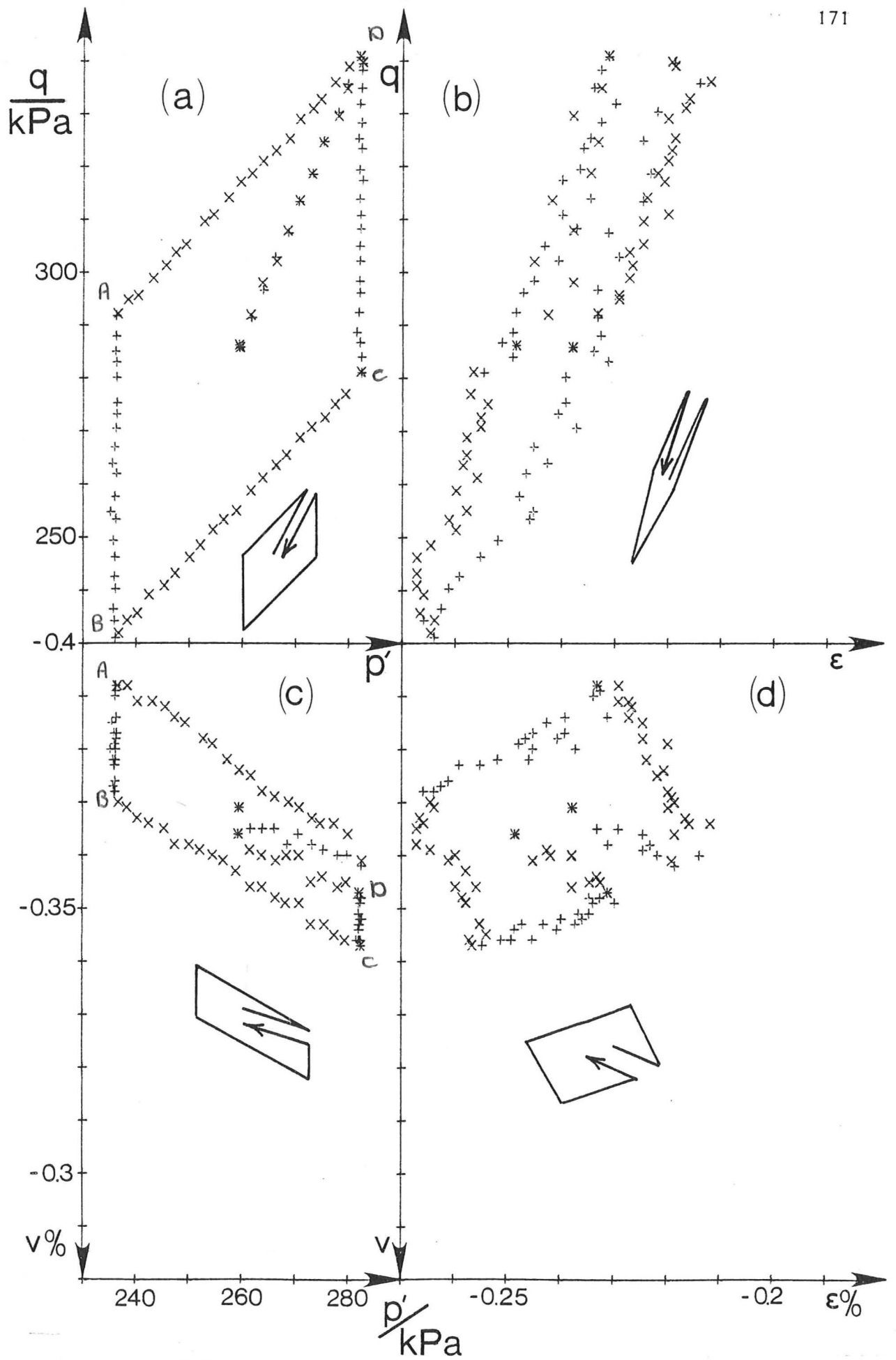


Figure 9.2 Test 2022, data for stress cycle starting at point 881

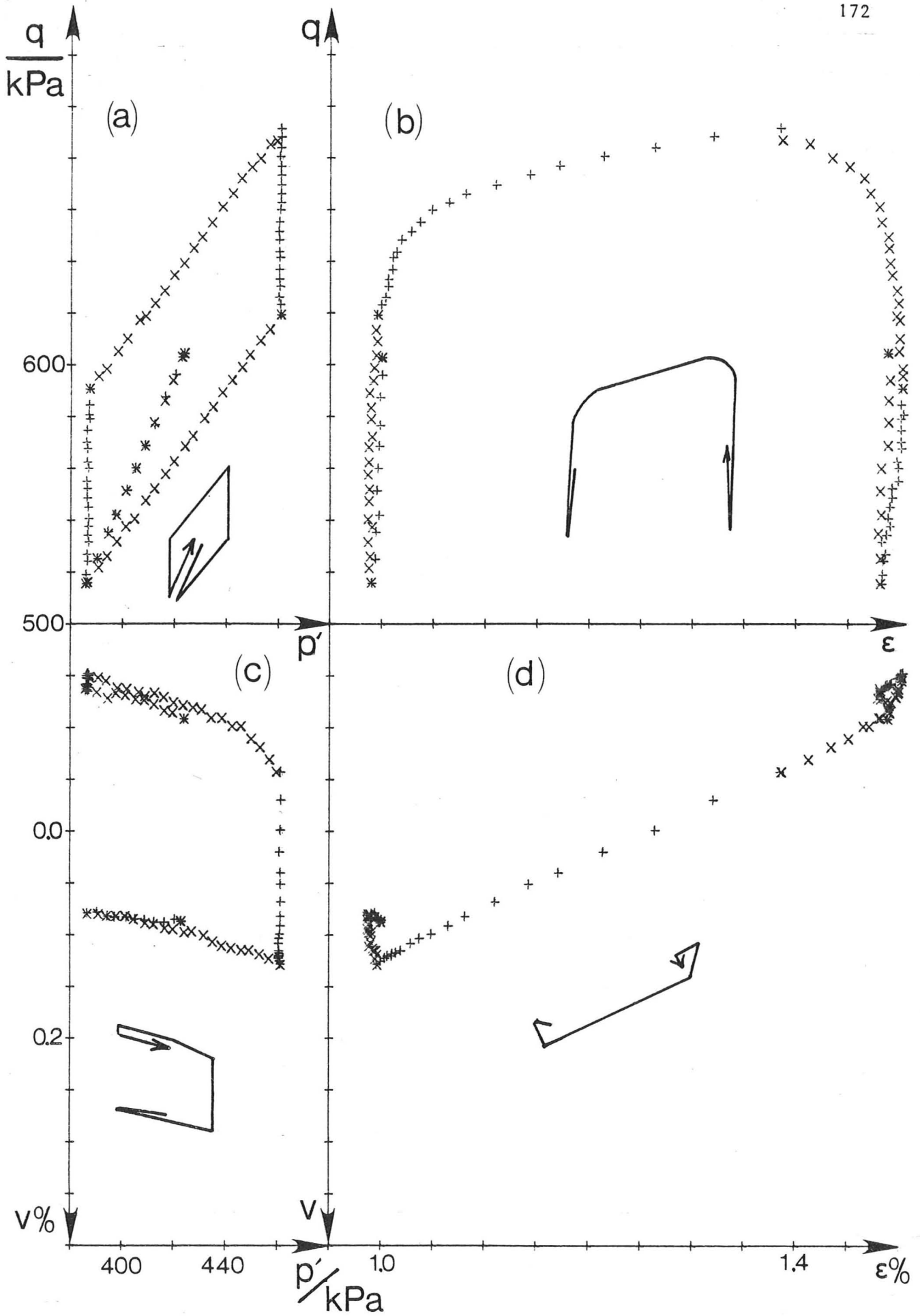


Figure 9.3 Test 2022, data for stress cycle starting at point 311

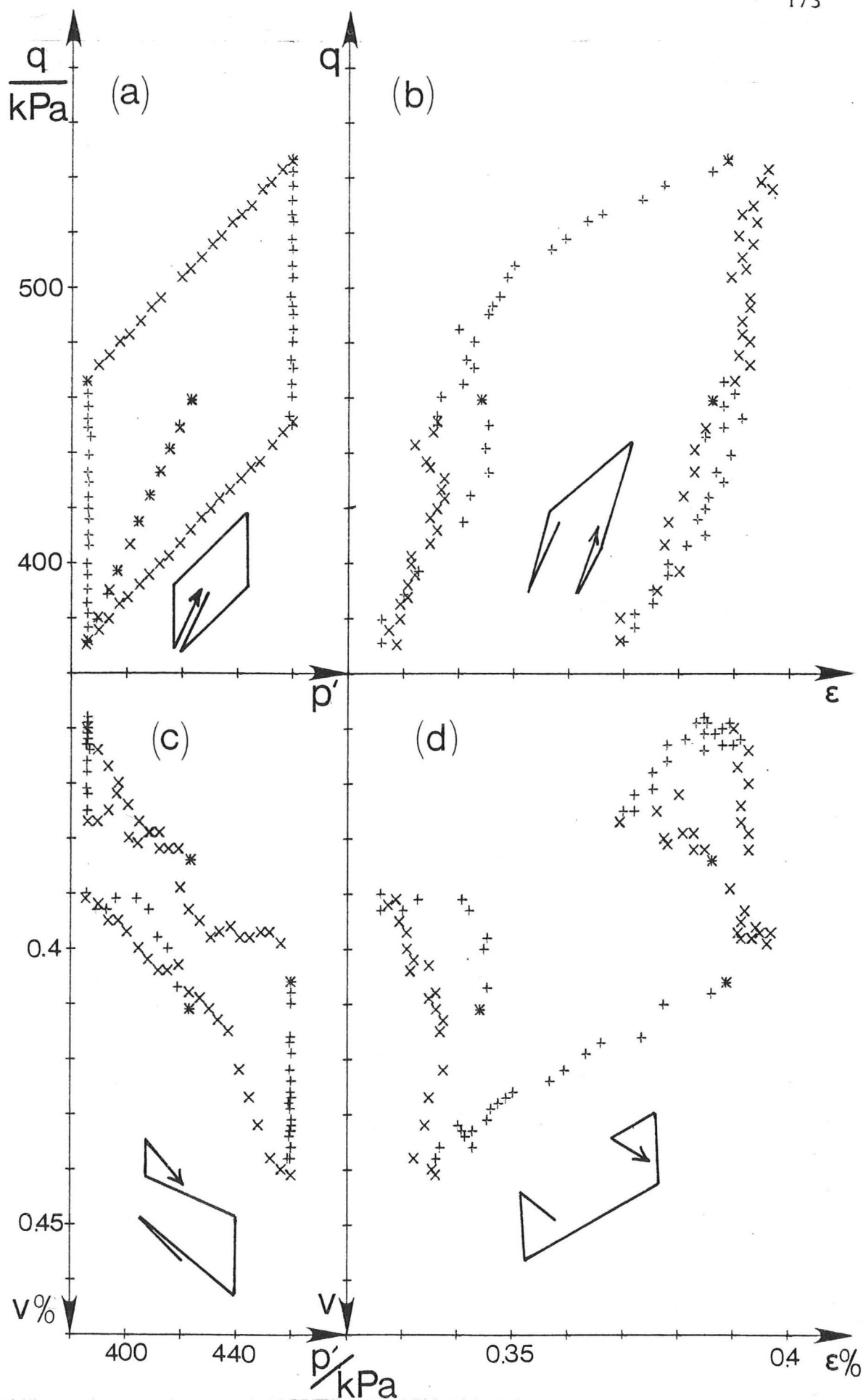


Figure 9.4 Test 1034, data for stress cycle starting at point 171

mainly elastic, but during changes of shear stress at constant pressure (AB and CD) there is a change in volume. This is due to the off diagonal terms in Equation (9.1.1) being non-zero, which is an indication of anisotropy.

Because of this complicating factor the elastic properties cannot simply be measured from the stress-strain plots. Equally well the plastic properties are not easily distinguished in a plot such as Figure 9.4. The third stage of the analysis, which is described in detail in the next Section, therefore involved the automatic fitting of elastic and plastic properties to each stress cycle using an optimisation routine. The final stage of the analysis then involved the collation and comparison of the properties measured for each cycle.

## 9.2 Optimisation of Elastic and Plastic Properties

The first stage in the derivation of the elastic and plastic properties involves the selection of an appropriate theoretical framework to describe the state of the sample. The elastic properties will be described by a constant stiffness matrix. The plastic properties will be described by a single straight yield locus, which remains parallel to its original location as it is translated by additional plastic deformation; a constant hardening modulus and a constant ratio between the plastic strain increments will be assumed. All these assumptions are made on the grounds that during any given stress cycle the changes in stress are small compared to the magnitudes of the stresses themselves (the size of the cycles was chosen so that the changes were approximately 10% of the current stresses). All the above properties were determined independently for each stress cycle.

As far as the (constant) elastic behaviour is concerned, it is reasonable to assume that a specimen of sand in a triaxial test, prepared by pouring and vibrating, will be orthotropic. For this case the elastic

mainly elastic, but during changes of shear stress at constant pressure (AB and CD) there is a change in volume. This is due to the off diagonal terms in Equation (9.1.1) being non-zero, which is an indication of anisotropy.

Because of this complicating factor the elastic properties cannot simply be measured from the stress-strain plots. Equally well the plastic properties are not easily distinguished in a plot such as Figure 9.4. The third stage of the analysis, which is described in detail in the next Section, therefore involved the automatic fitting of elastic and plastic properties to each stress cycle using an optimisation routine. The final stage of the analysis then involved the collation and comparison of the properties measured for each cycle.

## 9.2 Optimisation of Elastic and Plastic Properties

The first stage in the derivation of the elastic and plastic properties involves the selection of an appropriate theoretical framework to describe the state of the sample. The elastic properties will be described by a constant stiffness matrix. The plastic properties will be described by a single straight yield locus, which remains parallel to its original location as it is translated by additional plastic deformation; a constant hardening modulus and a constant ratio between the plastic strain increments will be assumed. All these assumptions are made on the grounds that during any given stress cycle the changes in stress are small compared to the magnitudes of the stresses themselves (the size of the cycles was chosen so that the changes were approximately 10% of the current stresses). All the above properties were determined independently for each stress cycle.

As far as the (constant) elastic behaviour is concerned, it is reasonable to assume that a specimen of sand in a triaxial test, prepared by pouring and vibrating, will be orthotropic. For this case the elastic

matrix is given by five constants (after Love (1927)):

$$\begin{bmatrix} \dot{\sigma}_{11} \\ \dot{\sigma}_{22} \\ \dot{\sigma}_{33} \\ \dot{\sigma}_{23} \\ \dot{\sigma}_{31} \\ \dot{\sigma}_{12} \end{bmatrix} = \begin{bmatrix} A & B & B & & & \\ B & C & D & & & \\ B & D & C & & & \\ & & & C-D & & \\ & & & & E & \\ & & & & & E \end{bmatrix} \begin{bmatrix} \dot{\epsilon}_{11} \\ \dot{\epsilon}_{22} \\ \dot{\epsilon}_{33} \\ \dot{\epsilon}_{23} \\ \dot{\epsilon}_{31} \\ \dot{\epsilon}_{12} \end{bmatrix} \quad (9.2.1)$$

in which the 1-direction is vertical. All other terms in the matrix are zero. In the triaxial test only non-rotating principal stresses may be applied, so no information may be deduced about E, and only the top  $3 \times 3$  matrix investigated. The further restriction that  $\sigma_{22} = \sigma_{33}$  and  $\epsilon_{22} = \epsilon_{33}$  is imposed, so that the matrix reduces to:

$$\begin{bmatrix} \dot{\sigma}_{11} \\ \dot{\sigma}_{33} \end{bmatrix} = \begin{bmatrix} A & 2B \\ B & C+D \end{bmatrix} \begin{bmatrix} \dot{\epsilon}_{11} \\ \dot{\epsilon}_{33} \end{bmatrix} \quad (9.2.2)$$

so that C and D cannot be determined independently in the triaxial test, which yields only three pieces of information about the four variables A,B,C,D. In order to estimate the values some assumption must be made. A reasonable assumption may be that the isotropic matrix:

$$\begin{bmatrix} \dot{\sigma}_{11} \\ \dot{\sigma}_{22} \\ \dot{\sigma}_{33} \end{bmatrix} = \begin{bmatrix} A & B & B \\ B & A & B \\ B & B & A \end{bmatrix} \begin{bmatrix} \dot{\epsilon}_{11} \\ \dot{\epsilon}_{22} \\ \dot{\epsilon}_{33} \end{bmatrix} \quad (9.2.3)$$

is modified by multiplying the second and third rows and columns by some "anisotropy factor" a to give:

$$\begin{bmatrix} \dot{\sigma}_{11} \\ \dot{\sigma}_{22} \\ \dot{\sigma}_{33} \end{bmatrix} = \begin{bmatrix} A & aB & aB \\ aB & a^2A & a^2B \\ aB & a^2B & a^2A \end{bmatrix} \begin{bmatrix} \dot{\epsilon}_{11} \\ \dot{\epsilon}_{22} \\ \dot{\epsilon}_{33} \end{bmatrix} \quad (9.2.4)$$

Although any number of alternative definitions of anisotropy could be used, each involving three elastic parameters, this definition represents a reasonable hypothesis that the anisotropy affects the values

of both C and D. Even if the real behaviour does not take the form assumed, the parameter a may still be derived from a triaxial test and used as a rational measure of anisotropy; more complex tests would be required to assess the validity of this assumed form of the elastic matrix. The quantity  $a^2$  represents the ratio of direct stiffnesses in the radial and axial directions. Isotropy is given by  $a = 1.0$ , and values of a less than unity indicate a sample stiffer vertically than horizontally. The stiffness matrix in triaxial parameters is:

$$\begin{bmatrix} \dot{p}' \\ \dot{q} \end{bmatrix} = \begin{bmatrix} (A+4aB+2a^2(A+B))/9 & (A+aB-a^2(A+B))/3 \\ (A+aB-a^2(A+B))/3 & (A-2aB+a^2(A+B))/2 \end{bmatrix} \begin{bmatrix} \dot{v}_e \\ \dot{\epsilon}_e \end{bmatrix} = \begin{bmatrix} K & E_{pq} \\ E_{pq} & 3G \end{bmatrix} \begin{bmatrix} \dot{v}_e \\ \dot{\epsilon}_e \end{bmatrix} \quad (9.2.5)$$

where K and G are retained and are similar to the bulk and shear moduli,  $E_{pq}$  is a modulus giving the cross effect between shear and volumetric behaviour. The inverse matrix will be denoted by:

$$\begin{bmatrix} \dot{v}_e \\ \dot{\epsilon}_e \end{bmatrix} = \begin{bmatrix} C_1 & C_2 \\ C_2 & C_3 \end{bmatrix} \begin{bmatrix} \dot{p}' \\ \dot{q} \end{bmatrix} \quad (9.2.6)$$

For an isotropic material the value of Poisson's ratio is given by  $\nu = B/(A+B)$ , and for the anisotropic material the same definition will be used for a parameter  $\nu^*$  which represents an analogous quantity to the conventional Poisson's ratio.

The plastic properties are given by assuming a yield locus and plastic potential in the forms:

$$f = q - M_y p' - 2c_y \quad (9.2.7)$$

$$g = q - M_f p' - 2c_f \quad (9.2.8)$$

where  $M_y$ ,  $c_y$ ,  $M_f$  and  $c_f$  are constants for each stress cycle. This does not imply that Equation (9.2.7) represents the whole yield locus, but only that it is locally approximated as a straight line; in particular, although  $2c_f$  represents the intercept of the locus on the

q-axis, it is not suggested that this in any way represents a true cohesion.

Adopting the Hill (1950) formulation the plastic strain is given by the expressions:

$$dv_p = \frac{1}{h} \frac{\partial g}{\partial p'} \left( \frac{\partial f}{\partial p'} dp' + \frac{\partial f}{\partial q} dq \right) \quad (9.2.9)$$

$$d\epsilon_p = \frac{1}{h} \frac{\partial g}{\partial q} \left( \frac{\partial f}{\partial p'} dp' + \frac{\partial f}{\partial q} dq \right) \quad (9.2.10)$$

where  $h$  is a hardening modulus. These expressions reduce to:

$$dv_p = -M_f(-M_y dp + dq)/h \quad (9.2.11)$$

$$d\epsilon_p = (-M_y dp + dq)/h \quad (9.2.12)$$

For the stress cycle tests these equations are implemented in the following way. As long as the cycle remains within the yield locus there is no plastic strain. If the stress point passes beyond the initial yield locus plastic strain is calculated proportional to the maximum distance the stress point has passed beyond the locus. The bracketed terms in Equations (9.2.11) and (9.2.12) represent the increment in the  $q$  direction from the initial yield locus, and for the finite stress change in the stress cycle tests this is equal to  $\Delta(q - M_y p' - 2c_y)$ . The maximum value of this quantity will be denoted as  $d$  (see Figure 9.5) and the plastic strains then given by:

$$dv_p = -M_f d/h, \quad d\epsilon_p = d/h \quad (9.2.13)$$

Finally it is useful to define a normalised hardening modulus  $h_n$  which gives the ratio between the perpendicular displacement of the initial yield locus ( $d_p$  in Figure 9.5) and the magnitude of the plastic strain increment:

$$h_n = d_p / (dv_p + d\epsilon_p)^{1/2} = h / [(1+M_f^2)(1+M_y^2)]^{1/2} \quad (9.2.14)$$

The plastic behaviour of the material during a stress cycle is described by four parameters ( $h, M_f, M_y, c_y$ ) and the elastic behaviour

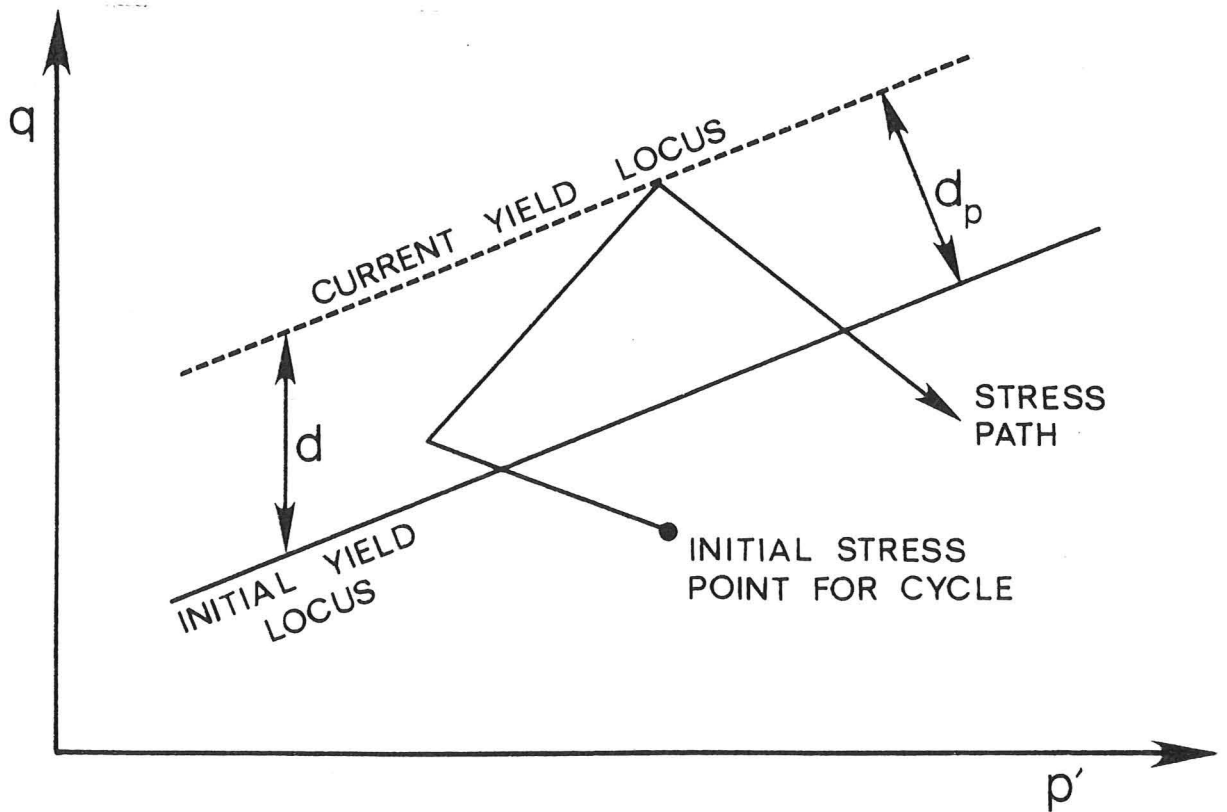


Figure 9.5 Calculation of plastic strain for a stress cycle test

by three parameters (either  $A, B, a$  or, more conveniently,  $C_1, C_2, C_3$  from which  $A, B$  and  $a$  may be derived). For any value of the stress increment in the cycle the strain increment depends therefore on seven parameters, and the actual strain will depend also on the strain at the start of the cycle  $(v_o, \epsilon_o)$ , giving nine unknown quantities altogether. The procedure for finding the properties for a given cycle involves the optimisation of nine quantities simultaneously to obtain the best fit to the experimental data. This was achieved by calculating for each data point the difference between the actual measured strain and the calculated strain:

$$v_{err} = v - v_o - C_1(p' - p'_o) - C_2(q - q_o) + M_f d/h \quad (9.2.15)$$

$$\epsilon_{err} = \epsilon - \epsilon_o - C_2(p' - p'_o) - C_3(q - q_o) - d/h \quad (9.2.16)$$

where  $d$  is equal to the maximum change of  $(q - M_y p' - 2c_y)$  since the beginning of the cycle. A root mean square error was then calculated:

$$e = \left( \sum_{1}^{N} (v_{\text{err}}^2 + \epsilon_{\text{err}}^2) \right)^{\frac{1}{2}} / N \quad (9.2.17)$$

where  $N$  is the number of data points in the cycle. The values of the nine parameters were systematically adjusted until  $e$  was minimised. Minimisation of such a function of many variables is not trivial, and there is no guarantee that a procedure will find an absolute rather than merely a local minimum. Neither in this case is there any definite knowledge that the minimisation will represent the true values of the parameters; but only that, using the error measure given above, they represent the best fit to the data.

Under these conditions a sophisticated minimisation technique was not justified, and a routine which minimised  $e$  by varying each parameter in turn, with the rest remaining constant, was used. The minimum was found by successively stepping the value of the control variable, with the step size being halved and reversed if the error increased (see Figure 9.6). The number of cycles of minimisation with respect to all the parameters was controlled manually and a check on the current error and parameter values made. The process was terminated when a satisfactory minimum was found.

### 9.3 Constraints on the Minimisation Procedure

Due to the presence of experimental error it is possible that the procedure outlined above would result in a minimum at unrealistic values of the parameters. For example the presence of a small amount of creep during unloading after a large plastic strain may be best fitted by a negative shear modulus. Even without experimental error unrealistic values may be derived if the idealisation is incorrect, for instance if the behaviour of sand requires the presence of a pointed yield locus for its description.

Any analysis involves the imposition of certain preconceived ideas

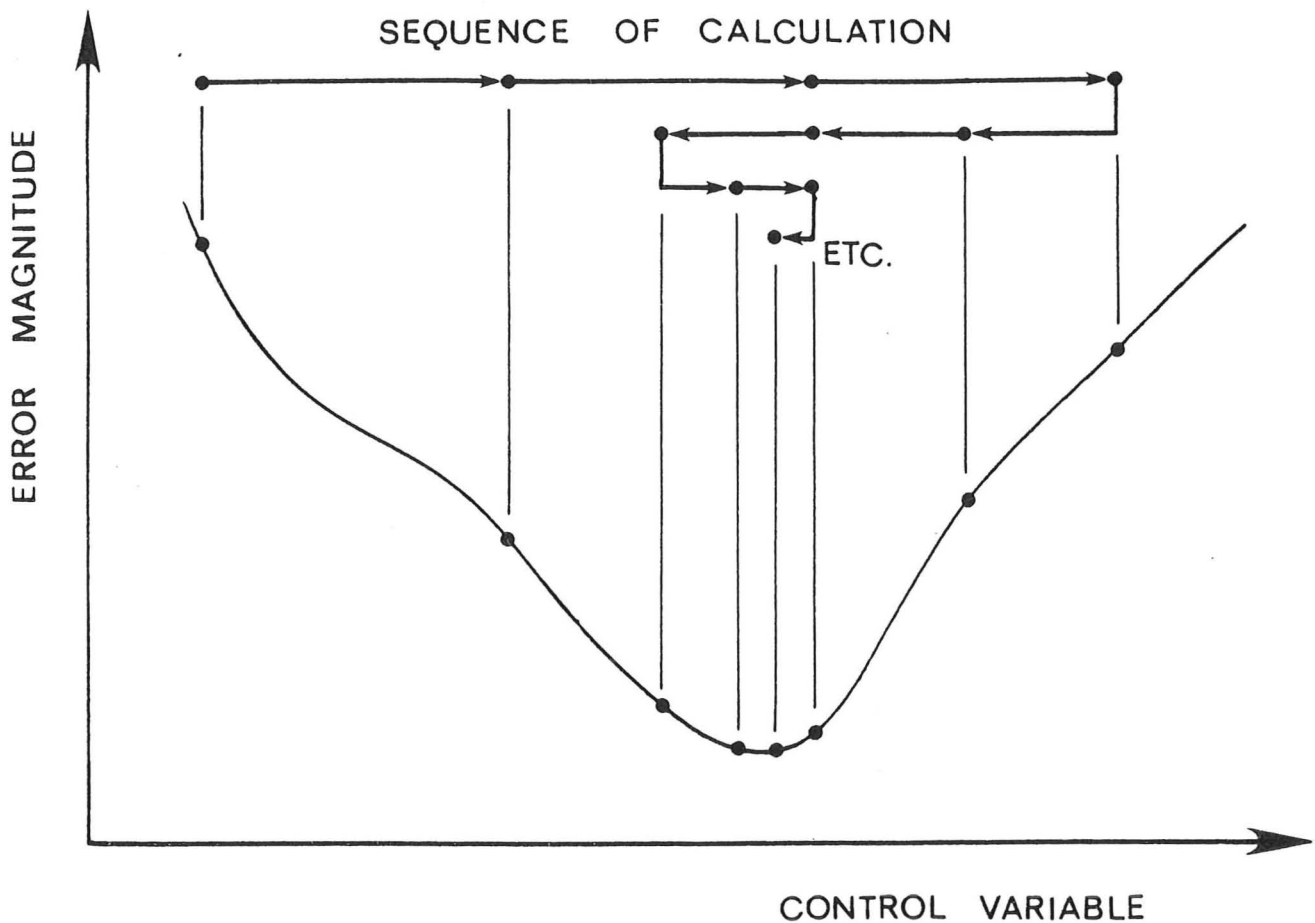


Figure 9.6 Error minimisation procedure

on the interpretation of experimental data, and in this case as well as the limitation of a simple elastic plastic model certain further constraints were imposed. It was assumed that the parameters  $A$ ,  $B$  and  $a$  were all positive. This is simply an extension of the constraint of a positive Young's modulus and Poisson's ratio so that none of the terms in the stiffness matrix is negative. Although there is no fundamental reason why the off diagonal terms of the matrix should be positive, no material is known which exhibits a negative Poisson's ratio, and such a material seems intuitively unlikely. These restrictions were usually achieved automatically in the optimisation program by limiting the value of  $C_3$  as a function of  $C_1$  and  $C_2$ , but in two cases arbitrary additional constraints were necessary.

As far as plastic behaviour is concerned the first restriction

imposed is that the plastic strain increment vector should be outward directed from the yield locus. Whilst normality is not required, certain further limits will also be put on the direction of the plastic strain increment. If a sand was idealised as a rigid-plastic material with no cohesion, described solely by angles of friction and dilation, then the angle of friction must always be greater than the angle of dilation, and this is indeed observed in practice. If this were not the case the material would exhibit negative dissipation: the limiting case of the angles being equal gives zero dissipation. It was found in Section 3.3 that for rigid-plastic materials lack of normality is related to the dependence of dissipation on stress. Examination of functions for dissipation shows also that, if the dissipation increases with stress, the plastic strain vector is deflected from normality in the direction of greater volumetric compression.

It seems intuitively unlikely that sand will show decreased dissipation on an increase in pressure, so the limitation will be made that the plastic strain increment should be in a direction giving no less volumetric compression than implied by normality. The allowable ranges of the strain increment direction are shown marked A on Figure 9.7 for a variety of orientations of the yield locus. This criterion is not the same as disallowing negative plastic work, since unlike the simple rigid-frictional material the yield locus does not necessarily pass through the origin. Frictional materials do not always behave in a way which is intuitively obvious, and this restriction may certainly be questioned.

The remaining restrictions are on the location of the yield locus. Firstly the initial point of a stress cycle is not allowed to lie outside the initial yield locus. Secondly, if the stress cycle has been approached from a particular direction then it will be clear that for certain orientations of the yield locus the initial point must

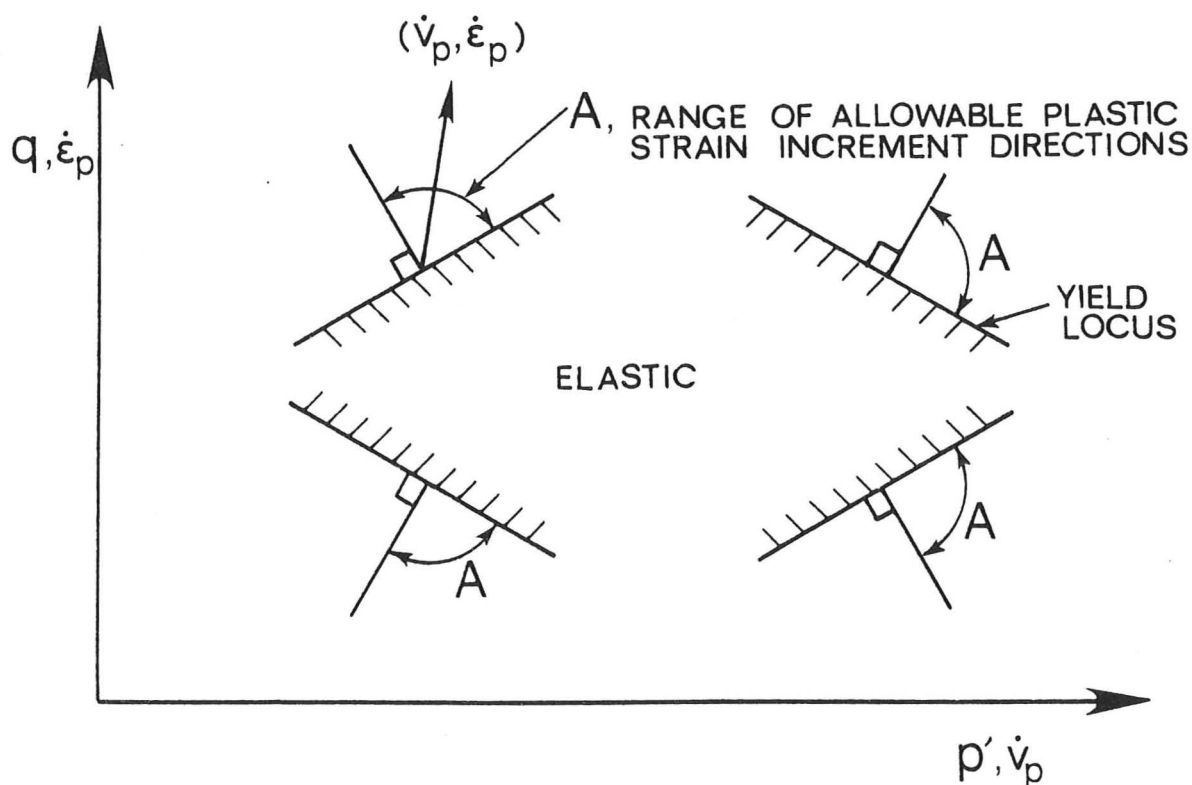


Figure 9.7 Allowable ranges of plastic strain increment directions lie on the locus (i.e. that the yield locus does not move 'ahead' of the stress point). This condition was imposed on certain cycles after examination of a preliminary analysis. The effect is usually minor, except that the value of the hardening modulus is increased.

#### 9.4 Representation of Stress Cycle Test Results

The derived values of the nine parameters were used to calculate the theoretical strain response for the cycle, and this compared with the actual response. Figure 9.8 shows the close fitting of a cycle in which the plastic strains predominate, and Figure 9.9 a cycle in which the elastic strains were larger than the plastic strains.

The properties derived from all the tests are given in Table 9.1, together with the average stresses for the cycle and the cycle history summarised by maximum past stress values. Those cycles for which the fitting of properties was unsatisfactory are noted in Table 9.1. The

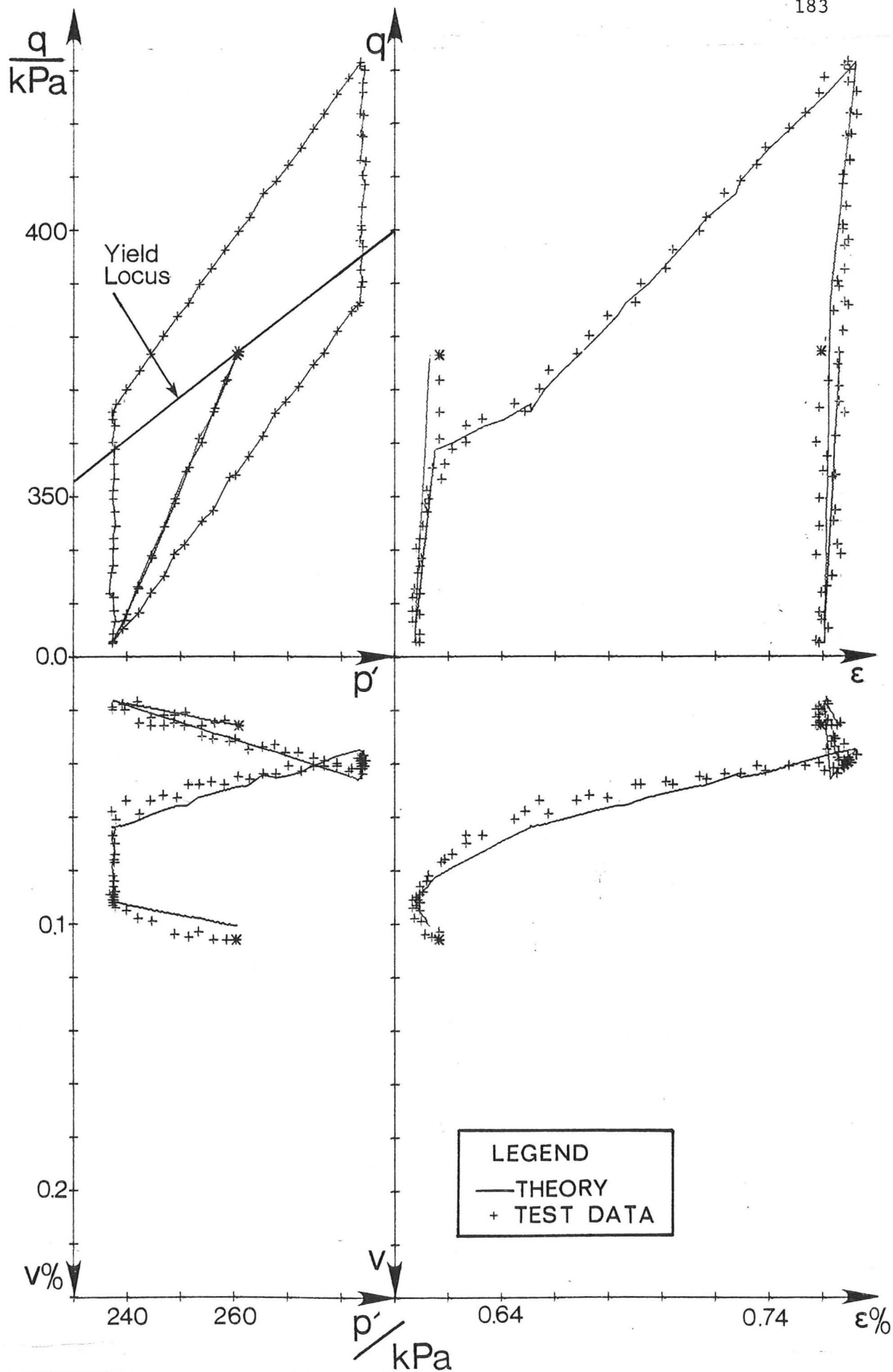


Figure 9.8 Test 2033, data and fitted properties for stress cycle starting at point 301

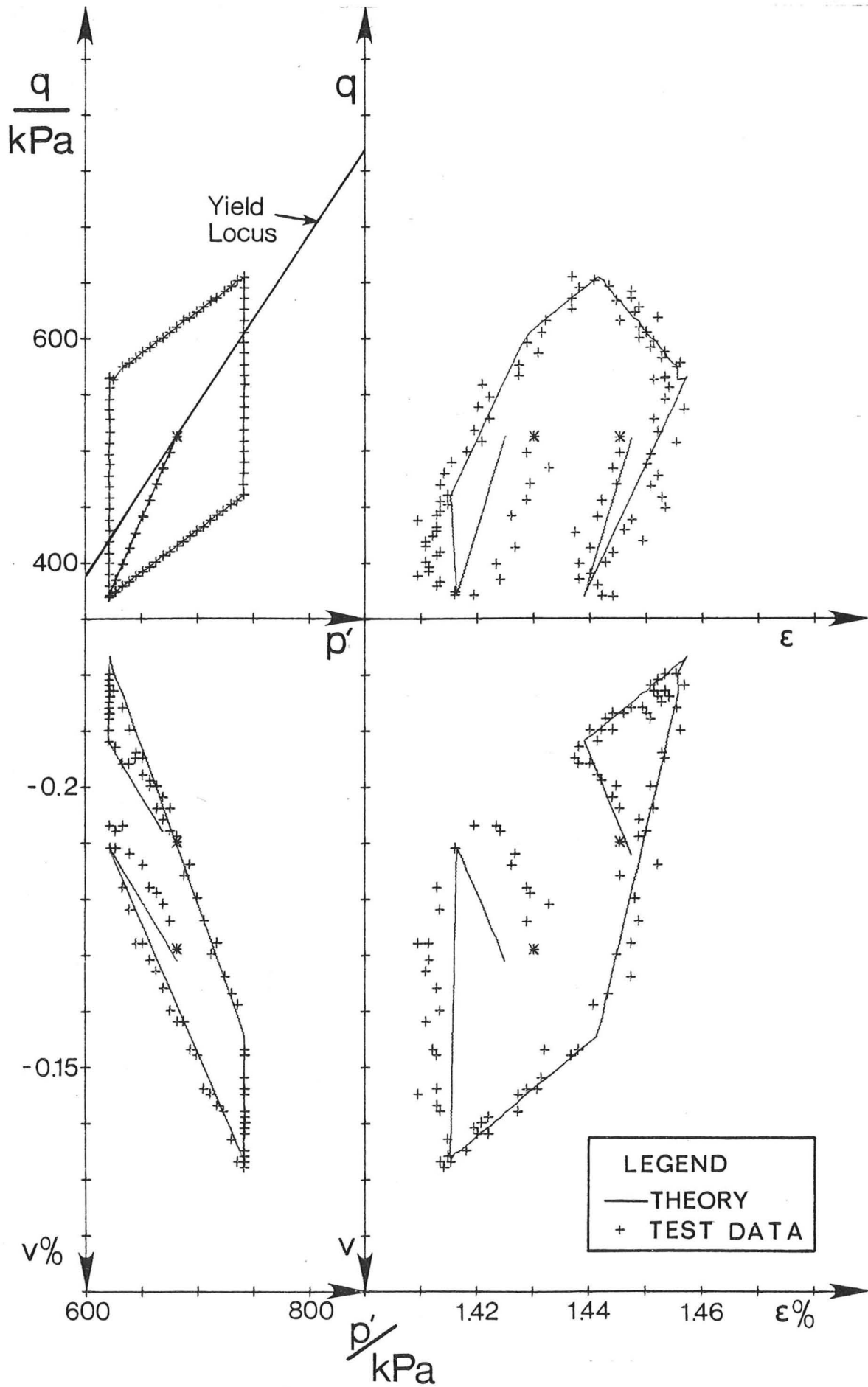


Figure 9.9 Test 2044, data and fitted properties for stress cycle starting at point 314

Code Numbers			Sample State			Sample History			Elastic Properties						Plastic Properties				Notes
Num	Test Num	Start Point	Mean p' (kPa)	Mean q (kPa)	Mean η	Max p' (kPa)	Max q (kPa)	Max η	K (MPa)	3G (MPa)	E <sub>pq</sub> (MPa)	A (MPa)	a	v*	M <sub>y</sub>	2c <sub>y</sub> (kPa)	M <sub>f</sub>	h <sub>n</sub> (MPa)	
1	2013	44	262.	193.	.736	289.	254.	.906	98.	362.	-51.	190.	1.345	.000	.785	-8.8	.785	64.2	U
2	2013	170	419.	451.	1.076	462.	549.	1.213	86.	449.	42.	342.	.792	.000	.540	230.8	.540	49.9	
3	2013	300	677.	964.	1.425	744.	1122.	1.534	143.	312.	127.	452.	.526	.328	1.033	274.5	.522	5.4	P
4	2013	458	689.	993.	1.442	789.	1219.	1.547	247.	484.	90.	582.	.775	.273	-1.875	2247.6	-1.875	-730.9	E
5	2013	600	688.	759.	1.103	789.	1219.	1.547	178.	549.	128.	592.	.642	.205	.087	682.6	.087	-1200.4	E
6	2013	742	688.	527.	.766	789.	1219.	1.547	177.	523.	85.	523.	.745	.186	.494	173.4	.793	-265.5	
7	2013	868	422.	324.	.769	789.	1219.	1.547	190.	427.	49.	445.	.842	.229	-1.032	741.9	-.536	-641.7	E
8	2013	994	262.	203.	.774	789.	1219.	1.547	169.	333.	48.	382.	.820	.262	-1.052	466.0	-1.052	-404.7	E
9	2014	47	258.	192.	.746	284.	253.	.919	232.	736.	-206.	285.	1.779	.000	.112	170.4	.112	76.5	LU
10	2012	171	419.	451.	1.076	461.	546.	1.213	245.	324.	-10.	375.	1.033	.304	1.316	-98.0	.400	33.7	P
11	2014	173	415.	452.	1.088	457.	547.	1.228	201.	328.	-16.	325.	1.061	.262	1.351	-105.8	.520	31.1	LP
12	2014	303	672.	964.	1.434	739.	1122.	1.541	149.	218.	93.	370.	.617	.366	1.550	-72.7	.416	4.2	P
13	2014	461	685.	993.	1.451	785.	1218.	1.554	192.	346.	118.	502.	.638	.325	1.797	-195.7	1.797	58.6	
14	2014	603	684.	760.	1.111	785.	1218.	1.554	162.	388.	121.	496.	.602	.280	-1.961	2075.0	-1.961	-486.9	E
15	2014	745	684.	526.	.770	785.	1218.	1.554	158.	404.	94.	462.	.679	.240	.220	359.6	.220	-314.2	
16	2014	871	417.	324.	.777	785.	1218.	1.554	159.	292.	85.	402.	.679	.310	-3.166	1622.0	-3.166	-239.8	
17	2014	997	258.	203.	.786	785.	1218.	1.554	128.	258.	70.	336.	.680	.292	-2.543	843.6	-2.543	-137.9	
18	2021	57	420.	307.	.732	460.	403.	.903	105.	495.	15.	344.	.934	.000	.221	215.4	.221	103.7	U
19	2021	183	419.	451.	1.075	461.	547.	1.212	111.	599.	79.	482.	.716	.011	.564	214.0	.265	52.2	
20	2021	309	420.	595.	1.418	461.	693.	1.521	165.	474.	220.	669.	.372	.348	1.113	132.7	.565	3.0	P
21	2021	611	426.	610.	1.431	794.	1221.	1.538	181.	706.	102.	631.	.736	.112	-1.103	1065.5	-1.103	-1203.3	E
22	2021	753	268.	383.	1.431	794.	1221.	1.539	146.	458.	18.	374.	.930	.126	1.301	56.1	1.301	20.0	P
23	2021	879	267.	292.	1.093	794.	1221.	1.539	143.	534.	58.	458.	.800	.107	.641	115.6	.641	-194.5	
24	2021	1005	267.	204.	.766	794.	1221.	1.539	146.	565.	61.	479.	.796	.097	.542	52.3	.991	-71.6	
25	2022	59	419.	307.	.734	461.	404.	.903	129.	380.	46.	359.	.807	.172	.658	35.5	.064	103.6	
26	2022	185	419.	450.	1.074	461.	548.	1.214	122.	511.	97.	478.	.649	.116	1.323	-97.3	.245	37.2	
27	2022	311	420.	595.	1.417	461.	691.	1.525	115.	290.	105.	383.	.534	.295	1.515	-37.3	.416	4.2	P
28	2022	469	691.	992.	1.435	794.	1222.	1.539	149.	511.	157.	585.	.518	.225	1.686	-151.9	.668	134.6	
29	2022	613	421.	608.	1.447	794.	1222.	1.555	158.	353.	101.	449.	.644	.281	-12.412	5773.6	-.945	-766.6	E
30	2022	755	262.	381.	1.457	794.	1222.	1.566	127.	256.	87.	356.	.613	.311	1.888	-103.4	1.888	147.9	
31	2022	881	262.	292.	1.116	794.	1222.	1.566	131.	256.	59.	324.	.729	.285	.569	138.2	.583	-270.2	
32	2022	1007	261.	202.	.772	794.	1222.	1.566	137.	268.	38.	307.	.823	.263	.903	-38.5	.981	-78.2	
33	2033	51	676.	497.	.736	787.	655.	.906	162.	810.	55.	595.	.849	.000	.146	412.8	.124	241.0	
34	2033	173	415.	450.	1.084	787.	655.	1.223	149.	875.	136.	720.	.657	.000	.429	278.7	.429	138.2	
35	2033	301	258.	372.	1.438	787.	655.	1.543	145.	697.	178.	692.	.512	.122	.784	172.3	.491	16.9	P
36	1034	49	680.	498.	.732	792.	654.	.900	184.	600.	61.	532.	.825	.139	.999	-173.4	-.318	205.9	
37	1034	171	419.	450.	1.073	792.	654.	1.210	146.	528.	81.	489.	.731	.135	1.231	-60.8	.424	71.9	
38	1034	299	263.	372.	1.417	792.	654.	1.519	129.	364.	59.	369.	.752	.196	1.475	-9.5	.516	7.1	P
39	2045	62	258.	372.	1.444	284.	433.	1.573	81.	536.	117.	475.	.511	.002	.944	138.3	.726	8.5	P
40	2045	188	415.	451.	1.088	456.	549.	1.573	124.	553.	-5.	364.	1.018	.000	1.739	-238.4	1.739	63.3	U

Notes: E: Elastic strains dominate, L: Arbitrary limit on elastic values, P: Plastic strains dominate, U: Poor fit to data

Table 9.1(a) Results of stress cycle tests

Code Numbers			Sample State			Sample History			Elastic Properties						Plastic Properties				Notes
Num	Test Num	Start Point	Mean p' (kPa)	Mean q (kPa)	Mean η	Max p' (kPa)	Max q (kPa)	Max η	K (MPa)	3G (MPa)	E <sub>pq</sub> (MPa)	A (MPa)	a	v*	M <sub>y</sub>	2c <sub>y</sub> (kPa)	M <sub>f</sub>	h <sub>n</sub> (MPa)	
41	2045	314	675.	499.	.739	742.	655.	1.573	182.	830.	7.	561.	.980	.000	2.272	-928.6	2.272	159.0	
42	2044	62	258.	372.	1.443	284.	432.	1.575	241.	334.	62.	471.	.823	.325	1.577	-33.2	.617	7.0	P
43	2044	188	414.	451.	1.088	455.	548.	1.575	200.	805.	106.	699.	.751	.096	1.601	-210.0	1.141	68.3	
44	2044	314	675.	499.	.738	742.	655.	1.575	219.	1225.	184.	1010.	.674	.012	1.519	-522.3	.834	266.0	
45	2051	77	262.	192.	.733	289.	285.	1.534	150.	485.	-128.	195.	1.722	.000	1.834	-261.9	1.834	26.1	U
46	2051	203	262.	282.	1.075	289.	345.	1.534	172.	630.	-96.	324.	1.374	.001	.910	47.4	.910	44.8	U
47	2051	329	263.	372.	1.417	289.	430.	1.534	85.	493.	74.	403.	.669	.000	1.105	114.8	.788	8.2	P
48	2051	487	419.	308.	.734	461.	430.	1.540	237.	758.	-206.	300.	1.749	.000	3.151	-1015.5	3.151	65.5	U
49	2051	613	419.	451.	1.076	462.	549.	1.540	169.	751.	-6.	494.	1.019	.000	.928	69.7	.928	80.6	
50	2051	739	420.	594.	1.416	462.	691.	1.540	133.	623.	125.	576.	.612	.092	1.024	179.5	.632	9.4	P
51	2051	897	680.	498.	.732	747.	691.	1.540	236.	934.	-86.	537.	1.216	.000	2.162	-971.1	2.162	170.3	
52	2051	1027	676.	731.	1.081	747.	883.	1.540	195.	844.	-23.	540.	1.062	.000	1.595	-342.9	1.595	136.0	
53	2051	1153	676.	963.	1.425	747.	1119.	1.540	210.	1019.	232.	972.	.559	.100	.978	329.6	.550	11.4	P
54	2052	77	262.	192.	.731	288.	285.	1.538	872.	343.	12.	1040.	.987	.438	3.122	-627.5	2.966	47.5	P
55	2052	203	263.	282.	1.075	288.	342.	1.538	536.	329.	-3.	678.	1.005	.404	1.816	-193.4	1.816	46.8	
56	2052	329	263.	372.	1.417	290.	433.	1.538	260.	379.	-9.	417.	1.026	.288	1.552	-36.1	.832	12.2	P
57	2052	487	419.	308.	.734	460.	547.	1.538	379.	448.	39.	629.	.923	.335	2.191	-609.4	2.191	100.8	
58	2052	613	419.	450.	1.075	460.	547.	1.538	278.	543.	49.	584.	.885	.251	1.638	-233.6	1.638	79.7	
59	2052	739	419.	594.	1.417	461.	692.	1.538	207.	422.	95.	521.	.727	.276	1.531	-43.9	.627	12.6	P
60	2052	897	680.	498.	.732	747.	692.	1.538	394.	679.	-4.	690.	1.008	.258	1.699	-653.5	1.699	156.8	
61	2052	1032	667.	727.	1.091	747.	883.	1.538	303.	655.	55.	667.	.885	.229	1.552	-305.2	1.396	119.5	
62	2052	1158	667.	959.	1.439	747.	1115.	1.549	176.	366.	140.	525.	.564	.323	1.524	-38.8	.489	5.5	P
63	2061	64	257.	377.	1.463	288.	444.	1.563	76.	413.	51.	327.	.733	.005	1.207	81.5	1.207	19.9	
64	2061	190	258.	288.	1.116	288.	444.	1.563	88.	268.	15.	227.	.901	.140	1.942	-200.0	1.924	60.2	
65	2061	316	257.	199.	.773	288.	444.	1.563	136.	271.	70.	350.	.697	.288	-.899	430.3	-.899	-269.5	
66	2061	458	415.	601.	1.449	457.	708.	1.563	133.	554.	-7.	371.	1.026	.019	1.562	-27.5	1.076	43.7	U
67	2061	584	414.	460.	1.109	457.	708.	1.563	117.	344.	34.	315.	.838	.164	2.456	-561.4	2.456	155.7	
68	2061	710	414.	319.	.769	457.	708.	1.563	153.	361.	77.	416.	.714	.249	-.087	351.1	.111	-428.9	
69	2061	852	677.	977.	1.444	744.	1142.	1.563	170.	663.	70.	558.	.799	.094	1.512	-42.3	.654	73.3	U
70	2061	978	676.	747.	1.105	744.	1142.	1.563	180.	531.	119.	575.	.663	.211	-.138	843.2	-.138	-752.2	E
71	2061	1104	675.	517.	.766	744.	1142.	1.563	182.	517.	93.	535.	.727	.201	.417	226.3	.563	-172.7	
72	2062	64	258.	376.	1.460	288.	443.	1.555	103.	611.	97.	504.	.650	.000	.890	153.7	.890	44.0	
73	2062	190	257.	287.	1.117	288.	443.	1.555	113.	366.	114.	428.	.528	.237	2.719	-413.7	2.719	106.5	
74	2062	316	257.	199.	.774	288.	443.	1.555	110.	417.	108.	439.	.561	.177	.294	117.1	.294	-224.3	
75	2062	458	415.	601.	1.449	457.	709.	1.555	153.	883.	171.	772.	.586	.029	.919	232.9	.919	109.2	
76	2062	584	414.	460.	1.111	457.	709.	1.555	129.	510.	129.	528.	.563	.166	-2.154	1357.8	-2.022	-463.5	E
77	2062	710	414.	318.	.769	457.	709.	1.555	148.	532.	133.	561.	.587	.182	.547	89.8	.547	-221.2	
78	2062	855	671.	975.	1.452	739.	1145.	1.555	198.	1309.	316.	1202.	.465	.022	.915	385.9	.543	125.9	E
79	2062	981	671.	745.	1.111	739.	1145.	1.555	188.	759.	217.	815.	.506	.182	-2.040	2127.0	-.837	-851.6	E
80	2062	1107	670.	515.	.769	739.	1145.	1.555	194.	751.	162.	744.	.622	.149	.717	26.0	.802	-208.3	

Notes: E: Elastic strains dominate, L: Arbitrary limit on elastic values, P: Plastic strains dominate, U: Poor fit to data

Table 9.1(b) Results of stress cycle tests (continued)

criterion adopted was that satisfactory fitting of the cycle should either reduce the root mean square error to 0.01% strain, or to one tenth of the average magnitude of strain measured during the cycle.

A graphical representation of the results is also required, and is given in the following way. On Figure 9.10 the mean stresses for three

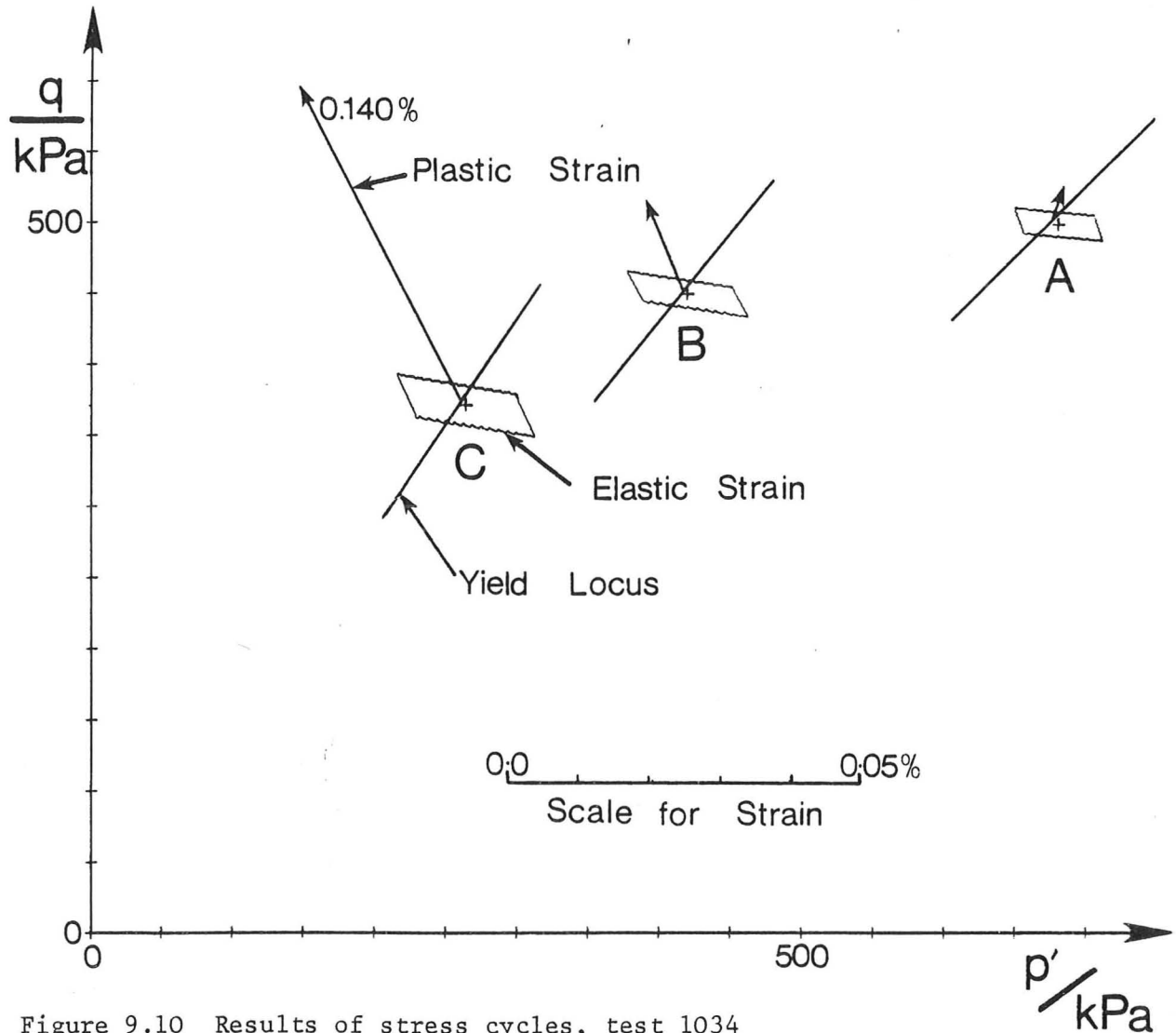


Figure 9.10 Results of stress cycles, test 1034

cycles at points A, B and C are shown as crosses, surrounding each cross is a parallelogram showing the elastic response to a small cycle of stress increments  $(\Delta p', \Delta q)$  of  $(1, 1)$ ,  $(1, -1)$ ,  $(-1, -1)$ ,  $(-1, 1)$ . For an isotropic material the parallelogram would reduce to a rectangle. The larger the parallelogram the more flexible the material, so in Figure 9.10 the sample is stiffer at higher pressures.

The plastic response is shown by plotting a short line segment

showing the location of the yield locus, and the plastic strain increment shown as a vector of length proportional to the strain given by a movement of the locus of one unit of stress (i.e. equal to  $1/h_n$ ). In Figure 9.10 much larger plastic strains and an increase in the angle of dilatancy are shown at higher stress ratios. For this sample with continuously increasing stress ratio the yield locus always passes through the initial point of the cycle. For tests where the plastic strain is very large it cannot be shown to the same scale as the elastic strain, and in these cases the vector is labelled with the magnitude.

The plot allows a rapid estimate of the relative significance of elastic and plastic deformation. For those tests dominated by large plastic strains it may be expected that the elastic properties may be inaccurate. Similarly if the response is virtually elastic the plastic properties will be unreliable. It was found in the latter case that although the flow rule might be quite well determined, the magnitude of the root mean square error was relatively insensitive to the location of the yield locus, so that the yield locus orientation is unreliable in this case. The tests dominated by elastic or plastic behaviour are noted in Table 9.1.

#### 9.5 Variation and Interpretation of Elastic Properties

Two aspects of the elastic behaviour of the sand will be considered, firstly the variation in stiffness (represented by moduli  $K$  and  $G$ ) and secondly the variation in structure (represented by the ratios between moduli, or simply by  $v^*$  and  $a$ ). Variations with current stress and with stress history are considered. For the stiffness the pressure and its past maximum are thought to be most important, and for the structure the effect of stress ratio will be studied. The behaviour is interpreted in terms of the conflicting hypotheses that elastic behaviour may be given by Hertzian contact theory or derived from a potential.

Figure 9.11 shows the variation of the modulus  $K$  with pressure for all cycles except where the plastic strain dominated. (The tests where satisfactory fitting of material properties was not achieved are shown by the symbol ' $\otimes$ ' or ' $\times$ '). Although there is a clear trend towards an

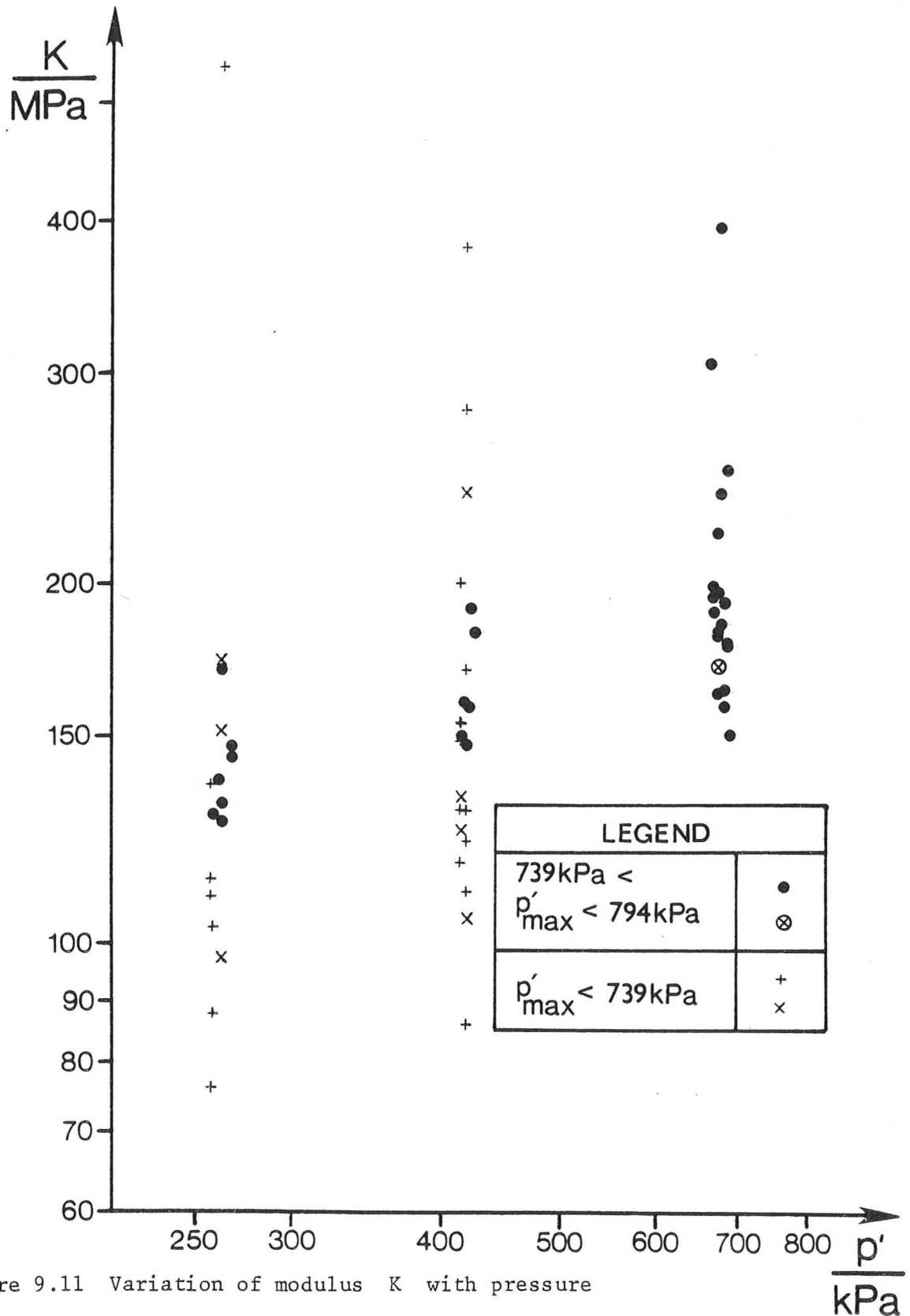


Figure 9.11 Variation of modulus  $K$  with pressure

increased modulus at higher pressure, any numerical relationship is obscured by the wide scatter of the data. The scatter is due to three effects:

- (a) The inherent variability of stiffness between samples.
- (b) The effect of variation of parameters other than pressure on the modulus.
- (c) Experimental error.

The measurement of the very small elastic strains in the stress cycles involves measurements of quantities close to the resolution of the triaxial machine, and so experimental error may be an important contributor. A further problem is that the membrane penetration correction is large (in the region of one third of the small elastic volumetric strains); variation of the penetration for different membranes will cause an additional error. The effects of (a) and (b) may, however, be eliminated by studying the variation for cycles with similar histories on a single specimen. Figure 9.12(a) shows the variation of bulk modulus for tests 2061 and 2062, in each test three cycles were carried out at three different stress levels, and the points show the geometric mean bulk modulus measured at each stress level. The tests at each stress had similar stress histories (stress ratio increasing and pressure approximately at its maximum value) so the data are directly comparable. Each test shows exactly the same trend of a power law dependence of modulus on pressure, with a difference in stiffness between the two samples.

The variation in shear modulus may also be studied in this way, and the geometric mean values for each of the three pressures in tests 2061 and 2062 are shown in Figure 9.12(b). It is clear that the shear modulus also increases as a power law with pressure, the mean exponent being given by  $G \propto p^{0.67}$  as compared to  $K \propto p^{0.61}$ . The difference in shear stiffness between the two tests is more marked than that of the

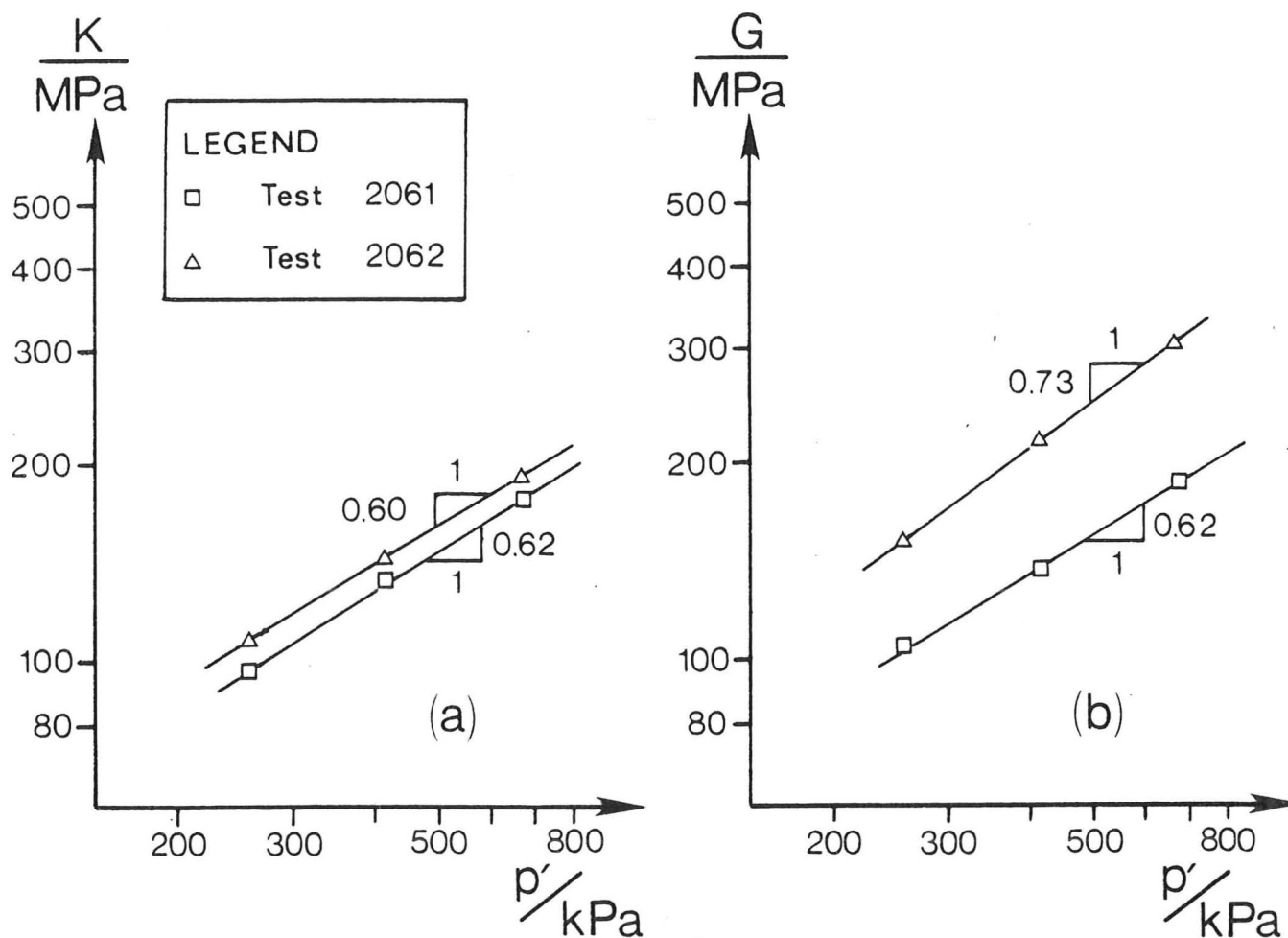


Figure 9.12 Variation of elastic properties, tests 2061 and 2062

bulk modulus.

The above results do not distinguish between the dependence of the moduli on the current stresses (non-linear elasticity) and a possible dependence on maximum past pressure (elastic-plastic coupling). If only those tests for which the maximum past pressure was in the range 739 - 794 kPa are selected from Figure 9.11, then an increase of modulus with pressure is still apparent, although less marked. A similar comparison for shear modulus shows no discernible difference. There is no doubt that non-linear elasticity is present, but these tests offer insufficient evidence as to whether elastic-plastic coupling also occurs.

Because of the problems of establishing elastic behaviour from the small stress cycles, a supplementary set of tests was carried out to establish the variation of moduli with pressure more accurately. It is

thought that the unloading of sand at constant stress ratio may give a substantially elastic response, so tests were carried out each involving loading and unloading at several different constant stress ratios. Elastic properties were fitted to the unloading portions of the constant stress ratio paths. Because each test involves the continuous measurement of strain over a much wider pressure range than for each of the stress cycle tests, a more accurate determination of the moduli is possible. These tests do not, however, allow a measure of anisotropy, and so were interpreted assuming the material to be isotropic. Several constant stress ratio tests were carried out on each sample, and no difference was observed for tests <sup>h</sup>were <sub>^</sub>  $\eta$  was increasing or decreasing between cycles.

The variation of the bulk modulus during the tests was assumed to take the form:

$$K/p_r = A(p'/p_r)^m \quad (9.5.1)$$

where  $p_r$  is a reference pressure (taken here as 1.0 kPa). This Equation leads to an unloading curve in the consolidation plot of:

$$v = v_o + (p'/p_r)^{(1-m)} / [A(1-m)] \quad (9.5.2)$$

and curves of this form were fitted to the data for the unloading part of the constant stress ratio paths. The mean value of  $m$  derived was 0.40 (standard deviation 0.005), and no variation of  $m$  with stress ratio is indicated. Using this mean figure, values of  $A$  were derived for each test and, as Figure 9.13(a) shows,  $A$  decreases very slightly with stress ratio, the total variation being only about 15%.

The exponent  $m$  in Equation (9.5.1) is established as 0.40 for this material with a constant maximum past pressure. In Figure 9.12(a) the average exponent is 0.61, and in this case the maximum past pressure increases with the current pressure. The data for both sets of tests would suggest a variation of bulk modulus taking the form:

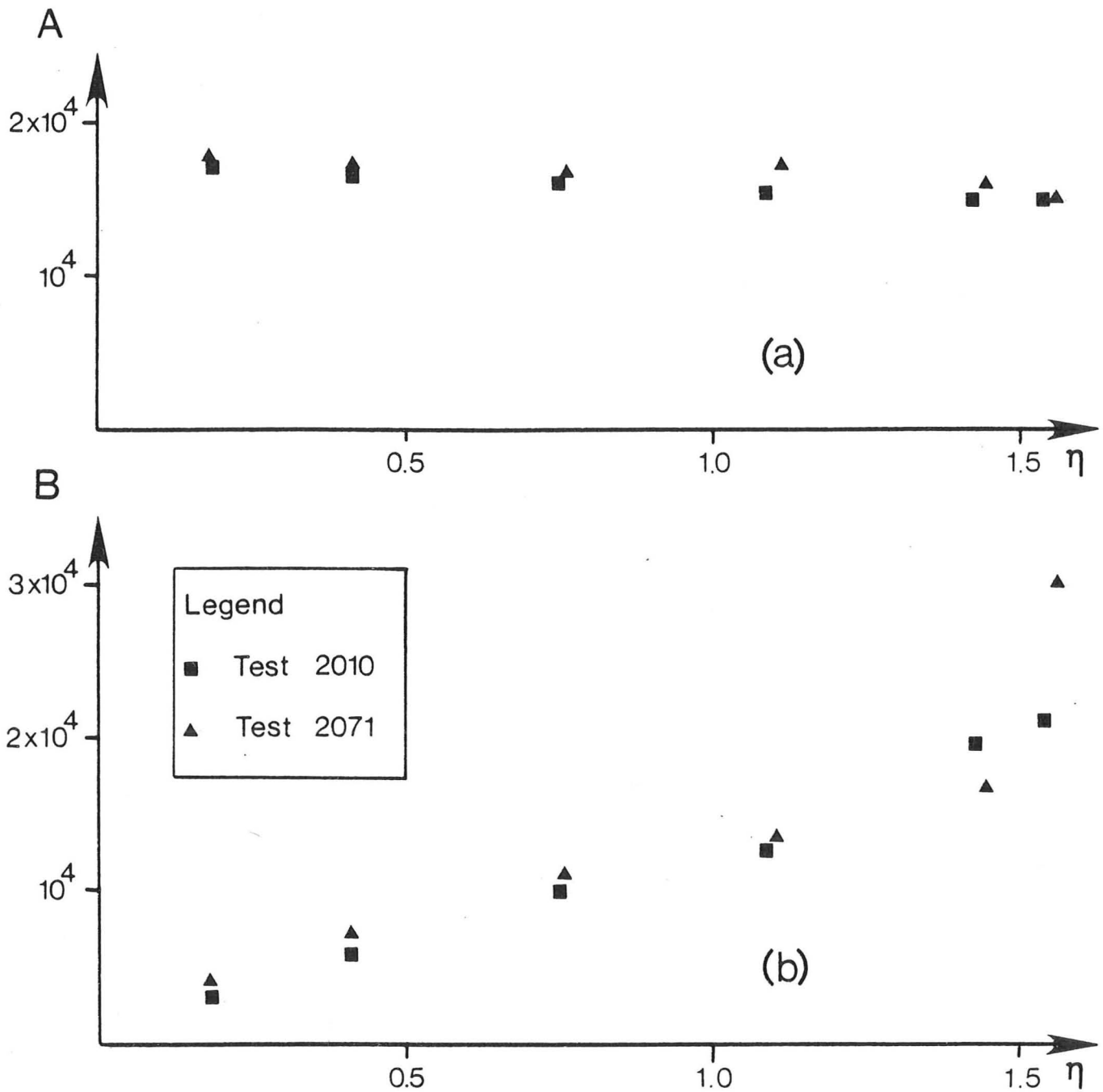


Figure 9.13 Variation of elastic properties, tests 2010 and 2071

$$K/p_r = A'(p'/p_r)^{0.4}(p'_{\max}/p_r)^{0.21} \quad (9.5.3)$$

The shear modulus in the constant stress ratio tests was also assumed to vary in the way:

$$G/p_r = B(p'/p_r)^n \quad (9.5.4)$$

which leads to shear strains of the form:

$$\varepsilon = \varepsilon_o + \eta(p'/p_r)^{(1-n)}/[3B(1-n)] \quad (9.5.5)$$

The mean value of  $n$  is 0.44 (standard deviation 0.042) and shows no variation with  $\eta$ . The variation of  $B$  is shown in Figure 9.13(b), and increases at a rate slightly less than proportional to stress ratio  $\eta$ . The result is that the term  $\eta/B$  which is present in Equation (9.5.5) increases only slightly with  $\eta$ , so that the amount of recoverable shear strain on a constant stress ratio path does not depend strongly on the stress ratio.

The average value of the exponent  $n$  of 0.44 compares with 0.67 from Figure 9.12(b) for the case where maximum pressure increases in proportion with the pressure; so that an expression for the shear modulus would be suggested in the form:

$$G/p_r = B'(p'/p_r)^{0.44} (p'_{\max}/p_r)^{0.23} \quad (9.5.6)$$

where  $B'$  is a function of stress ratio.

The power law relationship for the variation of the bulk modulus is most readily understood in terms of Hertzian contact theory. When two elastic bodies with curved surfaces are in contact over only a small area it can be shown that the approach of the two bodies is proportional to the two thirds power of the normal force between them. This power law is a result of the approximation of sections of the undeformed surfaces near the contact to parabolas. If on the other hand the geometry of the contact is idealised as a pyramidal or conical indentation problem, then dimensional analysis shows that the approach will be proportional to the square root of the normal force.

Extending this type of analysis to regular assemblies of elastic particles in contact on small areas, the bulk modulus of the assembly in an isotropic stress state may be shown to be proportional to the one third power of the pressure for rounded bodies (Hertzian contact theory) and to the square root of the pressure for angular bodies in contact at edges and corners. Variation of the modulus with pressure was found to depend

on  $p^{0.4}$ , which lies between these extremes.

At the pressures at which the tests were carried out the diameter of a typical particle contact may be calculated as between  $2.0 \mu\text{m}$  and  $5.0 \mu\text{m}$  (assuming  $0.2 \text{ mm}$  diameter particles packed in a face centred cubic array, with properties  $E = 90 \times 10^6 \text{ kPa}$  and  $\nu = 0.13$  appropriate for Quartzite). Examination of micrographs of the corners of the particles, Figure 9.14, shows that at this scale the contacts may either

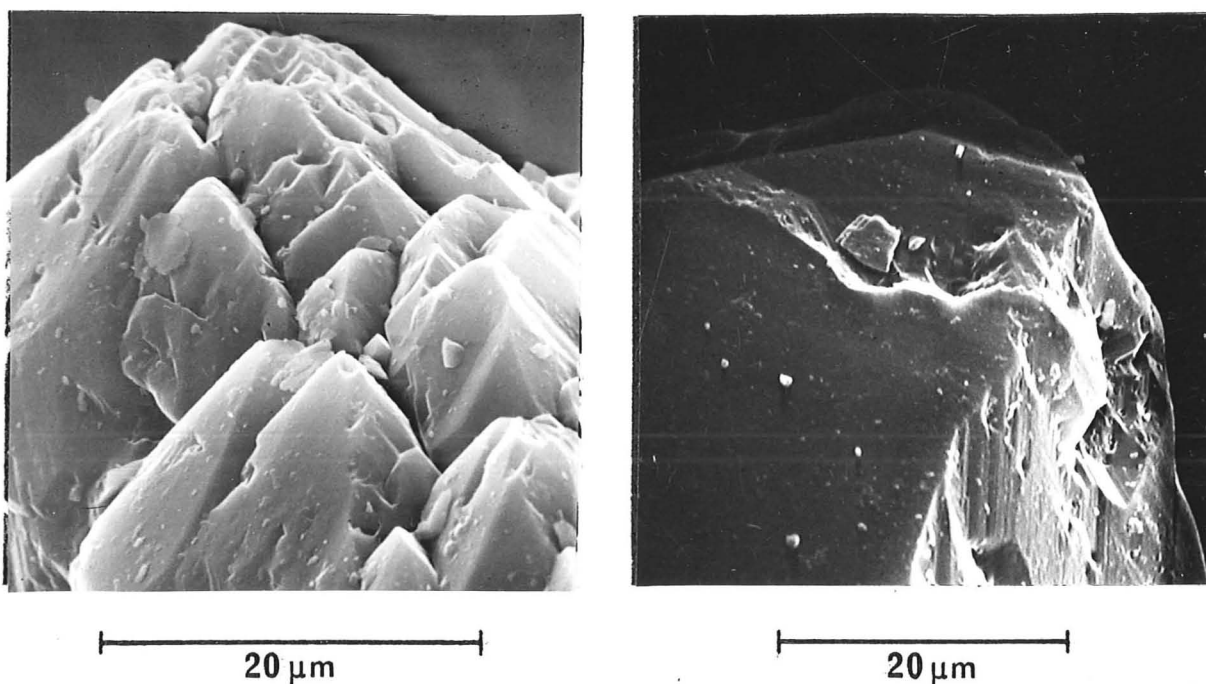


Figure 9.14 Micrographs of corners of sand particles

be rounded or angular. This is consistent with the result that the pressure variation of the modulus lies also between the results for rounded and angular particles. The idealisation of small contact areas is clearly appropriate since the contact diameter is only 1-2.5% of the particle diameter.

Under the action of tangential loads at the rounded contacts the stiffness is also proportional to the one third power of the pressure, but the stiffness also becomes strongly path dependent (see Mindlin and Deresiewicz (1953)). The behaviour of a face centred cubic array of spheres has been analysed to establish the stiffness on constant stress ratio paths (details of the calculation are not given here) and the

results may be compared with those for the constant stress ratio tests.

The results imply that a constant stress ratio path will involve also a constant strain rate ratio. In practice the strain paths were curved (giving larger shear strains at lower pressures) and this may be an indication that even on a constant stress ratio unloading some plastic deformation occurs. The apparent bulk modulus is predicted as increasing very slightly with stress ratio; for the values appropriate to the tests the increase is only 2.5% from the value at  $\eta = 0.0$ . In practice (Figure 9.13(a)) the bulk modulus fell very slightly with increasing stress ratio: the tests confirm the insensitivity of bulk modulus to stress ratio changes. The variation of the apparent shear modulus with stress ratio is also predicted as very small, whereas the tests (Figure 9.13(b)) clearly show the apparent shear modulus as increasing markedly with stress ratio.

Although Hertzian contact theory explains some of the elastic phenomena, it does not fully describe the behaviour of the sand. Because of the path dependence in particle contact theories, the elastic behaviour given by them cannot be derived from a potential. This is because, even for completely conservative behaviour, the theory needs internal parameters to describe the sample history. It is advantageous to describe elastic behaviour by a potential, and essential within the thermodynamic framework. The significance of this approach rather than a particle contact theory lies partly in the ratios between the moduli implied by the theories. These may be examined by studying the variation of  $v^*$  and  $a$  with stress and stress history. It is thought that the most important factor affecting the structure of the sand is the stress ratio, and Figure 9.15 shows the variation of  $v^*$  and  $a$  with  $\eta$  for all tests except those dominated by plastic variation.

A wide variation in the anisotropy is measured as would be expected in view of the variation in moduli observed. It is clear, however, that

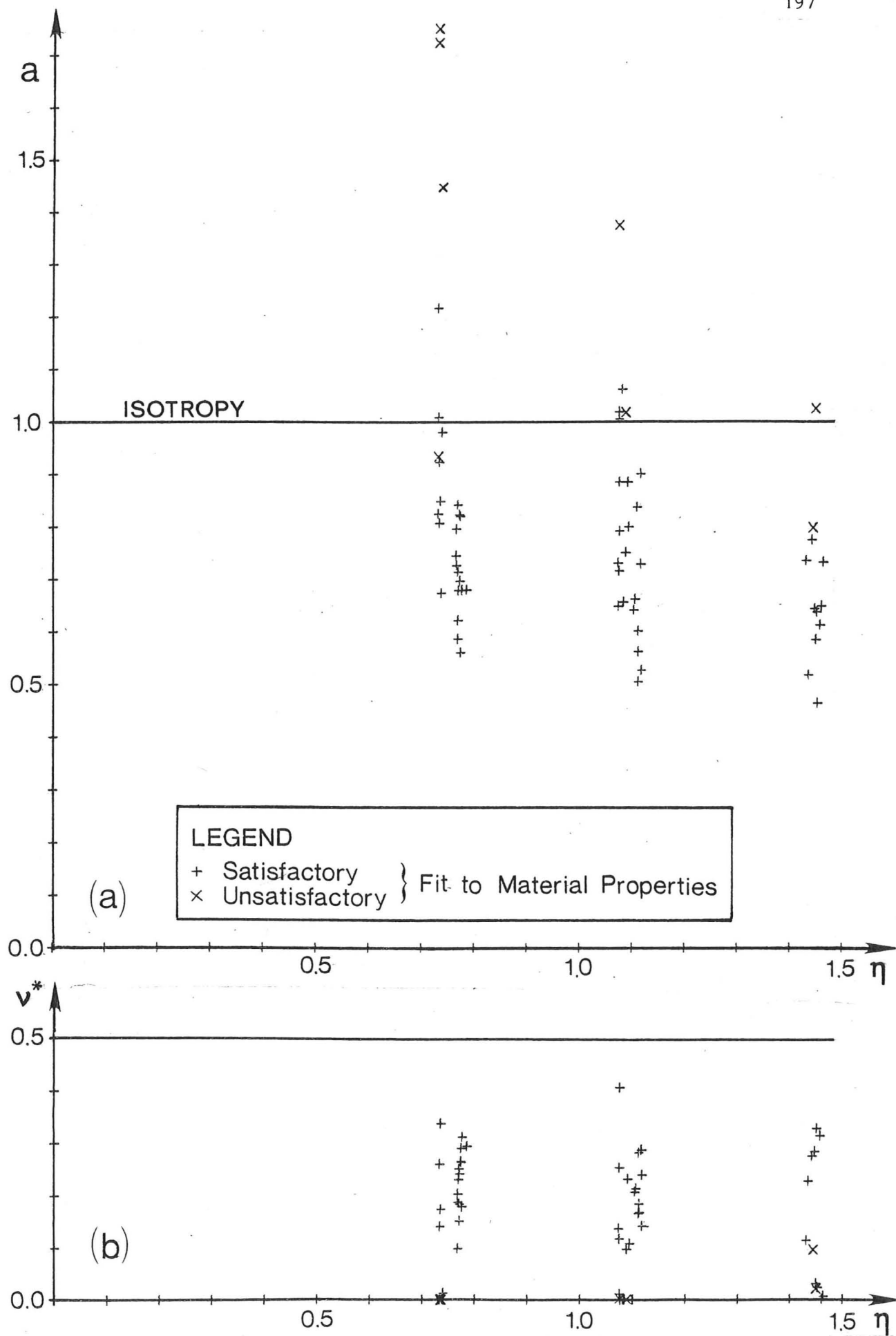


Figure 9.15 Variation of  $v^*$  and  $a$  with  $\eta$

the samples are predominantly stiffer in the vertical direction ( $a < 1.0$ ) with the ratio of direct stiffness ( $1/a^2$ ) in the region of 2.0. The anisotropy appears to be more pronounced at higher stress ratios, and it is reasonable to expect that the sample would increase in elastic stiffness vertically as vertical stress is increased.

The parameter  $v^*$  shows no sign of variation with  $\eta$ , and apart from several calculated values of 0.0 (mainly as a result of the limit on  $v^*$  and for tests which were not fitted satisfactorily) the mean value is in the region of 0.2. This compared well with values of  $v$  frequently used for sands (e.g. Lade (1977)).

The plots in Figure 9.15 include the effect of the maximum past stress ratio as well as its current value, but the two effects may be studied independently by selecting only those points at a fixed value of  $\eta_{\max}$ , and also plotting against  $\eta_{\max}$  for a fixed  $\eta$  value. Neither of these produce conclusive evidence, and the question as to whether the anisotropy is caused by the current stress state or induced by the plastic deformation caused by the past maximum stress ratio remains unresolved.

In order to assess whether this behaviour may be related to an elastic potential, some implications of the potential function introduced in Section 5.3 (which involved both bulk and shear moduli proportional to pressure) may be noted. Although it is possible to derive a function which gives the moduli proportional to some lower power of the pressure, the case where they are proportional to pressure will be considered since the mathematics is considerably simplified. Similar trends may be expected for other powers.

The first result is that a constant stress ratio path is predicted as producing no change in shear strain. The shear strains on these paths were indeed small, and their magnitude varied little with stress ratio. Allied to this is the fact that contours of shear and volumetric strain are constant stress ratio lines and parabolas (see Figure 5.6). The

tests on dense sand were insufficient to establish these contours, but Pappin and Brown (1980) report tests on crushed rock which give elastic strain contours closely approximating to this form. The bulk modulus on a constant stress ratio line is predicted as being independent of the stress ratio (cf. Figure 9.13(a)).

The model with moduli proportional to pressure implies that the structural parameters  $a$  and  $v^*$  will be unique functions of stress ratio. The values depend on the quantity  $\alpha\kappa^*$ , and the variation with  $\eta$  gives a similar trend to that observed in the tests (although a stronger dependence on  $\eta$ ). It is suggested therefore that a potential in which bulk and shear moduli depend on some lower power of pressure may be suitable for the description of a sand. If, however, the elastic behaviour may be derived from a potential and  $G$  depends on  $p'$ , then conversely  $K$  must depend on  $q$ . The variation of  $K$  with  $q$  at a fixed pressure has been studied and no such variation is confirmed.

Hertzian contact theory therefore can explain well the power law relation for the elastic moduli, but does not explain the variation of behaviour at different stress ratios. Use of an elastic potential gives the correct trends for the variation of moduli with stress ratio, and a potential could be chosen with the appropriate power law. The cross effect of  $q$  on  $K$  which would then be necessary is not confirmed. The increase of modulus with past maximum pressure has not been explained in detail, but is probably associated with the plastic increase in particle contact area, rather than the increase in density due to maximum past pressure since the latter effect is very slight.

#### 9.6 Variation of Plastic Properties

As would be expected, the plastic properties of the sand depend strongly on the past stress history. The most important parameter is thought to be the previous maximum stress ratio, so those tests in which

the stress ratio was continuously increasing will first be examined. These tests are divided into three groups: those for which  $p'$  is increasing, constant or decreasing.

The local yield loci and the flow rules are shown by bold lines on Figure 9.16 for the tests with  $p'$  constant and  $\eta$  increasing. There is a

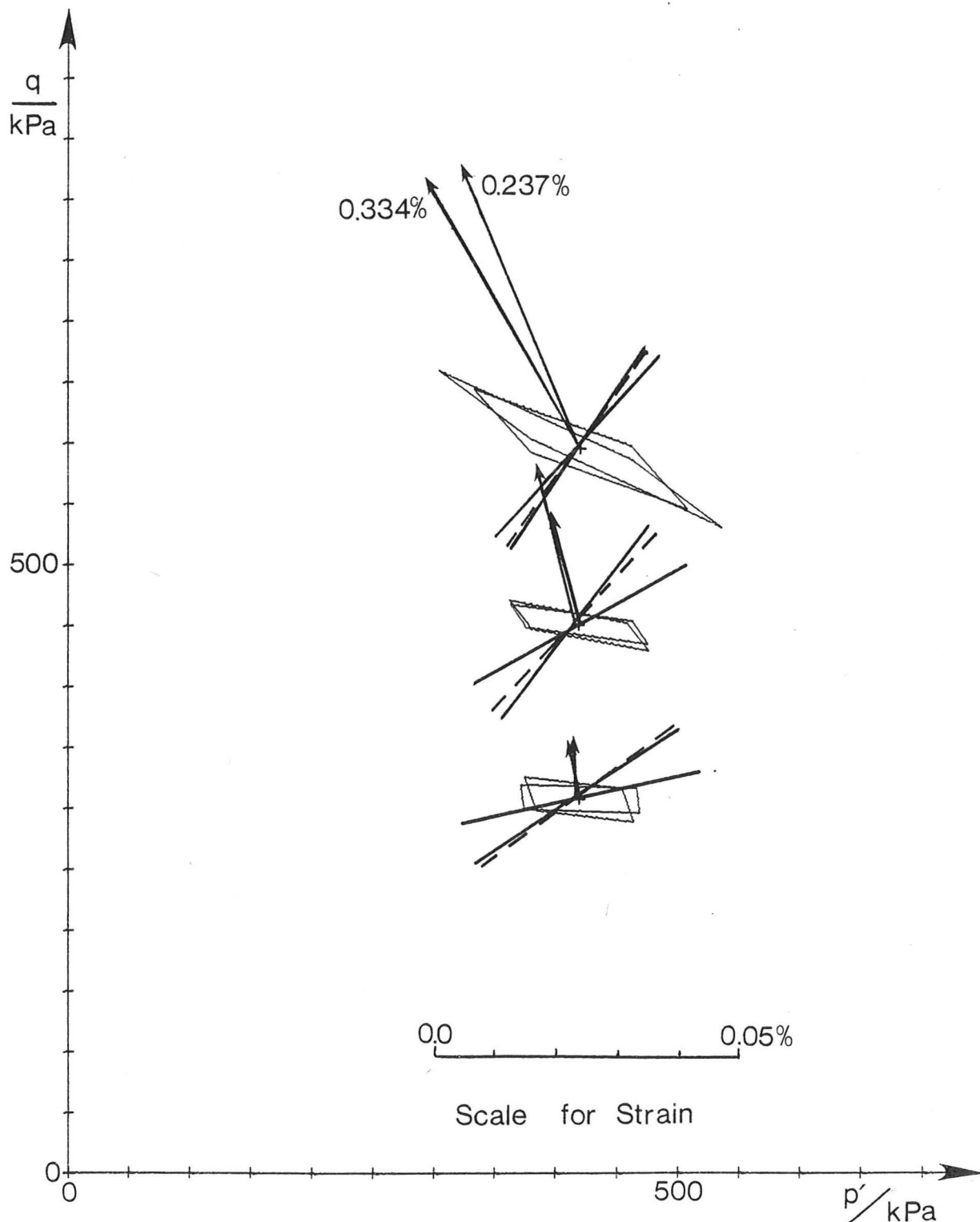


Figure 9.16 Results of tests 2021, 2022,  $\eta$  increasing,  $p'$  constant

small difference in the orientation of the yield locus for the tests in which the stress cycle was traversed clockwise or anticlockwise, and in most cases the yield locus is rotated in the same direction as the traverse of the cycle. The explanation of this phenomenon would appear probably to be the presence of creep, although there may be some other cause.

Before the start of each stress cycle the stresses were held constant for 30 minutes, during which a small amount of creep, strongly dependent on the current stress ratio, occurred. Each stage of the cycle was executed in 30 minutes, and so further creep would be expected during the cycle. If a stress state is reached during the cycle so that large plastic strains occur, then some part of this strain may be expected to occur as creep after that stress state had been passed. Because the resulting strain is then attributed to a later stage in the cycle, the yield locus will appear rotated in the direction of the cycle in order that the later points appear further from the initial locus.

Shown as dashed lines on Figure 9.16 are the lines at constant stress ratio through the initial points of the stress cycles, these represent the simplest hypothesis that the sample yields if the stress ratio increases. The data are certainly consistent with this hypothesis, but would also be consistent with a curved locus close to a line of constant stress ratio but at a flatter slope (e.g. as used by Lade (1977)). It should be borne in mind that the determination of the yield locus is least accurate for the tests at low stress ratios when plastic strains are small. The yield loci determined from the tests with  $\eta$  increasing and  $p'$  either increasing or decreasing indicate exactly the same form of yield locus as for the constant  $p'$  tests.

The flow rule for all the tests with  $\eta$  increasing is shown in Figure 9.17, where the slope of the plastic potential  $M_f$  is plotted against stress ratio  $\eta$ . The solid line gives the stress-dilatancy

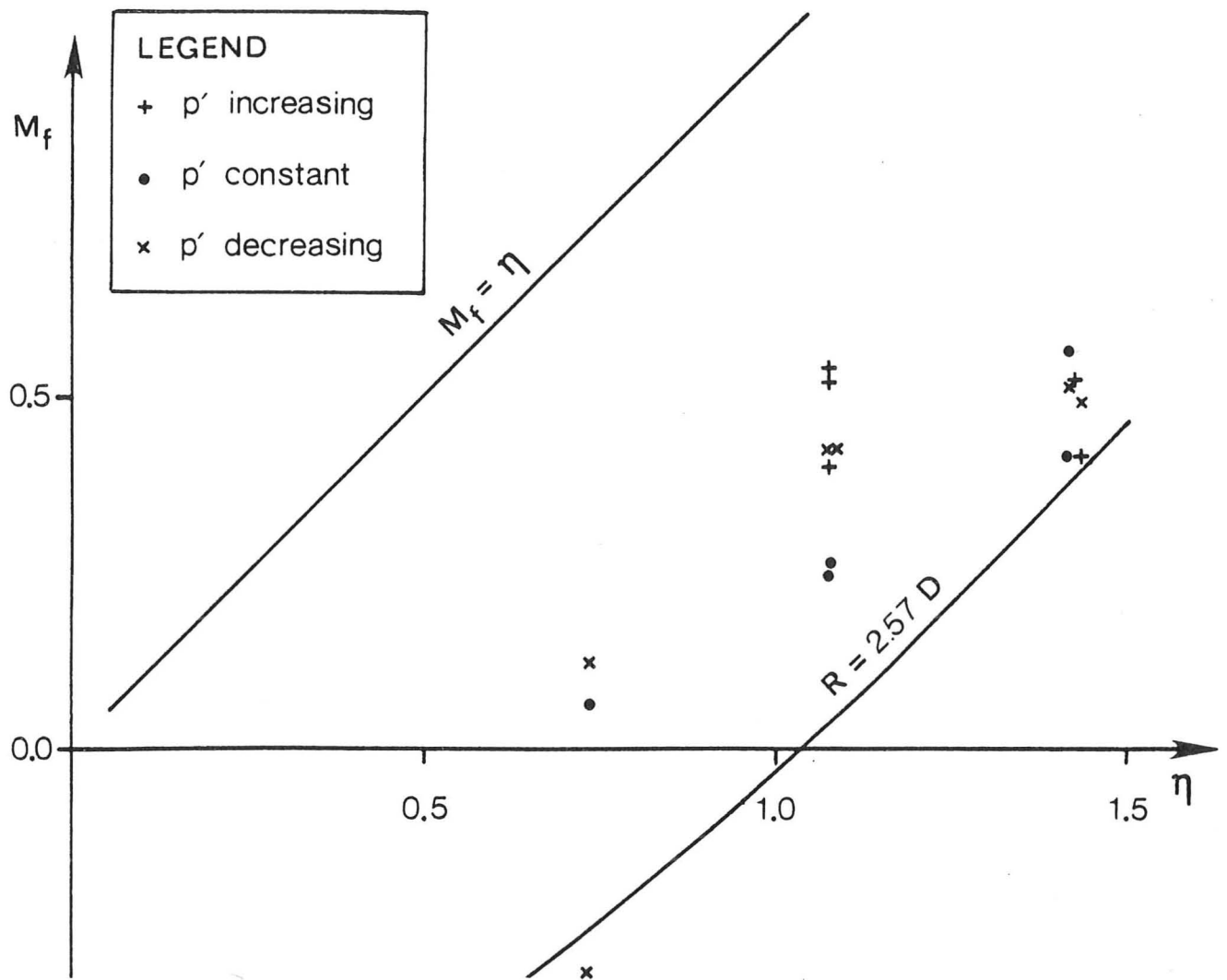


Figure 9.17 Flow rule for tests with  $\eta$  increasing

relationship  $R = 2.57 D$  which was found to fit the behaviour of a conventional monotonic triaxial test. Clearly this relation does not fit the behaviour of the stress cycle tests, which show a non-unique flow rule with a higher dilatancy; at high stress ratios the stress dilatancy relationship is, however, approached. Although the dilatancy is higher than for the monotonic test it is still considerably lower than that implied by associated flow on a constant stress ratio yield locus which would give  $M_f = \eta$ .

The data at low stress ratios show a wide scatter due to the inaccuracy of determination of plastic properties for these tests, and there is no discernible trend of change of the flow rule according to whether  $p'$  is increasing, constant or decreasing.

The value of the hardening modulus decreases dramatically with stress ratio increase, as is shown in the semi-logarithmic plot of Figure 9.18. The variation of the modulus with pressure is also of

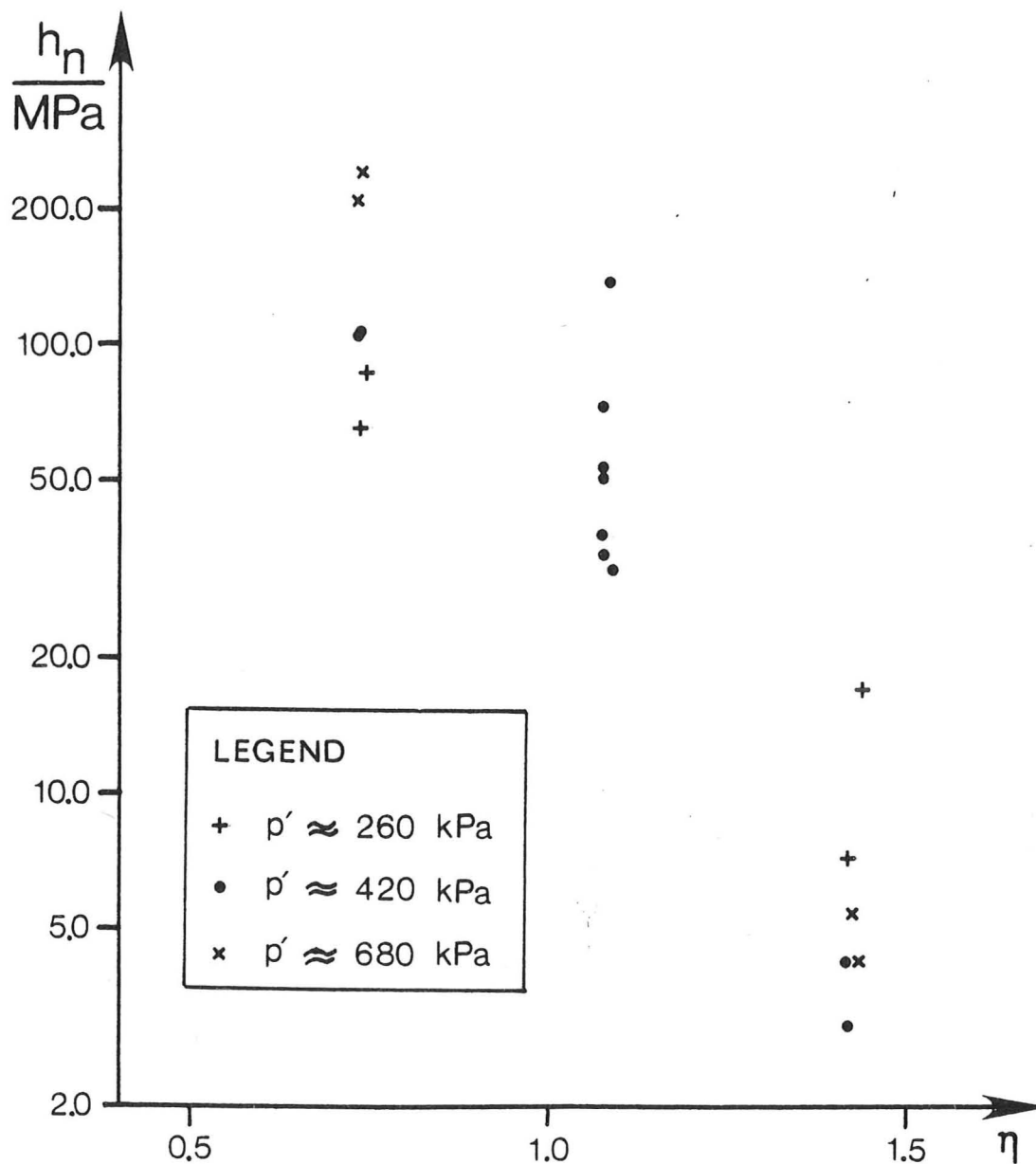


Figure 9.18 Variation of hardening modulus with stress ratio,  $\eta$  increasing

interest. The tests at the same stress ratios and different pressures unfortunately have slightly differing histories ( $p'$  at or below maximum) and so may not be fully comparable, but some comparison is nevertheless valuable. An increase of  $h_n$  rather less than in proportion to pressure is expected since:

(a) The behaviour of an ideal assembly of rigid grains should show a

full scaling of plastic behaviour with pressure, i.e.  $h_n \propto p'$ .

- (b) It is, however, well known that sands can sustain higher stress ratios at lower effective stresses, and a proportional increase of  $h_n$  at low pressure may be expected.

There is evidence of an increase of  $h_n$  with pressure at low stress ratio, but not at a high stress ratio, but this effect is obscured by the generally stiffer response of those samples for which  $p'$  was decreasing.

At the opposite extreme of behaviour are the tests for which both  $\eta$  and  $p'$  are decreasing. For these the plastic strains are expected to be very small, and it is also found that for this type of stress history the behaviour is strongly path dependent. The most obvious characteristic of the behaviour is that as  $p'$  decreases the yield locus is generally approximately perpendicular to the recent stress path, and as  $\eta$  decreases it is closer to a line of constant stress ratio; thus the state depends on the recent history of the sample. An example of the case where first  $p'$  then  $\eta$  decreases is shown in Figure 9.19.

Some exceptions are that on first unloading of Test 2014 (cycle 13) there is a small strain similar to that on monotonic loading (this point will be discussed later) and that on the next cycle the locus is again anomalous, but is associated with a very small strain. When the pressure is reduced at a high stress ratio a further shearing occurs for one test (cycle 22, Figure 9.19). This would indicate that the yield locus for primary loading curves to smaller stress ratios on either side of the maximum loading point (see Figure 9.20) not just on the higher pressure side as used by Lade (1977). Although a plastic volumetric expansion is shown for the cycles as  $p'$  is reduced at constant  $\eta$ , this does not necessarily mean that plastic expansion would occur on the unloading parts of constant stress ratio tests. The stress cycle tests involve small changes in stress ratio making them not truly constant  $\eta$  paths.

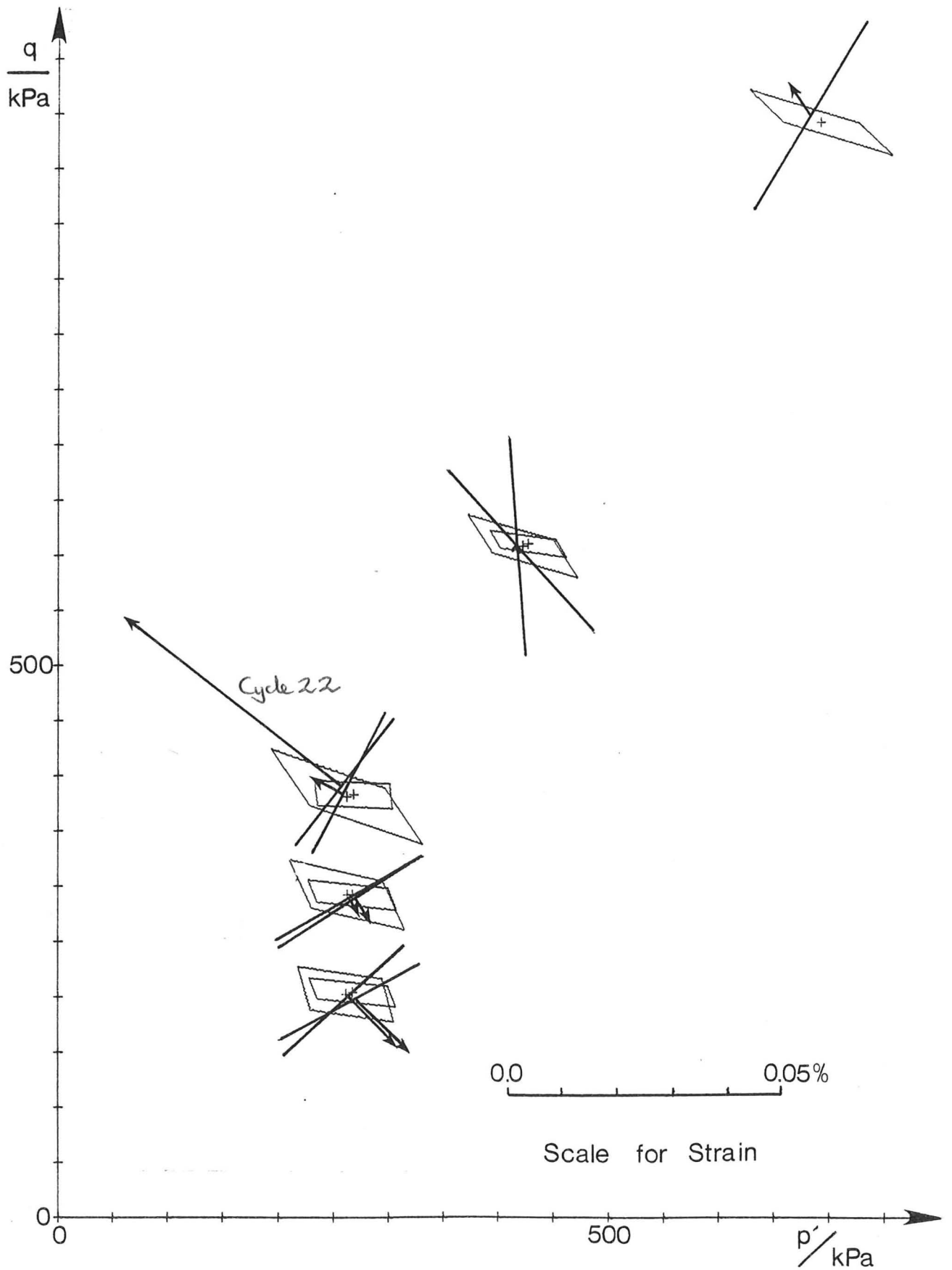


Figure 9.19 Results of tests 2021, 2022,  $p'$  decreasing then  $\eta$  decreasing

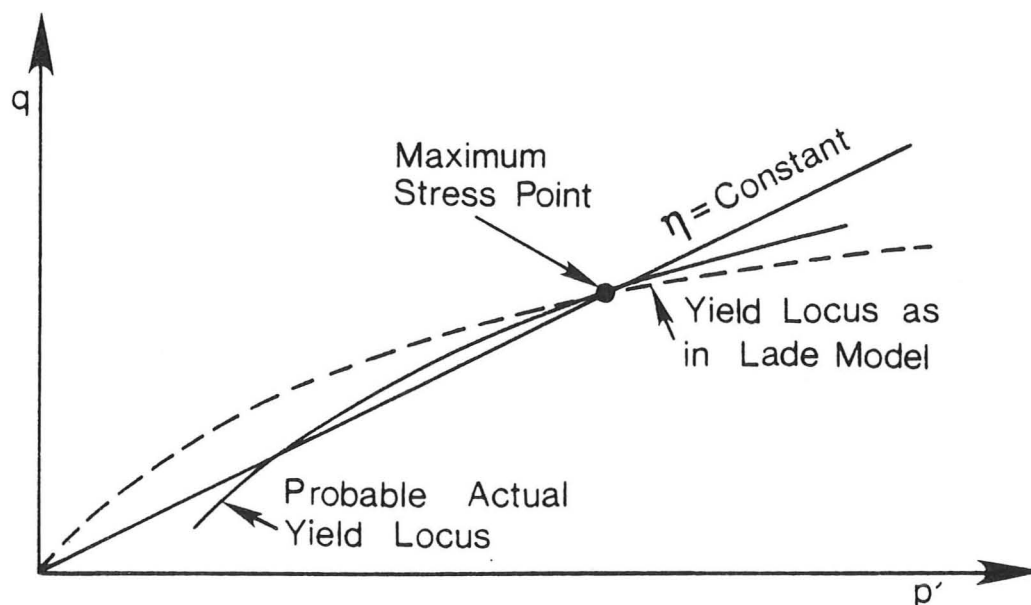


Figure 9.20 Curvature of yield loci for primary loading

Tests were also carried out in which the pressure was increasing while the stress ratio decreased, and the interpretation of these tests is more difficult. On first unloading from a high stress ratio the yield locus is indicated as a curve passing through the previous maximum stress ratio point (consistent with the earlier findings). For the tests at lower stress ratios the yield locus is oriented so that plastic strain occurs as the stress returns towards the point where the previous cycle was executed. Clearly this is an oversimplification of the real behaviour: the yield locus, if it exists, must include the last part of the stress path in the elastic region. It is thought that the explanation lies in the fact that any change in stress ratio induces plastic strain. During the cycle the stress ratio is reduced, causing a small plastic strain, and later increased, causing a different plastic strain. For these tests the latter strain is larger and so it appears that the yield locus does not include the recent stress path (the

elastic region is in fact smaller than the size of the stress cycle). This type of behaviour was also noted in one test on first unloading at a high stress ratio.

Two final series of tests served mainly to establish elastic properties. Those shown in Figure 9.21 involve  $\eta$  increasing at a value below its maximum and  $p'$  constant. The type of behaviour just described occurs again in these tests, and possible main yield loci through the points A, B and C at which maximum stresses had occurred are indicated by broken lines on Figure 9.21. These loci may be of the form observed by Tatsuoka and Ishihara (1974). Tests with  $\eta$  decreasing and  $p'$  constant show a largely elastic response, although the above effects cause plastic strains in some cases as large as the elastic ones, particularly after a large change of stress ratio.

These last series of tests confirm that although the major plastic strain occurs when a yield locus, approximating to a maximum past stress ratio line (but almost certainly curved), is crossed; there is also a small plastic strain for most stress changes. A detailed picture of the changes in the yield locus and flow rule for these secondary plastic strains has not been established, but both on loading and unloading the magnitude of the plastic strain increases as the stress point moves further in a fixed direction.

The behaviour of a dense sand in triaxial compression may broadly be described as follows. On first increasing the stress ratio plastic strains, increasing greatly with  $\eta$ , occur. The yield locus associated with these strains is curved, but oriented approximately as a constant stress ratio line. The flow rule is non-associated and does not seem to be well defined except for

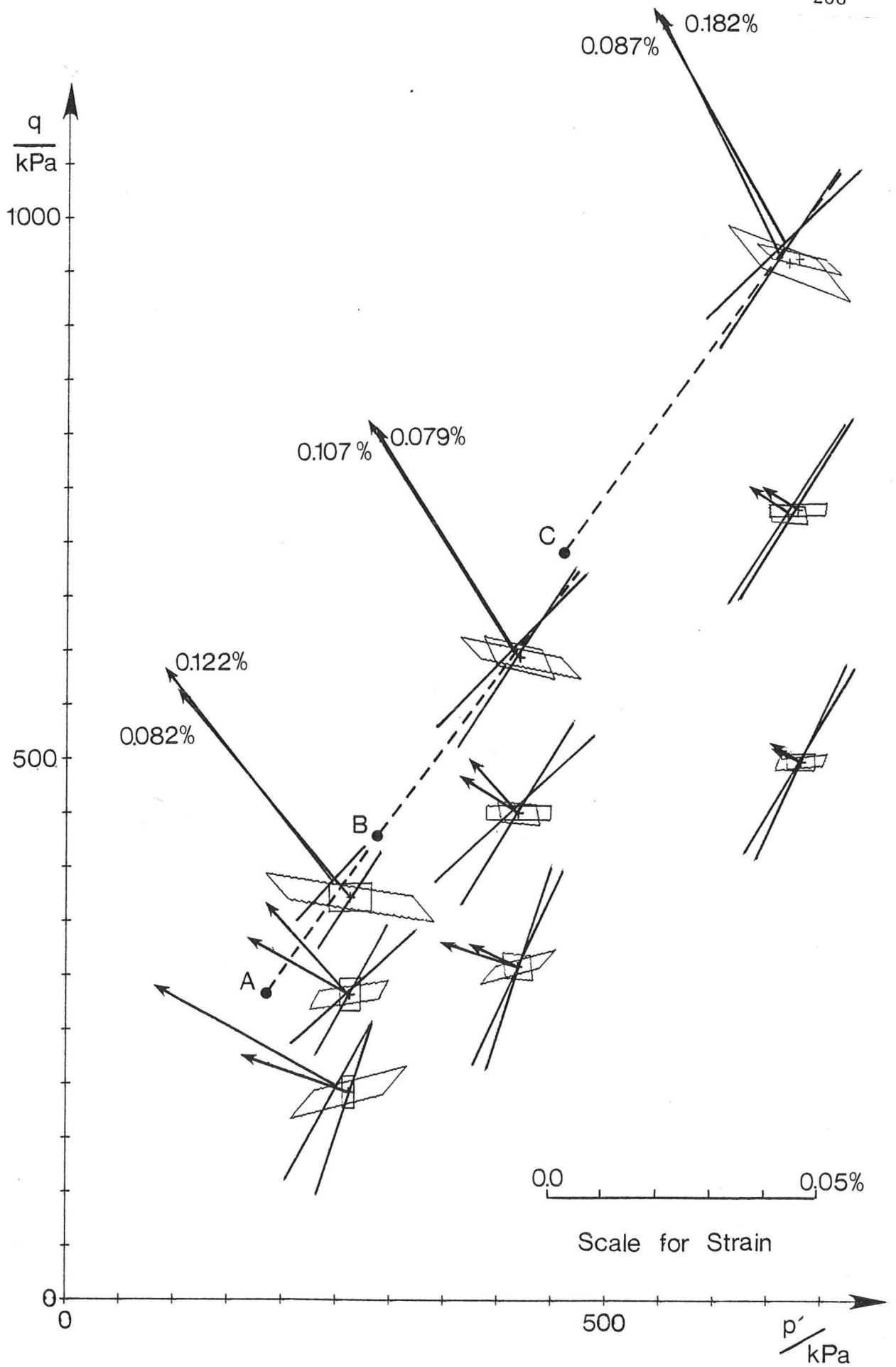


Figure 9.21 Results of tests 2051, 2052,  $\eta$  increasing below maximum,  $p'$  constant

monotonically loaded tests. If the material is unloaded smaller plastic strains occur, these being strongly path dependent. Although small, these strains are often comparable to or larger than the elastic strains, and a more detailed study of their variation would be of great importance. Finally the elastic strains are very small; both shear and bulk moduli increase with both pressure (this aspect being well explained by particle contact theory) and to a lesser extent with maximum past pressure. The elastic properties are anisotropic, with the anisotropy increasing with stress ratio.

## CHAPTER 10

## CONCLUSIONS

Some general conclusions are drawn from the evidence presented in the preceding Chapters. The most important points are re-emphasised and some suggestions for future developments made.

### 10.1 The Use of Thermomechanics in Soil Modelling

The thermomechanical approach to plasticity theory developed in Chapter 3 is a promising method for the description of soil behaviour. In particular it has achieved the primary objective of developing a formulation which guarantees thermodynamic admissibility, whilst allowing the description of "non-associated" plastic flow.

The rigorous development of thermomechanical methods in continuum mechanics is not under scrutiny here, but a brief comment may be made on the validity of the theories. At the very least the methods described in this dissertation represent a restricted class of materials, somewhat wider than those classes limited by the postulates of Il'iushin and Drucker, and the relevant question becomes whether soils approximate reasonably to materials in this class.

The use of an extremum principle, Ziegler's "orthogonality principle" is central to the development of the thermomechanical approach. Although regarded by some as controversial, the principle is linked to certain well established ideas, for instance the reciprocity relations of Onsager (Ziegler (1975)). Whilst many formulations make use (directly or indirectly) of extremum principles, some specifically exclude them. The rigid-plastic model of de Josselin de Jong (1977) for instance makes use only of a weaker dissipation inequality. The resulting model therefore has an additional degree of freedom, and for many problems yields a range of possible solutions rather than a single solution. This sort of model in which the initial and boundary conditions

play a greater role in determining the subsequent response, represents a different philosophy from that used throughout this dissertation in which the constitutive relations provide a complete framework for determining the response. Much further investigation is required to establish whether the simplifications introduced by the use of an extremum principle are justified.

An important result of the formulation, related directly to the choice of a limited number of internal variables, was the existence of a distinct yield locus in stress space. Whilst acceptable for a small number of loading cycles this assumption is expected to lead always to "shakedown" to elastic conditions after many cycles, and so this approach may be inappropriate for the analysis of cyclic behaviour.

A limited normality relationship was proven for rigid-plastic materials, and normality conditions also noted for some specific plasticity models. The proof of normality and convexity conditions is an essential preliminary to the establishment of any bound theorems, and is seen as an important subject for future study. If sufficient generality is to be achieved this will involve work mainly in applied mathematics rather than soil mechanics.

Thermomechanical methods can be used to include the principle of effective stress in a model, making use of the work input equations derived in Section 2.1. The effective stress principle becomes therefore an integral part of the method and need not be invoked as a special condition.

## 10.2 The Modified Cam-Clay Models

In Chapter 4 the application of the thermomechanical method to the description of a single soil model was given in detail. The Modified Cam-Clay model is well established from conventional plasticity theory, and it was of interest to examine how it may also be described by

thermomechanical methods. The importance of the approach lies in the treatment of developments of the model. The extension to large strain theory allows for instance an assessment of the necessity or otherwise of this complication, and for many problems it was deemed unnecessary.

More important are some of the secondary effects described in Chapter 5. The consequences of a pressure dependent elastic shear modulus could have been arrived at from conventional elastic potential theory, but the effects of elastic-plastic coupling are more complex. The alteration of the shape of the yield locus is a surprising result, and whilst it did not prove to be important in the case considered it would seem to be an area where more work could be fruitful. Although the coupled model is quite complex, it is important that the full implications of the thermomechanical approach for this case should be considered. An advantage of the thermomechanical method for coupled plasticity is that it achieves a clarification of the meaning of the internal variables and their relation to the irreversible strain increment.

Some conclusions on important subjects for future study may be drawn from the theoretical developments outside thermomechanics, and bringing these ideas within the thermomechanical framework is an obvious step. The necessity and possibility of non-circular generalisations of yield loci in the octahedral plane is noted, and the importance of anisotropy is also recognised. The development of the analysis of anisotropy will depend principally on the availability of more precise and systematic data for a few materials. The existence of pointed yield loci and plastic potentials is a question which remains open.

### 10.3 Results of Stress Cycle Tests on Dense Sand

Both successes and failures are noted for the computer controlled triaxial machine used for tests on dense sand. The use of stress control

based on a digital feedback system was entirely successful. Stress paths could be followed accurately, allowing tests to be carried out which would be impossible in a conventional apparatus. The use of a computer for both the logging and feedback system allows particularly accurate following of stress paths since all the necessary corrections may be made continuously. A dependence on purely electronic measurement techniques, with their associated problems of unreliability and instability, is a disadvantage.

A fundamental problem was encountered in the measurement of the very small elastic strains (typically 0.03%) during stress cycles in the triaxial test. The problem cannot be overcome by more accurate measurements since it lies in the corrections which must be applied to the measurements to allow for membrane penetration and other effects. These corrections become quite large when compared to the very small elastic deformations. If accurate elastic properties are to be obtained from stress cycle tests on stiff samples in the triaxial apparatus, then a more direct method of measurement of soil deformation is required (perhaps similar to the system reported by Boyce and Brown (1976)).

The stress cycle tests represent a new method of testing soils and were designed specifically to separate out the elastic and plastic properties of the material; the programme of tests was then arranged to study the variation of these properties. The tests proved to be a useful and instructive method of investigation of soil properties, and pose an extremely rigorous test of the applicability of plasticity theory. A computer was essential for the fitting of elastic and plastic properties to the stress cycle data. The quality of fit of the properties confirmed that the behaviour of a dense sand could be expressed within the framework of elastic-plastic behaviour. The main causes of lack of fit are thought to be the effects of a small amount of creep, and the occurrence of reverse plastic strains on some cycles. The latter effect would suggest that an endochronic or hypoelastic theory may have some relevance, and a

detailed study of the quality of the fit which could be achieved using these theories would be of interest.

Measurement of accurate elastic properties proved difficult using the triaxial apparatus, but the following results were noted. Both the bulk and shear moduli increase with pressure, with the power law relation between modulus and pressure being approximately as would be expected from particle contact analysis. The moduli also increase with past maximum pressure, indicating elastic-plastic coupling. The tests carried out also allowed a measure of elastic anisotropy to be made. The anisotropy increases with stress ratio, as would be expected from elastic potential theory with a shear modulus increasing with pressure. It was impossible to resolve completely the elastic behaviour between the conflicting theories of Hertzian contact (which gives a response which cannot be derived from a potential) and potential theory. Dense sand seems to reflect aspects of both types of behaviour and only more detailed measurements may resolve the problem.

On loading with increasing stress ratio a clear yield locus is observed. The locus is oriented approximately as a line of constant stress ratio, but may be at a rather flatter slope. Evidence of curvature of the yield locus to lower stress ratios at pressures both higher and lower than that at which the primary loading occurred (Figure 9.20) was provided by tests involving reloading. As would be expected, the plastic strains increase greatly at high stress ratios. The flow rule is non-associated but is not well determined, depending on stress history as well as stress ratio, although the stress-dilatancy flow rule of Rowe (1962) fitted monotonic triaxial tests well. At high stress ratios the flow rule from stress cycle tests becomes better established and is closer to stress-dilatancy.

Secondary plastic strains of a magnitude comparable to (and frequently larger than) the elastic strains were observed for tests with

unloading. These strains were identified by their different character from that of elastic strains (a process impossible in many conventional tests). They occurred both on unloading of stress ratio and of pressure, and the orientation of the yield locus associated with them was highly path dependent. A more detailed study of these strains is as important as the study of elastic behaviour.

Clearly it would be of interest and importance to carry out stress cycle tests on other materials, and also to extend the study of a single material to give more extensive information, for instance by including tests in the triaxial extension region. The information from tests within the triaxial plane does not yet seem to be sufficiently complete to warrant a similar exploration using a true triaxial device. Tests of a similar type could, however, be carried out in other two degrees of freedom devices such as the simple shear apparatus. If the triaxial machine is to be used further a more satisfactory method of measuring the small elastic strains is necessary.

#### 10.4 The Applicability of Plasticity Theory to Soils

This theoretical and experimental investigation has provided further evidence for the applicability of plasticity theory to soils. The thermomechanical framework provides a new approach in which plasticity theories are derived from a completely different set of assumptions from those used in the conventional approach. As well as being able to accommodate theories with non-associated flow rules without violating any thermodynamic restriction, the formulation is also able to offer some useful insights, for instance into phenomena such as elastic plastic coupling. Most importantly the inclusion of elastic nonlinearity, work hardening, non-associated flow and other phenomena observed in soils within a single rigorous formulation makes that method directly applicable to soils.

The investigation into the elastic and plastic properties of dense sand using stress probe tests confirmed that plasticity theory offers a suitable framework for describing that material. The soil is, however, complex and exhibits non-linear elasticity, elastic-plastic coupling and a complicated plastic response. A more detailed study of the secondary plastic strains for stress changes below maximum stress values is seen as a necessary extension of the study.

The most important subject raised in this dissertation is, however, the application of thermomechanical ideas to derive plasticity theories for soils. It is recommended that future work on this subject should be twofold. Firstly a fundamental study is necessary of the general derivation of plasticity theories within this approach, particularly in the exploration of normality conditions and a search for possible bound theorems. Secondly specific forms of the theory, including such effects as anisotropy and non-associated flow, should be developed to provide numerical models for real soils.

NOTATION

a	anisotropy factor
$a_k$	kinematic variable
$a_1 - a_3$	constants for triaxial control
A	modulus
$A_k$	generalised force
A, B	stiffness factors
A, ... E	moduli
b	$(\sigma_2 - \sigma_3) / (\sigma_1 - \sigma_3)$
$c, c_u$	shear strength, undrained shear strength
$c_{ijkl}$	compliance
$C_1, C_2, \dots$	compliances
d	displacement of yield locus
D	dissipation per unit volume, dilatancy parameter
e	error
E	error factor, potential function
$E_{pq}$	modulus
f	yield locus function
$f_i$	pore fluid velocity
g	plastic potential function
$g_i$	gravitational acceleration
G	shear modulus
$h, h_n$	hardening parameter, normalised hardening parameter
k	permeability
K	bulk modulus, stress-dilatancy constant
L	power input per unit volume
n	porosity
$p, p'$	pressure, effective pressure, $p = (\sigma_1 + \sigma_2 + \sigma_3) / 3$
$p'_c$	preconsolidation pressure

$p_r$	reference pressure
$p'_x$	critical state pressure
$q$	shear stress parameter , $q = \sigma_1 - \sigma_3$
$q^*$	dissipation parameter
$Q$	heat supply
$R$	$\sigma'_1/\sigma'_3$
$s, S$	specific entropy, entropy
$s'$	$(\sigma'_1 + \sigma'_3)/2$
$t$	$(\sigma'_1 - \sigma'_3)/2$
$u, u'$	total, excess pore pressure
$u^{(a)}, u^{(w)}$	pore air, water pressure
$U$	internal energy
$v$	volumetric strain
$v_i$	skeleton velocity
$V$	specific volume
$w_i$	artificial seepage velocity
$W$	work input per unit volume
$W_d, W_s$	dissipated, stored work per unit volume
$x_i$	spatial coordinate
$x_{ij}$	temporary
$\alpha$	shear modulus parameter
$\alpha_{ij}$	internal variable
$\beta$	shear modulus parameter
$\beta_{ij}$	internal force
$\gamma$	unit weight
$\Gamma$	reference specific volume
$\delta_{ij}$	Kronecker delta, 1 if $i = j$ , 0 if $i \neq j$
$\epsilon$	strain, shear strain parameter
$\epsilon_{ij}$	strain
$\eta$	$q/p'$

$\theta$	temperature
$\kappa, \kappa^*$	swelling parameters
$\lambda$	Lame's constant, consolidation parameter
$\lambda^*$	consolidation parameter
$\Lambda$	$(\lambda^* - \kappa^*) / \lambda^*$
$\mu$	Lame's constant
$M$	critical state parameter
$\nu$	Poisson's ratio, scalar factor
$\nu^*$	structural parameter
$\nu_i$	unit normal
$N$	additional critical state model parameter
$\xi$	intrinsic time
$\rho$	density
$\sigma$	stress
$\sigma_{ij}, \sigma'_{ij}$	stress, effective stress
$\phi$	angle of friction, specific dissipation function
$\phi_\mu$	angle of material friction
$\Phi$	dissipation function
$\chi$	pore pressure parameter
$\psi, \Psi$	specific free energy, free energy

## Subscripts and superscripts:

a	axial	q	quasiconservative
d	dissipative	r	radial
e	elastic	w	pore fluid
i	irreversible	1	major
m	maximum	2	intermediate
o	initial	3	minor
p	plastic		

## REFERENCES

- BALASUBRAMANIAM, A.S. (1969) Some Factors Influencing the Stress Strain Behaviour of Clays, Ph.D. Thesis, University of Cambridge
- BAZANT, Z.P. and KRIZEK, R.J. (1976) Endochronic Constitutive Law for Liquefaction of Sand, Jour.Eng.Mech.Div., Proc.ASCE, Vol.102, No.EM2, Apr., 225-238
- BISHOP, A.W. (1959) The Principle of Effective Stress, Teknisk Ukeblad No.39
- BOYCE, J.R. and BROWN, S.F. (1976) Measurement of Elastic Strain in Granular Material, Geotechnique, Vol.26, No.4, Dec., 637-640
- BUTTERFIELD, R. (1979) A Natural Compression Law for Soils (an Advance on  $e - \log p'$ ), Geotechnique, Vol.29, No.4, Dec., 469-480
- CALLADINE, C.R. (1963) The Yielding of Clay, Correspondence, Geotechnique, Vol.13, No.3, Sept., 250-255
- CALLADINE, C.R. (1971) A Microstructural View of the Mechanical Properties of Saturated Clay, Geotechnique, Vol.21, No.4, Dec., 391-415
- CALLEN, H.B. (1960) Thermodynamics, John Wiley and Sons, New York
- CASAGRANDE, A. (1936) Characteristics of Cohesionless Soils Affecting the Stability of Slopes and Earth Fills, Jour. Boston Society of Civil Engineers, Jan.
- DAFALIAS, Y.F. and HERRMANN, L.R. (1980) A Bounding Surface Soil Plasticity Model, Proc.Int.Symp. on Soils under Cyclic and Transient Loading, Swansea, 7-11 January, 335-345
- DAVIDSON, C.S. (1980) The Shear Modulus of Clays, Engineering Tripos, Part II, Group A, Project Report, Cambridge University
- DE JOSSELINE DE JONG, G. (1977) Mathematical Elaboration of the Double Sliding, Free Rotating Model, Archives of Mechanics, Vol.29, No.4, 561-591
- DRUCKER, D.C. (1951) A More Fundamental Approach to Plastic Stress Strain Relations, Proc. 1st US National Congress on App.Mech., Pub. ASME, June, 487-491
- DRUCKER, D.C. (1954) Coulomb Friction, Plasticity and Limit Loads, Jour.App.Mech., Vol.21, Trans.ASME, Series E, Vol.76, 71-74
- DRUCKER, D.C. (1956) On Uniqueness in the Theory of Plasticity, Quat.App.Maths., Vol.14, No.1, Apr., 35-42
- DRUCKER, D.C. (1959) A Definition of a Stable Inelastic Material, Jour.App.Mech., Vol.26, Trans.ASME, Series E, Vol.81, 101-106
- DRUCKER, D.C. (1964) On the Postulate of Stability of Material in the Mechanics of Continua, Jour. de Mech., Vol.3, No.2, June, 235-249

- DRUCKER, D.C., GIBSON, R.E. and HENKEL, D.J. (1957) Soil Mechanics and Work-Hardening Theories of Plasticity, Trans.ASCE, Vol.122, 338-346
- DUNCAN, J.M. and CHANG, C.-Y. (1970) Nonlinear Analysis of Stress and Strain in Soils, Jour. Soil Mech.Found.Eng.Div., Proc.ASCE, Vol.96, No.SM5, Sept., 1629-1653
- GEROGIANNOPOULOS, N. and BROWN, E.T. (1978) The Critical State Concept Applied to Rock, Int.Jour. Rock Mechanics and Mining Science and Geomechanics Abstracts, Vol.15, 1-10
- GUDEHUS, G. and KOLYMBAS, D. (1979) A Constitutive Law of the Rate Type for Soils, Proc. 3rd Int.Conf. on Numerical Methods in Geomechanics, Aachen, 319-329
- HEYMAN, J. (1972) Coulomb's Memoir on Statics, Cambridge University Press
- HILL, R. (1950) The Mathematical Theory of Plasticity, Oxford University Press
- HORNE, M.R. (1965) The Behaviour of an Assembly of Rotund, Rigid, Cohesionless Particles, I and II, Proc.Roy.Soc., Series A, Vol.286, 62-97
- HORNE, M.R. (1969) The Behaviour of an Assembly of Rotund, Rigid, Cohesionless Particles, III, Proc.Roy.Soc., Series A, Vol.310, 21-34
- HOULSBY, G.T. (1979) The Work Input to a Granular Material, Geotechnique, Vol.29, No.3, Sept., 254-258
- HUECKEL, T. and NOVA, R. (1979) Some Hysteresis Effects of the Behaviour of Geologic Media, Int.Jour. Solids and Structures, Vol.15, 625-642
- HVORSLEV, J. (1936) Condition of Failure for Remoulded Cohesive Soils, Discussion, Proc.Int.Conf. Soil Mech.Found.Eng., Vol.3, Cambridge, Mass., 51-53
- IL'IUSHIN, A.A. (1960) Problems of the General Theory of Plasticity, Jour.App.Maths. and Mech., Vol.24, No.3, 399-411
- IL'IUSHIN, A.A. (1961) On the Postulate of Plasticity, Jour.App.Math. and Mech., Vol.25, No.3, 746-752
- JOWITT, P.W. and MUNRO, J. (1975) Influence of Void Distribution and Entropy on the Engineering Properties of Granular Media, Proc. 2nd Int.Conf. Applications of Statistics and Probability in Soil and Structural Engineering, Vol.2, Aachen, Germany, Sept., 365-385
- KOLYMBAS, D. and GUDEHUS, G. (1980) A Constitutive Law for Sands and Clays - Position, Prediction and Evaluation, Proc.NSF/NSER North American Workshop on Plasticity and Generalised Stress-Strain Modelling of Soils, Montreal, May 28-30

- LADD, C.C., BOVEE, R.B., EDGERS, L. and RIXNER, J.J. (1971) Consolidated-Undrained Plane Strain Shear Tests on Boston Blue Clay, Research in Earth Physics, Phase Report No.15, Research Report R71-13, Soils Publication 273, Massachusetts Institute of Technology, Mar.
- LADD, C.C. and FOOTT, R. (1974) New Design Procedure for Stability of Soft Clays, Proc.ASCE, Jour.Geotech.Eng.Div., Vol.100, No.GT7, July, 763-786
- LADE, P.V. (1972) The Stress-Strain and Strength Characteristics of Cohesionless Soils, Ph.D. Thesis, University of California, Berkeley
- LADE, P.V. (1977) Elasto-Plastic Stress-Strain Theory for Cohesionless Soil with Curved Yield Surfaces, Int.Jour. Solids and Structures, Vol.13, 1019-1035
- LADE, P.V. and DUNCAN, J.M. (1975) Elastoplastic Stress-Strain Theory for Cohesionless Soil, Proc.ASCE, Jour.Geotech.Eng.Div., Vol.101, GT10, Oct., 1037-1053, Closure Vol.104, Jan. 1978, 134-141
- LADE, P.V. and DUNCAN, J.M. (1976) Stress-Path Dependent Behaviour of Cohesionless Soil, Jour.Geotech.Eng.Div., ASCE, Vol.102, GT1, Jan., 51-68
- LAGONI, P. (1976) Kornede Materialers Mekanik, Thesis, Soil Mechanics Laboratory, Technical University of Denmark
- LEE, I.K. (1978) End Restraint Effects on Undrained Static Strength of Sand, Proc.ASCE, Jour.Geotech.Eng.Div., Vol.104, No.GT6, June, 687-704
- LEWIN, P.I. (1970) Stress Deformation Characteristics of a Saturated Soil, M.Sc. Thesis, University of London
- LEWIN, P.I. (1973) The Influence of Stress History on the Plastic Potential, Symp. on the Role of Plasticity in Soil Mech., Ed. Palmer, A.C., Cambridge, 96-106
- LEWIN, P.I. and BURLAND, J.B. (1970) Stress Probe Experiments on Saturated Normally Consolidated Clay, Geotechnique, Vol.20, No.1, Mar., 38-56
- LOVE, A.E.H. (1927) A Treatise on the Mathematical Theory of Elasticity, Cambridge University Press
- MAIER, G. and HUECKEL, T. (1977) Nonassociated and Coupled Flow Rules of Elastoplasticity for Geotechnical Media, Proc. 9th Int.Conf. Soil Mech.Found.Eng., Session 9, Constitutive Equations for Soils, Tokyo, July
- MATSUOKA, H. (1974) Stress Strain Relationships of Sands Based on the Mobilised Plane, Soils and Foundations, Vol.14, No.2, June, 47-62
- MATSUOKA, H. (1976) On the Significance of the 'Spatial Mobilised Plane', Soils and Foundations, Vol.16, No.1, Mar., 91-100

- MATSUOKA, H. and NAKAI, T. (1974) Stress-Deformation and Strength Characteristics of Soil Under Three Different Principal Stresses, Proc.JSCE, No.232, Dec., 59-70
- MINDLIN, R.D. and DERESIEWICZ, H. (1953) Elastic Spheres in Contact Under Varying Oblique Forces, Jour.App.Mech., Vol.20, No.3, Sept., 327-344
- MITCHELL, R.J. (1970) On the Yielding and Mechanical Strength of Leda Clay, Canadian Geotechnical Journal, Vol.7, 297-312
- MOLENKAMP, F. (1980) Some Aspects of Constitutive Equations for Sand, Proc.Int.Symp. on Soils Under Cyclic and Transient Loading, Swansea, Vol.1, 411-420
- NAMY, D. (1970) An Investigation into Certain Aspects of Stress-Strain Relationships for Clay Soils, Ph.D. Thesis, Cornell University
- NOVA, R. and WOOD, D.M. (1978) Accessibility and Material Stability, Internal Report CUED/C-Soils TR44, University of Cambridge
- OHTA, H. and WROTH, C.P. (1976) Anisotropy and Stress Reorientation in Clay Under Load, 2nd Int.Conf. on Numerical Methods in Geomechanics, Blacksburg, Virginia, USA, Vol.1, Ed. Desai, C.S., Pub.ASCE, June, 319-328
- ODA, M. (1972) The Mechanism of Fabric Changes During Compressional Deformation of Sand, Soils and Foundations, Vol.12, No.2, June, 1-18
- ODA, M. (1974) A Mechanical and Statistical Model of Granular Material, Soils and Foundations, Vol.14, No.1, Mar., 13-27
- PALMER, A.C. (1967) Stress Strain Relations for Clays: An Energy Theory, Geotechnique, Vol.17, No.4, Dec., 348-358
- PAPPIN, J.W. and BROWN, S.F. (1980) Resilient Stress-Strain Behaviour of a Crushed Rock, Proc.Int.Symp. on Soils under Cyclic and Transient Loading, Swansea, 7-11 Jan., 169-177
- PARRY, R.H.G. (1965) Shear Strength of Saturated Remoulded Clay, Proc. 6th Int.Conf. Soil Mech.Found.Eng., Montreal, Vol.2, 333-337
- H
- PARRY, R.H.G. and AMERASINGE, S.F. (1973) Components of Deformation in Clay, Symp. on the Role of Plasticity in Soil Mechanics, Ed. Palmer, A.C., Cambridge, 13-15 Sept., 108-126
- PEARCE, J.A. (1970) The Behaviour of Soft Clay in a New True Triaxial Apparatus, Ph.D. Thesis, University of Cambridge
- POOROOSHASB, H.B., HOLUBEC, I. and SHERBOURNE, A.N. (1966) Yielding and Flow of Sand in Triaxial Compression, Part I, Canadian Geotechnical Journal, Vol.3, No.4, Nov., 179-190
- PRAGER, W. and HODGE, P.G. (1951) Theory of Perfectly Plastic Solids, John Wiley and Sons, New York

- PREVOST, J.H. (1979) Mathematical Modelling of Soil Stress-Strain-Strength Behaviour, Proc. 3rd Int.Conf. Numerical Methods in Geomechanics, Aachen, Vol.1, 347-361
- RANDOLPH, M.F., CARTER, J.P. and WROTH, C.P. (1979) Driven Piles in Clay - The Effects of Installation and Subsequent Consolidation, Geotechnique, Vol.29, No.4, Dec., 361-393
- RENDULIC, L. (1936) Relation Between Void Ratio and Effective Principal Stresses for a Remoulded Silty Clay, Discussion, Proc.Int.Conf. Soil Mech.Found.Eng., Vol.3, Cambridge, Mass., 48-51
- ROSCOE, K.H. and BURLAND, J.B. (1968) On the Generalised Stress-Strain Behaviour of 'Wet' Clay, Engineering Plasticity, Ed. Heyman, J. and Leckie, F.A., Cambridge University Press, 535-609
- ROSCOE, K.H., SCHOFIELD, A.N. and WROTH, C.P. (1958) On the Yielding of Soils, Geotechnique, Vol.8, No.1, Mar., 22-53
- ROWE, P.W. (1962) The Stress Dilatancy Relation for Static Equilibrium of an Assembly of Particles in Contact, Proc.Roy.Soc., Series A, Vol.269, 500-527
- ROWE, P.W. and BARDEN, L. (1964) The Importance of Free Ends in Triaxial Testing, Proc.ASCE, Jour. Soil Mech.Found.Eng.Div., Vol.90, No.SM1, 1-27
- SARSBY, R.W. (1978) The Deformation Behaviour of Particulate Media Subjected to Constant Stress Ratio Paths, Ph.D. Thesis, University of Manchester
- SCHOFIELD, A.N. and WROTH, C.P. (1968) Critical State Soil Mechanics, McGraw Hill, London
- SOKOLOVSKII, V.V. (1965) Statics of Granular Media, Pergamon, Oxford
- TATSUOKA, F. and ISHIHARA, K. (1974) Yielding of Sand in Triaxial Compression, Soils and Foundations, Vol.14, No.2, June, 63-74
- TAYLOR, D.W. (1948) Fundamentals of Soil Mechanics, Wiley, New York
- TERZAGHI, K. (1943) Theoretical Soil Mechanics, Wiley, New York
- THORNTON, C. and BLACKBURN, D.J. (1980) Yield Conditions for Body Centered Tetragonal Arrays, Internal Report, SM1080, Dept. of Civil Eng., University of Aston, Birmingham
- THURAIRAJAH, A. (1961) Some Shear Properties of Kaolin and of Sand, Ph.D. Thesis, University of Cambridge
- VALANIS, K.C. (1971) A Theory of Viscoplasticity Without a Yield Surface, I and II, Archives of Mechanics, Vol.23, No.4, 517-551
- VAN EEKELEN, H.A.M. and POTTS, D.M. (1978) The Behaviour of Drammen Clay Under Cyclic Loading, Geotechnique, Vol.28, No.1, Mar., 173-196
- WOOD, D.M. (1974) The Mechanical Behaviour of Kaolin, Ph.D. Thesis, University of Cambridge

- WROTH, C.P. (1977) The Predicted Performance of a Soft Clay Under a Trial Embankment Loading Based on the Cam-Clay Model, Finite Elements in Geomechanics, ed. G. Gudehus, John Wiley and Sons, London, 191-208
- WROTH, C.P. and HOULSBY, G.T. (1980) A Critical State Model for Predicting the Behaviour of Clays, Proc.NSF/NSERC North American Workshop on Plasticity and Generalised Stress-Strain Modelling of Soils, Montreal, May 28-30
- WROTH, C.P., RANDOLPH, M.F., HOULSBY, G.T. and FAHEY, M. (1979) A Review of the Engineering Properties of Soils with Particular Reference to the Shear Modulus, CUED/D-Soils TR75, Cambridge University
- WROTH, C.P. and ZYTYNSKI, M. (1977) Finite Element Computations Using an Elasto-Plastic Soil Model for Geotechnical Problems of Soft Clay, Proc. 9th Int.Conf. Soil Mech.Found.Eng., Computers in Soil Mechanics: Present and Future, Tokyo, July, 193-243
- YONG, R.N. and SILVESTRI, V. (1977) Plastic Yielding of a Sensitive Clay in True Triaxial Testing, Proc. 9th Int.Conf. Soil Mech. Found.Eng., Constitutive Equations for Soils, Session 9, Tokyo, 271-277
- ZIEGLER, H. (1975) Non-Linearity in Thermomechanics, Int.Jour. of Non-Linear Mechanics, Vol.10, 145.154
- ZIEGLER, H. (1977) An Introduction to Thermomechanics, North-Holland, Amsterdam
- ZYTYNSKI, M., RANDOLPH, M.F., NOVA, R. and WROTH, C.P. (1978) On Modelling the Unloading-Reloading Behaviour of Soils, Int.Jour. Numerical and Analytical Methods in Geomechanics, Vol.2, No.1, Jan., 87-93

## APPENDIX A

Geotechnique, Vol.29, No.3, September 1979, pp.354-358.

354

TECHNICAL NOTES

## The work input to a granular material

G. T. HOULSBY\*

### INTRODUCTION

Some recent theoretical models for soils are based on hypotheses about the rate at which the input work to the soil is either stored or dissipated. It is therefore necessary to evaluate the rate of work input to the soil in terms of the stresses, strain rates and other variables. For a single-phase material the power input per unit volume is simply the product of the stresses and the strain rates; but this result does not apply for the two-phase material, such as a saturated soil, where both the stresses within the two phases and the velocities of the two materials will be different. The total power input per unit volume to a soil must therefore be derived by considering the rate at which all the forces on both the soil grains and the pore fluid do work.

The principle of effective stress as described by Terzaghi (1943) states that the mechanical behaviour of a soil is governed by the difference between the total stress and the pore pressure, this quantity being termed the effective stress. If it is accepted that the mechanical behaviour of a material reflects the storage and dissipation of the power input, then it would be expected that this power input for a soil would depend on effective, not total stress. Such a result was obtained by Schofield and Wroth (1968) where they showed that, for an infinitely slow process, the mechanical work input to a soil is given by the product of the effective stress and the strain. (The result was obtained only for the special case of the triaxial test, but could be readily extended to more general stress states.)

Alternatively, if there is no deformation of the soil skeleton, the work input derives solely from the loss of excess pore pressure as the pore fluid seeps through the soil skeleton. The power input per unit volume may be calculated for this case as the product of the excess pore pressure gradient and the artificial seepage velocity.

The above two special cases represent extremes of soil behaviour: in the first, the entire power input is associated with the deformation of the soil skeleton, and in the second, the entire input is due to the viscous flow of the pore fluid. In many cases of engineering importance however, the two processes of deformation and seepage occur simultaneously, the best

---

\* Cambridge University Engineering Department.

known example of this being the consolidation of a soil. For the general case it must be determined whether the total power input is simply the sum of the two terms above (effective stress times deformation rate and excess pore pressure gradient times artificial seepage velocity) or whether there are additional power terms representing some coupling between the two processes of seepage and skeleton deformation.

Note that such a coupling between various terms in the expression for the input power is not to be confused with the inter-relation between seepage and skeleton deformation which arises from the conditions of compatibility and equilibrium. These latter relationships form the basis of conventional consolidation analysis.

#### ANALYSIS

In the following analysis the total power input per unit volume to a soil is derived under the simplifying assumption that both the individual soil grains and the pore fluid may be considered as incompressible; the analysis is therefore applicable to saturated soils only. Since the analysis is in terms of continuum mechanics (in which the microscopically non-homogeneous soil is replaced by an equivalent homogeneous continuum) the region under consideration must be sufficiently large so that the definitions of stress, strain and porosity are meaningful. It is assumed that there is no overall shear stress in the pore fluid on the scale of the element under consideration. However, in order that there should be any loss of excess pore pressure there must be shear stresses in the pore fluid on the scale of the grain size.

The analysis is carried out in terms of tensors, since this notation allows a convenient shorthand for the many components of the different variables. As only strain rates are considered (which may be treated as small strains) there is no loss of generality in the use of Cartesian tensors. The summation convention over a repeated index is used, and the symmetric and skew-symmetric parts of the tensor  $a_{ij}$  are given by  $a_{(ij)}$  and  $a_{[ij]}$  respectively. Partial differentiation with respect to spatial co-ordinate only is given by a comma notation; thus  $\partial a / \partial x_i = a_{,i}$ . Such differentials may be treated as tensors. The symbol  $\delta_{ij}$  is the Kronecker delta ( $\delta_{ij} = 1$ ,  $i = j$ ;  $\delta_{ij} = 0$ ,  $i \neq j$ ).

Let the total stress on an element of soil be  $\sigma_{ij}$  and the total pore pressure be  $u$ , the effective stress  $\sigma'_{ij}$  is then defined as

$$\sigma'_{ij} = \sigma_{ij} - u\delta_{ij} \quad \dots \dots \dots (1)$$

If the porosity is  $n$  and a plane cutting through both particles and voids is considered, then the average stress within the grains is given by  $s_{ij}$ , where

$$\sigma_{ij} = nu\delta_{ij} + (1-n)s_{ij} \quad \dots \dots \dots (2)$$

Denoting the densities of the soil grains and the pore fluid by  $\rho^{(s)}$  and  $\rho^{(w)}$  respectively, then the overall density  $\rho$  is given by

$$\rho = n\rho^{(w)} + (1-n)\rho^{(s)} \quad \dots \dots \dots (3)$$

If  $g_i$  is the gravitational acceleration the variation of excess pore pressure  $u'$  may be defined as

$$u'_{,i} = u_{,i} - \rho^{(w)}g_i \quad \dots \dots \dots (4)$$

The velocity of the soil skeleton is given by  $v_i$  and the strain by  $\hat{\epsilon}_{ij}$ ; the strain rate may then be defined as

$$\dot{\hat{\epsilon}}_{ij} = -v_{(j,i)} \quad \dots \dots \dots (5)$$

where the superposed dot indicates partial differentiation with respect to time, and the negative sign arises from a definition of compressive strains as positive. Denoting the actual mean velocity of the pore fluid by  $f_i$ , the artificial seepage velocity  $w_i$  (as used in conventional seepage calculations) is then defined by

$$w_i = n(f_i - v_i) \quad \dots \quad (6)$$

The above equations define the various quantities which are of interest, and correspond exactly to the conventional definitions used in soil mechanics. The conditions of equilibrium and compatibility now impose certain relationships between these quantities. The equation of total stress equilibrium, taking compressive stress as positive, may be written as

$$-\sigma_{ij,j} + \rho g_i = 0 \quad \dots \quad (7)$$

Since both the pore fluid and the individual soil grains are considered as incompressible the total flow of material into an arbitrary volume  $V$  fixed in space must be zero. If  $A$  is the surface bounding  $V$ , and  $v_j$  a unit vector in the direction of the outward normal to an element of this surface  $dA$ , then this condition may be written

$$\int_A [nf_j + (1-n)v_j]v_j dA = 0$$

Substituting the definition of artificial velocity (equation (6)) and making use of the divergence theorem of Gauss<sup>1</sup>

$$\int_V (w_j + v_j)_{,j} dV = 0$$

Carrying out the differentiation and noting that since  $V$  is arbitrary the integrand must always be zero

$$w_{j,j} + v_{j,j} = 0 \quad \dots \quad (8)$$

which is the final form of the compatibility condition for incompressible soil grains and pore fluid.

The power input to any arbitrary volume fixed in space is obtained from the sum of the products of the various forces (body forces and surface tractions) acting on the material with their respective velocities. If the average power input per unit volume within  $V$  is  $L$ , then summation of these terms gives

$$\int_V L dV = - \int_A [nu\delta_{ij}f_i + (1-n)s_{ij}v_i]v_j dA + \int_V [\rho^{(w)}ng_i f_i + \rho^{(s)}(1-n)g_i v_i] dV$$

where the negative sign arises from the compressive positive convention for the stresses. Substituting equations (2) and (3) gives

$$\int_V L dV = - \int_A (nu\delta_{ij}f_i - nu\delta_{ij}v_i + \sigma_{ij}v_i)v_j dA + \int_V (\rho^{(w)}ng_i f_i - \rho^{(w)}ng_i v_i + \rho g_i v_i) dV$$

Substituting the definition of artificial velocity (equation (6)) and then noting that  $\delta_{ij}w_i = w_j$ , the divergence theorem of Gauss may then be applied to give

<sup>1</sup> The divergence theorem of Gauss states that if  $y$  is an analytical function of  $x_i$ , ie  $y = y(x_i)$ , then, using the terminology defined above,

$$\int_A y v_j dA = \int_V y_{,j} dV$$

$$\int_V L dV = \int_V -(uw_j + \sigma_{ij}v_i)_{,j} + (\rho^{(w)}g_iw_i + \rho g_i v_i) dV$$

Again noting that since  $V$  is arbitrary this may be written in its local form, expansion of the differential then results in

$$L = -u_{,j}w_j - uw_{j,j} - \sigma_{ij,j}v_i - \sigma_{ij}v_{i,j} + \rho^{(w)}g_iw_i + \rho g_i v_i$$

Altering the dummy indices of the first term allows substitution of the definition of excess pore pressure gradient (4). Substitution of the compatibility condition (8) then allows re-arrangement to

$$L = -u_{,i}'w_i - \sigma_{ij}v_{i,j} + uv_{j,j} - \sigma_{ij,j}v_i + \rho g_i v_i$$

The last two terms may be eliminated by use of the equilibrium condition (7). Using the relationship  $v_j = \delta_{ij}v_i$

$$L = -u_{,i}'w_i - \sigma_{ij}v_{i,j} + u\delta_{ij}v_{i,j}$$

Substituting the definition of effective stress (1)

$$L = -u_{,i}'w_i - \sigma_{ij}'v_{i,j}$$

Note that because of the symmetry of  $\sigma_{ij}'$ ,  $\sigma_{ij}'v_{[i,j]} = 0$ , so  $\sigma_{ij}'v_{i,j} = \sigma_{ij}'v_{(i,j)}$ . Making use of the symmetry of  $v_{(i,j)}$  to interchange indices, the substitution of the definition of strain rate (5) then yields the final result

$$L = \sigma_{ij}'\dot{\epsilon}_{ij} - u_{,i}'w_i$$

#### DISCUSSION

It has been proven that there are no terms in the power input expression other than the two discussed above. The simple expression for the power input per unit volume therefore continues to apply for the case of finite deformation rate combined with seepage, the two terms being the product of the effective stress with the strain rate and the (negative) excess pore pressure gradient with the artificial seepage velocity. (The negative sign results simply from the sign convention for excess pore pressure gradient.)

This result may be used to give a new interpretation of the principle of effective stress. If the Terzaghi definition of effective stress is adopted it is observed that the total rate of work input per unit volume to the soil is given by the two terms  $(\sigma_{ij}'\dot{\epsilon}_{ij})$  and  $(-u_{,i}'w_i)$ . Clearly these may be interpreted as the rates of work input per unit volume to the soil skeleton and to the pore fluid respectively, and there is no coupling between the two processes of skeleton deformation and seepage. This result may be inverted to state that if there is no coupling between the work input to the soil skeleton and to the pore fluid, then the power input per unit volume to the soil skeleton is given at all times by the product of the effective stress with the strain rate. If it is further stated that the mechanical behaviour is simply a reflection of the way in which work is stored and dissipated, then if the processes of skeleton deformation and seepage are uncoupled, the mechanical behaviour of the skeleton will depend on the effective stress as defined by Terzaghi.

Although this gives an alternative interpretation of the principle of effective stress in terms of continuum mechanics, no statement is made here about whether soil would be expected to obey the principle, and hence show the uncoupling of the work terms. Any justification of the principle of effective stress for soils still rests on the arguments of particulate mechanics (notably Bishop, 1959) and the extensive body of experimental support for the theory. The

present analysis offers, however, a new interpretation in terms of continuum mechanics, in that the principle of effective stress is seen as a principle of the independence of the mechanical work input to the soil skeleton and to the pore fluid.

#### ACKNOWLEDGEMENT

The Author is grateful to the Science Research Council for financial support, and thanks Dr C. P. Wroth for his advice and encouragement.

#### REFERENCES

- Bishop, A. W. (1959). The principle of effective stress. *Tek. Ukebl.* No. 39.  
Schofield, A. N. & Wroth, C. P. (1968). *Critical state soil mechanics*. London: McGraw-Hill.  
Terzaghi, K. (1943). *Theoretical soil mechanics*. New York: John Wiley and Sons.

## APPENDIX B

## HOMOGENEITY OF RESPONSE

It is usually assumed without question in plasticity theory that the response of a continuum will remain homogeneous; and this assumption has been made throughout all other parts of this dissertation. A criterion for the homogeneity of response can, however, be established within the thermodynamic framework, and is examined briefly in this Appendix.

The equilibrium state of a system in thermal contact with a heat reservoir at constant temperature is such that the free energy is a minimum. The use of a minimum free energy criterion is not appropriate to other conditions (e.g. adiabatic or isentropic) and so the following analysis is appropriate only to the isothermal case, which represents a reasonable approximation to the conditions in soil mechanics problems. Ziegler's formulation requires an explicit statement of the free energy expressions for either internal energy or entropy *in order* to extend the minimum energy criterion to other conditions. The minimum free energy condition is used in Section 4.2 to establish the criterion for plastic loading or unloading. It is here adapted as a criterion for homogeneity of response: if a non-homogeneous mode of deformation can result in a lower free energy than homogeneous deformation, then this non-homogeneous mode will occur.

The mode of bifurcation into non-homogeneous deformation which is studied is the case where a homogeneous material splits into a series of infinitesimally thin layers of material undergoing alternatively elastic and plastic deformation; the following discussion is therefore only relevant to a material in which the stress point is on the yield locus. Only bifurcation from an initially homogeneous state is

considered. The proportion of the material which behaves elastically is  $\alpha$  and that which behaves plastically is  $(1-\alpha)$  (see Figure B.1).

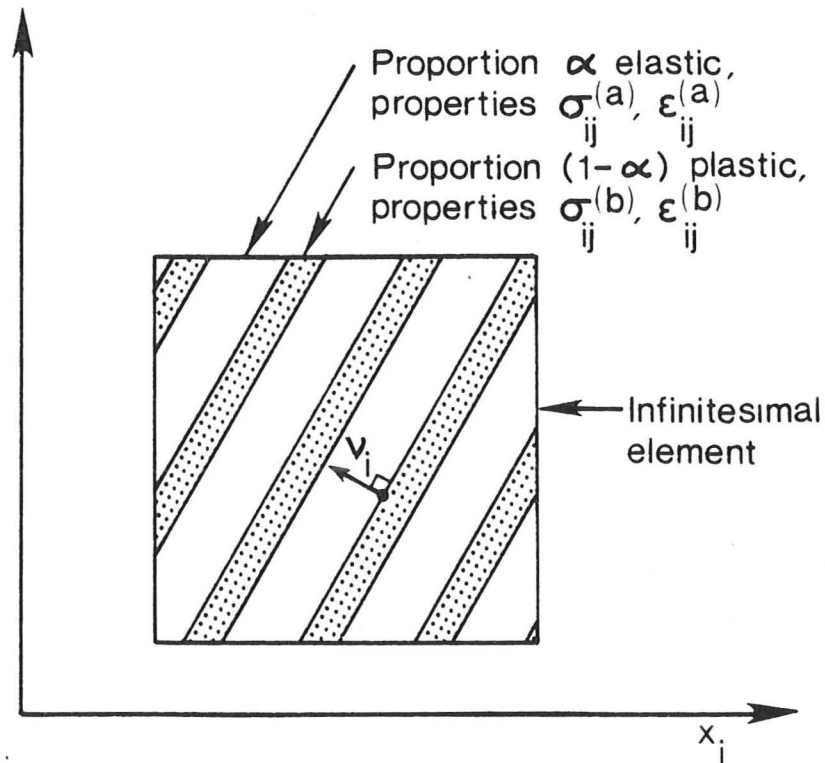


Figure B.1 Mode of bifurcation into non-homogeneous deformation

If superscripts (a) and (b) refer to the strains and stresses in these two regions then the overall increments of these quantities will be:

$$\dot{\sigma}_{ij} = \alpha \dot{\sigma}_{ij}^{(a)} + (1-\alpha) \dot{\sigma}_{ij}^{(b)} \quad (\text{B.1})$$

$$\dot{\epsilon}_{ij} = \alpha \dot{\epsilon}_{ij}^{(a)} + (1-\alpha) \dot{\epsilon}_{ij}^{(b)} \quad (\text{B.2})$$

Provided the layers are infinitesimally thin, then any boundary conditions may be met by the non-homogeneous material, since any element of the continuum will exhibit macroscopically the above overall properties. Thus the non-homogeneity discussed here is of a truly intrinsic nature to the material, and cannot be prevented by an

appropriate choice of boundary conditions.

The conditions of compatibility and equilibrium require that, for small strains:

$$\dot{\sigma}_{ij}^{(a)} v_j - \dot{\sigma}_{ij}^{(b)} v_j = 0 \quad (\text{B.3})$$

$$\dot{\epsilon}_{ij}^{(a)} - \dot{\epsilon}_{ij}^{(b)} = \frac{1}{2}(d_i v_j + d_j v_i) \quad (\text{B.4})$$

where  $v_i$  is the unit normal to the planes of bifurcation and  $d_i$  is a vector of arbitrary magnitude. For a given stress state and imposed strain increment it is now possible to calculate the free energy change in terms of the strain increment, the orientation of the planes of bifurcation  $v_i$  and the variable  $\alpha$ . If the stress point lies on the yield locus  $\alpha$  may vary between 0 and 1, and takes the value which minimises the free energy increase. In most cases the minimum is either at  $\alpha = 0$  or  $\alpha = 1$ , and homogeneous plastic or elastic response is given (with the selection being identical to that in the conventional approach). Under certain circumstances, however, an intermediate value may give a lower free energy, and bifurcation into the non-homogeneous mode is predicted.

The analysis for three dimensional models is lengthy, and no standard approach to the problem has been evolved, but the implementation of the homogeneity criterion is here illustrated by the case of a one-dimensional analogue. Consider the fairly general one-dimensional elastic-plastic material specified by the functions:

$$\rho\psi = f_1((\epsilon - \epsilon^{(p)})) + f_2(\epsilon^{(p)}) \quad (\text{B.5})$$

$$\rho\phi = f_3(\epsilon, \epsilon^{(p)}) |\dot{\epsilon}^{(p)}| \quad (\text{B.6})$$

The stress and internal force are given by:

$$\sigma = \frac{\partial f_1}{\partial \epsilon} \quad (\text{B.7})$$

$$\sigma = \frac{\partial f_1}{\partial \epsilon(p)} + \frac{\partial f_2}{\partial \epsilon(p)} + f_3 \text{sg}(\dot{\epsilon}^{(p)}) \quad (\text{B.8})$$

where the function  $\text{sg}(x)$  is equal to 1 for  $x > 0$  and -1 for  $x < 0$  and is undefined at  $x = 0$ . Noting that, because of the form of  $f_1$ ,  $\frac{\partial f_1}{\partial \epsilon(p)} = -\frac{\partial f_1}{\partial \epsilon}$ , so that:

$$\sigma = \frac{\partial f_2}{\partial \epsilon(p)} + f_3 \text{sg}(\dot{\epsilon}^{(p)}) \quad (\text{B.9})$$

Further differentiation and the elimination of  $\dot{\epsilon}^{(p)}$  results in the two cases:

$$\dot{\sigma} = \frac{\partial^2 f_1}{\partial \epsilon^2} \left[ \frac{\frac{\partial^2 f_2}{\partial \epsilon(p)} + \left( \frac{\partial f_3}{\partial \epsilon(p)} + \frac{\partial f_3}{\partial \epsilon} \right) \text{sg}(\dot{\epsilon}^{(p)})}{\frac{\partial^2 f_1}{\partial \epsilon^2} + \frac{\partial^2 f_2}{\partial \epsilon(p)^2} + \frac{\partial f_3}{\partial \epsilon(p)} \text{sg}(\dot{\epsilon}^{(p)})} \right] \dot{\epsilon} \quad (\text{B.10})$$

in the case of  $\dot{\epsilon}^{(p)} \neq 0$ , and for the elastic case ( $\dot{\epsilon}^{(p)} = 0$ )

$$\dot{\sigma} = \frac{\partial^2 f_1}{\partial \epsilon^2} \dot{\epsilon} \quad (\text{B.11})$$

These equations may more conveniently be written in terms of (variable) plastic and elastic moduli:

$$\dot{\sigma} = E^{(p)} \dot{\epsilon} \quad \text{for Equation (B.10)} \quad (\text{B.12})$$

and 
$$\dot{\sigma} = E^{(e)} \dot{\epsilon} \quad \text{for Equation (B.11)} \quad (\text{B.13})$$

If the non-homogeneous case is considered, with a proportion  $\alpha$  elastic and  $(1-\alpha)$  plastic, there is no strain compatibility condition for the one-dimensional case and the equilibrium condition reduces to:

$$\dot{\sigma}^{(a)} = \dot{\sigma}^{(b)} \quad (\text{B.14})$$

Noting that in the elastic case:

$$\rho \dot{\psi}^{(a)} = \sigma \dot{\epsilon}^{(a)} \quad (\text{B.15})$$

and in the plastic case:

$$\rho \dot{\psi}^{(b)} = \sigma \dot{\epsilon}^{(b)} + \left( \frac{\partial f_1}{\partial \epsilon^{(p)}} + \frac{\partial f_2}{\partial \epsilon^{(p)}} \right) \dot{\epsilon}_p^{(b)} \quad (\text{B.16})$$

after some manipulation and the substitution of the overall strain the overall free energy change is given by:

$$\rho \dot{\psi} = \alpha \rho \dot{\psi}^{(a)} + (1-\alpha) \rho \dot{\psi}^{(b)} = \sigma \dot{\epsilon} - f_3 \text{sg}(\dot{\epsilon}_p^{(b)}) \left( 1 - \frac{E^{(p)}}{E^{(e)}(1-\alpha) + E^{(p)}\alpha} \right) \dot{\epsilon} \quad (\text{B.17})$$

Provided that the current stress point satisfies the yield condition,  $\alpha$  may vary from zero to unity. Consider the case satisfying the yield condition with  $\dot{\epsilon}_p^{(b)} > 0$ ; then  $\text{sg}(\dot{\epsilon}_p^{(b)})$  is positive and  $f_3$  also positive (since the dissipation must be positive). The minimum increase of the free energy will be given by the minimum value of  $\frac{E^{(p)}}{E^{(e)}(1-\alpha) + E^{(p)}\alpha}$  when  $\dot{\epsilon}$  is positive and the maximum value when  $\dot{\epsilon}$  is negative. It is clear that these will be at  $\alpha = 0$  and  $\alpha = 1$  respectively if  $E^{(e)}$  and  $E^{(p)}$  are both positive and  $E^{(e)} > E^{(p)}$ ; so that homogeneous plastic or elastic behaviour occurs for  $\dot{\epsilon}$  positive or negative in this case.

If, however,  $E^{(p)}$  is negative ( $E^{(e)}$  is assumed to be always positive) a value of  $\alpha$  can be chosen between zero and unity for which  $\frac{E^{(p)}}{E^{(e)}(1-\alpha) + E^{(p)}\alpha}$  becomes infinite (of either sign), thus for this case a bifurcation to a non-homogeneous state, in which a finite drop in the free energy would occur for an infinitesimal strain, would be predicted for either sign of  $\dot{\epsilon}$ . In a monotonically strained body with  $E^{(e)}$  positive and a changing  $E^{(p)}$ , bifurcation will occur when  $E^{(p)}$  falls to zero, i.e. the transition from hardening to softening behaviour (see Figure B.2). No analysis of the post bifurcation behaviour has been attempted.

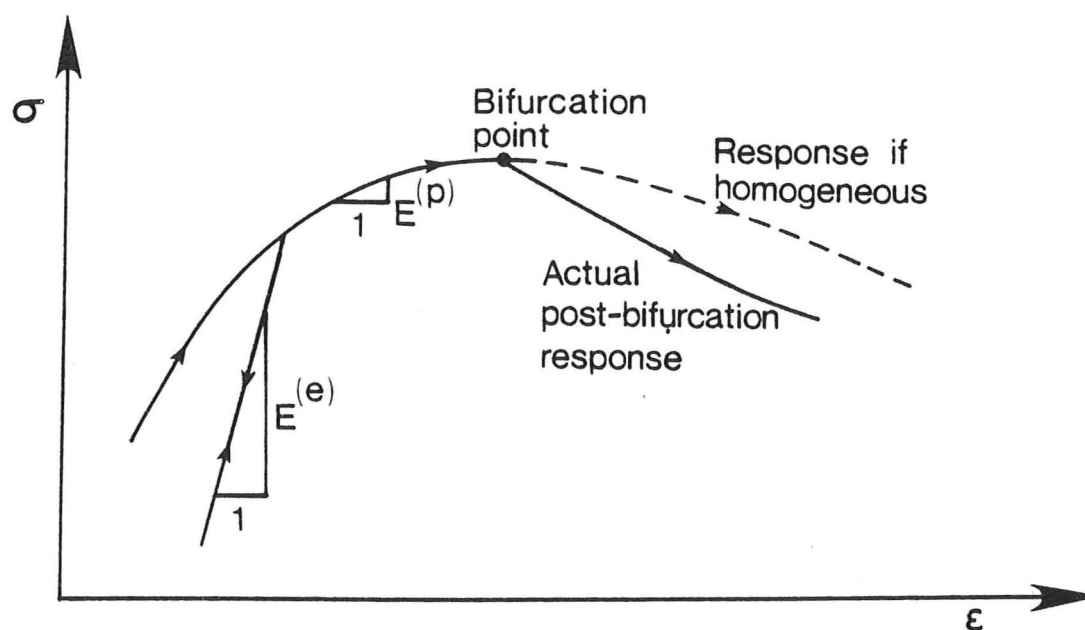


Figure B.2 Bifurcation of a one-dimensional elastic-plastic material into non-homogeneous mode

It is worthwhile noting that for this simple one-dimensional analogue the homogeneity criterion defined from free energy considerations is identical to the condition for 'stability' as defined by Drucker (1959) and also the stability criterion of Nova and Wood (1978) based on accessibility of stress states. It is not definite, however, whether this would also be true in the three-dimensional case.

## APPENDIX C

## STRESS AND STRAIN CALCULATIONS FOR TRIAXIAL TESTS

The triaxial sample is assumed to deform as a right circular cylinder: deviation from this form may arise from several effects, all of which are thought to have been small. Rotation of the top end cap was prevented by the detail of the ram connection (Figure 8.2) and lateral movement of the cap did not occur.

The most important effect is that of end friction, which causes barrelling of the sample; this effect is reduced, but not entirely eliminated, by the use of polished brass end caps coated with silicone grease and covered by a latex rubber membrane. Balasubramaniam (1969) gives radiographic evidence that this achieves an approximately uniform distribution of strains in clay with a sample of 2:1 height to diameter ratio at axial strains up to approximately 8.0% , with increasing non-uniformity at larger strains. Multiple layers of grease and rubber give a more effective reduction of the end friction (Lee (1978)), but have the disadvantage of introducing an additional flexibility between the sample and the measuring point for axial strain. The friction is in part due to the penetration of grains into the rubber membrane, and with an average grain size of 0.2 mm compared with a membrane thickness of 0.35 mm this effect is not thought to be important. With lubricated end caps it is possible to adopt samples with lower height to diameter ratios than in the conventional triaxial test, and Lade (1972) found that the 1:1 ratio adopted for these tests was most satisfactory.

A small non-uniformity may be caused by the constraints of the shaped sample membrane where it is moulded around the enlarged end caps and by the stretching of the end membranes. Both membranes are,

however, very flexible and any restraint should be small by comparison with the stresses. Calculations indicate an approximate radial restraint from the sample membrane of 0.0025 N/mm at each end of the sample at 2.0% radial strain, compared with typically 3.0 N/mm on the end 10 mm of the sample from a cell pressure of 300 kPa .

Non-uniformity may be induced as a result of density gradients in the sample, but the method of preparation is expected to produce a uniform density. No check on internal density variation was possible. Finally non-uniformity may be caused by an inherently non-homogeneous response of the soil. Such an effect, usually manifested in the form of shear bands is not usually observed until at or near peak stress ratio (Rowe and Barden (1964)). All the stress cycle tests were carried out before peak stress ratio was achieved.

Measurements of the initial and final dimensions of a triaxial sample are given on Figure C.1, showing signs of both barrelling and possible density variation. After an axial strain of 13.4% the

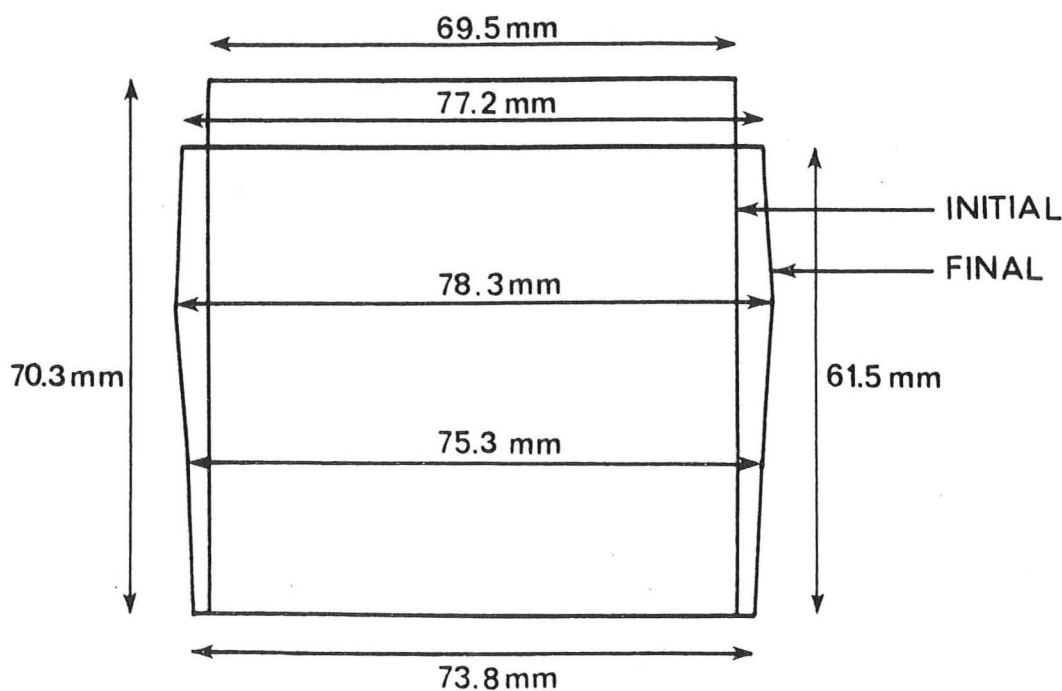


Figure C.1 Deformation of triaxial sample number 1002

maximum variation of lateral strain is from -6.0% to -11.9% . At the small strains achieved during the stress cycle tests (axial strain usually less than 4.0% ) a more uniform strain variation is to be expected.

The height of the sample is calculated from the initial measured height and the axial deformation measured by the LVDT , with a correction for the compressibility of the loading ram and lubricated end cap assembly. The magnitude of the correction was determined from a loading test with a cylinder of aluminium replacing the usual sand sample.

Each correction to either measured stress or deformation may be converted to an equivalent stiffness by referring it to the dimensions of the 70 mm  $\times$  70 mm cylindrical sample. The corrections may then be compared with the stiffnesses measured for the sample (elastic bulk moduli of approximately 100 - 200 MPa and shear moduli of 150 - 300 MPa were measured). A small correction to the measured deformation converts to a high stiffness and a small stress correction to a low stiffness. The magnitude of the axial deformation correction depends linearly on the ram load and converts to an equivalent stiffness of 1213 MPa and is therefore relatively small.

The volume of the sample is calculated from initial height and diameter values, changes in the burette reading during the sample preparation and measurements from the volume change device. In the analysis program, but not in the control program for the tests, a correction is also made for the variation of the membrane penetration with cell pressure. The magnitude of the penetration was measured using the billet method, in which consolidation tests were carried out on a normal sample and a sample containing a 65 mm  $\times$  65 mm cylinder of aluminium completely surrounded by sand. The volume changes for the

essentially elastic unloading were plotted against pressure and the difference extrapolated according to the volumes of sand present in each test to give the equivalent curve for a sample containing no sand: this curve represents the measured volume change due to membrane penetration, see Figure C.2. The curve was closely fitted by the expression

$$V_m = 235.0 \ln(\sigma_c / \sigma_{co}) \quad (C.1)$$

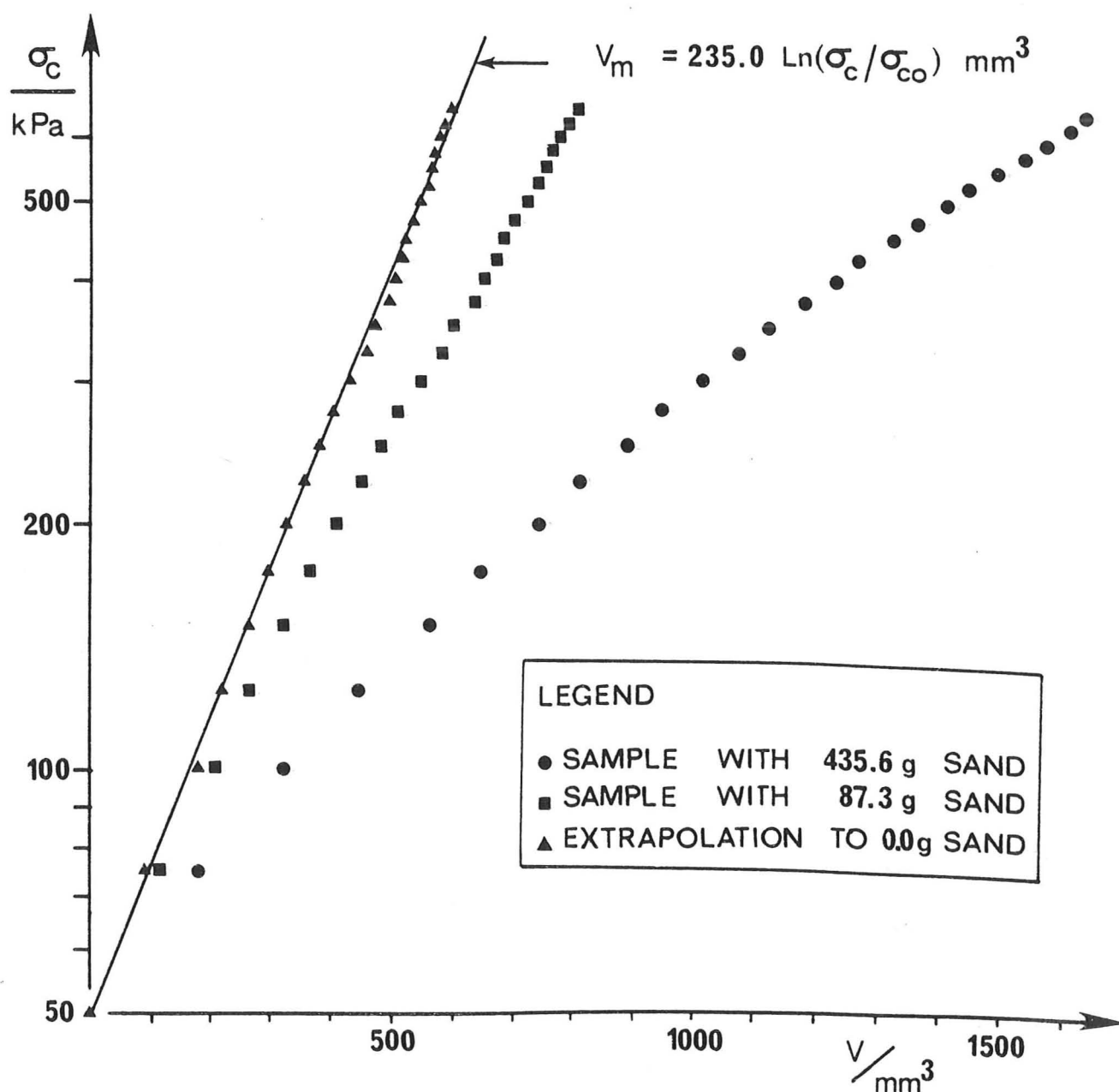


Figure C.2 Establishment of membrane penetration correction

where  $V_m$  is the volume correction in  $\text{mm}^3$  and  $\sigma_c$  is the cell pressure. The above correction converts to an equivalent stiffness of 160 - 600 MPa for the cell pressures of approximately 140 - 520 kPa used for the stress cycle tests. The magnitude of the correction agrees well with values measured by Sarsby (1978) in an extensive study of this problem; but represents a substantial correction to the measured volumetric strain.

Axial and lateral strains are then calculated directly from the corrected height and volume measurements. In the control program the Cauchy small strain is used for speed and simplicity, but in the subsequent analysis program the Hencky logarithmic strain is used.

The lateral stress is calculated according to the expression:

$$\sigma'_3 = \sigma_c - u + \left(2\left(\frac{d-d_o}{d_o}\right) + \left(\frac{h-h_o}{h_o}\right)\right) \frac{2Et}{3d} \quad (\text{C.2})$$

where  $u$  is the pore pressure,  $d$ ,  $d_o$ ,  $h$  and  $h_o$  the current and undeformed diameters and heights of the sample membrane,  $E$  the membrane stiffness and  $t$  its thickness. The final term simply represents the correction for the shell effect of the membrane (Poisson's ratio for the membrane rubber being taken as 0.5). The axial stress is given by:

$$\sigma'_1 = \sigma_c - u + (P + P_c - A_r \sigma_c) / A + \left(\left(\frac{d-d_o}{d_o}\right) + 2\left(\frac{h-h_o}{h_o}\right)\right) \frac{4Et}{d} \quad (\text{C.3})$$

where  $P$  is the axial load,  $P_c$  the submerged weight of the top cap,  $A_r$  the ram area and  $A$  the current sample area. The membrane shell effect on the two stresses may be expressed as a correction stiffness matrix with the following values in MPa for a 70 mm 70 mm sample:

$$\begin{bmatrix} \dot{\sigma}'_1 - \dot{\sigma}'_1 \text{ corr} \\ \dot{\sigma}'_3 - \dot{\sigma}'_3 \text{ corr} \end{bmatrix} = \begin{bmatrix} 0.0172 & 0.0086 \\ 0.0043 & 0.0086 \end{bmatrix} \begin{bmatrix} \dot{\epsilon}_1 \\ \dot{\epsilon}_3 \end{bmatrix}$$

Note that these very low stiffnesses indicate a very small stress correction.